Engineering of Polymeric Nanoparticles Based on Structure-Activity Relationships (SARs) for Oral Drug Delivery

---

A thesis submitted in partial fulfilment of the requirements for the degree of Doctor of Philosophy

July 2018

Uchechukwu Odunze

Research Department of Pharmaceutical and Biological Chemistry

UCL School of Pharmacy

Declaration

This thesis describes research conducted in the School of Pharmacy, University College London between October 2014 and April 2018 under the supervision of Prof. Andreas G Schatzlein and Prof. Ijeoma Uchegbu. I certify that the research described is original and conducted by me and that I have written all the text herein and have clearly indicated by suitable citation any part of this dissertation that has already been published.

Uchechukwu Odunze Date:

Abstract.

The self-assembling polymer *N*-palmitoyl-*N*-monomethyl-*N*,*N*- dimethyl-*N*,*N*,*N*-trimethyl-6-*O*-glycolchitosan (GCPQ) has been shown to improve the oral and parenteral delivery of various drugs. GCPQ contains a number of chemical 'building blocks' that are amenable to independent modification. The ability to finely control the level of modification for those moieties allows systematic modulation of polymer chemistry to become a tool to understanding the role and relative importance of specific modifications for the process of oral drug delivery.

GCPQ polymers with varying molar percentages of palmitoyl (DP) and quaternary ammonium (DQ) groups were synthesized and the effects on physicochemical properties, aggregation, stability and therapeutic applications were examined. Results obtained show that the critical micelle concentration is very low (below 10μM) compared to ≈8mM for sodium dodecyl sulphate and ≈80mM for sodium caprate (C10) and that micelle formation is spontaneous at room temperature. Structural modifications also resulted in a switch from an entropy to an enthalpy driven aggregation at room temperature. The colloidal stability of the synthesized polymers was found to increase with increasing ratio of DQ to DP (QPR) and is greater at acidic pH than at neutral pH. The structural modification also resulted in different morphological characteristics of drug loaded nanoparticles, producing nanocrystals and nano-micelles with varying drug loading capacities.

Additionally, *in vitro* transport studies showed that GCPQ enhances paracellular transport in a graded, modification dependent manner. When compared with C10, GCPQ was found

to be a much safer permeation enhancer, potentially more efficient for drug delivery and at least as potent as C10. The mechanism of these effects was found to involve temporary, size-selective distortions on the tight junctions which limit the passage of molecules larger than 3.2nm in hydrodynamic radius. Furthermore, it was observed that these modifications did not affect the uptake of encapsulated hydrophobic drugs by transcytosis in an *in vivo* rodent model.

Impact statement

The oral route of delivery is central to most therapies due to its convenience, ease of use and safety for a wide range of medications. To facilitate the delivery of pharmaceutical actives and excipients though this route, various delivery systems have been designed and used in preclinical settings as well as in some clinical applications. These applications, while largely beneficial are not without limitations, some of which result in failures in clinical trials. The ability to successfully utilise the oral route to achieve efficient systemic delivery of therapeutic agents therefore hinges on a thorough understanding of the relationships between the physicochemical properties of the compounds and their biological effect. This project seeks to provide relevant knowledge that will be useful as predictive tools for designing ideal delivery systems for orally administered pharmaceuticals.

One of the outcomes of this project is the successful association of specific structural modifications on GCPQ to physicochemical property changes which translate into varied biological effects. For example, this project revealed that by having a range of hydrophilic to hydrophobic surface modification, we can effectively modulate tight junctions to achieve graded paracellular transport enhancement. This information will potentially be useful to researchers seeking to achieve titratable paracellular transport enhancement. Furthermore, the clear association between some of these surface modifications and toxicities will be useful as a predictive tool to scientists designing new delivery systems to avoid potential toxicities.

Additionally, we show that specific structural modifications result in different morphologies of cargo-carrying nanoparticles. This clear insight into how polymer properties can be used to achieve targeted nanoparticle shapes and sizes will be useful to pharmaceutical industries and drug delivery researchers for designing the ideal delivery system for their specific target compounds.

Ultimately, we show that by having the right structural modifications, we can achieve significant systemic delivery, through the oral route of administration, of paclitaxel, a p-glycoprotein substrate used widely in cancer chemotherapy. Paclitaxel is currently only administered by the intravenous route which comes with associated costs and the inconvenience of being restrained as well as a higher risk of toxicities. This will potentially have an impact in the clinical management of cancer patients using paclitaxel and potentially other similar chemotherapeutic agents.

Acknowledgement

First, I will like to thank my supervisors Professors Andreas G. Schätzlein and Ijeoma F. Uchegbu for allowing me to work in their group. I also want to thank them for their menorship as well as their scientific, moral and material support in the course of this program.

I will also like to thank Dr. Fionn O'Brien, for helping me get started on my project and for providing invaluable pieces of advice that helped me go through this work. I am also very grateful to my colleagues in Lab 105 and 326 past and present: Dr. Lisa, Dr. Lorenzo, Dr Antonio, Dr. Sunish, Dr. Nicholas, Dr. Xian, Dr. Ramesh, Dr. Erazuliana, Dr. Preethi, Dr. David, Dr Rui, Dr. Ilona Dr. Manuel, Clemens, Abdulrahman, Gang, Asya, Zilan, Moutaz and Raquel. Thanks to you guys for being a great community of friends and scientists. I am also grateful to Katja, Michelle, Grace, Xiao and Akunna for helping out on some of the projects in this work. To Dr David Gathercole, thank you for helping with confocal microscopy, to Steve Coppard and the staff at the Animal Unit, thank you for your support and assistance.

My gratitude also goes to my parents, Prof. Azubuike and Dr. Ihuoma Odunze. Thank you for supporting me through my academic journey and for always being there. To my siblings: Favour, UD, Onyi and OC, thank you for the laughs, the fun times and for understanding when I am not able to be with you guys. To my family- Yemidale and Munachiso, you guys made the wheel move so smoothly. Thank you for the value you give to me, your patience and understanding and thank you for making it all worth the journey.

Finally, I will like to thank the Presidential Special Scholarship for Innovation and Development (PRESSID), the National Universities Commission (NUC) and the European Union Seventh Framework Program (FP7/2007-2013) under grant agreement no 281035 for providing the funds for this project.

To Adonai.

Table of Contents

Table of Figures

Abbreviations

^{1}H NMR	Proton nuclear magnetic resonance
BBB	blood brain barrier
C_{10}	sodium caprate
CLSM	confocal laser scanning microscopy
CMC	critical micelle concentration
Da	Dalton
dGC	degraded glycol chitosan
DLVO	Derjaguin, Verwey, Landau and Overbeek
DP	molar percentage of palmitoyl functionalization
DQ	molar percentage of quaternary ammonium functionalization
FD4	FITC-dextran (4000Da)
FD10	FITC-dextran (10000Da)
FD20	FITC-dextran (20000Da)
FD40	FITC-dextran (40000Da)
FD70	FITC-dextran (70000Da)
FITC	fluorescein isothiocyanate
GC	glycol chitosan
GCPQ	*N*-palmitoyl-*N*-monomethyl-*N*,*N*-dimethyl-*N*,*N*,*N*-trimethyl-6-*O*-glycolchitosan
HBSS	Hanks' balanced salt solution
ITC	Isothermal titration calorimetry
kDa	kilodaltons

LDH	Lactate dehydrogenase
MALLS	multi-angle laser light scattering
MDCK	Madin-Darby canine kidney cells
Mw	molecular weight
MWCO	molecular weight cut off
MTT	3-(4,5-dimethylthiazol-2-yl)-2,5-diphenyltetrazolium bromide
NMP	*N*-Methyl-2-pyrrolidone
NMR	nuclear magnetic resonance
pGC	palmitoyl glycol chitosan
PNS	palmitic acid N-hydroxysuccinimide
TMC	trimethyl chitosan
SARs	Structure Activity Relationships
ZP	zeta potential

Chapter 1. Polymeric Nanoparticles: Enhancement of Oral Delivery

1.0 Introduction

Oral delivery is the preferred route of drug administration because of benefits including relative safety, ease of administration and better compliance compared with most other routes of administration (Hamman et al., 2005). However, many potential therapeutics, including almost all peptides, are not available for oral administration since they exhibit poor oral bioavailability due to factors including poor absorption, inadequate solubility in gastrointestinal fluids or rapid degradation in the gut (Goldberg and Gomez-Orellana, 2003a, des Rieux et al., 2006). As a result, many compounds that are known to be pharmacologically active, and which may be of therapeutic benefit, have not been successfully developed as medicines to date. This challenge contributes to the unmet clinical demand for more effective treatments for several diseases, including cancer and chronic pain (Hill, 1995, Melzack and Wall, 1983, Scholz and Woolf, 2002). Hence, there is an urgent need for the development of effective drug delivery strategies to enhance the oral bioavailability of such compounds, thereby rendering them viable options as medicines. Much attention has focused on the considerable potential of nanoparticle-based approaches to achieve this goal (Uchegbu and Siew, 2013).

Polymeric nanoparticles have become the subject of extensive research in drug delivery because of their potentially favourable properties including biocompatibility, biodegradability, passive tumour targeting, high encapsulation-efficiency, superb

endocytosis efficiency and versatility in delivering a wide range of therapeutic agents (Faraji and Wipf, 2009, des Rieux et al., 2006).

Polymeric nanoparticles are synthesized using a variety of materials and methods depending on the properties of the drug to be encapsulated and the intended use of the formulation. The method and materials used result in varied structural conformations of the delivery systems including nano capsules, polymeric micelles and dendrimers with the encapsulated drugs entrapped within a core or bound covalently to the polymer matrix (Cho et al., 2008).

Some of these nanoparticle-based drug delivery systems will be discussed further with emphasis on formulations for enhanced oral delivery of various drugs.

1.1 Barriers to Oral Uptake

1.1.1 Biological Barriers:

Overview of the Gastrointestinal tract (GIT):

The digestive tract is an open-ended tube extending from the mouth to the anus, lined by an epithelium and associated with accessory organs and glands which contribute to the digestive process. The GIT is divided into four layers: the mucosa, submucosa, muscularis and serosa. The mucosa is the innermost layer consisting of a mucous epithelium, a loose connective tissue called the lamina propria and an outer smooth muscle layer called the muscularis mucosae. The epithelial cells of the mucosa are primarily responsible for absorption and they are specialized depending on the functions of the regions of the GIT. The mucosa of some regions of the mouth consists of keratinized epithelium, the pharynx and oesophagus have moist stratified squamous epithelium while the mucosa of the absorbing portions of the GIT have simple columnar epithelium. The mucosa of the intestine also contains modifications

which increase absorptive surface area such as villi, crypts and plicae as well as goblet cells that secrete mucus thus making it the secretory and absorptive layer of the small intestine.

The submucosa is a thick and highly vascular layer which also has a rich nerve plexus called the sub-mucosa plexus. Substances absorbed through the mucosa pass into the blood vessels in the sub-mucosa. The muscularis is a thick layer of muscles containing an outer layer of longitudinal smooth muscles and an inner layer of circular smooth muscles. The muscularis also contains the myenteric plexus which is vital for the peristaltic movements of the GIT. The serosa is an avascular connective tissue layer which serves for protection and support. Down the tube, the GIT is divided into regions: the mouth, pharynx, oesophagus, stomach, small intestine, large intestine and the anus. The functions of the tract include ingestion; mastication of ingested foods to facilitate digestion; propulsion of ingested materials through the canal; mixing; secretion of enzymes; digestive juices and mucus; digestion; absorption and elimination of waste. These functions are carried out at different regions of the digestive tract.

The mouth is the common route of ingestion and the site of mastication. Digestion of starch by the enzyme amylase also begins in the mouth. The pharynx and oesophagus serve as pathways for the transfer and propulsion of the ingested materials from the mouth to the stomach. The muscular stomach serves as the site for the mixing of the ingested and masticated materials secreted enzymes and juices to form chyme. Protein digestion begins in the stomach due to the action of hydrochloric acid and the enzyme pepsin. Very little absorption, mostly of water, alcohol and some weakly acidic and basic drugs such as aspirin

and warfarin occurs in the stomach. The stomach then propels the chyme produced into the small intestine which is the major site for digestion and absorption of nutrients, water and electrolytes. The small intestine is divided along its length into the duodenum, the jejunum and the ileum. The small intestine is lined by tiny projections called villi which increase the surface area for absorption, most of which occurs in the jejunum and ileum. The epithelial cells which line the villi contain protease and carbohydrate enzymes which are responsible for the final stage of digestion of proteins and carbohydrates. Bile salts and vitamin B12 are also absorbed in the small intestine. The large intestine is the final site of absorption of water and electrolytes as well as vitamins produced by bacteria, such as vitamin K, biotin and B12. It also serves as the final site of mixing and subsequently the propulsion of faeces towards the anus for elimination (Tate et al., 2003a).

Absorption in the Small Intestine:

The anatomical and physiological features of the regions of the small intestine influence digestion and absorption. The duodenum which receives chyme directly from the stomach is supplied with bile acids through the bile duct and enzymes from the pancreas which are important for digestion of proteins and emulsification of fats. It feeds the jejunum, where most of the absorption occurs and the jejunum then feeds the ilium which has relatively fewer villi and plicae (circular folds) but is abundant in lymph nodules called Peyer's patches. The Goblet cells, duodenal glands and intestinal glands secret mucus which serves to protect the wall of the intestine from the irritating effects of enzymes and the acidic chyme. The role of these features on influencing absorption will be discussed briefly.

Villi and Crypts:

The mucosa of the small intestine is characterized by the presence of finger-like projections called villi as well as deep-lying mucosal glands called crypts (Khan and Islam, 2012). The villi, each of which is about 0.5-1.5mm in height are covered with simple columnar epithelial cells (enterocytes) and have a network of blood capillaries and lymphatic capillaries called lacteal. Most of the cells of the villi contain 1μm cytoplasmic projections called microvilli which increase the surface area of absorption on the intestinal surface (Tate et al., 2003b). The enterocytes are connected by an apical junctional complex consisting of tight junctional proteins including the Zonula Occludens (ZO) proteins, claudins, occludin and Junctional Adhesion Molecules (JAM) which form an important part of the intestinal barrier, regulating the absorption of substances. Absorption through the enterocytes of the villi can either be by transcytosis or by paracellular transport. The cells of the crypts are mostly precursors to the enterocytes and goblet cells which are later found on the villi. They also contain Paneth cells which secret antimicrobial peptides such as lysozymes.

Peyer's patches and M cells:

Gut Associated Lymphoid Tissue (GALT) is a collection of lymphoid cells distributed throughout the lamina propria, sub mucosa and the epithelium of the GIT. An aggregation of these nodules found in the jejunum and mostly in the ileum is called Peyer's patches. The epithelium which covers the Peyer's patch, the follicle associated epithelium (FAE) is made up of specialised antigen sampling 'M' (Membranous epithelial) cells (Bye et al., 1984, Khan and Islam, 2012) which carry out trans epithelial transport and delivery of foreign antigens and micro-organisms to the organized lymphoid tissue of the intestinal mucosa (Kraehenbuhl and Neutra, 2000)- a function which has made them become subjects of

extensive research as a possible pathway for oral delivery of drugs and vaccines (Shakweh et al., 2004, Van der Lubben et al., 2001b).

Bile Acids

Bile, which is stored in the gall bladder and released into the duodenum consists of both organic and inorganic molecules, mostly conjugated bile acids (Hofmann and Eckmann, 2006). Bile acids (or bile salts) are products of the enzymatic modification of cholesterol and are water soluble amphipathic compounds with hydrophilic and hydrophobic groups. Bile serves as an excretory secretion to eliminate wastes like cholesterol and bilirubin. It is also a digestive secretion necessary for the digestion of fats and lipids- it solubilises lipids and fatty acids, forming micelles and thus enhancing their absorption at the proximal small intestine (Hofmann and Mysels, 1987, Hofmann and Eckmann, 2006). Bile acids are involved in extensive enterohepatic circulation after they are absorbed by an active transport system in the epithelium of the terminal ileum, which results in efficient recycling of conjugated bile acids, thus maintaining large amounts for digestion (Forte and Schultz, 1989). This bile acid transport system has been explored in drug delivery system to improve intestinal absorption and sustain systemic concentrations of therapeutic agents (Sievänen, 2007, Cundy et al., 2005).

Digestive enzymes:

An important function of the pancreas is to produce digestive enzymes which are released into the duodenum through the pancreatic duct to aid the digestion of proteins, fats, carbohydrates and other complex compounds. These enzymes include the proteases, lipases, amylases, co-lipases, phospholipase A_2 carboxylesterases, carboxypeptidases, nucleases and the elastases. Besides the pancreas, the enterocytes of the small intestine mucosa produce other enzymes including aminopeptidases, endo-peptidases, diesterases, nucleotidases and dipeptidases (Walker, 2004, Whitcomb and Lowe, 2007, Beck, 1973). These enzymes are responsible for breaking down ingested macromolecules to absorbable units. It is very important to consider the activity of these enzymes in drug delivery especially when the intended therapeutic agent is a substrate to some digestive enzyme(s). Strategies to overcome the challenge posed by these enzymes to uptake include structural modification of peptides such as the bio-reversible cyclization of peptide back bone to protect the C-terminal carboxyl and N-terminal amino groups from carboxypeptidases and aminopeptidases (Gangwar et al., 1997); macromolecular conjugation such as the PEGylation of proteins (Hinds and Kim, 2002); encapsulation in nanoparticles (Van Der Lubben et al., 2001a, Shen, 2003) and co-administration of peptide inhibitors (Langguth et al., 1997, Lee et al., 1991). The activity of these enzymes can equally be exploited in designing prodrugs which can be activated after cleavage of specific bonds by an endogenous enzyme (Han and Amidon, 2000, Sinha and Kumria, 2001).

Mucus

Goblet cells which secret mucin, are mostly located in the crypts but some can be found on the villi. Mucin is a heterogeneous glycoprotein of about 1-2 X 10^6 Daltons in weight (Norris et al., 1998, Neutra, 1987) which is a major component of a mucus layer that covers the surface of the mucosa. The mucus layer serves as a functional and physical barrier; helping to maintain the pH difference between the GI lumen and the mucosal surface (Allen et al., 1993) as well as restricting the diffusion of small and large compound to the mucosal surface (Norris et al., 1998). In forming a diffusional barrier, the mucus has been shown to serve two purposes: On the one hand, it forms a barrier to the absorption of particles, trapping and preventing them from getting to the absorptive surfaces of the intestine before they eventually get eliminated by mucociliary clearance (Lai et al., 2009, Norris et al., 1998). On the other hand, the mucus layer also helps particle uptake by increasing the residence time of muco-adhesive particles on the absorptive surface of the intestine, preventing them from being displaced during intestinal motility and thus providing a means for delayed and controlled uptake (Takeuchi et al., 2001, Pridgen et al., 2015)

1.1.2 Physicochemical Properties of the Compound

The ability of a drug candidate to overcome the biological barriers to absorption is dependent on a collection of factors. The Lipinski's rule-of-five (RoF) was an early attempt to describe the properties of an ideal drug which is expected to have good solubility and absorption (Lipinski et al., 2001). This rule states that poor solubility and absorption of a chemical compound is more likely when the log P is greater than 5, molecular mass is greater than 500 Daltons, there are more than five hydrogen-bond donors (determined as the sum of OHs and NHs) and there are more than ten hydrogen bond acceptors (determined as the sum of Nitrogens and Oxygens). Exceptions to the rule are substrates for biological transporters as well as natural products (Zhang and Wilkinson, 2007, Lipinski, 2016). Generally, these factors are mostly related to the physicochemical properties of the chemical compound and include drug solubility, dissolution rate, pKa, size and susceptibility to enzymatic degradation

The ability of a drug to be solubilised is an important limiting factor to its rate of absorption, the other being the rate of drug permeation through the membrane. The solubility of the drug in aqueous environments is usually a determinant of its dissolution rate so that drugs that are poorly soluble in aqueous environments will have a slower rate of dissolution which will ultimately slow down the rate of absorption (Hörter and Dressman, 2001). The dissolution rate is thus a more important limiting factor for lipophilic poorly soluble drugs than for hydrophilic drugs. This property has been used as a predictive tool for oral absorption. The Biopharmaceutical Classification System (BCS) (Amidon et al., 1995) has grouped

compound into four groups based on their solubility and permeability properties as shown in the table below:

Table 1-1 BCS classification of drugs

BCS Class	Properties	Examples
Class I	High permeability, high solubility	Metoprolol
Class II	High permeability, low solubility	Glibenclamide
Class III	Low permeability, high solubility	Cimetidine
Class IV	low permeability, low solubility	Bifonazole

Properties which affect the solubility of drugs include the particle size and effective surface area, drug pKa and lipophilicity. Bioavailability is reportedly not significantly affected by size when drug molecules are below 500 Daltons in size but significant decrease in bioavailability occurs with increasing size beyond 500 Daltons (Donovan et al., 1990, Goldberg and Gomez-Orellana, 2003b). While hydrophilicity is important for solubility, it is vital that there is some level of lipophilicity to allow passive permeation by transcytosis through the biological membranes, without which the alternative will have to be the very restrictive paracellular pathway which allows the passage of hydrophilic molecules smaller than 200 Daltons in size (Goldberg and Gomez-Orellana, 2003b, Camenisch et al., 1998).

Several drug compounds are weak acids and bases with different ionisation constants (*Ka*). The solubility of these compounds will depend on the pH of the solvent or dissolving medium as well as the pKa of the drug. For weak acids, the solubility increases with

increasing pH while weakly basic drugs have increasing solubility with decreasing pH. Weakly acidic drugs such as aspirin and salicylic acid are therefore less dissociated in the gastric pH and thus readily absorbed in the stomach while basic drugs like quinine and ephedrine are mostly dissociated in the gastric environment and not absorbed in the stomach (Hogben et al., 1957). Consequently, weakly basic drugs which are more soluble in acidic pH have a faster dissolution rate while poorly soluble weak bases like the imidazole antifungals have a lower dissolution rate, resulting in malabsorption (Hörter and Dressman, 2001).

The surface area of the drug exposed to the dissolving medium is directly proportional to the dissolution rate. The smaller the particle size, the greater the effective surface area and thus the faster the dissolution rate. It has been reported that particle sizes around 3-5μm are sufficient to achieve enhanced dissolution rates (Hörter and Dressman, 2001) hence the use of approaches like micronization to achieve small particle sizes. Newer technologies including nanoparticle drug formulation allows the achievement of smaller particle sizes which are expected to have better bioavailability because of enhanced uptake. Studies using some of these nanoparticle sized formulations show an inverse relationship between the particle size and the rate of uptake (Banerjee et al., 2016, Maisel et al., 2015, Dizaj et al., 2015, Ran et al., 2018).

In addition to these parameters, the absorption of macromolecules is hugely affected by their vulnerability to enzymatic degradation as is the case with protein and peptide drugs (Goldberg and Gomez-Orellana, 2003a). The goal for these compounds will be to protect

them from degradation long enough to allow for meaningful uptake. Strategies to achieve this goal include encapsulation, co-administration with enzyme inhibitors, peptidomimetics and delivery as pro-drugs (Hamman et al., 2005, Brayden and Alonso, 2016, Muheem et al., 2016).

1.2 Strategies to Overcome Barriers to Oral uptake

1.2.1 Nanoparticle Drug Delivery Systems

Nanoparticle drug delivery systems are typically submicron sized particles ranging in size from 3 to 200nm, synthesized from a range of materials including lipids, polymers, viruses and organometallic compounds (Cho et al., 2008). These particles can be designed for different purposes including the enhanced delivery of insoluble drugs to specific tissues in the body. Their small size allows them to be more efficiently taken up by cells and through passive or active targeting, carry their cargo to specific tissues such as tumours, thus reducing systemic toxicity. The use of some of these nanoparticle systems to enhance the oral uptake of drugs will be discussed briefly:

Lipid-based Nanoparticle Systems (Liposomes)

Liposomes are colloidal systems formed by the self-assembly of phospholipid molecules into spherically shaped vesicles surrounded by a lipid bilayer and an aqueous core (Kim, 2016, Cho et al., 2008). The phospholipid molecules have a hydrophilic head and a hydrophobic tail of lipids which assemble together to avoid the water in the aqueous core and the external environment. Their unique structure implies that they are useful in

encapsulating a wide range of drugs, both hydrophilic and hydrophobic. They are typically made using a couple of compounds including phosphatidyl choline, phosphatidyl glycerol, phosphatidyl inositol, phosphatidyl ethanolamine (cephalin), phosphatidyl serine and occasionally cholesterol (Daraee et al., 2016). Liposomes are sometimes classified based on the mechanisms through which they deliver items into cells as pH sensitive liposomes, cationic liposomes, long circulating liposomes, immune liposomes and convectional liposomes (Alavi et al., 2017, Daraee et al., 2016). They can also be classified based on their structure into as illustrated in Figure 1-1. They can be small unilamellar vesicles (SUV) which are less than 100 nm in diameter (Hoffmann et al., 2018, Klingler et al., 2015), large unilamellar vesicles (LUV) which are between 100 nm and 1000 nm in diameter, giant unilamellar vesicles (GUV), multilamellar vesicles (MLV) and multivessicular vesicles (MVV) (Rols, 2017, Stein et al., 2017).

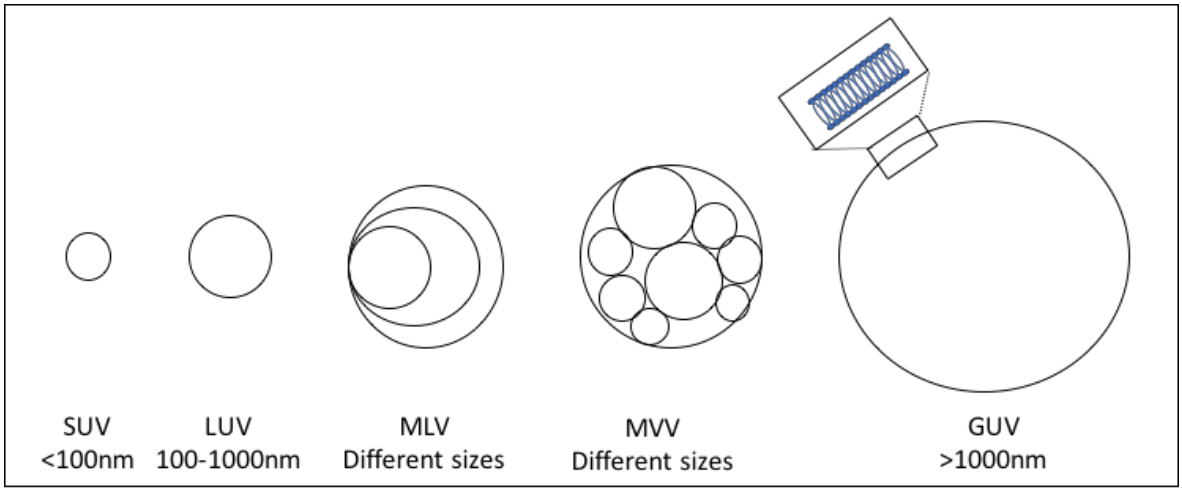

Figure 1-1: Schematic representation of types of liposomes

Liposome formulated drugs have a fairly long history of use in the clinic already, with the FDA approval of Doxil®, a PEgylated liposomal formulation of doxorubicin for the management of ovarian cancer and AIDS related Kaposi's sarcoma considered a milestone achievement (Working and Dayan, 1996). Since then, other formulations have received regulatory approval including Myocet® by Elan Pharmaceuticals, Mepact ® by Takeda pharmaceuticals and recently (in 2015), Onivyde^{TM} by Merrimack Pharmaceuticals which is a liposomal formulation of fluorouracil and leucovorin for the treatment of metastatic adenocarcinoma (Bulbake et al., 2017).

Liposomes have the structural advantage of having compartments that can be used to incorporate a wide range of substances. They are also structurally amenable to surface modifications which allows them to be applied for a variety of uses including site specific targeting. Additionally, their morphological similarity to cellular membranes also makes them easily degradable by cellular enzymes. They are however limited by their rapid clearance from circulation and capture by cells of the reticulo-endothelial system (Torchilin, 2005). There have also been recent reports of effects on cellular metabolism and mitochondrial function which could result in off-site unwanted effects (Gebhardt and Matz-Soja, 2015).

Magnetic Nanoparticles

Magnetic nanoparticles are made using a variety of compounds including metallic oxides such as iron oxide (Fe_3O_4) (Huber, 2005); metals (Sun et al., 2008) such as nickel, cobalt and iron; as well as bimetallic compounds such as iron-platinum (FePt) (Sun, 2006) and iron-

cobalt (FeCo) (Reiss and Hütten, 2005). These nanoparticles have a wide range of application owing to their amenability to modifications including in structure: surface chemistry and morphology, as well as in size and composition. They have been applied largely in use as contrast agents in magnetic resonance imaging and also as carriers for therapeutic purposes, making them useful both in diagnosis and in treatment of a number of diseases such as cancer and neurological diseases (Corot et al., 2004, Ferrari, 2005, Dobson, 2006).

Magnetic nanoparticles are usually susceptible to oxidation and more so because of their small sizes. They therefore usually need to be protected or stabilised using a variety of methods and materials. Examples of approaches to protect the magnetic nanoparticles from oxidation include:

1. Coating the surface of the nanoparticles with polymer stabilizers such as polyethylene glycol (PEG) (Lutz et al., 2006), poly(vinyl alcohol) (PVA) and chitosan (Tran et al., 2018).
2. Coating the surface of the nanoparticles with layers of inorganic materials including other metals such as gold (Jeong et al., 2006, Azhdarzadeh et al., 2016) and non-metals such as silica (Butterworth et al., 2001, Srikanth et al., 2017)and graphite.
3. Forming a lipid coating around the magnetic core of the nanoparticle. The lipid coatings could be in the form of liposomes or lipid nanoparticles (Liang et al., 2017).

A good number of magnetic nanoparticles have gone through clinical trials, with some of them already approved for use. For example, some polymer coated iron oxide nanoparticles have been approved by the FDA for iron replacement therapies including INFed®, Dexferrum®, Feraheme® and Venofer® which have been approved for the treatment of

anaemia associated with chronic kidney disease (CKD). Also, an aminosilane coated superparamagnetic iron oxide nanoparticle (SPIONs), Nanotherm^{TM} was approved in the EU for use in treatment of glioblastoma and is currently seeking FDA approval for the same indication in the USA (Bobo et al., 2016)

Polymeric Nanoparticle Systems

Polymeric nanoparticles are nanoparticles synthesized from polymer materials typically obtained from a variety of sources, natural and synthetic. They take different forms and are synthesized using different approaches. They are also typically suited for cargos having different physical and chemical properties. Some examples of these systems will be discussed in this section:

Polymeric Nano capsules

Nano capsules are nano-sized vesicular systems which have a core-shell structure in which there is a central reservoir for the encapsulated drug (core) and a polymer membrane surrounding the core (shell). The drug contained in the reservoir can be a liquid, solid or a molecular dispersion depending on the method of synthesis, the nature of the reservoir and the properties of the polymer used. For example, a Nano capsule with a hydrophilic core is more likely to be used for encapsulating hydrophilic actives which are more likely to be in solution. A hydrophobic core is more likely to entrap hydrophobic materials which can be solids or molecular dispersions. Understandably, the method used in synthesis will

determine the characteristics of the Nano capsule formed and the type of materials encapsulated (Mora-Huertas et al., 2010).

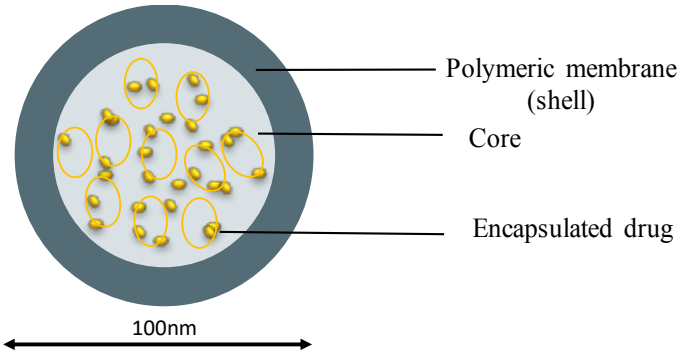

Figure 1-2: Representation of a polymeric Nano capsule

Several methods are used in the synthesis of Nano capsules including solvent displacement/ nanoprecipitation, emulsion diffusion, double emulsification and polymer coating methods (Mora-Huertas et al., 2010).

Nanoprecipitation is a method wherein the polymer and drug, dissolved in an organic, water miscible solvent is dispersed/precipitated in an aqueous solvent, usually water, forming a colloidal oil in water dispersion where the drug is trapped within an oily core surrounded by the polymer in an aqueous environment. A stabilizer is usually incorporated in the aqueous phase to keep the system stable. Also, a surfactant can be included to reduce the surface tension of the water and allow miscibility of the organic phase (Nagavarma et al., 2012). Polymers typically used for this method include biodegradable polyesters such as Poly (lactide) (PLA) (de Assis et al., 2008), poly (lactide-co-glycolic acid) (PLGA) (da Silva Santos et al., 2006) and poly-ε-caprolactone (PCL) (Pohlmann et al., 2008).

Polymeric Nano capsules have been extensively studied as platforms for enhanced oral delivery of a couple of compounds. Min-Jeong Park et al showed that a Nano capsule formulation of cyclosporine using poly ($_{D,L}$-lactide) significantly increased the bioavailability of cyclosporine in rats compared with the non-encapsulated formulation (Park et al., 2013). Similarly, a study showed that Nano capsule formulations of Lychnopholide in PEG-PLA Nano capsules and PCL nano capsules achieved significantly higher cure rates in mice infected with *Trypanosoma cruzi* compared with the non-encapsulated Lychnopholide after oral and intravenous administration (de Mello et al., 2016).

Dendrimers

Dendrimers are highly branched core-shell nanostructures with repeating units of stem-like projections emanating from the core, forming many branches affixed with terminal functional groups at the periphery (shell). They are synthesized in layers referred to as 'generations' and form precise globular structures that have low polydispersity, uniform size distribution and surface functionality (Svenson, 2009). These properties confer on dendrimers some advantages over conventional linear polymers use for drug delivery. For example, their low polydispersity will confer superior reproducibility in physicochemical properties of batches. This, coupled with their globular structure will imply a more homogenous pharmacokinetic behaviour of formulations in vivo. Their multi valency and unique branching characteristic also allow for attachment of chemically varied groups including drug molecules, targeting ligands and solubilising agents onto the dendrimer (Gillies and Frechet, 2005)

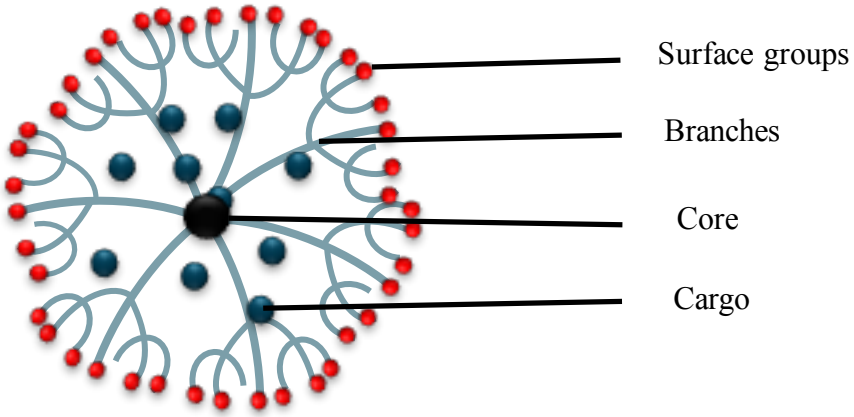

Figure 1-3: Representation of a Dendrimer

Some dendritic polymers that have been explored for use in drug delivery include polyamidoamine (PAMAM), polypropylimine (PPI), poly-l-lysine, polyethylene glycol (PEG), poly(glycerol-co-succinic acid), poly(glycerol), and poly[2,2-bis(hydroxymethyl)propionic acid] (Kesharwani et al., 2014). For example, a doxorubicin-PAMAM complex was reported to result in bioavailability of doxorubicin 200 times greater than that of free doxorubicin in a rat model (Ke et al., 2008) while another study showed a significantly better anti-inflammatory effect of Quercetin-PAMMAM complexes compared with quercetin suspensions after oral administration in a rat model (Madaan et al., 2016).

Polymeric Micelles

Polymeric micelles are core-shell nanostructures consisting of a typically hydrophilic surface (shell) and a hydrophobic core. They are formed from amphiphilic polymers which typically self-assemble in aqueous solution. Their hydrophobic core enables them to solubilize poorly soluble drugs and thus facilitate their uptake through the absorptive surfaces of the intestine. The micelles are formed due to the interplay of hydrophobic interactions and entropy due to release of water of solvation. The hydrophobic tails of the amphiphilic polymers associate with the hydrophobic drug in the core in a bid to limit

exposure to the aqueous environment. This association is energetically driven by the entropy of dissociation of water molecules from the hydrophobic tails. The water molecules interact by hydrogen bonding, with the hydrophilic heads of the amphiphile, forming a lattice structure around the molecule which establishes the shape of the micelle.

Amphiphilic polymers self-assemble in solution, therefore, methods for formulation of polymeric micelles attempt to facilitate this process of self-assembly. Examples of approaches employed include: thin-film formation/solvent evaporation and reconstitution, direct dissolution, change of ionic strength or pH or step-wise dialysis (Webber, 1998, Simões et al., 2015).

Examples of polymeric micelles employed in oral drug delivery include: chitosan derivatives such as trimethyl chitosan, block copolymers such as derivatives of poly(ethylene oxide) (PEO) formed with hydrophobic poly (propylene oxide) (PPO) and some triblock co polymers such as the poloxamers (PPO-PEO-PPO) some of which have been used in oral and parenteral formulations approved by the US FDA and the European Medicines Agency (EMA) (Simões et al., 2015)

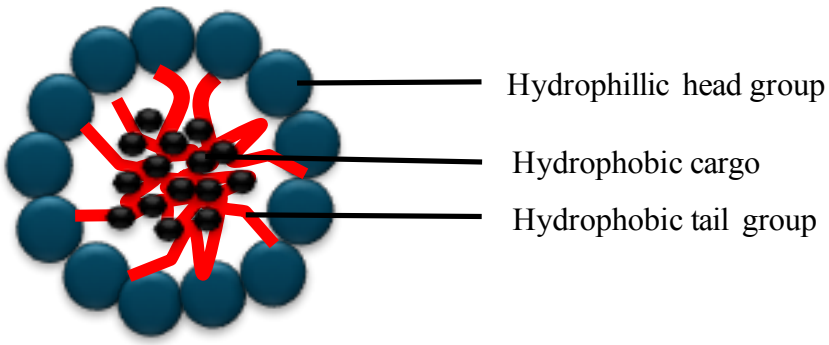

Figure 1-4: Representation of polymeric micelles

Physico-chemical properties of nanoparticles for enhanced absorption

Size

The widely researched and generally accepted observation that absorption increases with decreasing size is one motivation for interests in drug delivery nanotechnologies that formulate sub-micron sized particles (Desai et al., 1996, Desai et al., 1997, Florence, 2005). A study on the mucin permeability of carboxylate – modified latex particles ranging in size from 0.1μm to 1μm showed a sharp decrease in permeability with increasing diameter, reaching a nadir at about 0.5 μm (Norris and Sinko, 1997). The nanoparticle size has also been shown to affect the mechanism of nanoparticle uptake. Studies with polystyrene latex in a female Sprague rat model showed that particles with 50-100 nm in size were transported more readily than particles with larger sizes and particles greater than 1 μm were trapped in Peyer's patches (Jani et al., 1990). Furthermore, a study showed that spherically shaped gold particles were taken up 500 % more than rod-shaped materials, probably due to the relative ease of membrane wrapping around the spherical particles compared to the rod-shaped materials (Verma and Stellacci, 2010, Jiang et al., 2008, Chithrani et al., 2006).

Surface charge

The surface charge of nanoparticles has been shown to affect the extent of interaction with mucin and the epithelial cell surface. The carbohydrate side chain of mucin is rich in negatively charged sulphate and sialic acid and can therefore interact electrostatically with positively charged particles. Studies have shown that cations with higher valence bind stronger to porcine gastric mucus (Crowther and Marriott, 1984, Quarterman, 1987). This electrostatic interaction has been suggested to be the major driving force for the muco-

adhesive property of chitosan (Sogias et al., 2008, He et al., 1998). The cell membrane is mostly negatively charged and so, like the mucus layer, will be expected to favour interactions with positively charged particles. However, several studies have shown that negatively charged particles also get adsorbed to the cell membrane but show lower internalization compared to the positively charged particles (Villanueva et al., 2009, Cho et al., 2009, Wilhelm et al., 2003). The internalization of negatively charged particles is likely due to non-specific binding and clustering of the particles on the relatively scarce cationic sites on the plasma membrane, resulting in their eventual endocytosis (Verma and Stellacci, 2010). Positively charged particles on the other hand readily bind to the anionic groups on the cell membrane by electrostatic interaction and eventually get internalized. The charge density on these particles has been shown to influence the mechanism of internalization as well as the fate of the particles. Chung et al reported that a clathrin and actin dependent endocytic mechanism was indicated for silica nanoparticle at lower charge density but both mechanisms were by-passed when the nanoparticles were more densely charged (Chung et al., 2007). Fuller et al also reported that positively charged silica nanoparticles can escape the endosomes and get into the cytoplasm and nucleus (Fuller et al., 2008). Furthermore, studies have shown that positively charged nanoparticles tend to form pores on the lipid bilayer of the plasma membrane which results in their internalization into cells, intracellular and extracellular diffusion of dye molecules and diffusion of cytosolic proteins out of cells (Hong et al., 2004, Verma and Stellacci, 2010).

1.3 Mechanisms of Nanoparticle Uptake

The uptake of nanoparticles by epithelial cells can be by transcellular transport (including transcytosis via invagination of the cell membrane and carrier mediated transport) or by paracellular diffusion through the tight junctions of epithelial cells (Malam et al., 2009). Both pathways are illustrated in figure 1-5.

1.3.1 Transcytosis

Transcytosis is an energy dependent transport of molecular cargo across an epithelial membrane (Frank et al., 2003, Komarova and Malik, 2010). It is a strategy used by cells to regulate the movement of macromolecules across its membrane and therefore control homeostasis. The process is dependent on factors such as the cell type, the mechanism involved and the type of cargo being carried across (Tuma and Hubbard, 2003). In the intestinal epithelium, transcytosis usually begins with a Clathrin-mediated endocytosis carried out mostly by M cells of Peyer patches but also by enterocytes (Florence and Hussain, 2001, Tuma and Hubbard, 2003, des Rieux et al., 2006, Lavelle et al., 1995).

Endocytosis is a fundamental process in eukaryotic cells that involves the internalization of extracellular materials by the invagination of plasma membrane forming vesicles (Nam et al., 2009, Canton and Battaglia, 2012). The process can be through different pathways including caveolae-mediated endocytosis, macropinocytosis, phagocytosis, clathrin and caveolae-independent endocytosis and the more established clarthrin-mediated endocytosis (Conner and Schmid, 2003b, McMahon and Boucrot, 2011).

Clathrin-mediated endocytosis has been implicated in the uptake of nutrients and toxins in the GIT. It has thus been the focus of much research on the mechanism of uptake of orally administered nanoparticles. Though it is currently the most studied endocytic pathway for particle uptake, several studies have shown that other pathways may equally be important for uptake, especially pathways that do not eventually fuse with the acidic lysosome. Macropinocytosis and caveolae-dependent endocytosis are both non-specific and neither digestive nor acidic and could serve as alternative uptake pathways (Nam et al., 2009, Swanson and Watts, 1995, Conner and Schmid, 2003b).

Reports suggest that the hydrophobicity and charges of particles are important for endocytosis. Nanoparticles composed of the relatively hydrophilic ethyl cellulose or cellulose acetate were transported less by M cells than nanoparticles composed of polystyrene, poly(methyl methacrylate), poly(lactic acids) (PLA) or poly(lactic-co-glycolic acids) (PLGA) (Shakweh et al., 2004). Improving mucoadhesion by coating with chitosan was also shown to increase the uptake of salmon calcitonin (Kawashima et al., 2000) and tetanus toxoid (Vila et al., 2002). GCPQ, a chitosan based amphiphilic polymer delivery system has been shown to enhance the uptake of Amphotericin B through the M cells of Peyer's patches (Serrano et al., 2015a).

1.3.2 Paracellular Transport

Paracellular transport refers to the movement of, usually ions and electrolytes in solution through pores at the intercellular junctions between cells. This movement is usually passive and down an electrical or chemical gradient. The presence of tight junctions between epithelial cells introduces size discrimination to paracellular transport (Van Itallie and Anderson, 2006) given the limited pore sizes of the tight junctions in humans: 0.8 nm in the jejunum and 0.3 nm in the ileum and colon (Powell, 1987). Several authors report that molecules greater than 1.2nm in diameter cannot be transported through the paracellular route (pore diameter between epithelial cells is between 0.3 and 1.0 nm (Nellans, 1991)) hence the use of hydrophilic molecules with smaller sizes as paracellular markers (Norris et al., 1998, Ma et al., 1990).

Hydrophilic proteins and polypeptides such as octreotide (Drewe et al., 1993), salmon calcitonin (Lee and Sinko, 2000) and analogues of vasopressin (Lundin and Artursson, 1990) are able to passively diffuse through the tight junction but most times at amounts below the potent concentration. Hence the need for ways to enhance paracellular transport. Several strategies have been employed to achieve this, including the use of surfactants and water soluble polymers such as chitosan, starch and thiolated polymers (des Rieux et al., 2006). These strategies usually involve modulating the tight junction with suggested mechanisms including chelation or depletion of Ca^{2+} which results in the activation of protein kinase C (PKC) which is mediated by the calcium dependent cell adhesion protein cadherin. This results in the internalization of cadherin family proteins and triggers a cellular signalling cascade that causes the disassembly of cellular junction components including Zonula

Occludens-1 (ZO-1) (Citi, 1992, Noach et al., 1993, Tomita et al., 1996, Salamat-Miller and Johnston, 2005). Unlike chitosan and some of its derivatives, most of the surfactants and chelating agents used to enhance paracellular transport produce irreversible modulation which has strong implications for toxicity (Prego et al., 2005). Chitosan and some of its derivatives have been reported to cause the depolymerisation and redistribution of cellular F-actin, the activation of PKC and the displacement of essential cations due to its interaction with anionic glycoproteins on the surface of epithelial cells (Kotzé et al., 1999, Dodane et al., 1999, Ma et al., 2005).

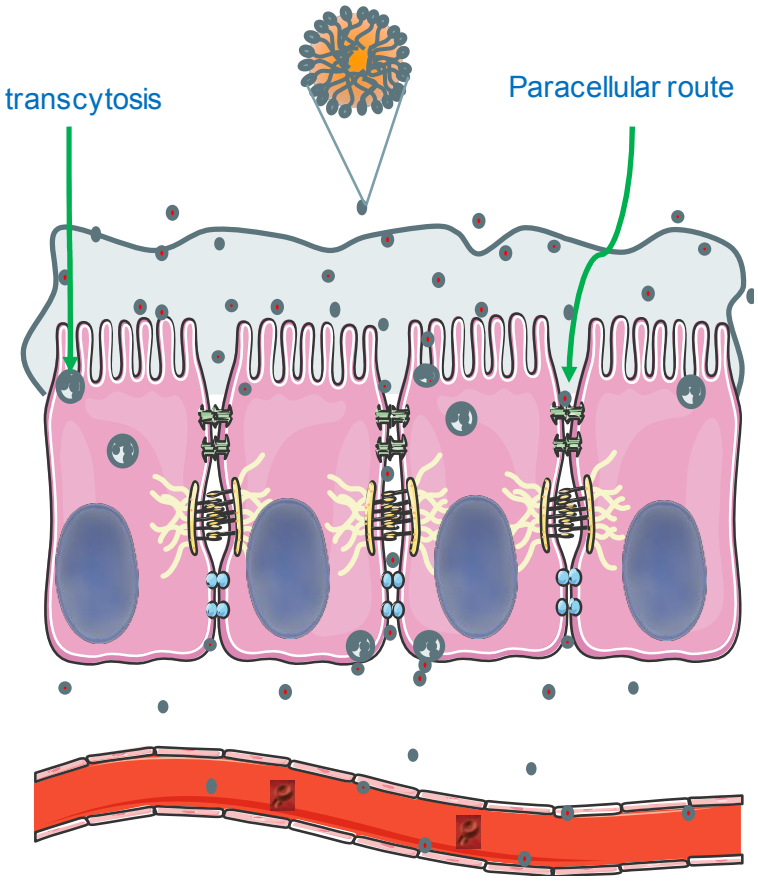

Figure 1-5: Schematic representation of pathways of particle uptake across the intestinal epithelium

1.4 Chitosan and Its Derivatives as Absorption Enhancers

Chitosan, α (1–4) 2-amino-2-deoxy-β-d-glucan is a polysaccharide comprising of polymers of glucosamine with some N-acetyl glucosamine impurities. It is a non-toxic, pH sensitive, bio-adhesive, bio-compatible and biodegradable polymer obtained by alkaline deacetylation of chitin, a component of the exoskeleton of crustaceans such as shrimps (Toan et al., 2006). Because of its favourable properties, it has found wide application in tissue engineering, targeted delivery and as an absorption enhancer (Suh and Matthew, 2000, Kumar, 2000, Dodane and Vilivalam, 1998). Chitosan is insoluble at neutral and at alkaline pH and forms salts with organic and inorganic acids and is known to swell when in solution (Thanou et al., 2001b). Its muco-adhesive property is reported to be related to its solubility and its protonated state in solution which enable it to interact with negatively charged groups on the mucosal surface (Prabaharan, 2008, Lehr et al., 1992). The mechanism by which chitosan enhances oral absorption is reported to be through a combination of bio-adhesion and the widening of tight junctions (Illum et al., 1994), thus favouring absorption through the paracellular route. Though its efficacy in absorption enhancement has been well researched, its poor solubility at neutral and alkaline pH makes it limited in its therapeutic potential at physiologic pH values. Furthermore, its tendency to swell in aqueous environments leads to fast release of its cargo, thus limiting its use in sustained release formulations (Prabaharan, 2008, Thanou et al., 2001b). These limitations necessitated the search for chemical modifications that improve chitosan's properties and widens its application. Over the years, several modifications, usually involving substitutions and grafting at the free $–NH_2$ of chitosan, have been developed with varied properties such as stimuli sensitivity, good

mechanical strength, controlled swelling and drug release and improved solubility at a wide pH range (Mourya and Inamdar, 2008). Modifications with groups having amphiphilic properties allow for the encapsulation of hydrophobic substances, thus expanding the utility of chitosan in drug formulation.

1.4.1 Trimethyl chitosan (TMC)

N,*N*,*N*-trimethyl chitosan chloride is a partially quarternised chitosan derivative which has permanent positive charges and improves the solubility and permeation enhancement of chitosan at neutral pH (Bayat et al., 2008, Kotzé et al., 1997). It can be synthesized to have varying degrees of quaternisation with absorption enhancing effects increasing with degree of quaternisation (Sieval et al., 1998, Thanou et al., 2000a). TMC has been shown to increase the in vitro permeability of paracellular transport markers across epithelial barriers (Kotzé et al., 1999) and has also been shown to increase the absorption of a couple of drugs in vivo following admiration through different routes (Amidi et al., 2006, Sandri et al., 2005, Thanou et al., 2001c, Ramalingam and Ko, 2015). It has also been used in combination with other compounds to achieve additional benefits including improved cohesiveness, mucus penetration, gene delivery (Yin et al., 2009, Xu et al., 2010, Bei et al., 2014, Zheng et al., 2009).

1.4.2 Thiolated chitosan

Thiolated chitosan derivatives are formed by coupling the primary amine groups of chitosan with thiol containing functional groups, forming a product which has superior mucoadhesive and permeation enhancement properties (Kast and Bernkop-Schnürch, 2001, Bernkop-Schnürch et al., 1999, Bernkop-Schnürch et al., 2003) and protease resistant properties (Bravo-Osuna et al., 2007). They also display in situ gelling properties at physiological pH which improves the stability of liquid formulations and makes them ideal for controlled release formulations (Hornof et al., 2003, Jayakumar et al., 2007). Their strong cohesive properties are mostly due to the formation of inter- and intra-molecular disulphide bonds between the thiol groups and cysteine rich domains of the mucus layer (Kast and Bernkop-Schnürch, 2001, Hornof et al., 2003). This property is also thought to be responsible for the enhanced permeation enhancement compared to chitosan. By forming an adherent and bulkier matrix at the membrane, thiolated chitosan derivatives can have a higher local concentration and thus a comparatively higher permeation enhancement effect (Bernkop-Schnürch et al., 2004).

1.4.3 Carboxymethyl chitosan

Carboxymethyl chitosan derivatives are synthesized by the N- and/or O- substitution of carboxymethyl groups onto the chitosan molecule (Upadhyaya et al., 2014). This produces polyampholytic polymers with improved solubility in both alkaline and acidic pH environments (Thanou et al., 2001a). This offers an advantage over chitosan and trimethyl chitosan since they are both insoluble at alkaline pH and form aggregates with highly anionic polysaccharides (Muzzarelli et al., 1982, Thanou et al., 2001a). Their amphoteric character makes them ideal for formulation of pH sensitive delivery systems (Chen et al., 2004a, Chen et al., 2004b). Carboxymethyl chitosan derivatives have been shown to enhance the uptake of a wide range of compounds (Wang et al., 2008, Ha et al., 2012, Thanou et al., 2001a)

1.4.4 Quaternary ammonium glycol chitosan

N-palmitoyl-*N*-monomethyl-*N*,*N*-dimethyl-*N*,*N*,*N*-trimethyl-6-*O*-glycolchitosan (GCPQ) is a polymer synthesized from glycol chitosan by the introduction of hydrophilic (positively charged quaternary ammonium) and hydrophobic (palmitoyl) moieties. Its amphiphilic nature means that GCPQ spontaneously forms micellar nanoparticles in aqueous solution, in which drug molecules can be encapsulated (Uchegbu et al., 2001a). Preclinical pharmacokinetic studies have demonstrated that the oral delivery of hydrophilic and hydrophobic drugs, as well as small peptides, can be enhanced by formulating with GCPQ (Lalatsa et al., 2012b, Siew et al., 2012, Serrano et al., 2015b). Furthermore, encapsulation within GCPQ Nano micelles has been shown to result in a pharmacodynamics effect of the centrally-acting analgesic peptide leucine (5)-encephalin after oral administration (Lalatsa et al., 2012c).

In common with several other chitosan-based nanoparticles, it is thought that GCPQ may act by protecting the drug from enzymatic degradation (Guggi and Bernkop-Schnürch, 2003, Zhang et al., 2015) and by mucoadhesion (Yin et al., 2009, Bernkop-Schnürch and Dünnhaupt, 2012). However, in contrast to other chitosan-based nanoparticles (Sonaje et al., 2012, Rosenthal et al., 2012, Kotzé et al., 1999), the available evidence suggests that the mechanism by which GCPQ augments oral bioavailability does not involve increased paracellular transport due to the opening of tight junctions between endothelial cells in the gut (Lalatsa et al., 2012a, Siew et al., 2012). In vitro transport experiments in the Caco-2 cell line found that GCPQ does not affect tight junction integrity, as measured by trans epithelial electrical resistance (TEER) and the transport of Lucifer Yellow, a marker of paracellular

transport (Siew et al., 2012). Moreover, studies involving the cutting-edge and label-free coherent anti-Stokes Raman scattering (CARS) microscopy approach, in combination with analysis of the pharmacokinetics of radiolabelled GCPQ, suggest that that GCPQ nanoparticles may be transcytosed by enterocytes in the GIT following oral administration, resulting in an oral bioavailability of ~24% (Lalatsa et al., 2012a, Lalatsa et al., 2012b).

It is thought to act by increasing the dissolution rate of hydrophobic drugs, adhering to and penetrating the mucus layer, thus enhancing the contact of the drug molecule with the absorptive cells of the intestine, and facilitating the transcytosis of the hydrophobic drugs (Siew et al., 2011). GCPQ was recently reported to increase the oral bioavailability of amphotericin B to 24.7% and increase its translocation by several folds to tissues in organs like the brain, lungs and liver, compared to other oral Amphotericin lipid based oral formulations (Serrano et al., 2015a). A 3D colorectal cancer model showed GCPQ to be more promising delivery system than a cationic liposomal system for delivery of AZD6244- a MEK inhibitor for potential treatment of cancer (López-Dávila et al., 2016). By increasing the oral bioavailability of a wide range of drugs and enhancing passage through epithelial barriers including the blood brain barrier (BBB), GCPQ lends itself to great prospects for use in drug delivery and is therefore an interesting molecule to study.

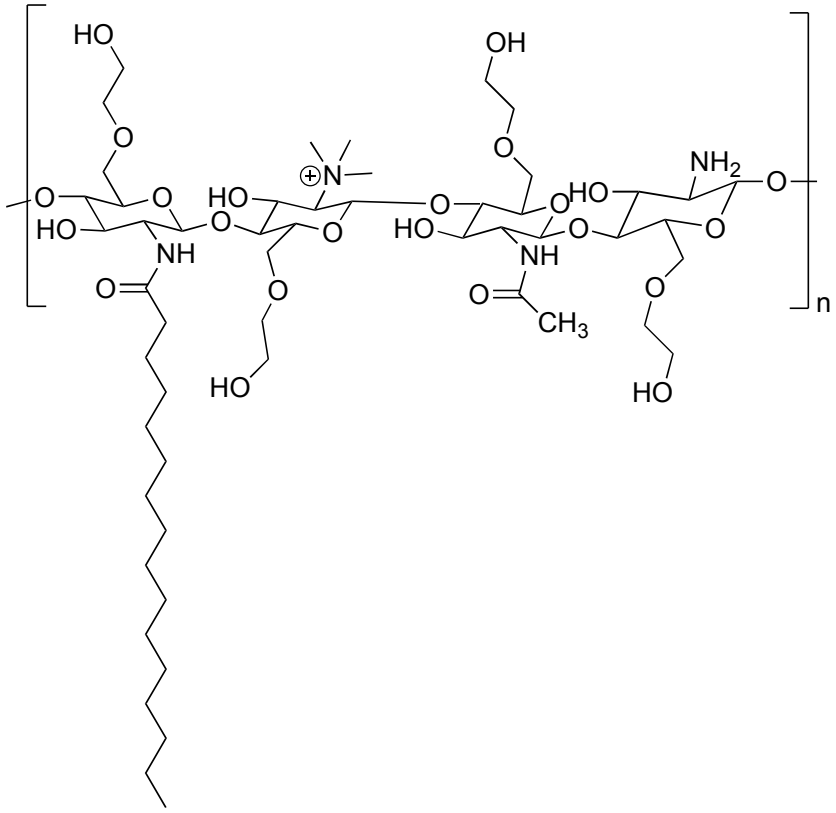

Figure 1-6: *N*-palmitoyl-*N*-monomethyl-*N*,*N*-dimethyl-*N*,*N*,*N*-trimethyl-6-*O*-glycolchitosan (GCPQ)

GCPQ has been reported to enhance the oral bioavailability of hydrophilic and hydrophobic drugs (Siew et al., 2011) and enhance the oral and intravenous delivery of peptides to the brain (Lalatsa et al., 2012d, Chooi et al., 2013).

1.5 Justification and Hypothesis

The physico-chemical properties of polymers play a vital role in their mechanism of absorption enhancement and their potential use for drug delivery. Properties such as the molecular weight, size, charge and pKa are critical to the mechanism of action of these polymers as well as their fate post-absorption.

GCPQ has been reported to enhance oral bioavailability of hydrophobic substances primarily through transcytosis. It is also reported to enhance the transport of hydrophilic proteins and peptides, presumably through the same mechanism. No significant involvement of the paracellular route was reported to be observed (Siew et al., 2011). The paracellular route of transport is however known to regulate the transport of hydrophilic substances and several reports have suggested that the degree of quaternisation of trimethyl chitosan, a derivative of chitosan, is important to the extent of paracellular transport enhancement (Thanou et al., 2000a, Kotzé et al., 1999). Also, the enhancement of paracellular transport by chitosan and its derivatives is suggested to be related to its positive charge and ability to interact with anionic glycoproteins (Kotzé et al., 1999, Dodane et al., 1999, Ma et al., 2005).

One of the hypotheses for this project will be that increasing the degree of quaternisation will increase the charge density of GCPQ, thus making it more hydrophilic and potentially increasing its ability to enhance paracellular transport. To test this, the effect of varying the proportion of quaternary ammonium groups on the mechanism of transport enhancement will be determined using tissue monolayer models and confocal microscopy. The effect of the degree of palmitoylation on hydrophilicity and potentially transport mechanisms will

also be determined using the same models. The molecular basis for the transport pathways (transcytosis and paracellular transport) will be examined based on the literature to establish the relationship between the functionalization of GCPQ and the pathway of transport enhancement. We will also test the relevance of this hypothesis on in vivo rodent models by examining the effect of structural modification of GCPQ on oral bioavailability of encapsulated drugs.

The stability of polymer formulations on the shelf and in physiological environments is critical to their utility. The size and charge of particles influence their stability in a liquid milieu as well as their mechanism of cellular uptake and passage across biological barriers (Sogias et al., 2008, Norris and Sinko, 1997). The stability of colloidal systems have also been explained in terms of forces influencing aggregation or disaggregation: Van Der Waal's force, Electrostatic forces, Hydration forces and hydrophobic interaction (Trefalt and Borkovec, 2014, Hwang et al., 2012) and the Derjaguin, Verwey, Landau and Overbeek (DLVO) theory of colloidal stability (Behrens et al., 2000, Instruments, 2011). GCPQ has been reported to form micelles 20-40nm in size which assemble into clusters of approximately 300nm in diameter and forms 200nm nanoparticles in dispersion (Chooi et al., 2014b, Siew et al., 2011). It is therefore hypothesized that the aggregation kinetics of GCPQ will be influenced by its physico-chemical properties which will potentially influence its biological effects. This hypothesis will be tested by determining the critical micelle concentration and thermodynamics of aggregation of GCPQ polymers containing varying proportions of DP and DQ, explaining the stability of the varied GCPQ polymers in different environments by the DLVO theory and determining if there is a relationship with the

observations on biological effects. The effect of structural modifications on drug encapsulation will also be examined to determine if the thermodynamics of aggregation and stability parameters influence the ability of the polymer to encapsulate different classes of drugs.

In summary, this project is aimed at understanding the relationship between the chemical structure and composition of GCPQ, its physico-chemical and biological properties, and the polymer structure-activity relationship (SAR) / molecular mechanisms of action. Polymer SAR may be used to tailor polymer properties to achieve enhanced oral delivery of for selected classes of drugs.

Chapter 2. Polymer Synthesis and Characterisation

2.0 Introduction:

This chapter outlines the methods used in the synthesis and characterisation of GCPQ, Quaternary ammonium decanoyl glycol chitosan (GCDQ) and a Texas-Red conjugate of GCPQ. Techniques used in characterisation will be discussed and include proton nuclear magnetic resonance (NMR), Gel permeation chromatography and multi angle laser light scattering (GPC-MALLS) and dynamic light scattering (DLS).

2.1 GCPQ Synthesis

2.1.1 Materials

Most chemicals and reagents used were purchased from Fischer Scientifics UK Ltd and Sigma Aldrich Chemical Company unless otherwise stated:

Reagents: Glycol Chitosan (WAKO), Sodium hydroxide, Palmitic acid N-hydroxysuccinimide ester, Sodium bicarbonate, Sodium iodide, Methyl iodide, N-methyl-2-pyrrolidone, Anhydrous Sodium acetate, Sodium Chloride, Glacial acetic acid, 1% w/v uranyl acetate aqueous solution, hydrochloric acid, triethyl amine,

Materials: Amberlite IRA-96 Resin PES Filters 0.22 μm, PTFE Filters 0.45 μm, Visking seamless cellulose dialysis tubing (3.5 kDa, 7 kDa, 12-14 kDa) (Medicell International Ltd., London, UK);

Solvents: Deionized water, Milli-pore double deionized water (<18Ω), Methanol-D4, Deuterated water, Methanol HPLC gradient, Absolute Ethanol, Diethyl Ether, Acetone, deuterium chloride, acetic acid-d6;

Equipment: Sonicator, Qsonica, LLC, GPC-MALLS equipped with: Dawn Heleos II MALLS detector (120mW solid-state laser operating at λ = 658 nm), Optilab rEX interferometric refractometer (flow cell: 7.4 uL, λ = 658 nm), quasielastic light scattering (QELS) detectors (Wyatt Technology Corporation, Santa Barbara, CA, USA), and Agilent 1200 auto sampler (Agilent Technologies, UK). Zetasizer Nano S90, (Malvern, UK) Transmission Electron Microscopy (TEM) (Philips CM 120), Biotwin NMR, (Bruker Avance, UK) 400 MHz NMR spectrometer, water bath, magnetic stirrer, magnetic stirrer bar, hot plate, oil bath.

2.1.2 Method

GCPQ synthesis and characterization were carried out according to protocols set up in the lab and previously reported (Uchegbu et al., 2001b, Chooi et al., 2014b, Siew et al., 2011, Lalatsa et al., 2012a). This typically involves an acid degradation step, following by a palmitoylation step and a final quaternisation reaction step as shown in Figure 2.1. These steps are outlined in this section:

Acid Degradation of Glycol Chitosan (GC)

GC [Molecular weight (MW) ~ 120 kDa, 20 g] was suspended in HCl (4 M, 760 mL) in a borosilicate glass vessel and allowed to dissolve under magnetic stirring for 20 min at room

temperature. This GC solution was then placed in a water bath at 50 °C and degraded for 8 hours (to obtain molecular weights of about 15 kDa) or 24 hours (to obtain molecular weights of about 6 -8 kDa) with continuous stirring. At the end of the reaction the degraded GC (dGC) was dialysed exhaustively against water using a dialysis membrane [molecular weight cut off (MWCO) = 3.5 kDa] and freeze dried to obtain a white fibrous solid. Yield = 35 – 80 %. The molecular weight of the GC was determined by gel permeation chromatography with multi-angle laser light scattering (GPC-MALLS) (Chooi et al., 2014c).

Palmitoylation of Degraded Glycol Chitosan

Dimethyl sulphoxide (DMSO, 220 mL) and triethylamine (0.06 moles, 8.4 mL) were mixed in a borosilicate glass vessel prior to the portion wise adding of the dGC HCl salt obtained from above [0.03 mole, 6.18 g (MW of GC sugar unit HCl salt = 242.68)] under vigorous magnetic stirring. Palmitic acid *N*-hydroxysuccinimide (PNS) was subsequently added to the solution of GC according to the target degree of palmitoylation: 2.23 g was added to obtain a level of palmitoylation of 20 %, 1.115 g was added to obtain a level of palmitoylation of 10 %. The reaction was left to proceed under magnetic stirring, protected from light for at least 15 hours at room temperature. Afterwards, the polymer was precipitated by slowly adding the DMSO solution into a mixture of acetone, ether (1: 2, 6 L) and the product, palmitoylated GC (PGC) left to precipitate overnight. After settling of the precipitate, most of the supernatant was removed, the solid washed three times with acetone (1 L), three times with diethyl ether (1 L), filtered using a glass sintered filter (porosity 3) and dried under vacuum. Yield of polymers synthesized is shown in Table 2.1. ^{1}H-NMR (CD_3OD, D_2O, CD_3COOD, 4:2:0.5) δ: 0.86 (3H, C**H**$_3$$CH_2$), 1.2-1.4 (24H, CH_3(C**H**$_2$)$_{12}$), 1.6

(2H, C**H₂**CH₂CO), 2.13 (3H, C**H₃**CO), 2.14 (2H, C**H₂**CO), 3.15 (1H, C**H** – C2 sugar monomer), 3.5 - 4.5 (9H, HOC**H₂**C**H₂** and H-3, H-4, H-5, H-6 CH –sugar monomer).

Quaternisation of Palmitoyl Glycol Chitosan

PGC (1 g) was dispersed in N-methyl-2-pyrollidone (NMP, 80 mL) in borosilicate glass vessel for 16 hours. Powdered sodium hydroxide (3.4 mM, 136 mg) was added to the PGC dispersion with continuous stirring at room temperature for 40 mins after which sodium iodide (1 mM, 155 mg) was added while saturating the vessel with gaseous nitrogen. Finally, methyl iodide (24 mM, 1.5 mL) was added to the pGC suspension and the reaction mixture left to react at 36 °C for 1.5 h – 8 h (depending on the level of quaternary ammonium groups required in the final product (1.5 hours for about 10% level of quaternisation, 3 hours for about 15 % quaternisation and 8hours for above 20% quaternisation) under a nitrogen atmosphere. Next, the product was precipitated with diethyl ether (6 X the volume of NMP) and left overnight. The diethyl ether was decanted, and the product washed twice more with diethyl ether (twice the original volume of NMP). Afterwards, the crude residue was solubilized in methanol (50 mL) and dialysed against 20 L of water (x5 changes every 2 h, 3.5 KDa MWCO, regenerated Cellulose). Finally, in order to obtain the chloride form of the polymer, GCPQ iodide solution was treated with ion exchange resin (IRA 410 Chloride), 6 g resin / 1 g polymer (starting material), filtered and freeze dried. ^{1}H-NMR (CD_3OD, DCl, 99.99:0.001) δ: 0.86 (3H, C**H₃**CH₂), 1.2-1.4 (24H, CH₃(C**H₂)₁₂**), 1.6 (2H, C**H₂**CH₂CO), 2.13 (3H, C**H₃**CO), 2.14 (2H, C**H₂**CO), 2.8 - 3.2 (9H, C**H₃**NH and (C**H₃)₂**N, 3.15 (1H, CH – C2 sugar monomer), 3.4 (9H, (C**H₃)₃**N^+), 3.5 - 4.5 (9H, HOC**H₂**C**H₂** and H-3, H-4, H-5, H-6 CH –sugar monomer).

The level of palmitoylation was calculated by comparing the ratio of palmitoyl methyl protons (δ = 0.86 ppm) to sugar protons (δ = 3.5 – 4.5 ppm) and the level of quaternisation by comparing the ratio of quaternary ammonium (δ = 3.4 ppm) to sugar protons.

$$\%\ \text{palmitoylation} = \frac{\frac{\text{integration value of } N\text{–palmitoyl methyl protons}}{3}}{\frac{\text{integration value of sugar protons}}{9}} \text{ x } 100 \qquad 2.1$$

$$\%\ \text{quaternisation} = \frac{\frac{\text{integration valueof trimethyl protons}}{9}}{\frac{\text{integration value of sugar protons}}{9}} \text{ x } 100 \qquad 2.2$$

The ratio of quaternary ammonium to palmitoyl groups (QPR) was calculated as follows:

$$QPR = \frac{Mole\ \%\ quaternisation}{Mole\ \%\ palmitoylation} \qquad 2.3$$

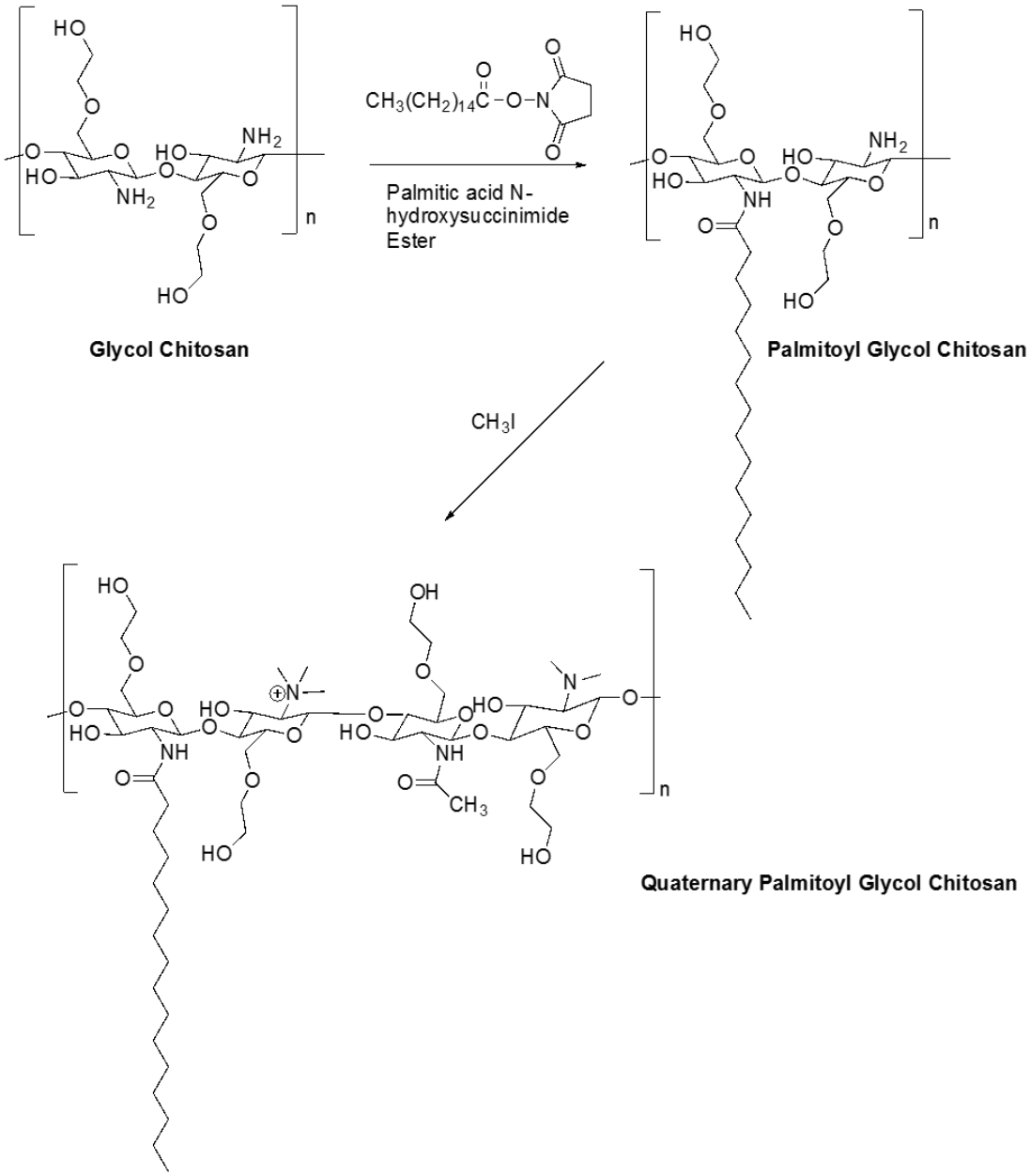

Figure 2-1: Scheme showing the steps in synthesis of GCPQ

2.2 Labelling of GCPQ with Texas Red-X

2.2.1 Materials and Method

Reagents: GCPQ polymers previously synthesized, Triethylamine, Texas Red-X succinimidyl ester, dimethylsulphoxide (DMSO), ethanol, diethyl ether, methanol, hydrochloric acid (HCl).

Method: To label the polymer, GCPQ was reacted with Texas Red-X succinimidyl ester (Life Technologies, UK) in a molar ratio of 4:1 as described briefly:

120 mg of GCPQ (mw: 10KD) was dissolved in 3 mL of DMSO in a 10 mL amber coloured round bottom flask and 100µL of Triethylamine added to the solution. 500 µL of a 5 mg/mL solution of Texas Red –X (mw: 0.816KD) in DMSO was added drop wise to the reaction mixture with continuous stirring and the reaction left to continue for 16 hours. The mixture was then transferred to a 100 mL conical flask, clamped at about 45 degrees for ease of aspiration of a supernatant and protected from light. 200 µL of a 1:4 mixture of ethanol: diethyl ether mixture was then added to the mixture and left to stand until complete precipitation of GCPQ-Texas Red, still protected from light. The supernatant was aspirated and the precipitate washed three times again with the same ethanol: diethyl ether mixture. The precipitate was then collected by filtration through a 10 µm glass filter under vacuum. The filtrate was then dissolved in 45 mL of a 60% methanol in water solution acidified with 1.35 mL of 4M HCl and purified by ultrafiltration using 3 kDa 15 mL Amicon filters spun at 9000 g for 30 minutes twice, with re-dissolution of the retentate. The filtration was

repeated until the filtrate became near colourless. The retentate was then collected, diluted with water and dialysed first against 0.01 M sodium bicarbonate with three changes over 6hours and then against water with six changes over 24 hours. Following dialysis, the product was collected, freeze dried and recovery determined as 45% by weight.

2.3 Synthesis of Quaternary Ammonium Decanoyl Glycol Chitosan (GCDQ)

2.3.1 Materials

Decanoic acid (DA), *N*-hydroxysuccinimide (NHS), *N*-(3-dimethylaminopropyl)-*N*'-ethylcarbodiimide hydrochloride (EDC), dichloromethane (DCM), hydrochloric acid (HCl), Sodium bicarbonate, Glycol chitosan, magnesium sulphate,

2.3.2 Method

Acid Degradation of Glycol Chitosan

GC [Molecular weight (MW) ~ 120 kDa, 20 g] was suspended in HCl (4 M, 760 mL) in a borosilicate glass vessel and allowed to dissolve under magnetic stirring for 20 min at room temperature. This GC solution was then placed in a water bath at 50 °C and degraded for 24 hours (to obtain molecular weights of about 6 -8 kDa) with continuous stirring. At the end of the reaction the degraded GC was dialysed exhaustively against water using a dialysis membrane [molecular weight cut off (MWCO) = 3.5 kDa] and freeze dried to obtain a white fibrous solid. Yield = 35 – 80%. The molecular weight of the GC was determined by gel permeation chromatography with multi-angle laser light scattering (GPC-MALLS) (Chooi et al., 2014c).

Synthesis of Decanoic acid N-hydroxysuccinimide ester

500 mg of decanoic acid (Mw=176.26) was weighed into a 7 mL reaction vessel. 0.351 g of NHS (Mw=115.09) and 0.584 g of EDC (Mw=191.7) were also weighed and the reaction mixture was dissolved in 2.5 mL of Dichloromethane to give a molar ratio of 1:1.07 for Decanoic acid: NHS and decanoic acid:EDC. The reaction was allowed to proceed overnight (16 hours) with stirring and protected from light. The product, a hard transparent solid was dispersed in 3 mL of DCM by vortexing and subsequent stirring for 1hour after which it was washed with 2 mL of 0.05M HCl with shaking. The top, aqueous layer was removed using a glass Pasteur pipette and the residue washed again with saturated sodium bicarbonate solution (about 3 mL). The top aqueous layer was again removed and the precipitate was collected by filtration. The product was dried under vacuum and analysed by NMR. ^{1}H-NMR (CD_3OD, D_2O, CD_3COOD, 4: 2: 0.5) δ: 0.86 (3H, C**H**$_3$$CH_2$), 1.2 - 1.4 (12H, CH_3(C**H**$_2$)$_6$), 1.6 (2H, C**H**$_2$$CH_2CO$), 2.65 (2H, C**H**$_2$CO), 2.8 (4H, (C**H**$_2$CO)$_2$ *N*-succinimide group).

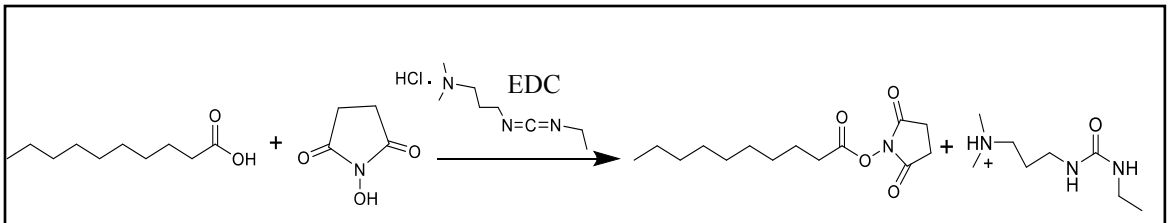

Decanoic acid N-hydroxysuccinimide Decanoic acid-*N*-hydroxysuccinimide Isourea

Figure 2-2: Structural representation of reaction for synthesis of Decanoic acid-*N*-hydroxysuccnimide ester

Synthesis of Decanoyl Glycol Chitosan (DGC)

Dimethyl sulphoxide (DMSO, 15 mL) and triethylamine (4.25 mM) were mixed in a borosilicate glass vessel prior to the portion wise adding of the GC HCl salt obtained previously [2.06 mM, 0.5g (MW of GC sugar unit HCl salt = 242.68)] under vigorous magnetic stirring. Decanoic acid *N*-hydroxysuccinimide (DNS) was subsequently added to the solution of GC (0.77 mM, 0.206 g) was added to obtain a level of decanoylation of 34%, 0.515g was added to obtain a level of decanoylation of 10 %. The reaction was left to proceed under magnetic stirring, protected from light for at least 15 hours at room temperature. Afterwards, the polymer was precipitated by slowly adding the DMSO solution into a mixture of acetone, ether (1: 2, 300 mL) and the product (DGC) left to precipitate overnight. After settling of the precipitate, most of the supernatant was removed, the solid washed three times with acetone (100 mL), three times with diethyl ether (100 mL), filtered using a glass sintered filter (porosity 3) and dried under vacuum. ^{1}H-NMR (CD_3OD, D_2O, CD_3COOD, 4: 2: 0.5) δ: 0.86 (3H, C**H**$_3$$CH_2$), 1.2 - 1.4 (12H, CH_3(C**H**$_2$)$_6$), 1.6 (2H, C**H**$_2$$CH_2CO$), 2.13 (3H, C**H**$_3$CO), 2.14 (2H, C**H**$_2$CO), 3.15 (1H, C**H** – C2 sugar monomer), 3.5 - 4.5 (9H, HOC**H**$_2$C**H**$_2$ and H-3, H-4, H-5, H-6 CH –sugar monomer).

Synthesis of Quaternised Decanoyl Glycol Chitosan

DGC (0.1g) was dispersed in *N*-methyl-2-pyrollidone (NMP, 80 mL) in borosilicate glass vessel for 16 hours. Powdered sodium hydroxide (0.34 mM, 0.014 g) was added to the PGC dispersion with continuous stirring at room temperature for 40 mins after which sodium iodide (0.1 mM, 0.016 g) was added while saturating the vessel with gaseous nitrogen. Finally, methyl iodide (2.4 mM, 0.15 mL) was added to the DGC suspension and the reaction mixture left to react at 36 °C for 1.5 h – 8 h (depending on the level of quaternary ammonium groups required in the final product (1.5 hours for about 10% level of quaternisation, 3hours for about 15% quaternisation and 8hours for above 20% quaternisation) under a nitrogen atmosphere. Next, the product was precipitated with diethyl ether (6 X the volume of NMP) and left overnight. The diethyl ether was decanted, and the product washed twice more with diethyl ether (twice the original volume of NMP). Afterwards, the crude residue was solubilized in methanol (10 mL) and dialysed against 2 L of water (x5 changes every 2 h, 3.5 kDa MWCO, regenerated Cellulose). Finally, in order to obtain the chloride form of the polymer, GCDQ iodide solution was treated with ion exchange resin (IRA 410 Chloride), 6 g resin / 1 g polymer (starting material), filtered and freeze dried. ^{1}H-NMR (CD_3OD, DCl, 99.99:0.001) δ: 0.86 (3H, C**H**$_3$$CH_2$), 1.2 - 1.4 (12H, CH_3(**C**$\mathbf{H_2}$)$_6$), 1.6 (2H, C**H**$_2$$CH_2CO$), 2.13 (3H, C**H**$_3$CO), 2.14 (2H, C**H**$_2$CO), 2.8 - 3.2 (9H, C**H**$_3$NH and (C**H**$_3$)$_2$N, 3.15 (1H, C**H** – C2 sugar monomer), 3.4 (9H, (C**H**$_3$)$_3$$N^+$), 3.5 - 4.5 (9H, HOC**H**$_2$C**H**$_2$ and H-3, H-4, H-5, H-6 CH –sugar monomer).

The level of decanoylation was calculated by comparing the ratio of decanoyl methyl protons (δ = 0.86 ppm) to sugar protons (δ = 3.5 – 4.5 ppm) and the level of quaternisation by comparing the ratio of quaternary ammonium (δ = 3.4 ppm) to sugar protons as was done for GCPQ.

2.4 Polymer Characterisation Techniques

2.4.1 ^{1}H NMR

Proton Nuclear Magnetic Resonance is an important technique for characterization of organic compounds. It is a technique that helps to identify a compound's unique structure by identifying the carbon-hydrogen framework of the compound.

The principle of NMR can be described thus: the nuclei in a sample can absorb energy if the sample is exposed to radiofrequency radiation at the right frequency in a magnetic field. The frequency of the radiation required for energy absorption depends on the type of Nucleus and the chemical environment of the nucleus (James, 1998). The presence of the external magnetic field compels the nuclei to align either with (parallel) or against (anti-parallel) to the magnetic field, creating high and low energy states. The difference in energy between the two states depends on the strength of the magnetic field. The nuclei in the low energy state is able to flip to the higher energy state if the absorbed energy is equal to the difference between the energy spin states. This results in a signal in the form of a peak on the NMR spectrum. In the proton NMR, it is the electron orbiting the nuclei that determines the peak's position (chemical shift, δ) on the spectrum. The position of the electron in relation to the

nuclei is influenced by the chemical environment -shielding or de-shielding effects caused by adjacent electron withdrawing or donating groups- and this gives each nuclei its own characteristic absorption peak. The NMR is thus able to utilize the information on the peak positioning, coupling and integration as well as 2D correlation to determine the structure of a given molecule.

2.4.1 Gel Permeation Chromatography and Multi-Angle Laser Light Scattering (GPC-MALLS)

The molecular weight of GCPQ was determined using the GPC MALLS. This is a technique used to characterize polymer molecular weight, size distribution and branching (Podzimek, 1994).

GPC is a size exclusion chromatography (SEC) technique which involves the use of a column filled with beads that contain pores of different sizes which make up the stationary phase and the solvent for the samples, which is the mobile phase. The sample dissolved in the mobile phase is then introduced into the column and allowed to run through the column continually at a given rate. During the separation, small sized molecules get trapped in the pore and therefore move through the column slowly. The larger sized molecules move faster through the column because they do not fit into the pores of the gel. Therefore, larger molecules elute first and smaller molecules elute last (Johnson and Porter, 1970)

The molecular weight of the molecules is then determined using a calibration standard to establish the relationship between the elution volume and the molecular weight. However,

this fractionation based on hydrodynamic volume is only sufficient for narrowly distributed polymers. Branched polymers are reported to have smaller sizes than linear polymers of the same molecular weight (Zimm and Stockmayer, 1949). For branched polymers therefore, a simultaneous measurement of light scattering intensity and concentration is required for determination of the molecular weight (Grcev et al., 2004). The multi-angle laser light scattering (MALLS) detector is therefore attached to the GPC for this measurement.

Because the light scattered signal is proportional to the product of the concentration of the solution, c, and the weight average molecular weight, Mw, a high concentration is required for detectable light scattering (LS) signals for polymers with very low Mw. In addition, an accurate dn/dc value (the refractive index increment of the polymer) is required for the interpretation of the light scattering data (Grcev et al., 2004). The dn/dc is determined by injecting a range of dilutions of the polymer solution into a refractive index detector. The higher the dn/dc, the greater the increase in refractive index of the polymer solution at a given increase in concentration.

The molecular weights of the GC and GCPQ polymers were thus determined using a Wyatt gel permeation chromatography−multi-angle laser light scattering instrument (GPC-MALLS) equipped with Dawn Heleos II MALLS detector (120 mW solid-state laser operating at λ = 658 nm), Optilab rEX interferometric refractometer (flow cell: 7.4 µL, λ= 658 nm) and quasielastic light scattering (QELS) detectors (Wyatt Technology Corporation, Santa Barbara, CA, USA). The mobile phase used was an acetate buffer (0.3 M anhydrous sodium acetate, 0.2 M glacial acetic acid, pH = 4.5) for GC and a mixture of acetate buffer and methanol (35: 65 v/v) for GCPQ. Filtered samples (0.2 µm, PES, Millipore Millex-HA,

100 μL) were injected using an Agilent 1200 series auto sampler (Agilent Instruments, Stockport, U.K.) on to a POLYSEPGFC-P guard column (35 × 7.8 mm, Phenomenex, Macclesfield, U.K.) attached to a POLYSEP-GFC-P 4000 column (300 × 7.8 mm, exclusion limit for PEG = 200 kDa, Phenomenex) at a loading concentration of 5 mg mL−1. Measurements in triplicate were performed at room temperature with a mobile phase flow rate of 0.9 mL min −1 (Agilent 1200 series isocratic pump attached to an Agilent 1200 series degasser). The data were processed using ASTRA for Windows version 5.3.4.14 software (Wyatt Technology Corporation) (Lalatsa et al., 2012a)

2.4.3 Size Measurement Using Dynamic Light Scattering (DLS)

Dynamic Light Scattering (DLS), also referred to as Photon Correlation Spectroscopy (PCS) and Quasi-Elastic Light Scattering (QELS), is a technique that is used to measure the size of particles usually in the nano-scale region. It is based on the tendency for particles in suspension undergoing Brownian motion to scatter light. The constant motion of these particles causes fluctuations in the light scattering intensity of the solution which allows for the measurement of particle size (Hoo et al., 2008)

Given that the size measurement by DLS is based on how the particles move in a solvent, the diameter measured is referred to as the hydrodynamic diameter and is given by the Stokes-Einstein equation:

$$d(H) = kT/3\pi\eta D \qquad 2.5$$

where d(H) is the hydrodynamic diameter, D is the translational diffusion coefficient, k is the Boltzmann's constant, T is the absolute temperature, η is the viscosity.

The hydrodynamic diameter thus measured is the diameter of a sphere that has the same translational diffusion coefficient as the particle in suspension and it depends on factors such as surface structure, ions in the medium and speed of diffusion.

The z-average is the cumulant average particle diameter and the Polydispersity Index (PDI) corresponds to the square of the normalized standard deviation of the underlying Gaussian size distribution (Nobbmann et al., 2007).

Method

Dynamic light scattering measurements were made on the fixed scattering angle Zetasizer Nano-S system (Malvern Instruments Ltd., Malvern, UK). Samples were measured in a 200 µL quartz cuvette at 25.0 ºC and the light scattering was detected at 173 º and collected in automatic mode, typically requiring a measurement duration of 150 seconds. The resulting data were analysed using the "DTS (Version 4.2)" software (Malvern Instruments Ltd., Malvern, UK).

2.4.4 **Zeta Potential Measurement**

Zeta potential (ζ) analysis is a method for determining the surface charge of nanoparticles in solution. It is a measure of the electrical potential at the boundary (slipping plane) of a double layer formed around the particle. The double layer consists of closely attached oppositely charged layer of ions around the surface of the nanoparticle (stern layer) and a more diffuse layer of loosely associated ions (Clogston, 2009, Kirby and Hasselbrink, 2004).

The measurement of zeta potential is important for predicting the stability of colloidal systems, with a measure of +30 or -30mV thought to be the dividing line between stable and unstable systems(Instruments, 2011). This stability can be explained by the contribution of the electrostatic repulsion force in the Derjaguin, Verwey, Landau and Overbeek (DLVO) theory of colloidal stability (Behrens et al., 2000, Instruments, 2011). The zeta potential is affected by factors such as the pH, ionic strength and concentration of a formulation.

To determine the zeta potential, an electric field is applied across the sample, causing electrophoretic mobility of charged particles. The zeta potential is related to the electrophoretic mobility by the Henle equation (Clogston, 2009, Instruments, 2011):

$$U_E = 2\,\varepsilon\, z\, f(\kappa a)/\, 3\eta \qquad 2.6$$

where U_E = electrophoretic mobility, z = zeta potential, ε = dielectric constant, η = viscosity and f(κa) = Henry's function and κa = a measure of the ratio of the particle radius to the Debye length.

The zeta potential of GCPQ was thus measured using the Zeta sizer Nano ZS (Malvern Instruments). 1mL Samples were loaded into folded capillary cells (zeta cells, polycarbonate

cell with gold-plated electrodes; Malvern Instruments, DTS1060C) and run at 25degrees, 40V.

2.5 Results and Discussion

Table 2-1 shows the yield and characteristics of degraded glycol chitosan and palmitoylated glycol chitosan synthesized and used for the synthesis of GCPQ polymers. The molecular weight of the polymers was determined using GPC-MALLS

Table 2-1: Glycol chitosan and palmitoyl glycol chitosan characterisation

Polymer	Yield (%)	Mw (kDa)	Mn (kDa)	PDI (Mw/Mn)	Mole% Palmitoyl
dGCFOB03	56	6.7	6.6	1.015	Not applicable
dGC.HCl.JF06	78	11.3	11.1	1.018	Not applicable
dGC.HCl.JF05	69	10.6	10.4	1.019	Not applicable
GC15	67	13.3	12.6	1.056	Not applicable
GC16	38	14.2	9.2	1.543	Not applicable
dGC.HCl.JF03	48	13.2	12.9	1.023	Not applicable
GCAI23	60	12.44	12.36	1.006	Not applicable
GCAI24	63	10.96	10.71	1.023	Not applicable
pGCFOB04	90	Not determined	Not determined	Not determined	19
pGC.HCl.AI06b	80	Not determined	Not determined	Not determined	25
pGC.HCl.AI05b	80	Not determined	Not determined	Not determined	23
pGC.HCL.AI03	82	Not determined	Not determined	Not determined	29
pGCAI23	89	Not determined	Not determined	Not determined	Not determined
pGCAI24	89	Not determined	Not determined	Not determined	Not determined
pGCAI06c	76	Not determined	Not determined	Not determined	27
pGC16	Not determined	Not determined	Not determined	Not determined	Not determined
pGCUO2	88	Not determined	Not determined	Not determined	46
pGCUO3	85	Not determined	Not determined	Not determined	10
pGC15	Not determined	Not determined	Not determined	Not determined	Not determined

Table 2-1 shows the % yield of different degraded GC (dGC) and palmitoylated GC (pGC) synthesized and their molecular weight parameters. The yield was calculated by comparing

the final mass of the products with the mass of the starting materials as shown in the equations below:

$$\%Yield\ of\ dGC = 100\ X\ \frac{mass\ of\ dried\ dGC\ product}{mass\ undegraded\ GC\ used}$$

$$\%\ Yield\ of\ pGC = 100\ X\ \frac{mass\ of\ dried\ pGC\ product}{mass\ of\ dGC\ used}$$

$$PDI = \frac{Mw}{Mn}$$

The reaction yield for the degradation of GC ranges from 38% to 78% while the reaction yield for the synthesis of pGC ranges from 72% to 90%. The molecular weights of the degraded GC were determined using the GPC-MALLS (a chromatogram is shown in Figure 2-9). The polydispersity (PDI) of the polymers, calculated as the ratio of the weight average molecular weight (MW) to the number average molecular weight (Mn) is less than 1.1 for all dGC synthesized except for dGC16 which is about 1.5. This shows a narrow molecular weight distribution of each batch of dGC after degradation in HCl.

Table 2-2: GCPQ Polymer characterisation. The nomenclature of GCPQ polymers is given as: GCxPnQm where 'x' is the molecular weight of the polymers, 'n' is the mole % of palmitoyl group substitution and 'm' is the mole % of quaternary ammonium group substitution.

Polymer	Yield (%)	Mw (kDa)	Mn (kDa)	Mole % Palmitoyl group	Mole % Quaternary ammonium group
GC13P24Q9	35	12.6	12.7	24	9
GC14P24Q12	68	13.9	13.2	24	12
GC11P22Q9	77	10.5	10.4	22	9
GC12P24Q10	85	12.2	12.0	24	10
GC13P23Q7	Not determined	13.1	11.1	23	7
GC15P24Q9	92	14.9	14.2	24	9
GCxP23Q14	100	Not determined	Not determined	23	14
GC14P12Q9	Not determined	14.3	14	12	9
GC14P8Q10	Not determined	14.4	13.5	8	10
GC14P20Q9	Not determined	14.5	14.4	20	9
GC9P19Q12	55	8.7	8.6	19	12
GC12P19Q9	71	12.4	12.0	19	9
GC10P20Q22	74	9.9	8.5	20	22
GC9P9Q36	89	8.8	8.3	9	36
GC8P10Q14	74	8.4	8.0	10	14
GCxP37Q23	86	Not determined	Not determined	37	23

Table 2-2 shows the reaction yield for the synthesis of GCPQ polymers, the molecular weight parameters as well as the mole percentage (mole %) of palmitoyl and quaternary ammonium group substitutions. As for dGC, the molecular weights of GCPQ polymers were determined using GPC-MALLS (a chromatogram can be seen in figure 2-10). The reaction

yield was calculated by comparing the mass of the synthesized GCPQ polymers with the mass of the pGC used as shown in the equation below :

$$\%yield = 100\ X\ \frac{mass\ of\ dried\ GCPQ}{mass\ of\ pGC\ used}$$

The PDI, calculated as for dGC was less than 1.2 for all determined molecular weight of GCPQ polymers, suggesting a narrow weight distribution of each batch of GCPQ polymer synthesized.

The mole % of palmitoyl (DP) and quaternary ammonium (DQ) group substitutions were calculated using equations 2.1 and 2.2 respectively. GCPQ polymers were synthesized to have range of DP substitution from 8% to 37% and DQ substitution from 7% to 36%.

Table 2-3: Size and Zeta potential of GCPQ nanoparticles

Polymers	polymers	Z-ave (d.nm)	PDI	Zeta pot. (ζ)	QPR
LG16_0.25	GC14P20Q9	171.4±3.39	0.49±0.03	49.53±0.31	0.45
GCPQ05	GC12P19Q9	72.74±4.95	0.53±0.01	49.73±1.50	0.47
GCPQ04	GC10P19Q10	54.44±2.90	0.95±0.05	39.27±2.06	0.53
GCPQ10	GCxP37Q23	47.45±0.92	0.48±0.01	50.13±0.80	0.62
GCPQ03	GC9P19Q12	45.71±1.32	0.45±0.02	36.47±1.21	0.63
LG15_0.15	GC14P12Q9	88.82±1.94	0.58±0.03	33.97±2.29	0.75
GCPQ06	GC10P20Q22	50.40±2.48	0.38±0.03	49.43±1.67	1.10
LG16_0.1	GC14P8Q10	86.40±10.68	0.87±0.22	27.90±0.50	1.25
GCPQ08	GC8P10Q14	128.8±2.07	0.46±0.03	41.23±3.31	1.40
LG14_0.05	GC15P4Q11	225.6±1.01	0.68±0.02	26.63±2.29	2.75
GCPQ07	GC9P9Q36	224.5±11.86	0.53±0.07	39.40±0.44	4.00
GCPQ04-TR		9.18±1.16	0.53±0.05	36.90±0.96	

Table 2-3 shows the physicochemical properties of the synthesized GCPQ polymers. Polymers with very low DP have the largest z-average size above 200 nm with the exception of GC14P20Q9 which also has a large size. There is no direct correlation between the DQ% and the zeta potential neither is there a direct correlation between the QPR and the zeta potential as is shown in Figure 2-3B. A weak correlation is seen between the QPR and the size of GCPQ particles (Figure 2-3A) where an increase in QPR is correlated with an increase in size of the particles. The size distribution of some of the GCPQ polymers are shown in figure 2-12.

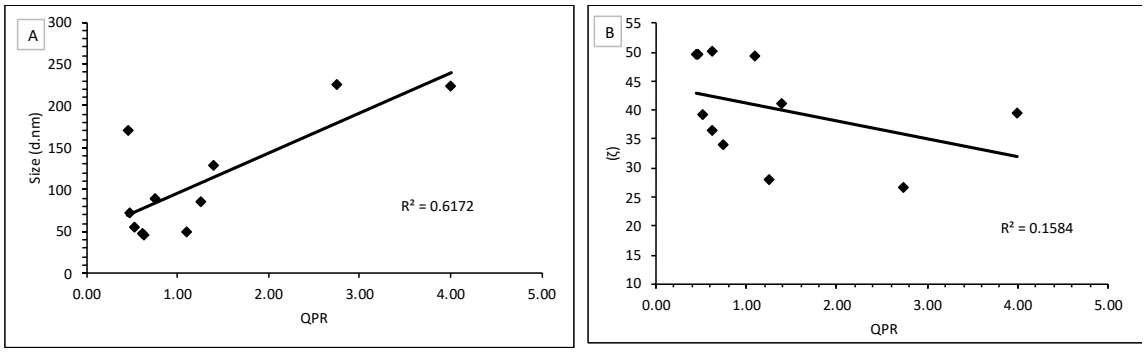

Figure 2-3: Graphical illustration of correlation between QPR and the size (A) as well as the zeta potential (B) of GCPQ polymers.

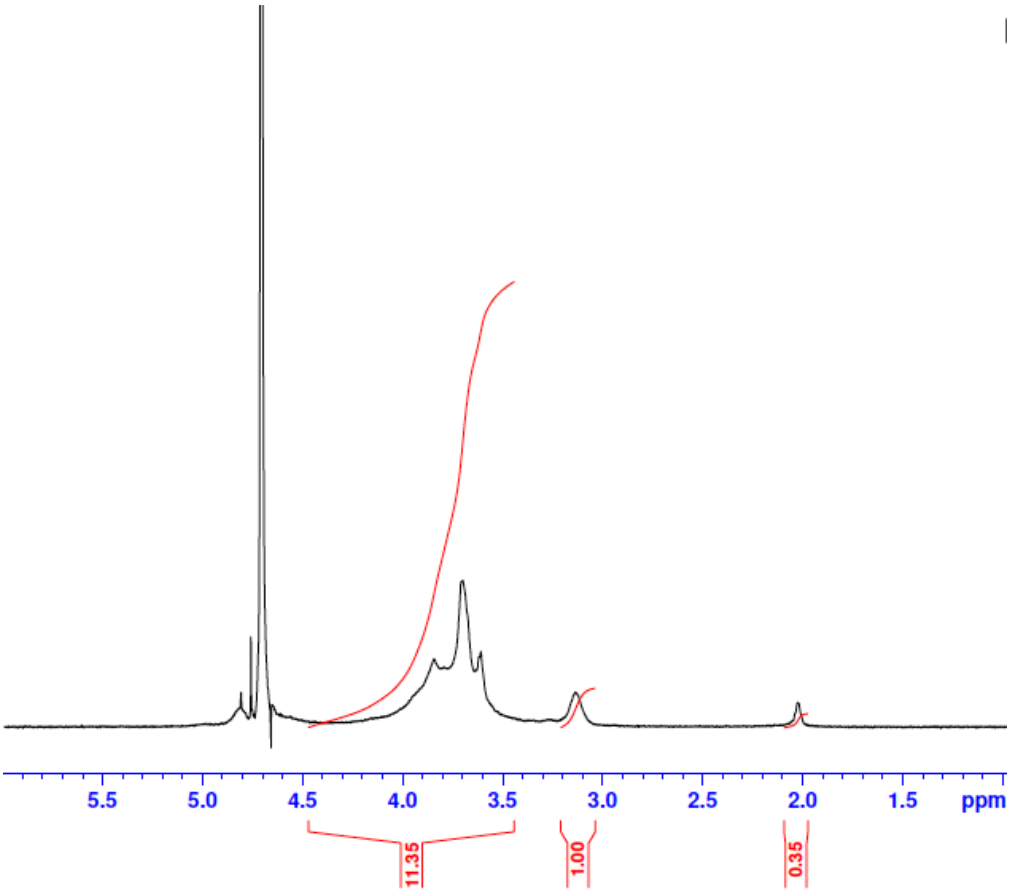

Figure 2-4: Proton NMR of glycol chitosan (dGC) degraded in 4 M HCl at 50 ^{o}C for 18 hours

^{1}H-NMR (D_2O) δ: 2.0 (3H, ***CH$_3$***-CONH-, acetyl GC), 2.14 (CH_2CO), 3.1 (1H, NH_2-***CH***-, GC), 3.15 (1H, C**H** – C2 sugar monomer), 3.4-4.3 (9H, HOC**H$_2$**C**H$_2$**-, -***CH***(OH)- and –***CH$_2$***-OH, GC sugar monomer), 4.75 (D_2O obscuring the GC anomeric proton),

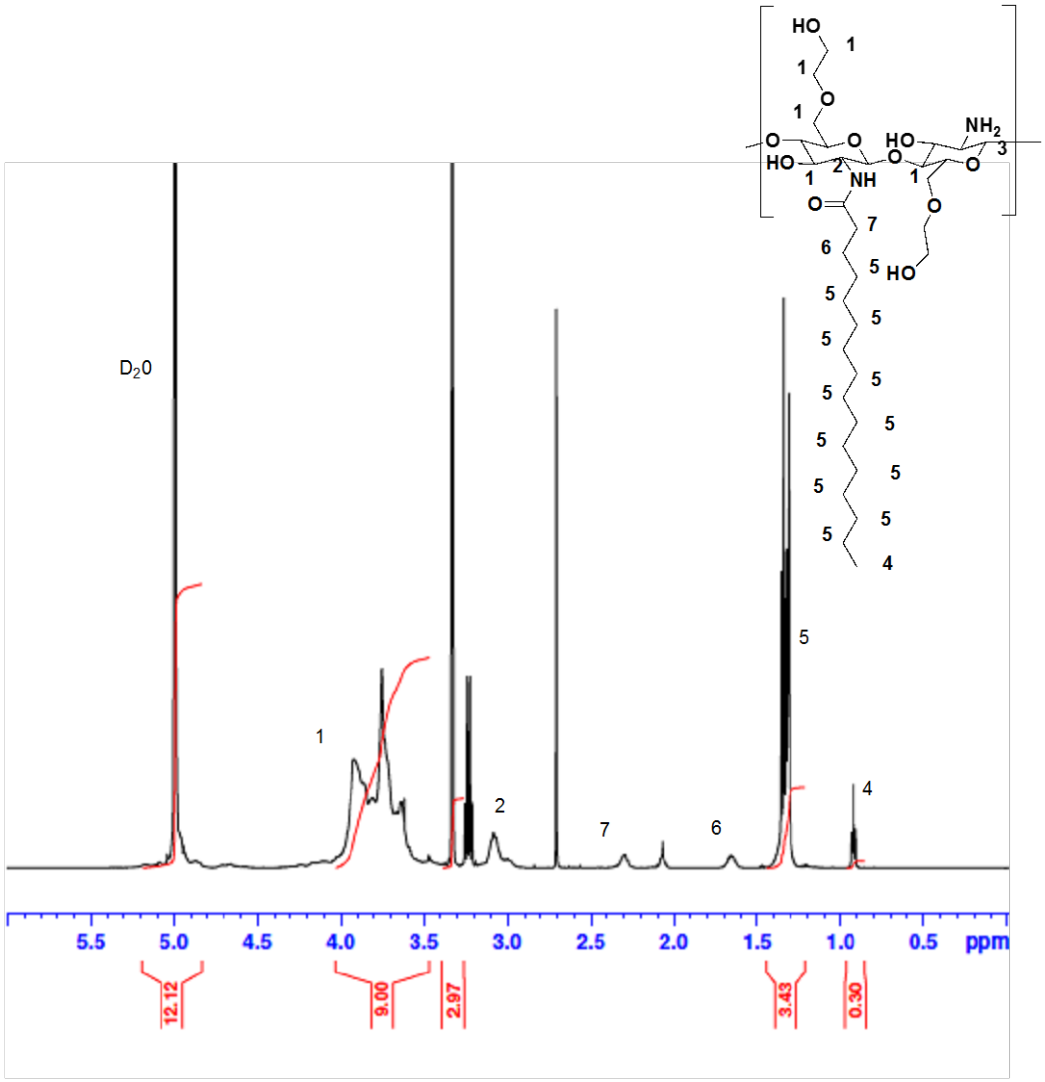

Figure 2-5: Proton NMR of palmitoylated glycol chitosan in CD_3OD:D_2O:CD_3COOD (8:4:1) showing 10% mole percent palmitoyl group substitution

^{1}H-NMR (CD_3OD, D_2O, CD_3COOD, 4:2:0.5) δ: 0.86 (3H, C**H**$_3$$CH_2$), 1.2-1.4 (24H, CH_3(C**H**$_2$)$_{12}$), 1.6 (2H, C**H**$_2$$CH_2CO$), 2.13 (3H, C**H**$_3$CO), 2.14 (2H, C**H**$_2$CO), 3.15 (1H, C**H** – C2 sugar monomer), 3.5 - 4.5 (9H, HOC**H**$_2$C**H**$_2$ and H-3, H-4, H-5, H-6 CH –sugar monomer).

The mole percentage (mole %) of palmitoyl group substitution was calculated using equation 2.1 and determined to be 25%.

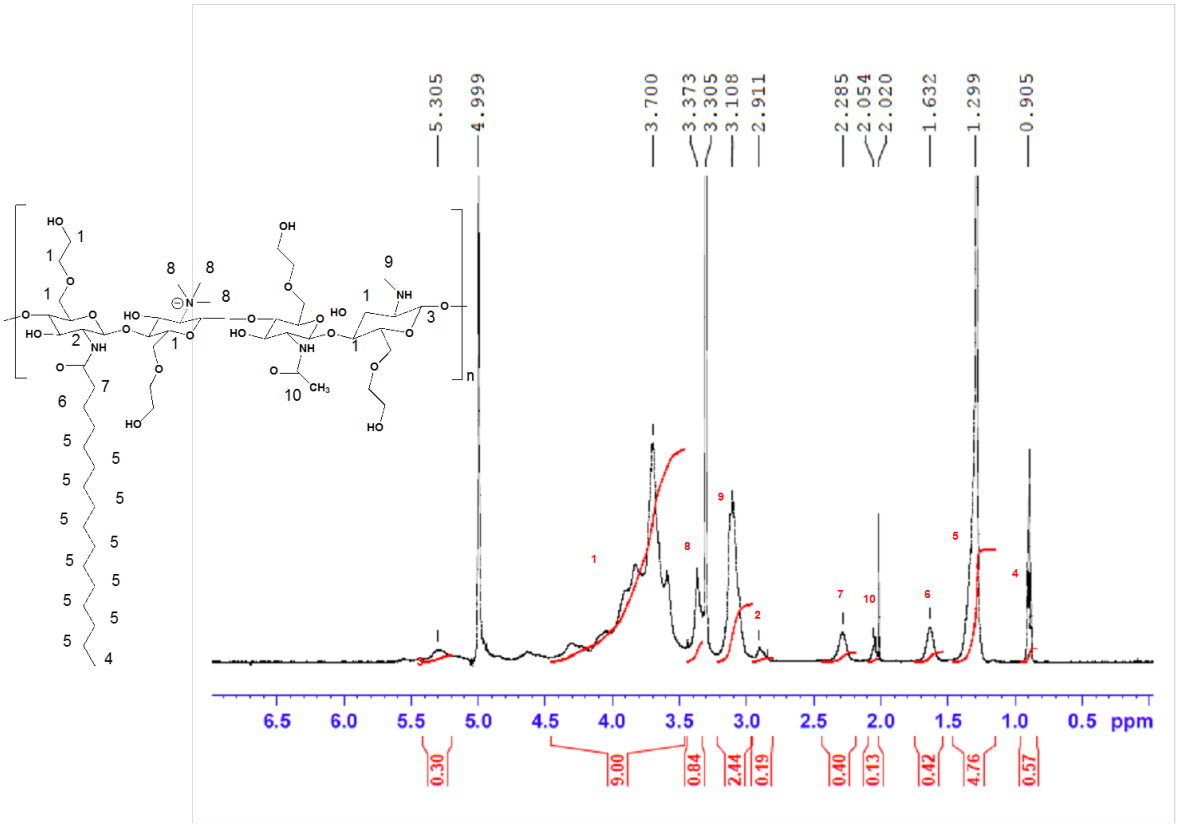

Figure 2-6: 1H NMR of GCPQ in MeOD with palmitoylation level of 19% and quaternisation level of 9.3%.

^{1}H-NMR (CD_3OD, DCl, 99.99:0.001) δ: 0.86 (3H, C**H₃**CH_2), 1.2-1.4 (24H, CH_3(C**H₂**)**₁₂**), 1.6 (2H, C**H₂**CH_2CO), 2.13 (3H, C**H₃**CO), 2.14 (2H, C**H₂**CO), 2.8 - 3.2 (9H, C**H₃**NH and (C**H₃**)**₂**N, 3.15 (1H, CH – C2 sugar monomer), 3.4 (9H, (C**H₃**)**₃**N^+), 3.5 - 4.5 (9H, HOC**H₂**C**H₂** and H-3, H-4, H-5, H-6 CH –sugar monomer).

The level of palmitoylation was calculated by comparing the ratio of palmitoyl methyl protons (δ = 0.86 ppm) to sugar protons (δ = 3.5 – 4.5 ppm) and the level of quaternisation by comparing the ratio of quaternary ammonium (δ = 3.4 ppm) to sugar protons as shown in equations 2.1 and 2.2.

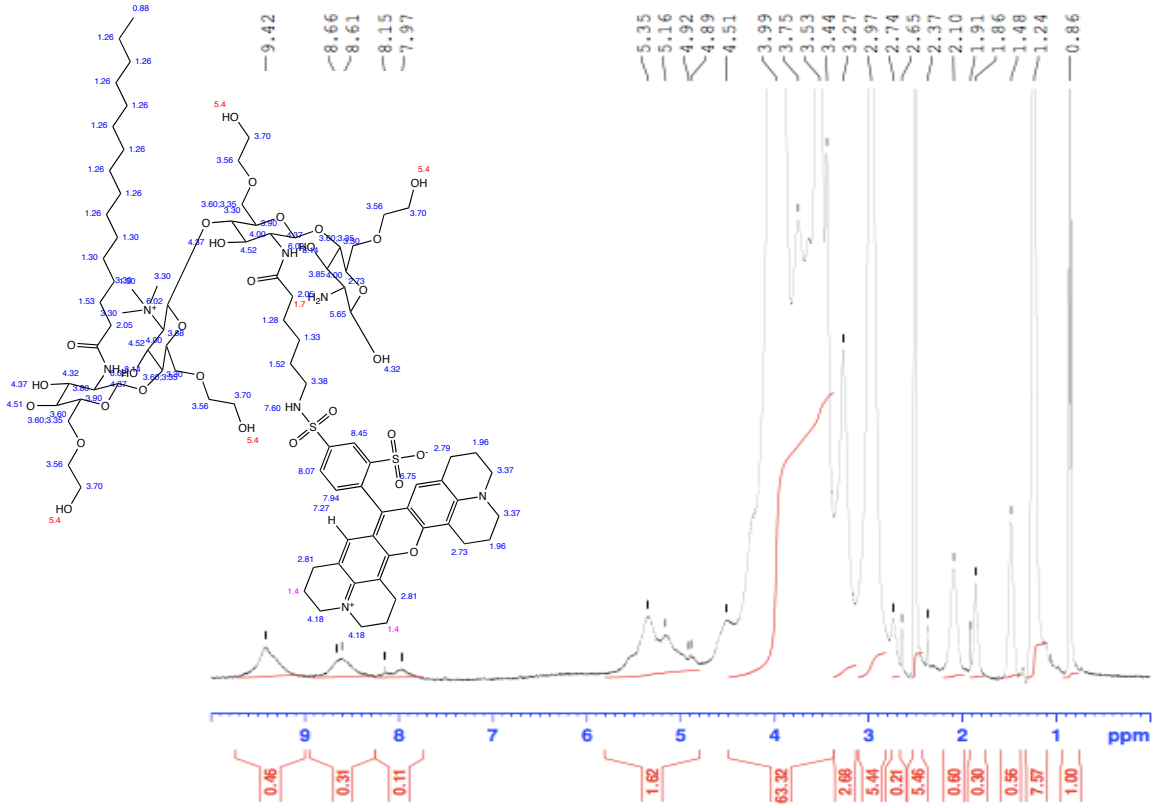

Figure 2-7: ^{1}H NMR of GCPQ-Texas Red conjugate in MeOD with palmitoylation level of 19% and quaternisation level of 10% and %Texas red substitution of 10%

^{1}H-NMR (DMSO-d_6) δ: 0.86 (3H, C**H**$_3$CH$_2$), 1.2-1.4 (24H, CH$_3$(C**H**$_2$)$_{12}$), 1.6 (2H, C**H**$_2$CH$_2$CO), 2.14 (2H, C**H**$_2$CO), 2.8 - 3.2 (C**H**$_3$NH and (C**H**$_3$)$_2$N, 3.15 (1H, C**H** – C2 sugar monomer), 3.4 (9H, (C**H**$_3$)$_3$N$^+$), 3.5 - 4.5 (9H, HOC**H**$_2$C**H**$_2$ and H-3, H-4, H-5, H-6 CH – sugar monomer), 4.5-5.5 (anomeric proton, 1H- sugar monomer), 9.4 (1H, ArH), 8.3-8.9 (2H, ArH), 7.8-8.3 (2H, 2 x ArH).

The mole % substitution with Texas Red was determined using the formula below:

$$Degree\ of\ TR = 100\ \times \left[\left(\frac{\frac{integral\ at\ \delta 8.0 - 9.4}{number\ of\ aryl\ protons}}{\frac{integral\ at\ \delta 0.88}{number\ of\ methyl\ protons}} \right) \times DP\ of\ GCPQ\ used \right]$$

$$Degree\ of\ TR = 100\ \times \left[\left(\frac{\frac{0.88}{5}}{\frac{1}{3}} \right) \times 0.19 \right] = 10.0\%$$

The yield of the Texas Red conjugate was determined by comparing the mass of the dried GCPQ-Texas Red conjugate with the mass of GCPQ starting material:

$$\%\ yield = 100\ \times \frac{mass\ of\ dried\ GCPQ - TR}{mass\ of\ GCPQ}$$

$$\%\ yield = 100\ \times \frac{48}{120} = 40\%$$

The purity of the labelled GCPQ polymers was determined using GPC-MALLS and is shown in figure 2-11. The pure conjugates were stored at -20 ^{o}C and away from light.

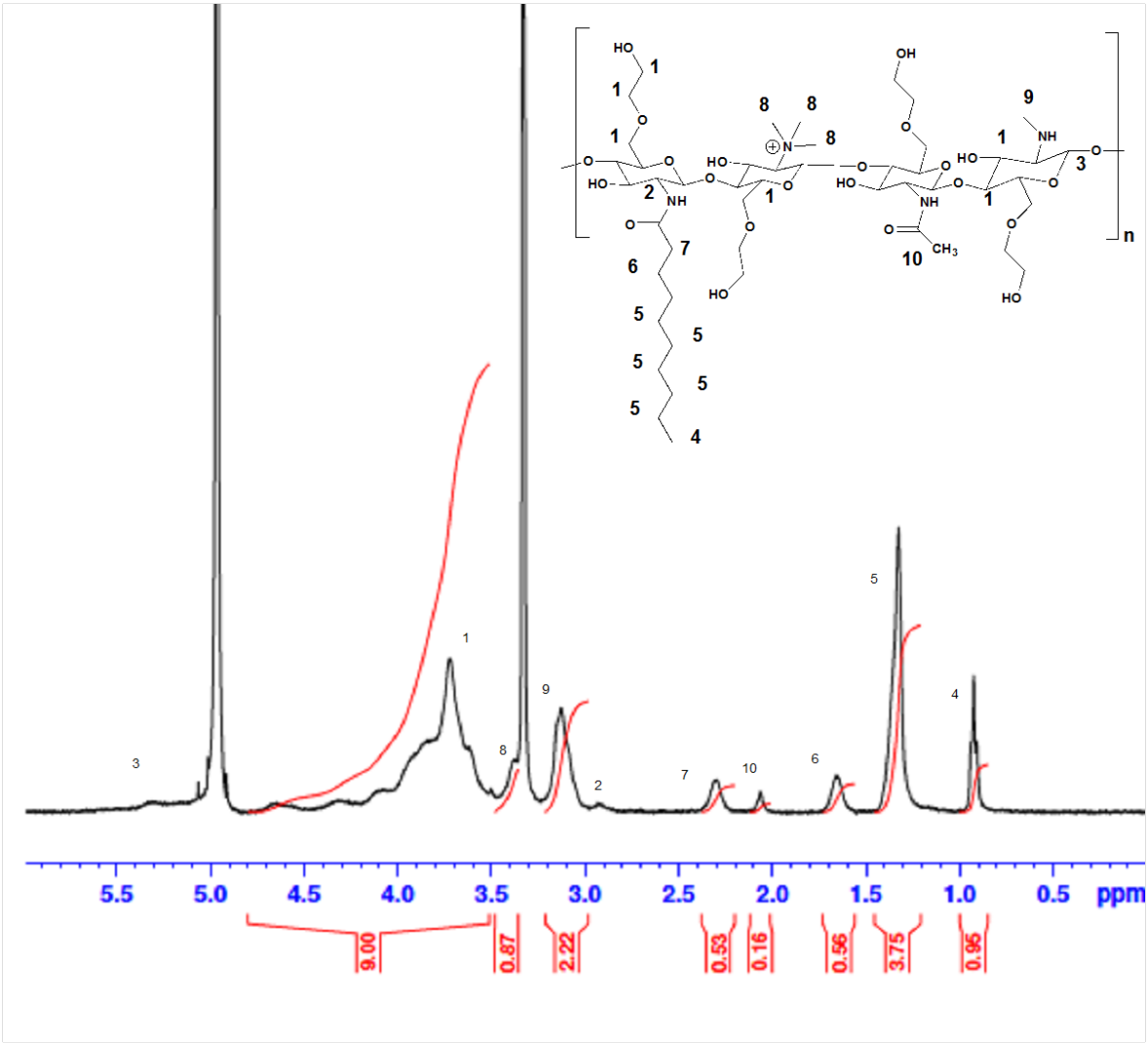

Figure 2-8: 1H NMR of GCDQ in MeOD with decanoylation level of 32 % and quaternisation level of 10 %

^{1}H-NMR (CD_3OD, DCl, 99.99:0.001) δ: 0.86 (3H, C**H**$_3$CH$_2$), 1.2 - 1.4 (12H, CH$_3$(C**H**$_2$)$_6$), 1.6 (2H, C**H**$_2$CH$_2$CO), 2.13 (3H, C**H**$_3$CO), 2.14 (2H, C**H**$_2$CO), 2.8 - 3.2 (C**H**$_3$NH and (C**H**$_3$)$_2$N, 3.15 (1H, C**H** – C2 sugar monomer), 3.4 (9H, (C**H**$_3$)$_3$N$^+$), 3.5 - 4.5 (9H, HOC**H**$_2$C**H**$_2$ and H-3, H-4, H-5, H-6 CH –sugar monomer).

The level of decanoylation was calculated by comparing the ratio of decanoyl methyl protons (δ = 0.86 ppm) to sugar protons (δ = 3.5 – 4.5 ppm) and the level of quaternisation by comparing the ratio of quaternary ammonium (δ = 3.4 ppm) to sugar protons as was done for GCPQ.

$$\%\ \text{decanoylation} = \frac{\frac{\text{integration value of } N - \text{decanoyl methyl protons}}{3}}{\frac{\text{integration value of sugar protons}}{9}} \text{ x } 100$$

$$\%\ \text{quaternisation} = \frac{\frac{\text{integration valueof trimethyl}}{9}}{\frac{\text{integration value of sugar protons}}{9}} \text{ x } 100$$

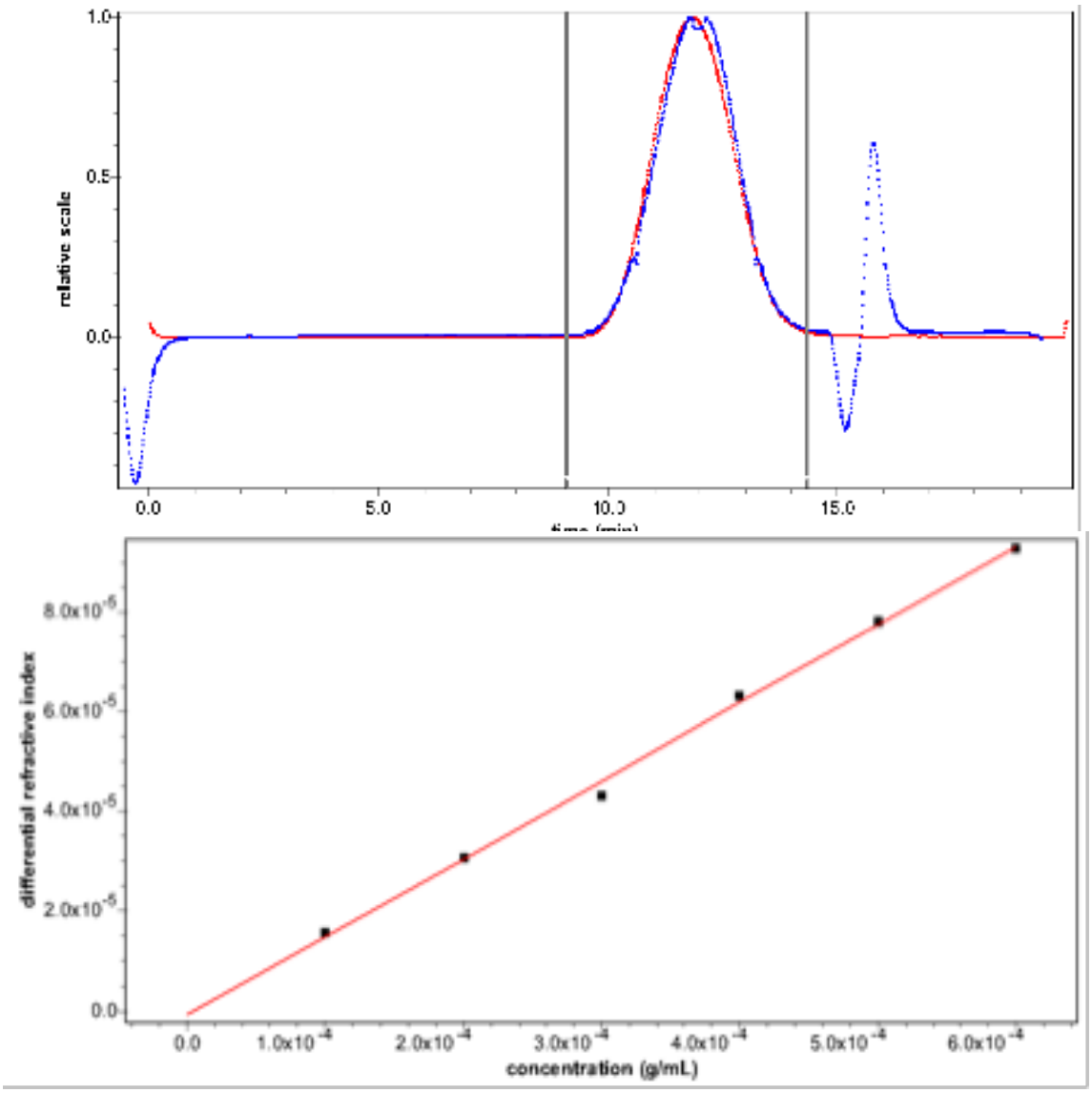

Figure 2-9: GPC chromatogram showing **Top:** dGC03; Mw: 6.7102e+3Da; Mw/Mn: 1.012 (1%); **Bottom**: dn/dc: 0.1562±0.0043. Red line: Light scattering. Blue line: Refractive index

The GPC MALLS shows an elution time of 12 minutes for degraded GC corresponding to 6.7102 kDa with polydispersity of 1.012. The dn/dc obtained for the degraded GC was 0.1562±0.0043. The refractive index shows a small peak at about 16 minutes which is likely a ghost peak due to the salts in the mobile phase.

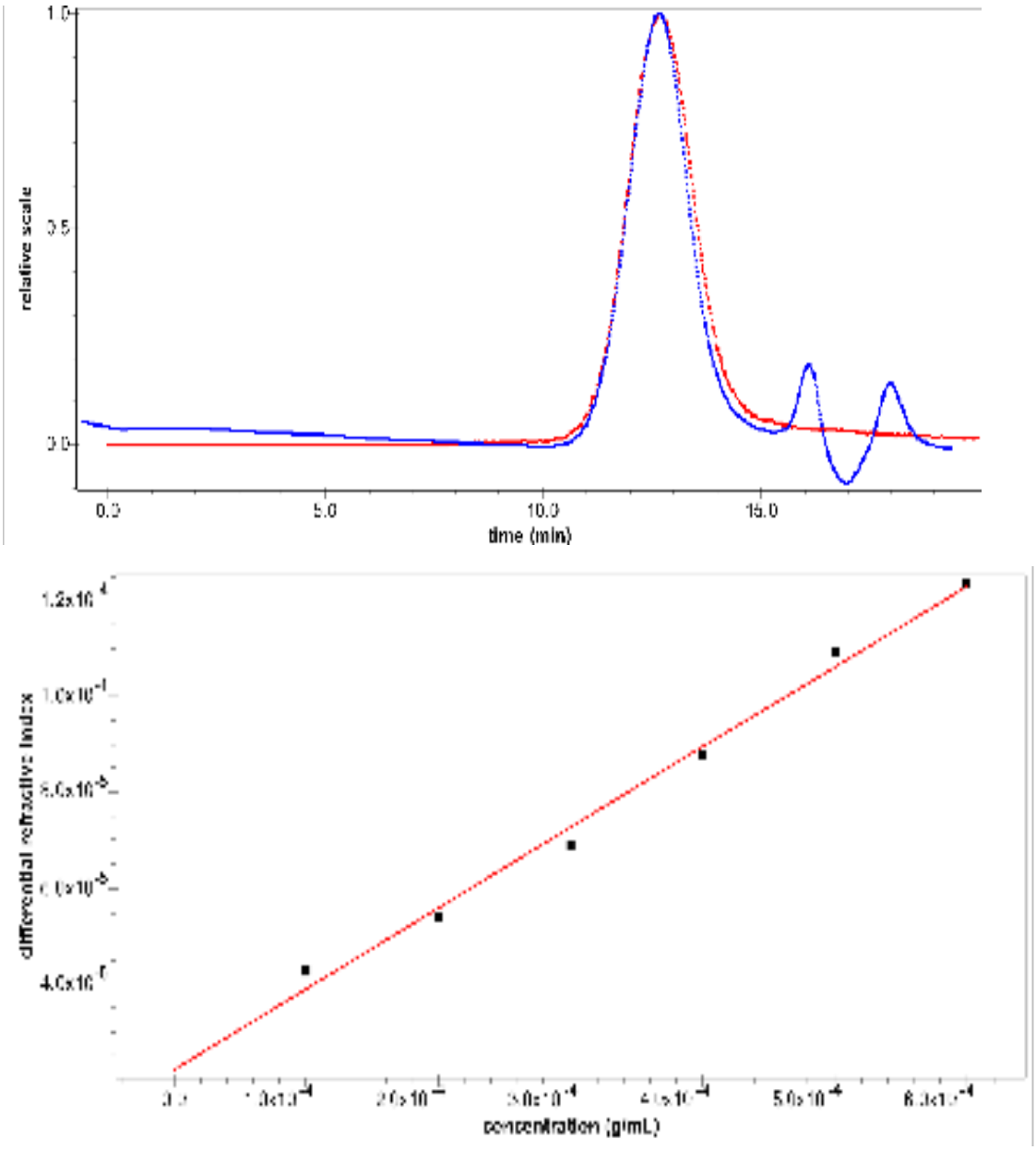

Figure 2-10: **Top:** $GCP_{19}Q_{12}$: Mw: 1.235e+4Da; Mw/Mn: 1.027(3%); **Bottom:** dn/dc: 0.1689±0.0080 mL/g. Red line: Light scattering. Blue line: Refractive index

The GPC MALLS data shows the elution time for GCPQ at about 12 minutes as was obtained for dGC. The polydispersity was 1.027 and dn/dc was 0.1689±0.0080 mL/g.

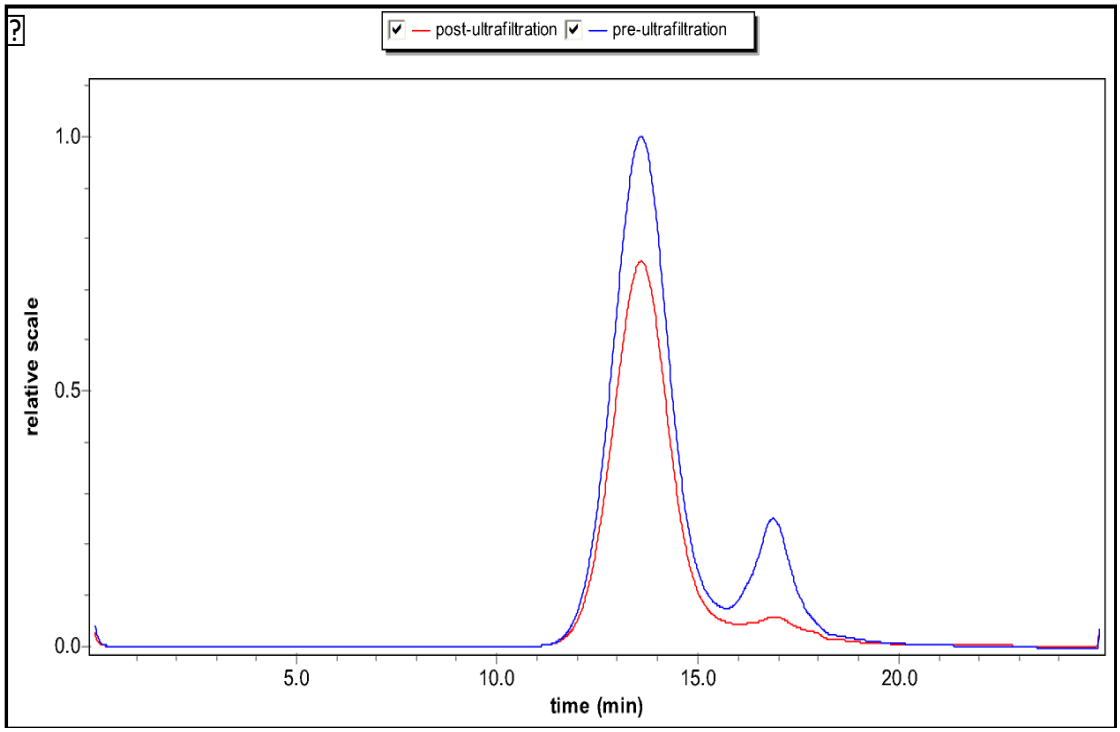

Figure 2-11: chromatograms showing the purified GCPQ-Texas red conjugate. Retention times for GCPQ and Texas-red are 12mins and 17 minutes respectively.

The GPC MALLS plot in figure 2-10 shows the elution time of GCPQ-TR at about 12 minutes, corresponding to the peaks of GCPQ and dGC, and the impure GCPQ-TR at about 17 minutes. But after purification, the impurity peak at 17 minutes is almost totally lost.

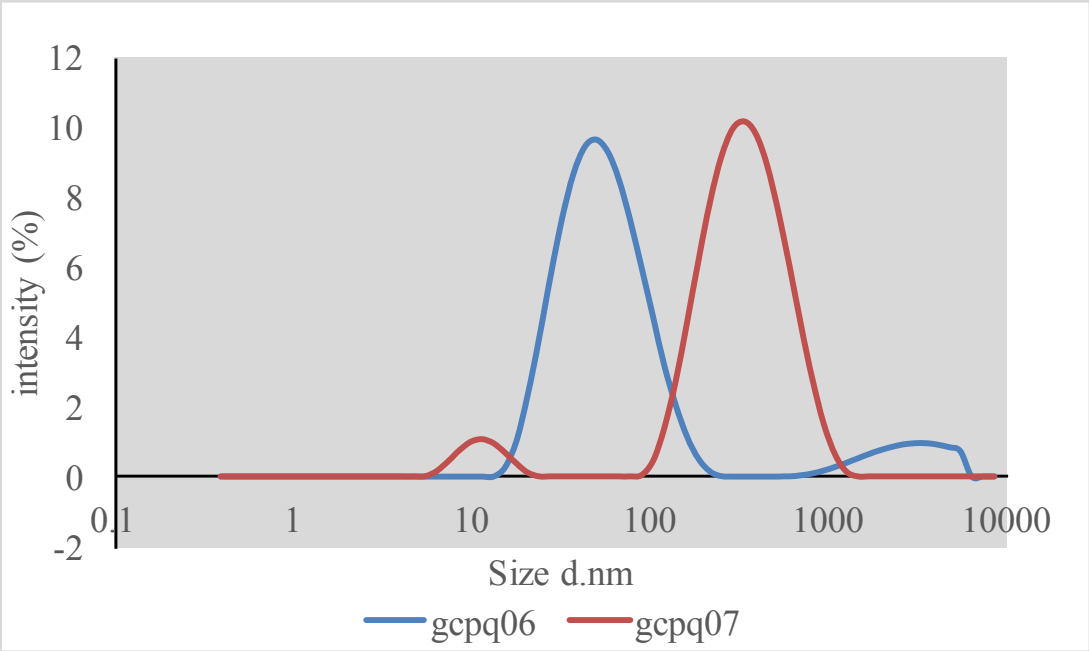

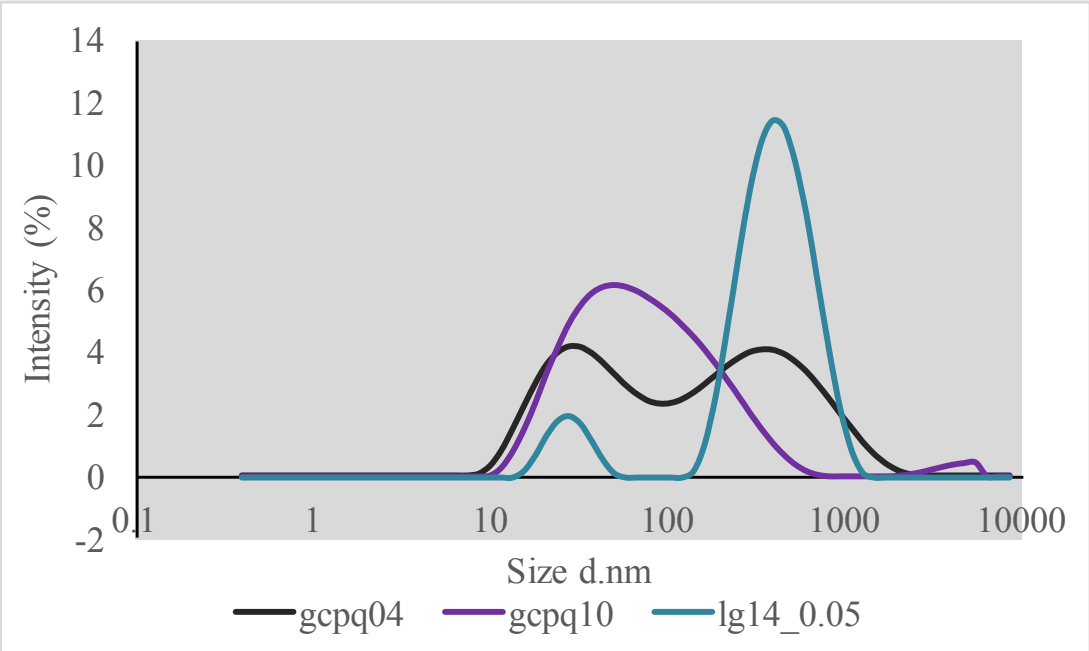

Figure 2-12*:* Size distribution of GCPQ polymers differs with hydrophilicity**. Top**: GCPQ 06 and GCPQ07 with QPR of 1.1 and 4.0 respectively. The more hydrophilic polymer (GCPQ 07) has a higher mean size distribution. **Bottom:** More hydrophobic polymers (GCPQ 04 and GCPQ10, QPR of 0.53 and 0.62 respectively) have broader size distribution than the more hydrophilic polymer (LG14_0.05, QPR of 2.75)

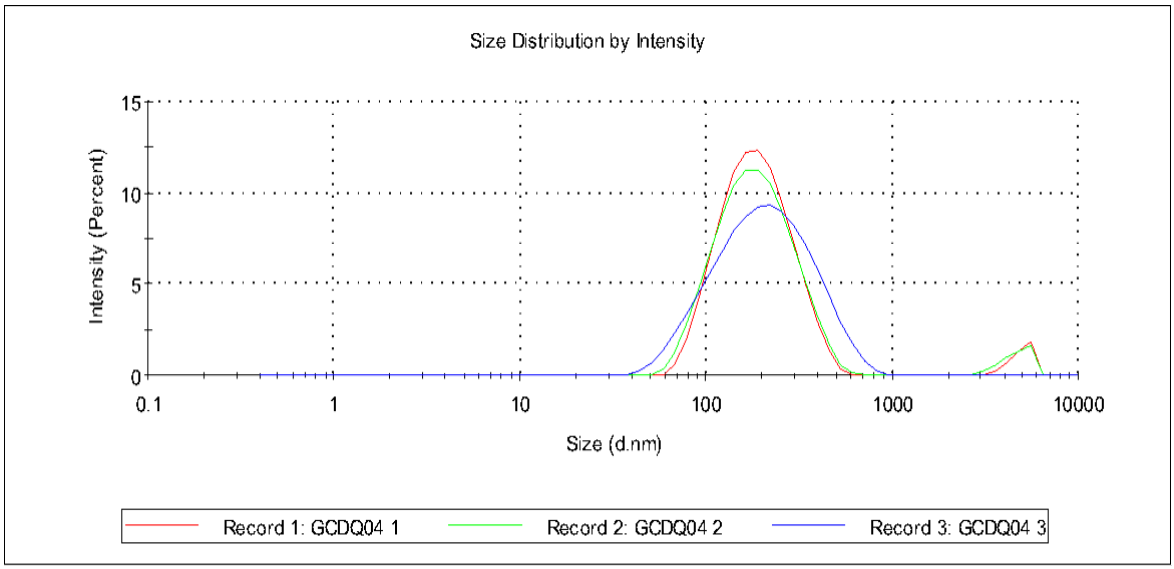

Figure 2-13: Size distribution of GCDQ polymer with DD% : 8.7%, DQ% of 7% , Z average= 172.0 ± 5.75; PDI= 0.351± 0.037.

Figure 2-12 shows the size distribution of GCDQ with degree of decanoylation of about 8.7 % and degree of quaternisation of about 7 %. The intensity mean distribution shows a large single peak at about 200 nm and a small peak greater than 1000 nm which could be very large aggregates. This implies that GCDQ forms a monomodal population of nanoparticles with a narrow size distribution since the PDI is about 0.35.

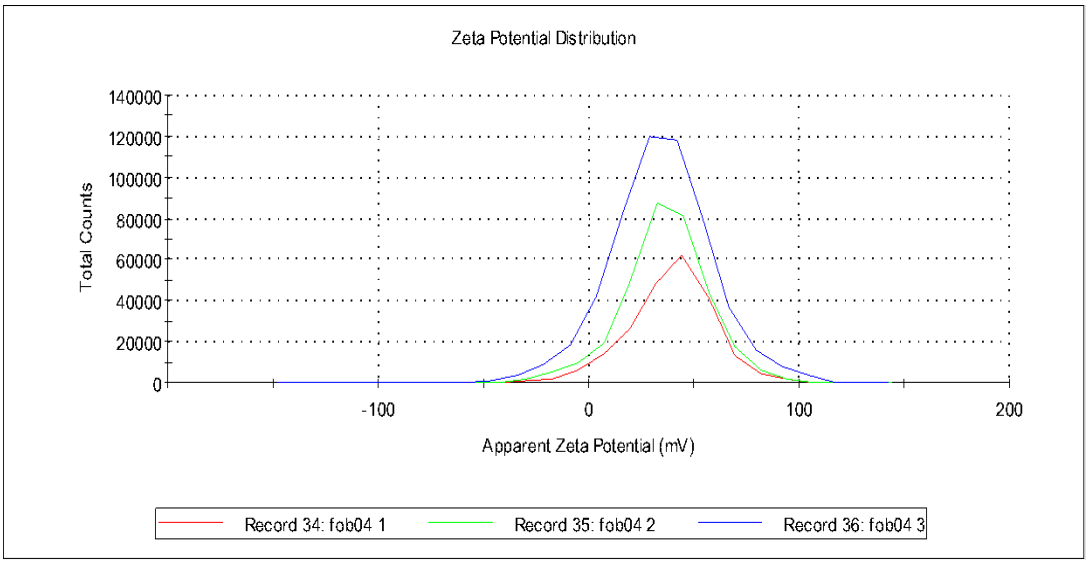

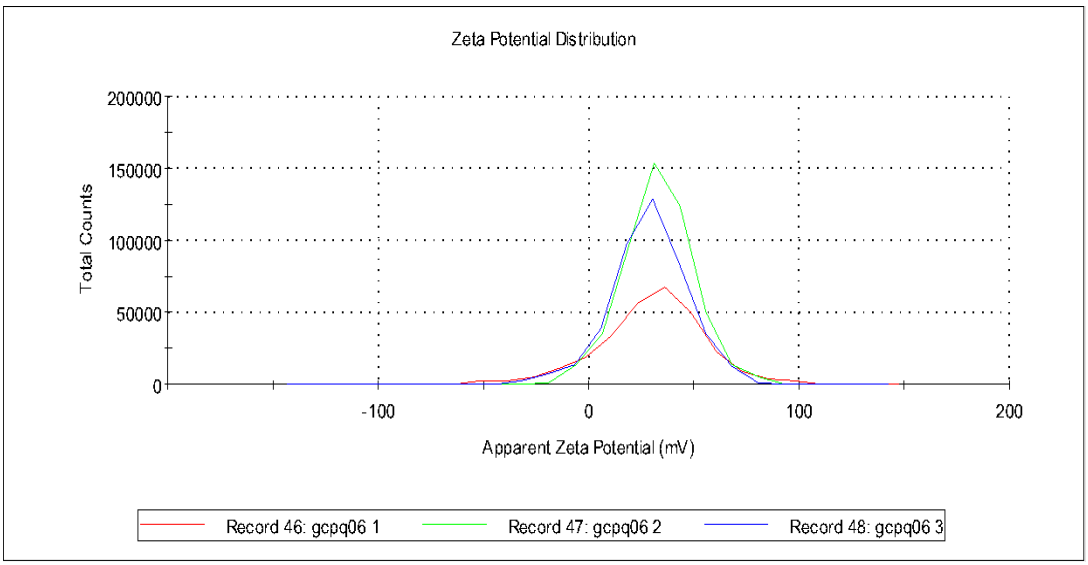

Figure 2-14: Zeta potential of a more hydrophobic GCPQ polymer, GCPQ04; QPR: 0.53, Zeta potential: 39.27±2.06mV (**Top**) and a more hydrophilic polymer, GCPQ06; QPR: 1.10, Zeta potential: 49.43±1.67mV (bottom).

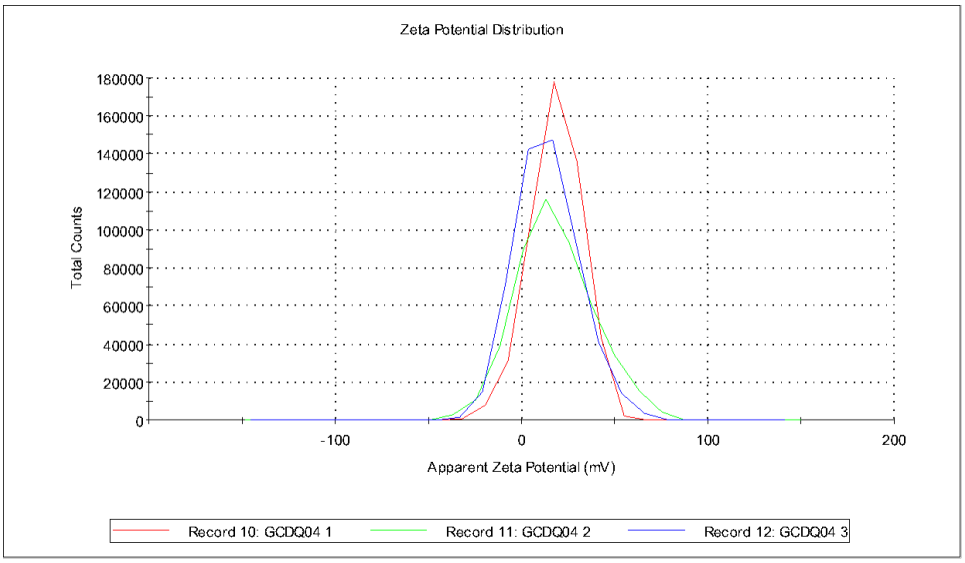

Figure 2-15: Zeta potential of GCDQ polymer with DD% : 8.7%, DQ% of 7%, Zeta potential=16.35 ± 1.75.

The zeta potential of GCDQ is much lower than that of GCPQ polymers. (see figure 2-13).

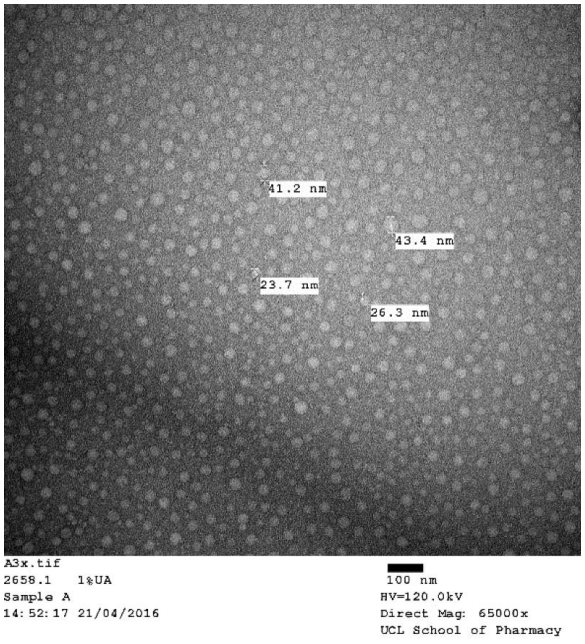

Figure 2-16: Transmission Emission Microscopy of GCPQ 04, GCP19Q10, QPR: 0.53, Conc: 10mg/mL.

GCPQ 04 forms a homogenous distribution of micelles with sizes between 20nm and 40nm in deionised water

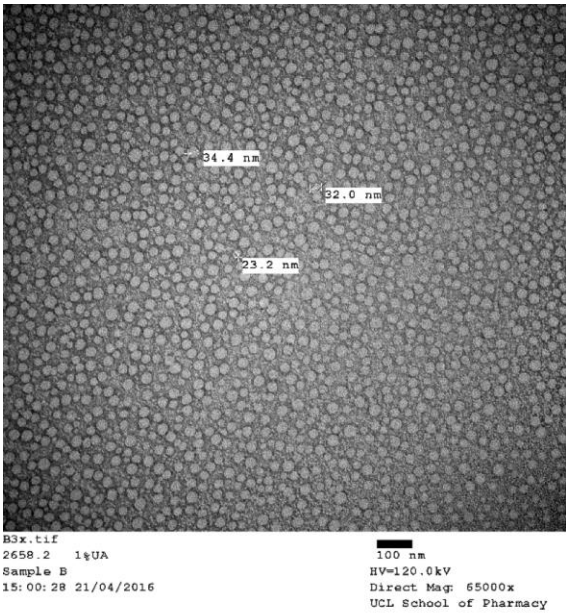

Figure 2-17: Transmission Emission Microscopy of GCPQ06: GCP20Q22, QPR: 1.10, Conc: 10mg.mL.

GCPQ06 forms a homogenous distribution of micelles with sizes ranging from 20nm-30nm in deionised water. There is no apparent difference in size of micelles between GCPQ04 (figure 2-16) and GCPQ06.

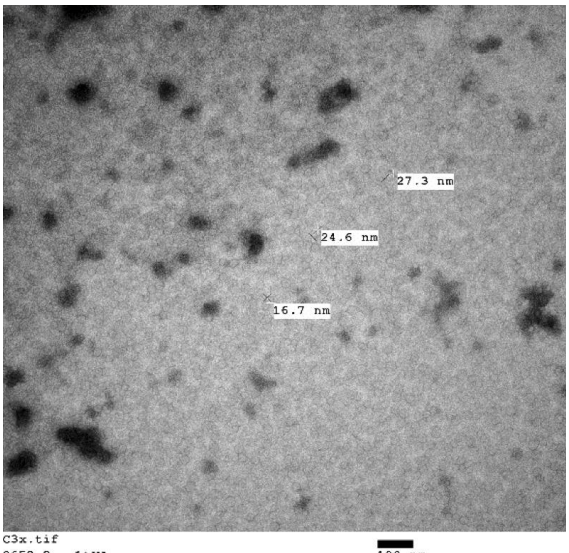

Figure 2-18: Transmission Emission Microscopy of GCPQ04-TR, GCP19Q10TR7, Conc: 10mg/mL.

GCPQ04-TR forms micelles which are slightly smaller than the micelles formed by GCPQ04, perhaps due to the more hydrophobic nature of the conjugate.

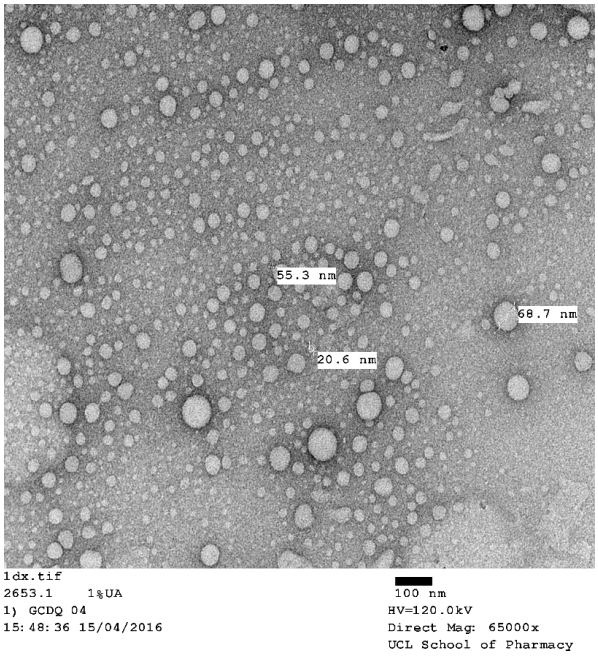

Figure 2-19: Transmission Emission Microscopy of GCDQ04, GCD8.7Q7, Conc: 10mg/mL.

GCDQ forms a more heterogeneous distribution of small and larger micelles than GCPQ perhaps owing to the shorter chain length of the hydrophobic decanoyl, making the system less thermodynamically stable.

GCPQ polymers were synthesized with a range of structural modifications and characterised using different techniques. The physicochemical properties of these polymers such as particle size, molecular weight and zeta potential were determined to observe the effects of the modifications on the characteristics of the polymers. The ratio of DQ% to DP% (QPR) did not influence the size or zeta potential of the polymers. An alternative polymer, GCDQ with a shorter chain decanoyl substituent was synthesized and compared with GCPQ polymers. GCDQ forms slightly larger aggregates (figure 2-19) than GCPQ and has a lower zeta potential. The lower zeta potential possibly encourages aggregation of the nanoparticle. Zeta potential of GCPQ polymers range from 30 to 50 mV while GCDQ has a zeta potential value below 20mV. TEM images show that GCPQ forms micelles ranging from 20-40nm in size while GCDQ forms micelles larger than 50nm. Both polymers apparently aggregate to form larger sized nanoparticle. **Table 2-3** shows that polymer with lower DP% have higher z-average values, some above 200nm while polymers with high DP% values have z-average values less than 100nm and some below 50nm. Conjugating with Texas red results in even smaller sized particles about 10nm in size. GCDQ however forms aggregate about 170nm in size. These observations are supported by previously reported data on the characterization of GCPQ (Uchegbu, 2013, Uchegbu et al., 2013b). For subsequent studies, GCPQ with varying degrees of DP and DQ will be used to understand the effect of structural modifications on aggregation kinetics, in vitro and in vivo applications of GCPQ. GCPQ-

TR will be used for microscopic observation of interactions between GCPQ and epithelial barriers in vitro and in vivo.

2.6 Conclusion

GCPQ polymers with varying degree of DP% and DQ% were synthesized and characterised. GCPQ- Texas red conjugate was also synthesized, purified and characterised. GCDQ polymers were equally successfully synthesized and characterised for comparison with GCPQ. These polymers will be used for further studies in mammalian cell and rodent model-based assays.

Chapter 3. Colloidal Stability and Thermodynamics of GCPQ Self Assembly

3.0 Introduction

Colloidal systems are defined as systems in which one phase is dispersed in another (Kralchevsky et al., 1997). Typically, the dispersed phase has a larger molecular weight or particle size than the dispersion medium or continuous phase. The dispersed phase is typically made up of particles of sizes less than 1 μm though exceptions exist for emulsions, paints and aerosols (Myers, 1999). Colloidal systems represent a large group of compounds with wide ranging applications in pharmaceuticals, construction, cosmetics, food and beverages, fashion and design. Table 1 shows examples of colloidal systems as well as their dispersed and continuous phases.

Table 3-1: Examples of colloidal systems

System	Example	Dispersed phase	Continuous phase
Micellar solutions	Detergents	Detergent molecules	Liquid
Suspensions	Paint	Solid	Liquid
Emulsion	Milk/Butter	Oil/Water	Water/Oil
Foam	Shaving cream	Gas	Liquid
Solid foam	Styrofoam	Gas	Solid
Liquid Aerosol	Fog, mist, deodorant	Liquid	Gas
Solid aerosol	Smoke	Solid	Gas
Gel	Jello	Macromolecules	Liquid

This chapter will cover experiments carried out to determine the colloidal stability of GCPQ polymers in different environments as well as the thermodynamics of self-aggregation of

GCPQ particles.

3.1 Stability of Colloidal systems

The stability of colloidal systems is very important given the wide range of applications of these systems. Pharmaceutical formulations prepared as suspensions or emulsions must stay stable for prolonged periods of time to preserve their utility. Aggregation is one of the important properties of colloidal systems, the kinetics of which is explained by van der waal's force, Electrostatic forces, Hydration forces and hydrophobic interaction (Trefalt and Borkovec, 2014, Hwang et al., 2012) and the Derjaguin, Verwey, Landau and Overbeek (DLVO) theory of colloidal stability (Behrens et al., 2000, Instruments, 2011, Derjaguin and Landau, 1941, Verwey et al., 1999). According to the DLVO theory, the stability of a colloidal system is controlled by two forces: an attractive force (V_A) and a repulsive force (V_R). The net effect of the forces is the sum of both (V_A+V_R) (Ortega-Vinuesa et al., 1996). For colloidal suspensions containing electrolytes, the DLVO theory is insufficient for predicting the stability of a colloidal system. While the repulsive force (electrostatic force) is typically influenced by the electrolyte concentration the attractive force consists mostly of the London/ van der waal's forces. However, the contribution of steric effects of hydrated electrolytes is not accounted for. An addition to the DLVO theory tries to account for this steric effect of electrolytes in a colloidal system described as hydration forces (V_H) as well as attractive hydrophobic interactions.

Van der Waal's forces of Attraction.

Van der waals forces are attractive intermolecular forces due to interactions between dipoles formed by the movement of electrons of atoms and molecules (Ohshima, 2012). The electrons on molecules are in a constant dynamic state, meaning that they ae constantly in motion. This movements creates regions that have a slight excess of electrons compared to other regions, thus resulting in dipoles. Because of the constant motion, however, these dipoles are temporary with constant fluctuations (Kronberg et al., 2014). This attractive force is inversely dependent on the dielectric constant of the dispersion medium. So, the attraction is highest in vacuum and organic solvents which have a relatively lower dielectric constant than water. It is also inversely proportional to the distance between particles, so that the close the particles are to each other, the greater the attractive force. The sum total of the attractive forces is however directly proportional to the size of the particles so that the bigger the particles, the greater the force of attraction. These relationships, together with the type of material the particles are made of determine the contribution of van der waal attractive forces to the stability of a colloidal system (Kronberg et al., 2014).

Electrostatic repulsive forces

Charged particles in solution have an electric double layer of oppositely charged ions surrounding them. The double layer consists of a Stern layer of more compact, stuck oppositely charged ions and a diffuse layer of ions. When these charged particles come close to each other, there is an overlap of their double layers which potentially creates a centre of sufficiently high charge density that causes a repulsion of the particles, keeping them from coming any closer. The zeta potential is used as a measure of the electrical potential at the stern layer. This potential decays proportional to the double layer thickness or the Debye length which is inversely proportional to the ionic concentration of dispersed electrolytes (Eastman, 2009). The greater the zeta potential, the greater the repulsive force and hence the greater the stability of the colloidal system.

The repulsive electrostatic forces (V_R) are opposed by the Van Der Waal's attractive forces (V_A). The sum of both forces in a colloidal system is explained by the Total potential (V_T)

$$V_T=V_A+V_R$$

According to the DLVO theory, the Total potential describes the tendency for a colloidal system to remain stable. The superposition of both the repulsive and attractive forces results in a primary maximum potential that provides an effective activation energy for activation. That implies that the collision between two particles has to be sufficient to overcome the activation energy for them to stick together and thus aggregate. Hence, the interplay between particle size, concentration and charge density will determine if the attractive forces will overcome the repulsive forces and thus give a lower primary maximum, creating an unstable colloidal system.

Non-DLVO Forces

The DLVO theory explains the stability of a colloidal system on the bases of mostly two forces: Van der Waal's attractive forces and electrostatic repulsive forces. It however leaves out the role of other forces that have been shown to contribute to the stability of colloidal systems. Two primary forces include hydrophobic interactions and hydration forces (Ghosh, 2012).

Hydrophobic interactions can be described as an interaction between molecules which have a low affinity for water and are typically attractive in nature (Grasso et al., 2002). Hydrophobic interactions seek to explain the force of attraction between molecules that cannot be explained by the van der Waal's forces, forces which are typically stronger or greater than can be explained by the DLVO theory. These hydrophobic interactions are usually explained by the decrease in entropy of water molecules due to the formation of a cavity consisting of hydrophobic moieties in solution.

Hydration forces are mostly structural forces formed due to the orientation of solvent molecules around dispersed particles. Where water is the solvent, a network of hydrogen bonds is formed around solubilised particles, creating a lattice structure that creates a boundary layer between separated particles. As the particles attempt to get closer, the pressure on the boundary later increases, causing a resistance to particle collision or aggregation (Grasso et al., 2002).

3.2 Polymeric Micelles

Amphiphilic polymers are polymers composed of hydrophilic units as well as hydrophobic units. By virtue of having the hydrophilic component, these polymers are mostly water soluble and are able to self-aggregate in aqueous solution, forming micelles (Borisov and Halperin, 1998) or vesicles (Wu et al., 2008) through interactions of their hydrophobic units. Generally, the hydrophobic units are n-alkyl chains of varying lengths (Giusti et al., 2012) while the hydrophilic units could be anionic (Petit-Agnely et al., 2000, Suwa et al., 2000), neutral (Feng et al., 2005, Sharma et al., 2012), cationic (Villari et al., 2013, O'Mahony et al., 2012) or zwitterionic (Diab et al., 2007). The characteristics of the units attached to the polymer typically influences the nature and thermodynamics of aggregation.

Self-assembly of polymers in solution is known to be driven largely by hydrophobic interactions (Chandler, 2005b, Sánchez-Iglesias et al., 2012) which in turn depends on factors such as temperature, the nature of hydrophobes, the structure of water around the hydrophobic entities as well as the presence of neighbouring immobilized ions (Ma et al., 2015b). The process of micelle formation is thus influenced by the interplay of molecular forces. Thermodynamics of this process is reliably described by the Gibbs free energy. The Gibbs free energy describes the tendency for the reaction to occur spontaneously and is dependent on two components: enthalpy and entropy. Thus;

$$\Delta G = \Delta H - T\Delta S \ldots\ldots. \quad (3.1.1).$$

The enthalpy describes the average potential energy of interactions between molecules while the entropy describes intermolecular correlations (Dill and Bromberg, 2010). David Chandler (Chandler, 2005b) explains the enthalpic component as being the result of processes that involve the breakage of hydrogen bonds, thereby increasing intermolecular

interactions while the entropic component involves specific spatial organization of hydrogen bonding patterns.

The introduction of a hydrophobe into an aqueous medium results in the breakage of hydrogen bonds between water molecules to accommodate the hydrophobe and then the formation of new hydrogen bonds around the hydrophobe, thus creating a hydrophobic cavity surrounded by clathrate-like water structures. The energy compensation provided by the formation of the new hydrogen bonds determines if the change in enthalpy is positive or negative (Chang, 2005). Polymers and surfactants containing a hydrophilic component have additional restrictions in configuration due to the accommodation of hydrophilic interactions which introduces an additional entropic effect (Chandler, 2005b). The process of micelle formation is therefore considered to be influenced by enthalpy changes due to the aggregation of charged heads, the destruction of organized water structures, the transfer of hydrocarbons from water to micelles (the first two events being endothermic and the latter exothermic (Adderson and Taylor, 1970)) as well as the magnitude of entropy contribution thus making the assembly process to be driven by energy difference between enthalpic and the entropic events (Chandler, 2005b).

3.1.1 **Thermodynamics of Aggregation of GCPQ micelles**

Aggregation is one of the important properties of colloidal systems. Describing the thermodynamics of aggregation is important for characterization of systems. This usually involves determining the critical micelle concentration (CMC), the change in enthalpy (ΔH_{mic}), the change in entropy (ΔS_{mic}) and the change in Gibbs free energy (ΔG_{mic}) at micelle formation using different techniques including tensiometry, conductometry, fluorimetry and calorimetry (Ray et al., 2006). Isothermal Titration Calorimetry (ITC) is a form of power compensated calorimetric measurement routinely used to characterize the thermodynamics of biopolymer binding interactions (Ray et al., 2006). It has however been adopted for use in determining the thermodynamics of micelle formation with the advantage over the other methods, of being highly sensitive, probe free and providing fast, reliable direct measurement of the CMC and the enthalpy of micellization (Koper et al., 2009, Raju et al., 2001). Here, we utilized the ITC to characterize the thermodynamics of micelle formation of *N*-palmitoyl-*N*-monomethyl-*N*,*N*-dimethyl-*N*,*N*,*N*-trimethyl-6-O-glycolchitosan (GCPQ)- an amphiphilic polymer system which can be designed to contain different proportions of charged quaternary ammonium and lipophilic palmitoyl group substitutions. There have been several reports on the effect of the water structure around non-polar molecular fragments on hydrophobic interactions (Chandler, 2005b, Meyer et al., 2006, Davis et al., 2012b). Derek Ma et al (Ma et al., 2015b) suggested that by judiciously placing charged groups close to hydrophobic domains, it is possible to tune the hydrophobic driving forces of self-assembly. They also showed that the protonation of amine groups doubles the strength of hydrophobic interaction. Since our previous reports on the micelle formation of GCPQ was based on a prototype with specific properties (Siew et al., 2011, Chooi et al.,

2014b, Uchegbu et al., 2014), we sought to determine the effect, if any, of a variation of the proportion of the hydrophobic palmitoyl and the protonated quaternary ammonium group on the self-assembly of the polymer and the possible implication on biological effects.

Here, the ITC technique was used to determine the CMC and thermodynamic quantities of GCPQ self-assembly.

3.2 Method:

3.2.1 Isothermal Titration Calorimetry

A MicroCal iTC200 (Malvern Instruments, Malvern UK) was used to determine the aggregation kinetics of GCPQ. The sample cell has a volume of 200μL and was filled with deionized water prior to each experiment. Polymer concentration of 1mg/ml was put in the injection syringe which holds 40μL. Prior to each experiment, a water-water run was done to ensure a good baseline was obtained. For each experiment, 19-30 aliquots of 0.8-2μL of the polymer was injected into the sample with constant stirring at 1000rpm and an interval of 120seconds between each injection at 25^{o}C or 35^{o}C. Each titration was performed three times to ensure reproducibility of the results. Data analysis was carried out using Microcal ORIGIN software version 7 and GraphPad Prism version 5.

The CMC was determined as the highest or lowest point of inflection on the plot of the first derivative of the heat of reaction against the concentration (Paula et al., 1995a).

The enthalpy of micellization (ΔH_{mic}) was determined from the enthalpy of demicellization (ΔH_{demic}) which was obtained by the integration of the raw signal (Bouchemal et al., 2009).

$$\Delta H_{mic} = -\Delta H_{demic}$$

The Gibbs free energy and entropy of micellization were determined using the Mass-action model (Tadros, 2005, Chatterjee et al., 2001):

$\Delta G_{mic} = RT\ln X_{cmc}$

And using the Gibbs-Helmoltz equation,

$\Delta S_{mic} = (\Delta H_{mic} - \Delta G_{mic})/T$

Where R is the gas constant ($8.314 JK^{-1}mol^{-1}$), T is the absolute temperature, X_{cmc} is the CMC in mole fraction units determined from the ITC titration.

3.2.2 Colloidal stability of GCPQ polymers

Stability in salt solutions

Several concentrations of sodium chloride and calcium chloride were prepared in deionised water. The concentrations used are : 0.016M, 0.04M, 0.008M, 0.11M, 0.18M, 0.26M, 0.35M, 0.5M, 0.6M, 0.75M, 0.8M, 0.9M, 1M and 2M. 2mg/mL of GCPQ polymer solutions was also prepared in deionised water and the pH adjusted to 4.2 and 7.4 using 0.1M NaOH or 0.1M HCl. A 1:1 dilution of the GCPQ polymers solution with each salt concentration was prepared by missing 100uL of each salt solution with 100uL of GCPQ solution in a cuvette to yield a mixture containing 1mg/mL of GCPQ polymers and one of 0.008M, 0.02M, 0.04M, 0.055M, 0.09M, 0.13M, 0.175M, 0.25M, 0.3M, 0.375M, 0.4M, 0.45M, 0.75M, 0.5M, 1M, 1.5M salt solution. The cuvette was then immediately placed in a Cary 100 UV-Vis spectrophotometer (Agilent Technologies, US) and the absorbance measured over 120 minutes in kinetics mode. A plot of Absorbance against time was obtained as represented in the figure below:

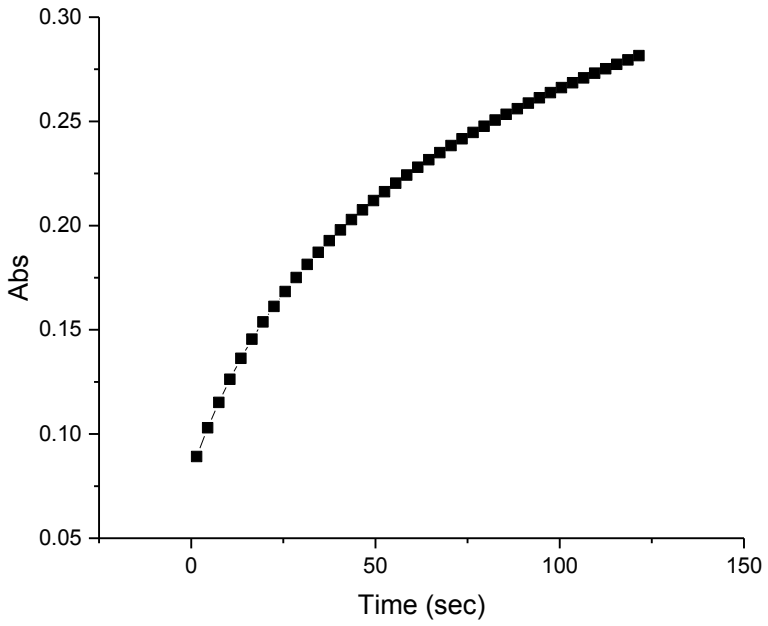

Figure 3-1: A curve representing a typical absorbance versus time plot, with light absorbance increasing with time at 570λ.

3.2.3 Nano-zetasizer measurements: Size and Zeta potential

Particle size and zeta potential of GCPQ dispersions under conditions used for kinetics measurements were obtained using a Nano-zetasizer (Malvern, UK).

3.2.4 **Data analysis**

OriginPro 2016 and Microsoft Excel were used to analyse the data obtained. The Fuchs factor, W, was used to quantify the instability of polymers in different conditions. The Fuchs factor is determined using the function:

$$W = \frac{kf}{ks} = \frac{\left(\frac{dAbs}{dt}\right)f}{\left(\frac{dAbs}{dt}\right)s}$$

Where *kf* represents the fastest slope and *ks* the slowest slope. A Fuchs factor of 1 represents a completely unstable system (Santander-Ortega et al., 2010). The Fuchs factor enables us to obtain the critical coagulation concentration (CCC) which is the salt concentration with the least stability and the critical stabilisation concentration (CSC) which is the salt concentration where restabilisation begins.

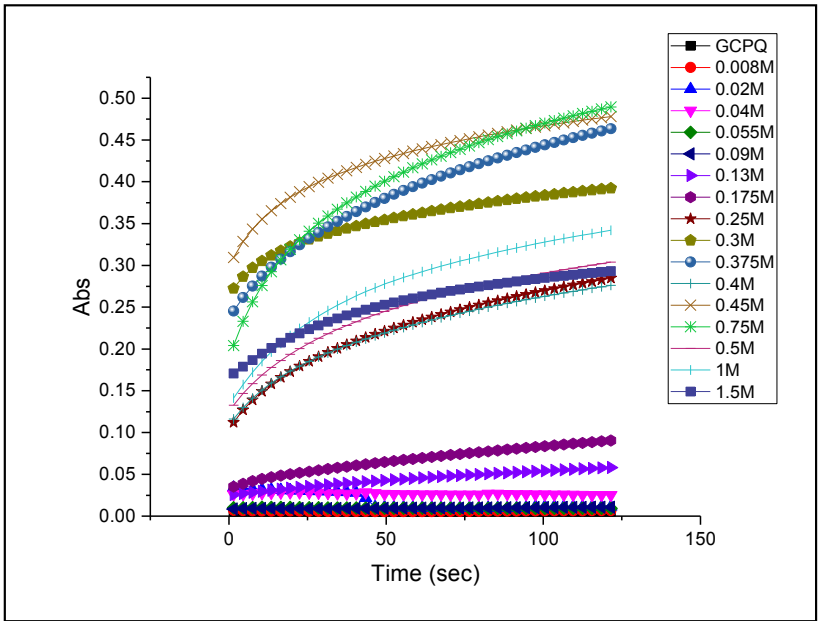

Figure 3-2: A representative plot of absorbance against time curves, on OriginPro 2016 showing curves representing different GCPQ-salt mixtures having different slopes. The curve with the steepest slope will have a Fuchs factor of 1.

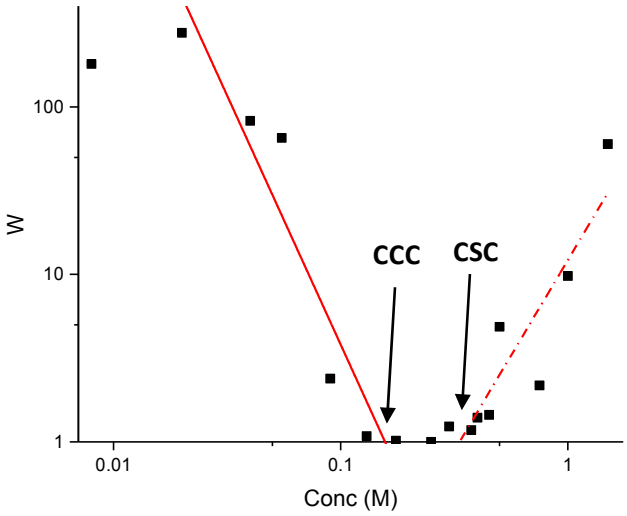

Figure 3-3: A representative plot of Fuchs factor against salt concentration generated in Excel, showing the critical coagulation concentration (CCC) and the Critical Stabilisation Concentration (CSC)

3.3 Results and Discussion

3.3.1 Thermodynamics of GCPQ aggregation

The various GCPQ polymers were named using the following nomenclature: GC(Mw in kDa)P(Mole% palmitoyl groups)Q(Mole% quaternary ammonium groups) and so a polymer with a molecular weight of 10 kDa and containing 20 mole% palmitoyl groups and 22 mole% quaternary ammonium groups would be named as follows: GC10P20Q22. The ratio of hydrophilic (quaternary ammonium groups) versus hydrophobic (palmitoyl groups) substitution is given by the quaternary to palmitoyl ratio (QPR).

$$QPR = \frac{Q}{P}$$

Where Q = mole% quaternary ammonium groups and P = mole% palmitoyl groups.

The polymers used are shown in table 3-2.

Isothermal calorimetry (ITC) was used to determine the various thermodynamics parameters of the micellization events. At the first injection of the micelles into the sample cell, the micelles are diluted to below their CMC values and the dilution enthalpograms reflect the resultant demicellisation of the micelles, as well as dilution of the resulting monomers. During the second set of injections the dilution enthalpograms reflect the end of the demicellisation events as the CMC is reached. The final stage of the enthalpograms indicates very little change in heat flows as more micelles are added to the sample cell. Large changes in enthalpy per injection volume, are an indicator that demicellisation is occurring; while the abrupt change in enthalpy events indicates that demicellisation is complete and any

additional micelles are simply diluted in the sample cell (Paula et al., 1995b). To detect the abrupt change in enthalpy events, the first derivative of the change in heat flow per injection volume was determined and plotted, with the peak in this plot used to determine the CMC (Paula et al., 1995b).

The enthalpy of demicellisation (ΔH_{demic}) is calculated from the difference between maximum and minimum heat change (Paula et al., 1995b) (Figure 3-4b). According to the law of mass action, the standard Gibbs free energy change of demicellisation (the transfer of one molecule of GCPQ from the micelle to water) is calculated from the equation:

$$\Delta G_{demic} = -RT \ln k$$

Where R is the gas constant (8.3144 J mol-1 K-1), T is the temperature in K and k is the CMC in mole fraction units. The product of temperature and the entropy change of demicellisation ($T\Delta S_{demic}$) may then be calculated from the Gibbs free energy equation:

$$\Delta G_{demic} = \Delta H_{demic} - T\Delta S_{demic}$$

All micellization parameters (X_{mic}) are equal in magnitude but opposite in sign to the demicellisation parameters.

$$\Delta G_{mic} = - \Delta G_{demic}$$

The Gibbs free energy equation of micellization is given by the equation:

$$\Delta G_{mic} = \Delta H_{mic} - T\Delta S_{mic}$$

Where ΔG_{mic}, ΔH_{mic}, ΔS_{mic} and T are the free energy change, enthalpy change, entropy change and temperature of micellization respectively.

At the start of the study, the CMC of sodium dodecyl sulphate was determined at 288K (8.29 mM, Figure 2a and b) from the dilution enthalpograms and found to be in agreement with values in the literature using ITC: 8.37 mM at 288K (Chatterjee et al., 2001). Table 3-2 shows the CMCs and micellization thermodynamics parameters of the various GCPQs.

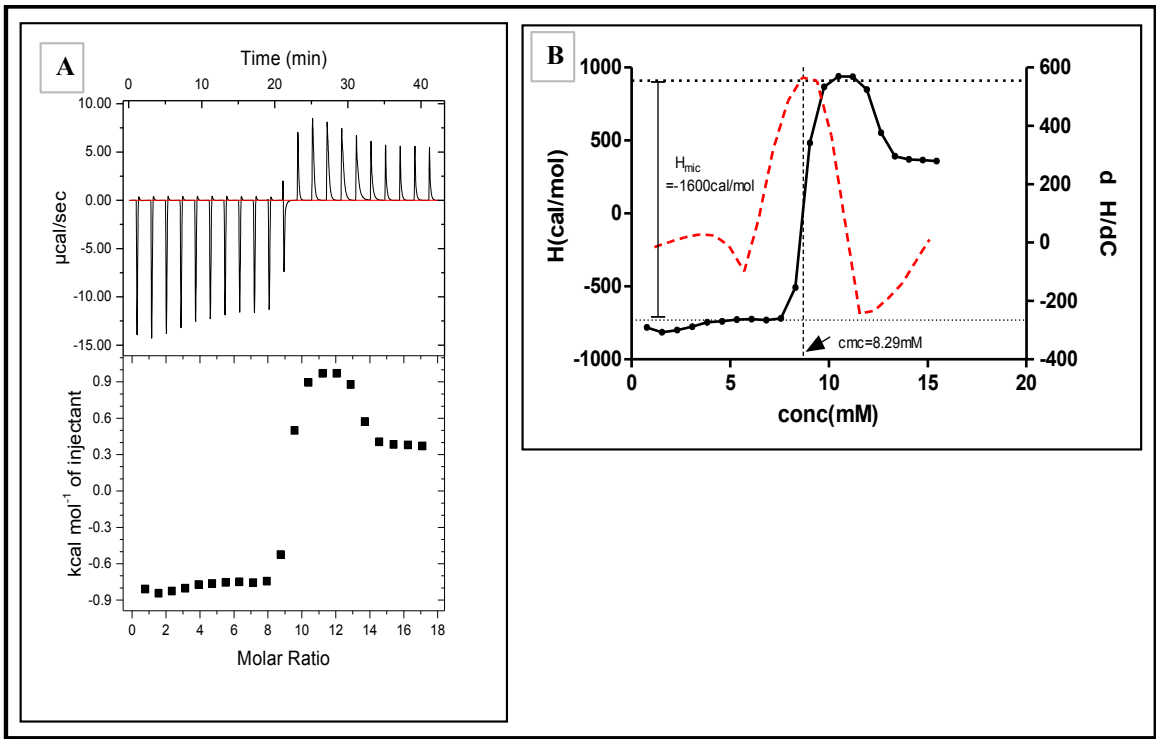

Figure 3-4: Data obtained from ITC experiments performed with Sodium dodecyl sulphate(SDS) solution (160mM) with 1µL of SDS per injection into 200µL of water at 15°C (288K). **A**. heat flow against time (top); enthalpy change per mole of SDS (bottom). **B** enthalpy change per mole of SDS plotted with first derivative of enthalpy with respect concentration (red dashed line)

Table 3-2: CMC values and Thermodynamic parameters of Micellization of GCPQ polymers expressed as the mean from three experiments with % RSD less than 15%. The number after 'P' in the nomenclature of GCPQ represents the molar percentage of palmitoyl groups (DP) and the number after 'Q' represents the molar percentage of quaternary ammonium groups (DQ).

Polymer	Mw (kDa)	CMC (µM)	Temperature (°K)	ΔH_{mic} (kJ mole^{-1})	ΔG_{mic} (kJ mole^{-1})	$T\Delta S_{mic}$ (kJ mole^{-1})	QPR
GC10P20Q22	9.9	2.4	298	96.2	-42.0	138.2	1.10
GC8P10Q14	8.4	1.7	298	25.1	-42.8	67.9	1.40
GC9P9Q36	8.8	1.5	298	-23.8	-42.3	18.5	4
GC14P12Q9	14.3	1.9	298	-83.7	-41.7	-42.0	0.75
GC14P12Q9	14.3	1.1	288	-62.8	-41.5	-21.2	0.75
GC9P19Q12	8.7	2.4	298	-60.8	-41.2	-19.7	0.63
GC9P19Q12	8.7	4.9	308	-75.3	-39.4	-35.9	0.63
GC10P19Q10	10.4	1.9	298	-71.1	-41.7	-29.4	0.53
GC12P19Q9	12.4	1.9	298	-79.5	-41.7	-37.8	0.47
GC15P4Q11	15.2	1.3	298	-184.1	-43.1	-141	2.75

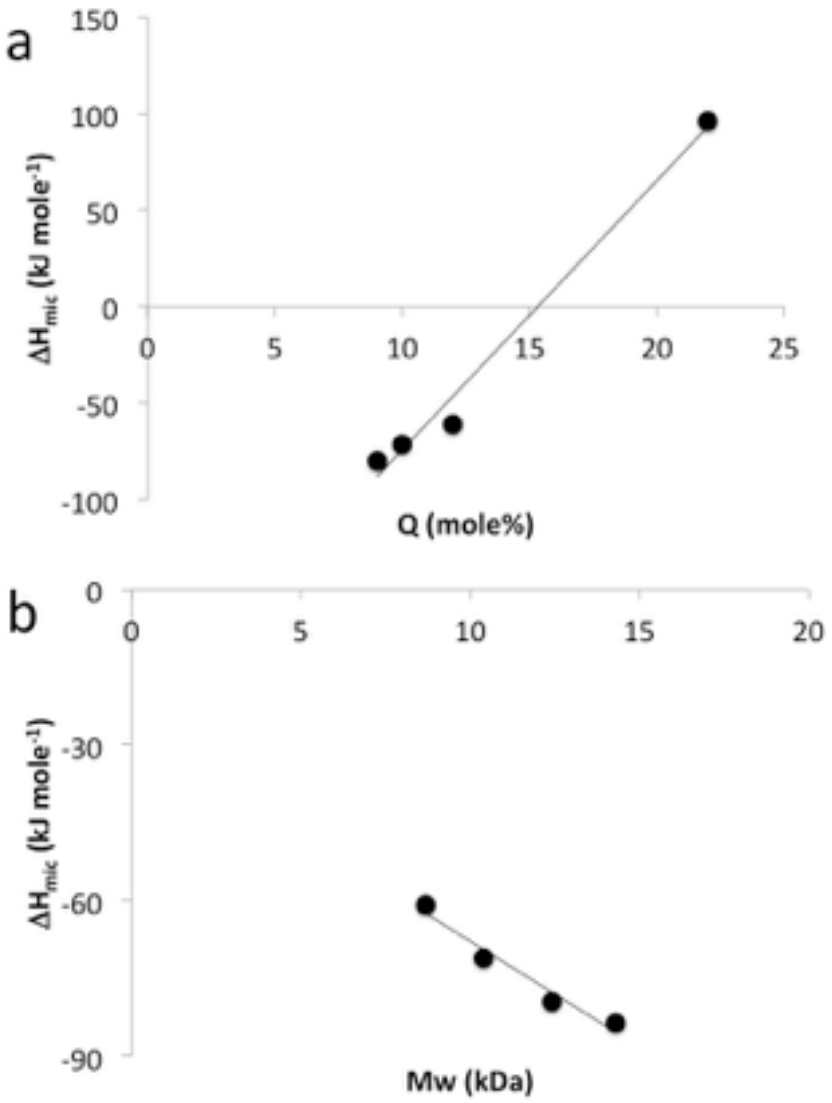

Figure 3-5: The influence of ΔH_{mic}: a) mole% quaternary ammonium groups (Q) within the 8 – 10 kDa polymers all with a palmitoylation (P) level of 19 mole% (ΔH_{mic} = 13.9Q -213, r^2 = 0.99) and b) molecular weight (Mw) within the polymers having a narrow range of Q (9 – 10 mole%) and P (12 – 19 mole %) substitutions (ΔH_{mic} = -4.1Mw – 27.0, r^2 = 0.96)..

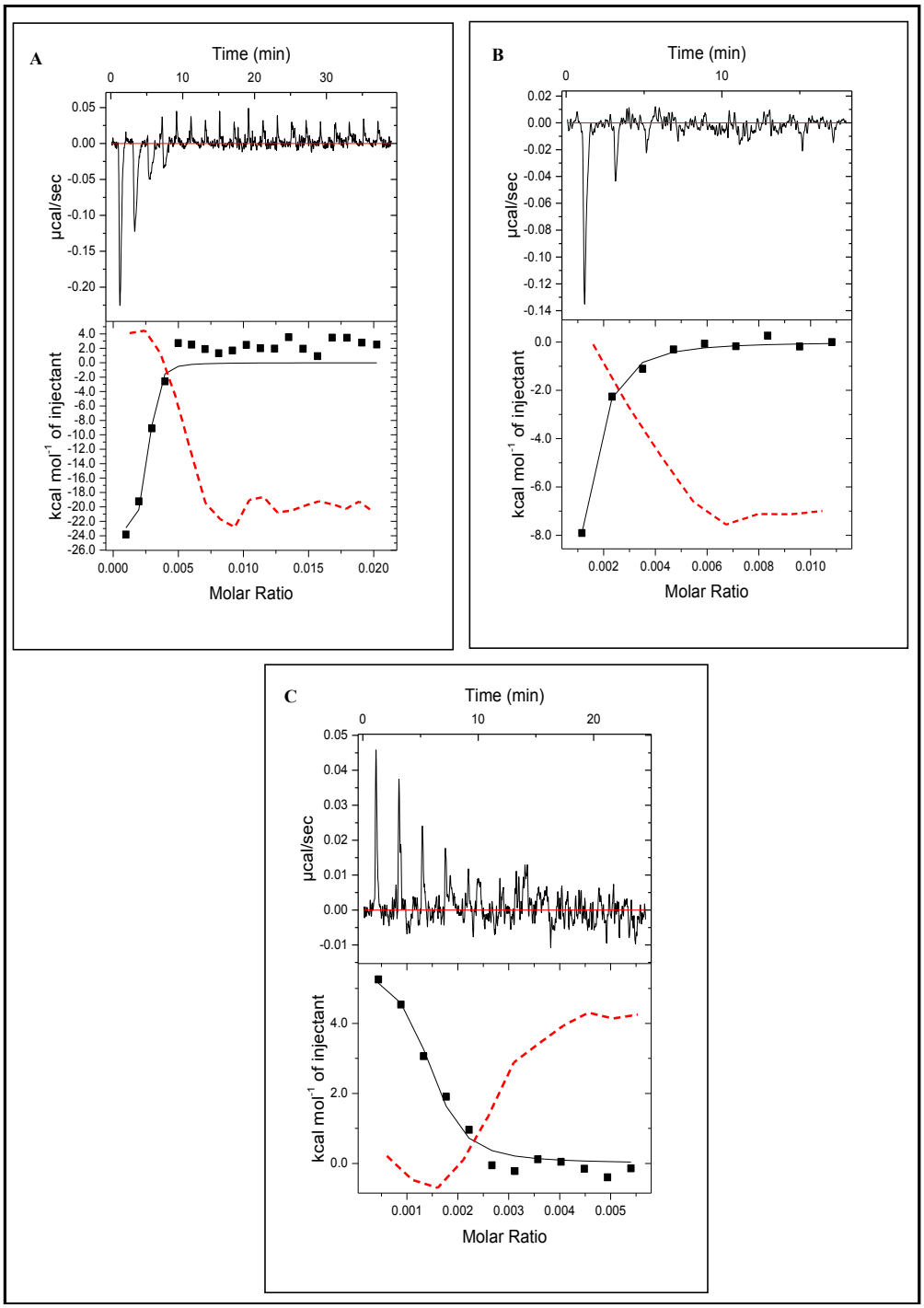

Figure 3-6: Data obtained from ITC experiments performed with GCPQ showing heat flow against time (top); enthalpy change per mole of GCPQ (bottom) and first derivative of enthalpy change per mole of GCPQ plotted against concentration (red dashed line). 2µL of GCPQ solution per injection into 200µL of water at 25ºC (298K). **A**. GCP20Q22. **B** .GCP10Q14. **C** GCP9Q36

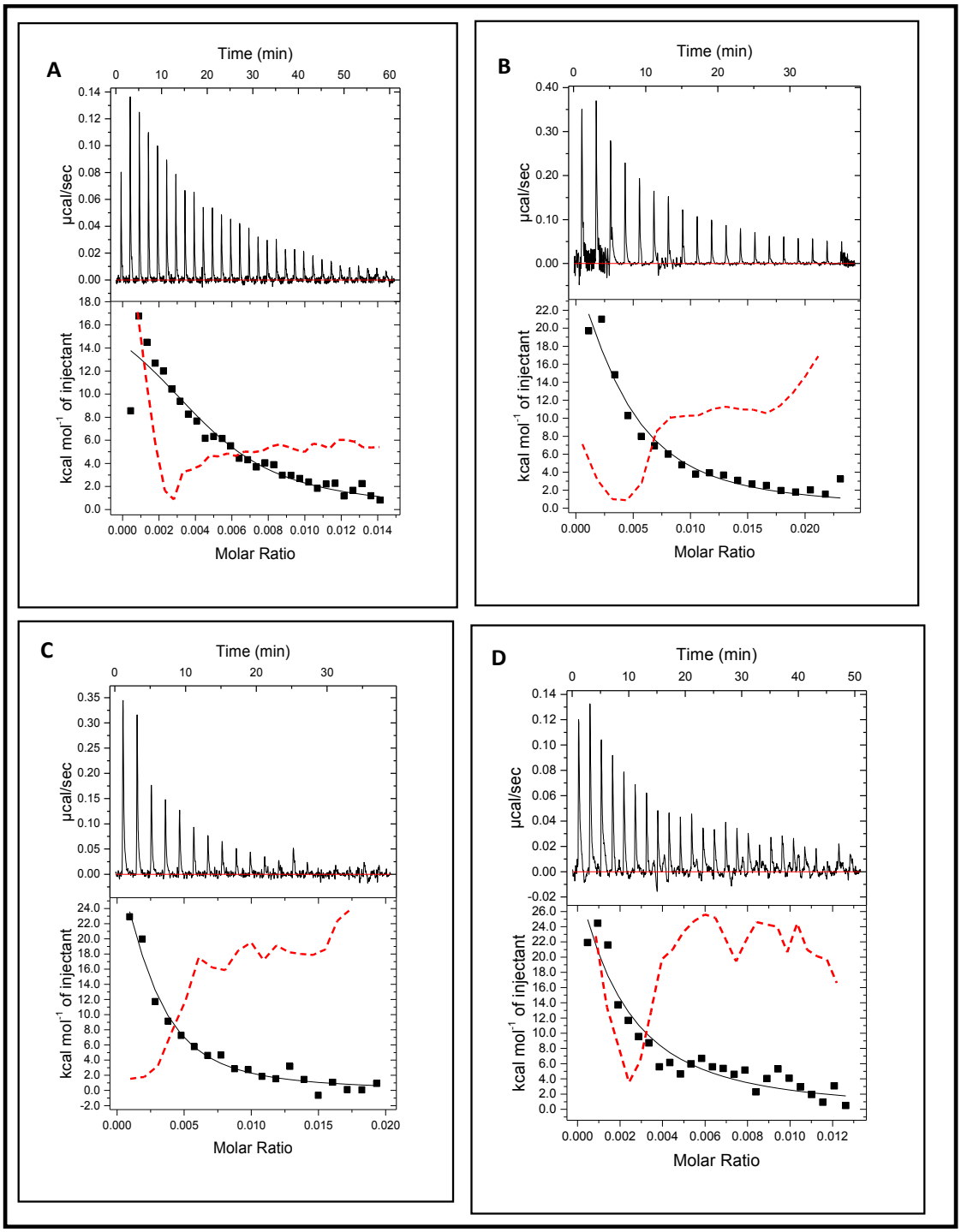

Figure 3-7: Data obtained from ITC experiments performed with GCPQ showing heat flow against time (top); enthalpy change per mole of GCPQ (bottom) and first derivative of enthalpy change per mole of GCPQ plotted against concentration (red dashed line). **A**. GCP19Q12 (298K). **B.** GCP19Q12 (308K) **C.** GCP19Q10. **D.** GCP19Q9.

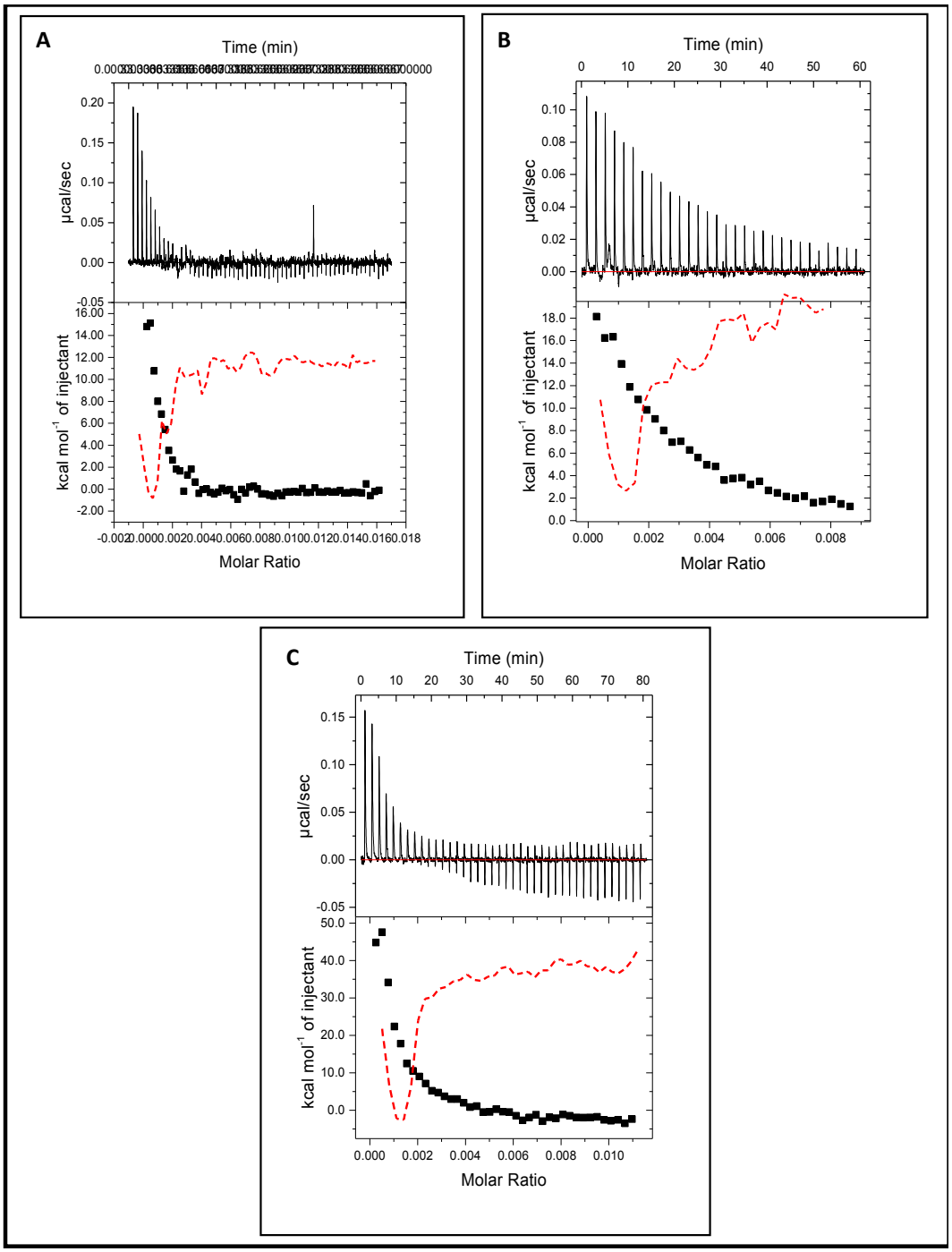

Figure 3-8: Data obtained from ITC experiments performed with GCPQ showing heat flow against time (top); enthalpy change per mole of GCPQ (bottom) and first derivative of enthalpy change per mole of GCPQ plotted against concentration (red dashed line). **A**. GCP12Q9 (298K). **B.** GCP12Q9 (288K) **C.** GCP4Q11

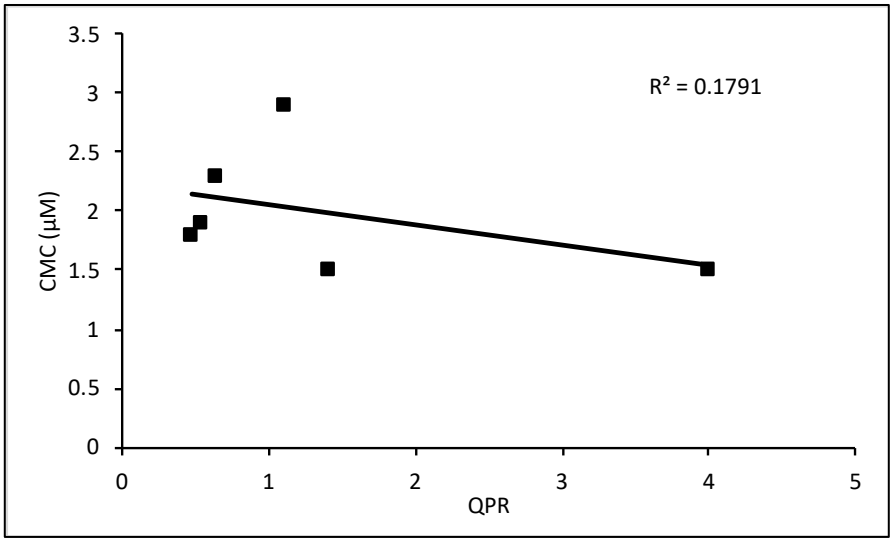

Figure 3-8. No correlation (R^2 =0.179) is seen between the critical micelle concentration and the QPR of GCPQ polymers

The micellization of all polymers is spontaneous as shown by the negative ΔG_{mic} values (Table 3-2) and the CMCs are in the very low micromolar range. The fact that we could measure heat flows in very dilute samples (< 1 μM) allowed us to capture the very early demicellisation events occurring in these polymers. The CMCs differ very little between all the polymers and we have not ruled out the possibility that with one of the polymers, the CMC may be below the limit of detection of the instrument as no plateau was observed on the first few injections with polymer GC8P10Q14 (Figure 3-6b).

However, there are some notable findings. On addition of an amphiphile to aqueous media, the initial transfer of the hydrophobic unit into the water phase results in the destruction of unrestricted hydrogen bonding by the water molecules, as a cavity is formed within which the hydrophobic moiety sits, with the water - hydrophobic moiety interface, akin to the water - vapour interface (Chandler, 2005a). The hydrophobic interactions, which drive self-

assembly, involve the transfer of the hydrophobic moiety from this water cavity to the interior of the micelle and the thermodynamics of this process are best described using the Gibbs Free energy equation (Equation 5). The hydrophobic cavity has water molecules unable to hydrogen bond freely in all directions (Tanford, 1980, Gill and Wadso, 1976, Kronberg et al., 1994). On self-assembly, the Gibbs free energy associated with the removal of the hydrophobic unit from the water phase to the interior of the micelle (ΔG_{mic}) is either driven by the positive change in entropy or the negative change in enthalpy. The micellization is entropy driven when the predominant free energy comes from the freeing of these water molecules from the cavity and their ability to hydrogen bond in all directions or is enthalpy driven when the freed water molecules form new bonds (including hydrogen bonds) (Chandler, 2005a, Gill and Wadso, 1976, Shimizu et al., 2004).

While the micellization events for the two of the more hydrophilic 8 – 12 kDa polymers (GC10P20Q22 and GC8P10Q14) are entropy driven, the micellization events of the more hydrophobic 8 – 12 kDa polymers (GC14P12Q9, GC9P19Q12, GC10P19Q10 and GC12P19Q9) are enthalpy driven. In essence the more hydrophilic 8 – 12 kDa polymers cause the freed water molecules to now enjoy additional hydrogen bonding opportunities and compensate for the entropy loss associated with GCPQ aggregation, whereas the more hydrophobic polymers suffer an entropy deficit (presumably due to aggregation of the hydrophobic polymer molecules) and an enthalpy gain associated with the formation of new hydrogen bonds by the water molecules freed from the hydrophobic cavity. It is conceivable that the more hydrophobic 8 – 12 kDa GCPQs (QPR $\leq$ 1.1) will have a higher surface area of hydrophobic content, when compared to the more hydrophilic GCPQs (QPR $\geq$ 1.4) and thus the water molecules within the hydrophobic cavity, prior to micellization, will have

fewer hydrogen bonds overall and once freed from the cavity will be able to make more stable hydrogen bonds thus contributing to the enthalpy gain seen. The formation of new hydrogen bonds on micellization is further supported by the fact that the enthalpy contribution increases as the polymers become more hydrophobic (Figure 3-5a) and increases as the polymer chains become longer (Figure 3-5b) as both an increase in hydrophobicity and an increase in molecular weight will result in the release of additional water molecules from the hydrophobic cavity on self-assembly. The heat capacity of demicellisation (Cp_{demic}) sheds more light on the competing influences of molecular weight and hydrophobicity on the demicellisation thermodynamics.

$$Cp_{demic} = \frac{d\ H_{demic}}{dT}$$ (Chooi et al., 2009)

The Cp_{demic} is linearly related to the exposure of hydrophobic surfaces to water during demicellisation and is derived from the change in the structure of water necessary to accommodate the hydrophobic unit, with the surface area of the hydrophobic faces reflected in the magnitude of the Cp_{demic} (Tanford, 1980, Gardiel et al., 2000, Costas et al., 1994). Comparing the Cp_{demic} values of GC14P12Q9 (Cp_{demic} = 2.09 KJ mole^{-1} K^{-1}) and GC9P19Q12 (Cp_{demic} = 1.59 KJ mole^{-1} K^{-1}) reveals that despite the higher hydrophobicity of GC9P19Q12 when compared to GC14P12Q9, there is not much difference in their Cp_{demic} values; i.e. a longer polymer with lower palmitoyl substitution exposes a similar hydrophobic surface area per mole as a shorter polymer with greater palmitoyl substitution. We deduce from this that molecular weight has a greater influence on the Cp_{demic} during demicellisation and in order to prepare stable aggregates an increase in molecular weight will have a greater contribution to improved stability than an increase in palmitoyl

substitution. We have earlier shown that polymer architecture has a profound influence on Cp_{demic} with star shaped amphiphiles (Chooi et al., 2010).

It has been reported that immobilised amine cations in close proximity to the hydrophobic units strengthen the hydrophobic interactions (Ma et al., 2015a) and since GCPQ comprises amine cations and hydrophobic units in close proximity to each other, we examined the effect of quaternary amine content on the thermodynamics of self-assembly. We would have expected to see a marked change in CMC as the polymers became more hydrophilic, however there is no correlation between CMC and QPR with the 8 – 12 kDa polymers (r^2 = 0.179, figure 3-8). There is good correlation (r^2 = 0.99) in the 8 – 12 kDa polymers between the level of quaternary ammonium groups (Q) and ΔH_{mic}, when the level of palmitoyl groups is fixed at 19 – 20 mole% (Figure 3a). This strong correlation between Q and ΔH_{mic}, when the palmitoyl units are fixed between 19 and 20 mole%, indicates that the quaternary ammonium groups are participating in the hydrophobic interactions occurring on micellization but as the Q increases the enthalpy contribution to micellization becomes less negative, indicating that hydrogen bond formation with the quaternary ammonium groups is not the source of the increase in the reaction's exothermic events. However, evidence that the presence of protonated amine groups in close proximity to the hydrophobic units could influence the hydrophobic bonds and self-assembly is seen in the polymers with high Q levels: polymer GC9P9Q36, where self-assembly is driven by a combination of entropy and enthalpy effects, and GC15P4Q11 where a strong enthalpy component drives the self-assembly. Both of these polymers have low CMCs.

This enthalpy driven micellization at room temperature is unusual as micellization is actually normally entropy driven at room temperature (Paula et al., 1995b, Chooi et al., 2010, Marsh, 2012), with a switch to being enthalpy driven as temperature rises (Chooi et al., 2010); the latter due to an increased level of disorder around the hydrophobic cavity at elevated temperature (Davis et al., 2012a), presumably as the molecules gain more kinetic energy as the temperature rises. We do observe an increase in the enthalpy change of micellization as the temperature rises as seen with GC9P19Q12, where ΔH_{mic} rises from -60.8 to -75.3 kJ $mole^{-1}$ as the temperature rises from 298 – 308 K and with GC14P12Q9 where ΔH_{mic} rises from -62.8 to -83.7 kJ $mole^{-1}$ as the temperature rises from 288 – 298 K, thus supporting the established explanation for the change in micellization thermodynamics with temperature and micellization is seen to increase as the temperature rises. Even when micellization is exothermic, the entropy contribution is hugely dominant and drives the self-assembly (Stodghill et al., 2004, Corkill et al., 1966).

Quite clearly the chemistry of these polymers is responsible for the unusual exothermic removal of the hydrophobic units from their water cavities. The quaternary ammonium groups may contribute to the exothermic nature of the micellization as even though the micellization of quaternary ammonium compounds is found to be mostly entropy driven, the demicellisation is endothermic and the micellization is exothermic (Tong et al., 2010). It is plausible that a reorganization of the molecules, as occurs with micellization, would offer an increased propensity for water molecules to hydrogen bond with the quaternary ammonium units as well as with each other, although this new water-amine bond formation does not drive the self-assembly. It appears as if the pendant nature of the hydrophobic

groups (resulting in a high surface area of hydrophobic units) is what contributes to the very low CMCs when compared to amphiphilic polymers of similar molecular weight (MW) such as the Pluronic block copolymers (Alexandridis et al., 1995) with P104 (MW = 5900 Da) having a CMC of 0.34 mM at 25°C and F108 (MW = 14,600 Da) having a CMC of 2.7 mM at 25°C.

3.3.2 Colloidal Stability of GCPQ polymer nanoparticles

The Fuchs factor is a measure of the stability of colloidal systems and is related to the number of collisions between particles that result in them sticking together. The double logarithmic plot of W against increasing salinity yields the CCC, which is W=1 and is indicative of the point of least stability (see figure 3-3). For some systems, there will be a second point, CSC where W begins to rise again with increasing salinity. This is indicative of restabilisation of the colloidal system (Santander-Ortega et al., 2010). The CCC gives information on the surface charge density and as a measure of stability, a colloidal system which has a low CCC has a low stability. The CSC gives information on hydrophilicity so that the restabilisation process is due to the structural barrier created by hydrated ions on the surface. Therefore, CSC increases as hydrophilicity decreases because there will be fewer hydrated ions on the surface of a hydrophobic system (Santander-Ortega et al., 2011).

Figure 3-9 shows a plot of the stability of GCP27Q11 in NaCl at different pH values while **Figure 3-10** shows a plot of the stability of GCP20Q14, a more hydrophilic polymer in $CaCl_2$ similar conditions. **Table 3-3** shows a summary of the stability parameters of both polymers. The stability plot for both polymers shows that the CSC was more defined and

further from the CCC, at higher pH than at lower pH, indicating that the systems become more hydrophobic at higher pH values. This is understandable, given that chitosan and most of its derivatives are known to become less soluble at near neutral pH values (Mucha, 1997, Szymańska and Winnicka, 2015). The more hydrophobic polymer, GCP27Q11 has a higher native pH value (5.35) than GCP20Q14 (4.9). GCP20Q14 was stable at its native pH value in NaCl while GCP27Q11 had a CCC value of 0.373M and a CSC value of 0.4M. Comparing both polymers in $CaCl_2$ at pH 7.4, GCP27Q11 has a lower CCC (0.15M) than GCP20Q14 (0.2M) but has a higher CSC (0.31M) than GCP20Q14 (0.29M). GCP20Q14 clearly has a lower pKa and is thus more hydrophilic and will have more surface charge density than GCP27Q11 at pH 7.4 and thus more hydrated ions at the same pH. It has a higher CCC, implying that it is more stable and it has a lower CSC implying that it is more hydrophilic than GCP27Q11.

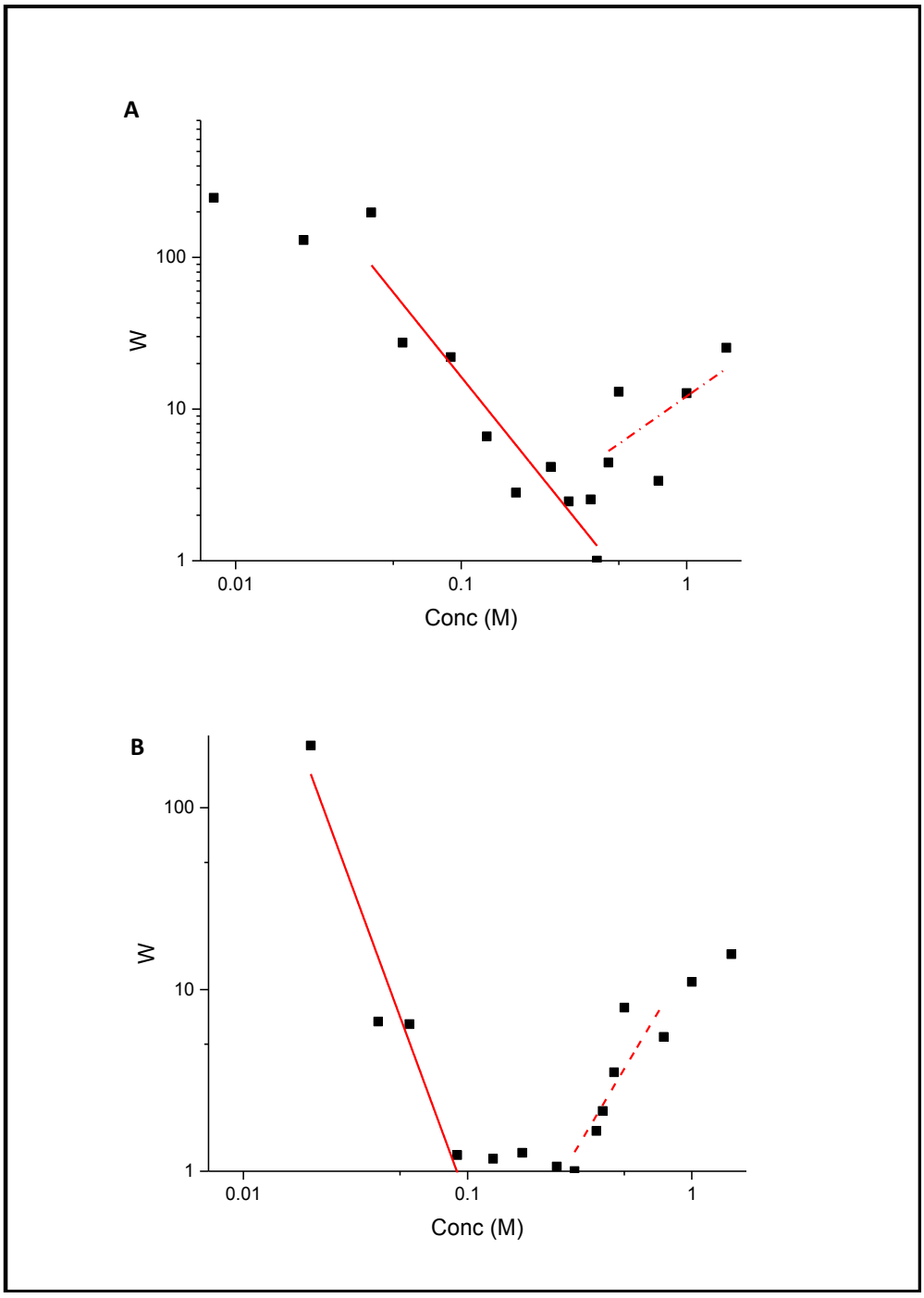

Figure 3-9: Plot of Fuchs factor (W) against concentration of NaCl showing stability of GCP27Q11 (1mg/ml) **A:** at pH 5.35 **B:** at pH 7.4. CCC values of the Polymer in NaCl were lower at pH 7.4 than at pH 5.35

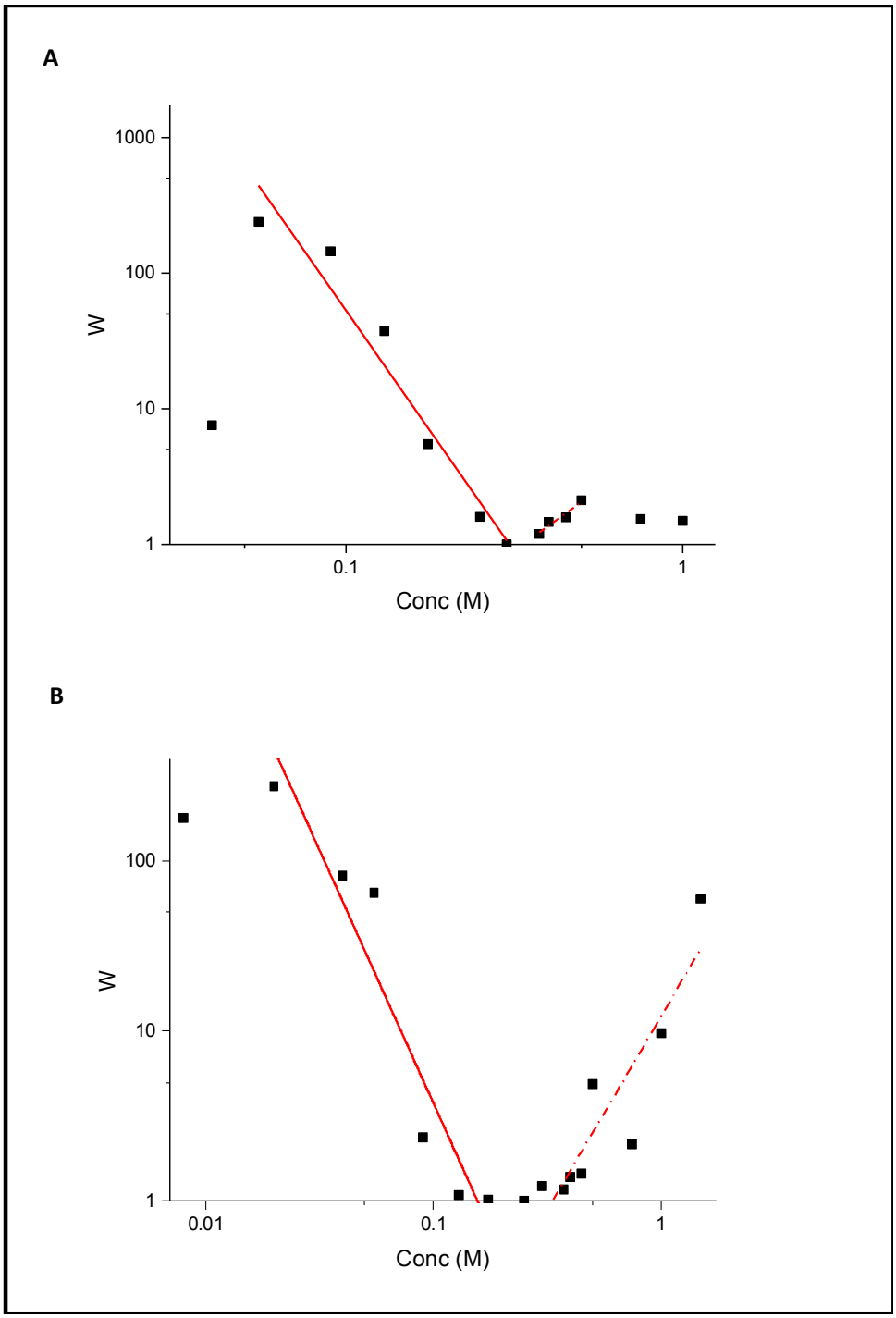

Figure 3-10: Plot of Fuchs factor (W) against concentration of $CaCl_2$ showing stability of GCP20Q14 (1mg/ml) **A:** at pH 4.9 **B:** at pH 7.4. CCC values are lower at pH 7.4 than at pH 4.9

Table 3-3 also shows that a higher concentration of GCP20Q11 (5mg/mL) at the native pH is more unstable than the 1mg/mL solution in $CaCl_2$ as it has a lower CCC (0.13M). This is understandable given that there will be 5 times more particle colliding with each other, hence an increased probability of a collision resulting in adhesion/aggregation. The CSC is lower (0.175M), however, because there is a higher concentration of hydrated ions owing to the larger number of ions coming from the polymer.

Table 3-3 CCC and CSC values of GCPQ polymers in different salt solutions at different pH.

Polymer	Concentration of polymer (mg/ml)	Salt	pH	CCC (M)	CSC (M)
GCP27Q11	1	$CaCl_2$	5.35	0.47	-
GCP27Q11	1	$CaCl_2$	7.4	0.15	0.31
GCP27Q11	1	NaCl	5.35	0.375	0.4
GCP27Q11	1	NaCl	7.4	0.3	-
GCP20Q14	1	$CaCl_2$	4.9	0.3	0.375
GCP20Q14	1	$CaCl_2$	7.4	0.2	0.29
GCP20Q14	5	$CaCl_2$	4.9	0.13	0.175

These results show that the DLVO theory can be used to explain the behaviour of GCPQ polymers having different structural modifications in different salt solutions and show that these polymers will behave differently depending on the nature of structural modification.

3.4 Conclusion

We have shown that the self-assembly of a group of amphiphilic chitosans is spontaneous and occurs at low micromolar concentration (1 – 2.4 μM at 25 °C) giving rise to highly stable aggregates. At room temperature, while aggregation is entropy driven for the more hydrophilic molecules, it is unusually enthalpy driven for the more hydrophobic group of chitosan amphiphiles. We attribute this unusual thermodynamic behaviour to the polymer architecture, which supports the formation of entropically unfavourable aggregates, but which releases water molecules from the hydrophobic cavity and allows these freed water molecules to form bonds with each other.

Structural modifications on GCPQ results in changes in physicochemical properties of the polymer. GCPQ can be engineered to form polymers that form more stable colloidal suspensions in different salt and pH environments. GCPQ can also be engineered to have a switch in aggregation kinetics from an entropy driven process to an enthalpy driven process while maintaining a similar Gibbs free energy of aggregation. These physicochemical differences can be exploited for targeted synthesis and for-purpose design of pharmaceutical formulations.

Chapter 4. Drug Encapsulation Studies

4.1 Introduction

Results obtained from the previous chapter show that GCPQ polymers undergo spontaneous aggregation in water to form particles or aggregates at very low single digit micromolar critical micelle concentrations (cmc). This very low cmc will likely imply that the formed micelles will remain stable even after significant dilution, for example after in vivo administration. The results also show that the kinetics of this aggregation changes when GCPQ is structurally modified to become more hydrophobic or more hydrophilic. Furthermore, stability studies showed that the level of structural modification affects the behaviour of the polymer aggregates and micelles in different pH and salt environments. These observations raise the question of how the formulation and stability of cargo - carrying nanoparticles formed using GCPQ polymers will be affected by structural modifications to the polymer. This chapter will attempt to answer this question by encapsulating different classes of drugs using GCPQ polymers with different degrees of structural modifications and examining their properties and stability profile. The drugs will be selected based on the Biopharmaceutical Classification System.

According to the Biopharmaceutical Classification System (BCS), drug substances are grouped into four classes: Class I which consists of substances that have high solubility and high permeability, Class II which consists of substances that have low solubility and high permeability, Class III which consists of substances that have high solubility and low

permeability as well as Class IV substance which have low solubility and low permeability (Lawrence et al., 2002). Classes II, III and IV are generally good candidates for drug delivery strategies aimed at enhancing solubility and/or permeability. The physicochemical properties of the drug candidates determine the type of approaches employed- where medicinal chemistry is unable to optimise solubility and/or permeability, formulation strategies are then employed. For example, the solubility of substances with ionisable groups can be enhanced by pH adjustments or salt formation while lipid-based formulations can be used to solubilise very lipophilic substances. Nanoparticles provide advanced opportunities to address some of these challenges, in particular, for hydrophobic compounds, where the solubility of the drug candidate is increased- that is, the amount that can be given in an aqueous volume, albeit in a colloidal suspension or dispersion. Polymeric nanoparticles have become an increasingly studied system being employed in the formulation of a wide range of drug substances intended for different delivery routes because of some of the benefits that they offer including biocompatibility, biodegradability, small sizes, tuneable surface properties, ubiquity in application protection against degradation and enhanced bioavailability (Kumari et al., 2010).

The choice of drug encapsulation strategy and polymers to be used must be made with consideration to the properties of the final formulation. Factors like the size of the nanoparticle, the shape and the charge of the formulation influence the behaviour of the formulation. Studies have shown that particles with sizes about 100nm have longer circulation half-lives and sub 100nm nanoparticles penetrate well into highly penetrable tumours (Cabral et al., 2011) while particles larger than 100nm are accumulated non-specifically in the liver. Particles less than 5nm in size are rapidly cleared by the kidney

(Choi et al., 2007) while particles greater than 200nm trend to be retained by the spleen (Chen and Weiss, 1973). The shape of the nanoparticles is also reported to influence the hemorheological behaviour, cellular uptake and in-vivo fate of the nanoparticle (Blanco et al., 2015). As an example, filamentous micelles are reported to have higher circulation half-lives than spherical micelles, owing partly to rate of clearance and uptake by phagocytes. The filamentous micelles tend to align themselves with blood flow, the shear of which pulls them away from phagocytic cells, keeping them longer in circulation (Geng et al., 2007).

The shape and size of the formulation is usually dependent on the nature of the polymer used and the method employed. Here, we use GCPQ to encapsulate cyclosporine A, a BCS class II drug and paclitaxel, a BCS class IV drug. We examine the effect of GCPQ structural modifications on the shape, size and encapsulation efficiency of these drugs with a view to achieving an optimal formulation for oral delivery of these drugs.

4.2 Materials and Methods

Most chemicals and reagents used were purchased from Fischer Scientifics UK Ltd and Sigma Aldrich Chemical Company unless otherwise stated.

Reagents and solvents: Paclitaxel (Cambridge Biosciences, Cambridge, UK), Cyclosporine A (Sigma-Aldridge, Sigma, UK) Deionized water, Milli-pore double deionized water (<18Ω), Methanol HPLC gradient, Glycerol, Absolute Ethanol, Acetone, uranyl acetate.

Equipment: MSE soniprep 150 sonicator (MSE UK Ltd), Zetasizer Nano S90, Malvern, UK Transmission Electron Microscopy (TEM), Philips CM 120, Biotwin NMR, Bruker Avance

400, vortex, Agilent 1220 infinity chromatographic system, Agilent Technologies 1200 series chromatographic system fitted with a vacuum degasser, quaternary pump, standard and preparative auto-sampler, column compartment with a thermostat and a UV detector, onyx monolithic CS18 column (100 x 4.6 mm; particle size, 5µm).

4.2.1 Encapsulation of Paclitaxel

A dried film hydration method was used to encapsulate paclitaxel with GCPQ. This method was adapted from previously reported methods used in the encapsulation of the hydrophobic compound, curcumin (Sahu et al., 2011) and modified for paclitaxel and the specific GCPQ polymers used. Encapsulation efficiency and drug loading were also determined based on previously reported methods (Sahu et al., 2011, Kakde et al., 2016). The steps involved in this synthesis is outlined below:

10 mg of Paclitaxel powder (Generon, Slough, UK) was weighed into a glass vial and dissolved in 2 mL absolute ethanol to make 5 mg/mL solutions. 20 mg of different GCPQ polymers was weighed in glass vials and dissolved in 1 mL of deionised water to make 20 mg/mL solution. 0.4 mL of GCPQ solution was transferred into a 1.5 mL Eppendorf and 0.2 mL of paclitaxel solution added for a ratio of 5: 1 of GCPQ to paclitaxel. The mixture was vortexed for 1 minute and the Eppendorf tubes were then placed in a Savant SPD131DDA vacuum evaporator (Thermo Scientific) at 45° C and spun under vacuum for 2 hours until a dry film was formed.

The film was then rehydrated by adding 1mL of deionized water and the mixture vortexed for about 5 minutes to disperse the film fully in water. The mixture was subsequently sonicated using an MSE soniprep 150 sonicator (MSE UK Ltd) at 8 amplitude microns for

20 minutes in an ice bath. The mixture was subsequently filtered through a 0.45 μm filter and encapsulation efficiency determined using an Agilent HPLC.

4.2.2 **Encapsulation of cyclosporine A**

GCPQ-Cyclosporine A formulation was prepared using a method developed by Dr. Lorenzo Capretto in the lab (unpublished). 1% glycerol in deionised water was prepared by adding 100μL of glycerol into 12mLs of deionised water. This glycerol solution was used to prepare 7.5 mg/mL of GCPQ by dissolving 15 mg of GCPQ in 2 mL of glycerol solution. 2 mg of Cyclosporine A was weighed into a glass vial and 2mLs of the prepared GCPQ solution was used to disperse cyclosporine A. The mixture was subsequently sonicated using an MSE soniprep 150 sonicator (MSE UK Ltd) at 8 amplitude microns for 20 minutes in an ice bath. After sonication, the mixture was placed in the fridge at 4^{o}C overnight. On the following day, the mixture was filtered using a 0.22μm filter and prepared for HPLC analysis. This method was originally used to formulate cyclosporine A application in the eye, hence the use of 1% glycerol as an osmotic agent. Glycerol was retained in this formulation because it was observed that it improved the encapsulation efficiency and stability of the formulation.

4.2.3 **Characterisation of Drug Formulations**

Encapsulation efficiency (EE), more specifically, the percentage of drug content in the colloidal fraction and drug loading (DL) were determined by HPLC analysis using an onyx monolithic CS18 column (100 x 4.6 mm; particle size, 5μm) for both compounds and calculated using the formula:

$$EE\ (\%) = \frac{colloidal\ drug\ content}{theoretical\ drug\ content} \times 100\%$$

$$DL\ (\%) = \frac{mass\ of\ colloidal\ drug\ content}{mass\ of\ polymer + drug} \times 100\%$$

HPLC Method Development

For Paclitaxel, an isocratic method was developed using a mobile phase consisting of acetonitrile: water (1:1), a flow rate of 1.5 mL min^{-1} and a run time of 8 minutes. Column temperature was maintained at 40°C and absorption monitored at 227 nm. Retention time of paclitaxel was 2.1 minutes. A standard curve was prepared using paclitaxel concentrations ranging from 0.1 to 100µg/mL in mobile phase ($y = 8.5785x + 3.6749$, $R^2 = 0.99996$). 100 µL of prepared paclitaxel formulations were diluted with 300µL of methanol to make a 1:3 dilution and vortexed prior to sample injection. 10 µL of each sample was injected and paclitaxel concentration determined from the standard curve.

For cyclosporine A, an isocratic method was developed using a mobile phase consisting of acetonitrile: water (1:1), a flow rate of 1.1 mL min^{-1} and a run time of 10.5 minutes. Column temperature was maintained at 40 °C and absorption monitored at 220 nm. Retention time of cyclosporine A was 3.6 minutes. A standard curve was prepared using cyclosporine A concentrations ranging from 4 to 2000µg/mL in methanol ($y = 27.196x + 601.81$, $R^2 = 0.99888$). 100µL of prepared cyclosporine A formulations were diluted with 300µL of the methanol to make a 1:3 dilution and vortexed prior to sample injection. 10µL of each sample

was injected and cyclosporine concentration determined from the standard curve.

The particle size and size distribution of the formulations were determined by Dynamic light scattering measurements made on the fixed scattering angle Zetasizer Nano-S system (Malvern Instruments Ltd., Malvern, UK). Samples were measured in a 200 µL quartz cuvette at 25.0 ºC and the light scattering was detected at 173 º and collected in automatic mode, typically requiring a measurement duration of 150 seconds. The resulting data were analysed using the "DTS (Version 4.2)" software (Malvern Instruments Ltd., Malvern, UK).

Transmission Electron Microscopy (TEM) was carried out using the Philips/FEI CM120 Bio Twin (Philips, Netherlands). Samples were prepared by drying a drop of the formulation on a copper TEM grid - a 300mesh-fomvar/carbon coated- and staining with a drop of uranyl acetate (1% w/v). The dried samples were then imaged under the microscope.

GCPQ formulations having different levels of DP and DQ were used for the formulations and are shown in Table 4.1

Table 4-1: Size and zeta potential of GCPQ nanoparticles used for drug encapsulation

Polymers	polymers	Z-ave (d.nm)	PDI	Zeta pot. (ζ)	QPR
GCPQ05	GC12P19Q9	72.74±4.95	0.53±0.01	49.73±1.50	0.47
GCPQ10	GCxP37Q23	47.45±0.92	0.48±0.01	50.13±0.80	0.62
GCPQ03	GC9P19Q12	45.71±1.32	0.45±0.02	36.47±1.21	0.63
GCPQ06	GC10P20Q22	50.40±2.48	0.38±0.03	49.43±1.67	1.10

4.3 Results and Discussion

4.3.1 Results

GCPQ – Paclitaxel formulations

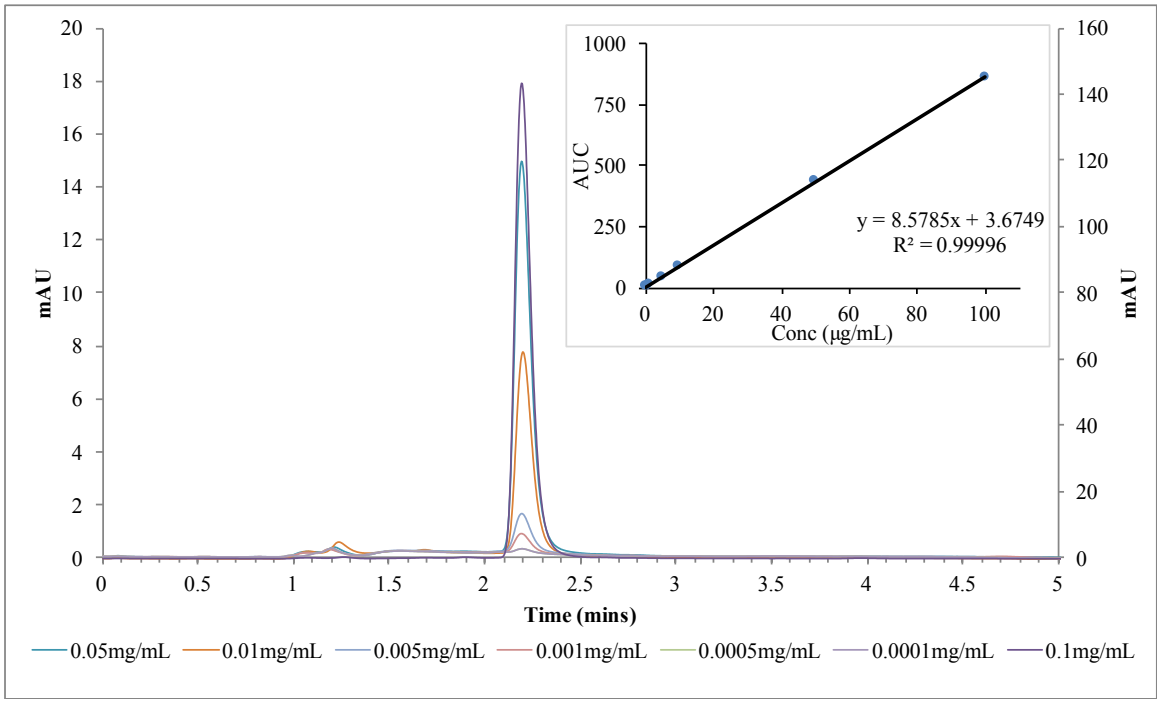

Figure 4-1: HPLC chromatogram for paclitaxel standard solutions with acetonitrile :water (50:50) as the mobile phase. Inset: standard curve plotted from the AUC values obtained from the chromatogram

The HPLC chromatogram shows a retention time of 2.3 minutes with a solvent front at 1.2 minutes. The standard curve plotted from this chromatogram shows good linearity with a correlation coefficient of 0.99996. The equation of the standard curve was used to determine the concentration of encapsulated paclitaxel in GCPQ-paclitaxel formulations and thus determine the EE and DL which are shown in Table 4.2. To determine the concentration of paclitaxel in formulations, the formula below was used:

$$conc\ (\mu g/mL) = \frac{AUC - 3.6746}{8.5785}$$

Table 4-2: Table showing encapsulation efficiency (EE%) and Drug Loading (DL%) of GCPQ-Paclitaxel formulations

Formulation	GCPQ	Z-average±SD (nm)	PDI±SD	EE(%)	DL(%)
GCPQ03+PTXL	GCP19Q12	156.6±1.64	0.12±0.05	56.70±3.5	9.50±0.58
GCPQ06+PTXL	GCP20Q22	158.5±1.16	0.10±0.01	96.63±5.27	16.11±0.88
GCPQ10+PTXL	GCP37Q23	327.8±51.77	0.47±0.06	99.81±3.12	16.64±0.52
GCPQ14+PTXL	GCP29Q11	196.5±1.45	0.17±0.02	53.40±1.95	8.90±0.33

GCPQ-paclitaxel (GCPQ+PTX) formulations were prepared with a starting concentration of 2mg/mL of paclitaxel to 10mg/mL of GCPQ. The encapsulation efficiency was determined after excluding unencapsulated paclitaxel using a 0.45 μm filter. The encapsulated paclitaxel was then quantified using HPLC after breaking up the micelle in methanol to free up all encapsulated paclitaxel. The results shown in table 4-2 indicate that encapsulation of paclitaxel was higher for polymers with DQ greater than 20%, with GCPQ06 and GCPQ10 both having encapsulation efficiencies of 96.63±5.27% and 99.81±3.12% respectively which is much higher than the 56.70±3.5% and 53.40±1.95% obtained with GCPQ03 (GCP19Q12) and GCPQ14 (GCP29Q11). GCPQ03 and GCPQ14 both have similar DQ but very different DP and have similar encapsulation efficiency (EE%) while GCPQ06 and GCPQ10 have similar DQ but much different DP and also have similar EE%.

Given the fact that paclitaxel is hydrophobic, it was expected that the more hydrophobic polymers will solubilise a higher amount of paclitaxel than the more hydrophilic polymers, making these results unexpected. To gain a better understanding of this observation, the formulations were further characterised using other techniques. The size of the formulations was determined as shown below:

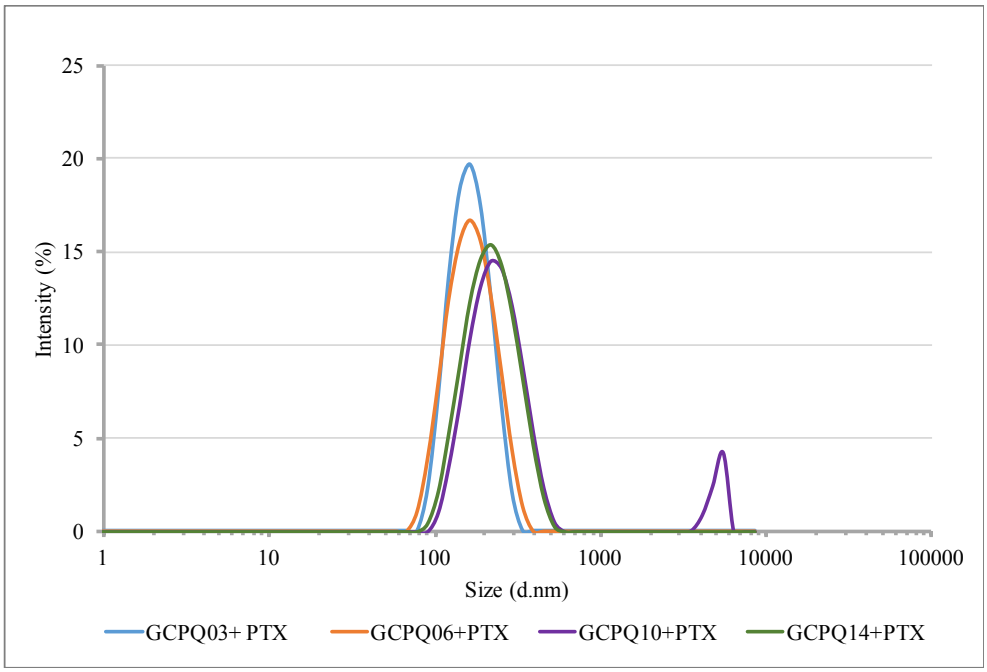

Figure 4-2: Size distribution of GCPQ-Paclitaxel formulations measured by Dynamic Light Scattering

GCPQ-paclitaxel formulations are larger in size than the nanoparticles formed by the naked GCPQ polymers. GCPQ03, GCPQ06 and GCPQ10 paclitaxel formulations have Z-average values of 156.6±1.64nm, 158.5±1.16nm and 327.8±51.77nm respectively (Table 4-2) while

the Z-average values of their naked nanoparticles are: 45.71±1.32nm, 50.40±2.48 and 47.45±0.92nm respectively (Table 4-1). The size distribution graph shown in figure 4-3 shows that the formulations were mostly monomodal except GCPQ10-PTX which had a large peak greater than 1000nm. It is interesting to observe however, that the particles formed from the formulation of different GCPQ polymers and paclitaxel have very similar size distribution. The size distribution data alone therefore doesn't explain the relatively higher EE observed with the very hydrophilic polymer formulation- GCPQ06+PTX compared with some of the more hydrophobic polymer formulations.

To further examine the characteristics of these formulations, electron microscopy was used to observe the morphology of the nanoparticles formed using different GCPQ polymers:

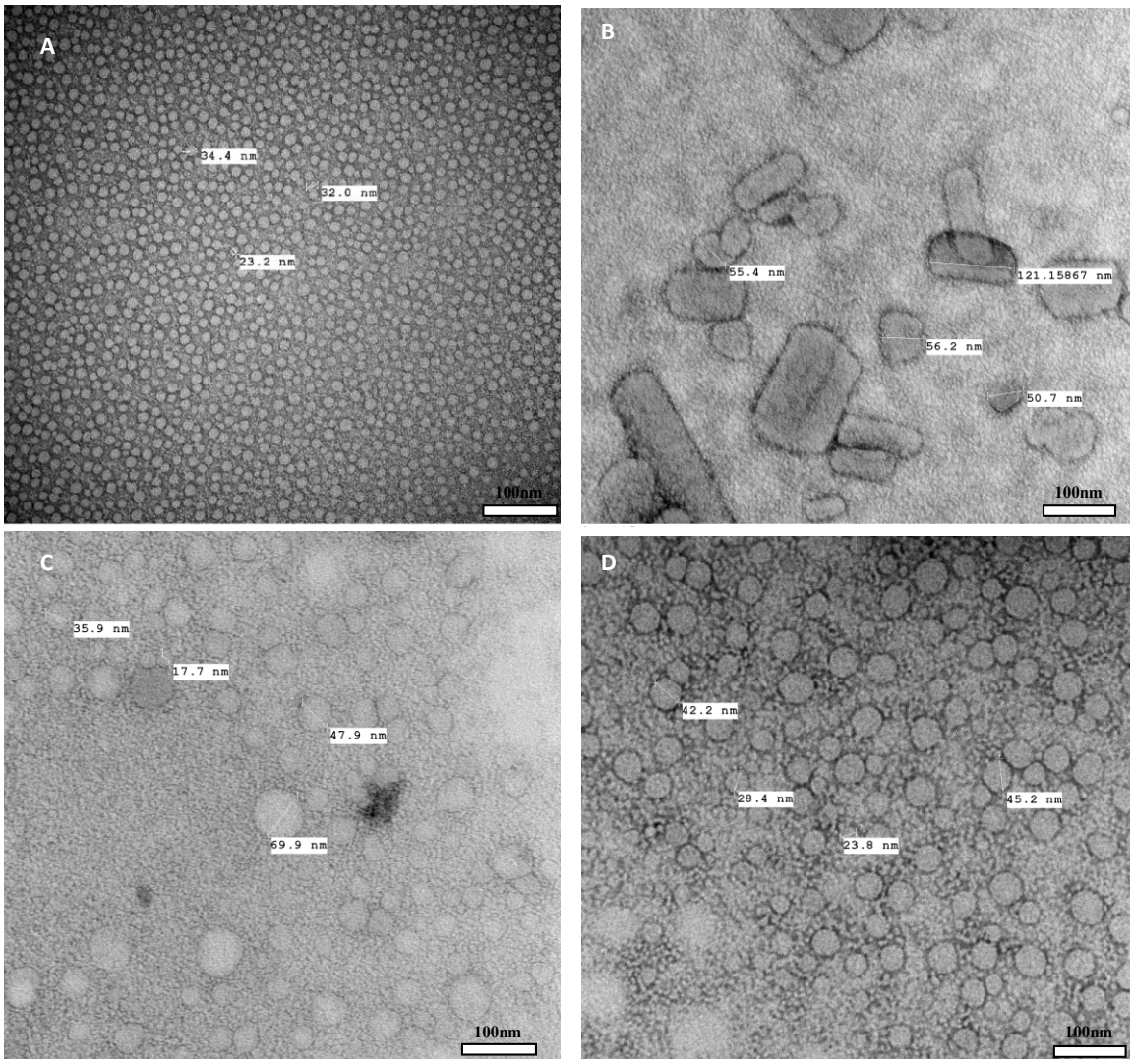

Figure 4-3: Transmission Electron Microscopy (TEM) image of GCPQ-Paclitaxel formulations showing. A. naked GCPQ 06 micelles B. GCPQ06+PTX nanocrystals C. GCPQ10+PTX micelles D. GCPQ14+PTX micelles.

Figure 4-3 shows that GCPQ+PTX formulations form larger spherical or rod-shaped vesicles which expectedly contains the encapsulated paclitaxel. In comparison with the size distribution and z-average values obtained using dynamic light scattering, the TEM images, which were taken using dried samples, suggest that the nanoparticles aggregate to form larger vesicles when in aqueous environments. It is also noteworthy that structural modifications of GCPQ resulted in formulations with different morphology- spherical and rod shaped (crystals). GCPQ06 which is the most hydrophilic polymer, having a ratio of quaternary ammonium to palmitoyl group (QPR) greater than 1 (see Table 4-1) formed large nanocrystals. While the other polymers, all having QPR less than 1 formed spherical vesicles. Also, it can be seen that GCPQ10+PTX formed larger, more heterogenous micelles than GCPQ14+PTX which appear more homogenous.

Table 4-3 and Figure 4-4 show the changes in size distribution and size parameters of GCPQ-paclitaxel formulations after storage in 4 ^{o}C for 28 days. The size distribution graphs show a narrowing of the size peaks and a general decrease in sizes of the formulations. Compared with the size data in table 4-3, GCPQ03+PTX had a slight increase in z-average size while the other formulations showed a slight decrease in z-average size. GCPQ03+PTX increased from about 157 nm to about 170 nm, an increase of about 8 %, GCPQ06+PTX stayed fairly similar with little no real decrease, GCPQ10+PTX decreased from about 328 nm to about 178 nm, a decrease of about 46 %, but which is likely attributable to a loss of the small population of very large sized particle (likely debris) as shown in the size distribution graphs on figure 4-5. GCPQ14 +PTX decreased from about 197 nm to about 180 nm, a decrease of

about 9 %. Generally, over a 28-day period, the data suggests GCPQ-PTX stayed stable when stored at 4 º C.

Table 4-3: Changes in size distribution of GCPQ-paclitaxel formulations over 28days

		Day1		Day 28	
Formulation	**GCPQ**	**Z-average±SD (nm)**	**PDI±SD**	**Z-average±SD (nm)**	**PDI±SD**
GCPQ03+PTXL	GCPQ03	156.6±1.64	0.12±0.05	171.07±1.60	0.09±0.024
GCPQ06+PTXL	GCPQ06	158.5±1.16	0.10±0.01	156.63±2.38	0.11±0.003
GCPQ10+PTXL	GCPQ10	327.8±51.77	0.47±0.06	178.57±0.35	0.06±0.003
GCPQ14+PTXL	GCPQ14	196.5±1.45	0.17±0.02	180.17±1.80	0.05±0.045

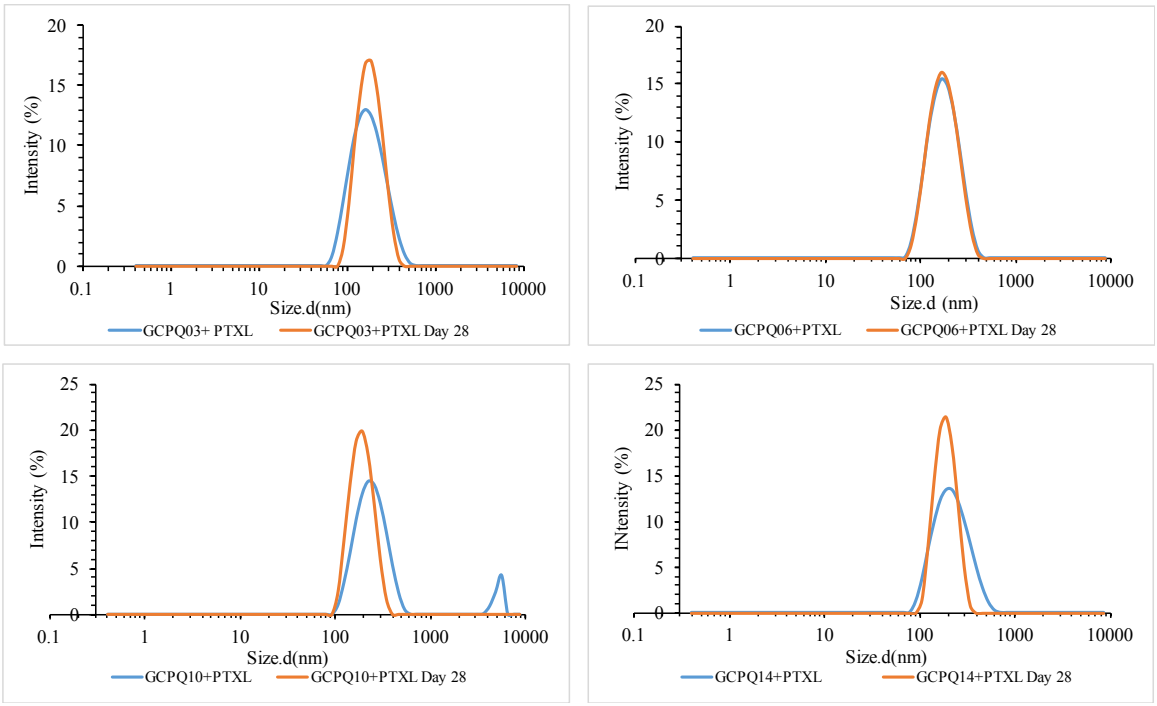

Figure 4-4: Size distribution of GCPQ paclitaxel formulations which were stored at 4ºC, 28 days after formulation compared with day 1 of the formulation.

GCPQ- Cyclosporine A formulations

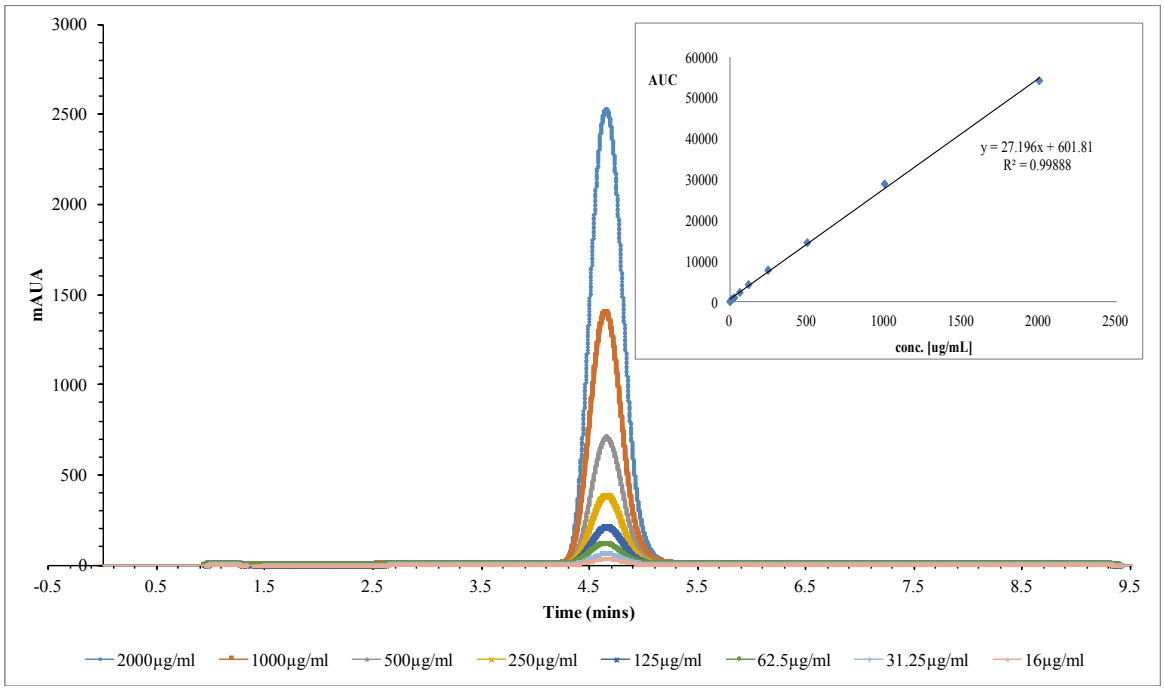

Figure 4-5: HPLC chromatogram, for cyclosporine A and calibration curve (inset) obtained from HPLC chromatogram in acetonitrile : water (50:50)

The HPLC chromatogram shows a retention time of 4.6 minutes and the standard curve plotted from this chromatogram shows a correlation coefficient of 0.99888. The equation of the standard curve was used to determine the concentration of encapsulated cyclosporine A in GCPQ-cyclosporine A formulations and thus determine the EE and DL which are shown in Table 4.3. To determine the concentration of cyclosporine A in formulations, the formula below was used:

$$conc\ (\mu g/mL) = \frac{AUC - 601.81}{27.196}$$

Table 4-4 shows the encapsulation efficiency of GCPQ-cyclosporine A formulations, % drug loading as well as the size parameters of the formulations. GCPQ05 (GCP19Q9) which has the lowest QPR (0.47) had the highest encapsulation efficiency of about 100%. GCPQ03 (GCP19Q12) and GCPQ10 (GCP37Q22), both with similar QPR of 0.63 and 0.62 respectively had similar encapsulation efficiency of about 84 %. GCPQ06 (GCP20Q22) with the highest QPR of 1.1 had the lowest encapsulation efficiency of about 69%. These values show that the more hydrophobic polymers were better for encapsulating cyclosporine A.

Table 4-4: Table showing Encapsulation efficiency (EE%) and Drug Loading (DL%) of GCPQ-cyclosporine formulations. Formulations prepared with GCPQ polymers having a low QPR ratio have higher encapsulation efficiency.

Formulation	GCPQ	QPR	Z-average±SD (nm)	PDI±SD	EE(%)	DL(%)
GCPQ03+CYS A	GCP19Q12	0.63	159.7±13.66	0.54±0.16	83.86±1.43	9.87±0.17
GCPQ05+CYS A	GCP19Q09	0.47	339.4±17.39	0.14±0.06	106.77±1.94	12.56±0.23
GCPQ06+CYS A	GCP20Q22	1.1	158.2±95.96	0.58±0.25	68.99±1.58	8.12±0.19
GCPQ10+CYS A	GCP37Q23	0.62	93.32±2.80	0.72±0.05	84.79±1.50	9.98±0.18

The size parameters of these formulations were determined using dynamic light scattering and are shown below:

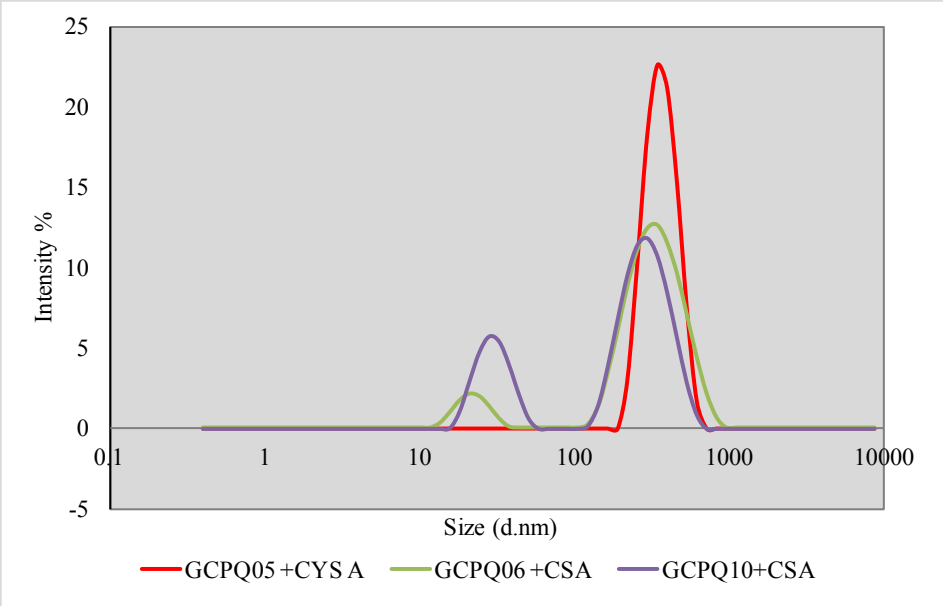

Figure 4-6: Size distribution of GCPQ-Cyclosporine formulations measured by Dynamic Light Scattering (DLS)

Figure 4-6 shows the size distribution of GCPQ-Cyclosporine A formulations. The size parameters are shown in table 4-4. The more hydrophobic polymer, GCPQ05 (GCP19Q9) with the lowest QPR of 0.47 formed particles which have a monomodal distribution and a larger mean size of about 300 nm. The more hydrophilic polymers formed particles with two distinct populations around 50 nm and 200 nm. These observations indicate a greater contribution of hydrophobic forces in the more hydrophobic polymers resulting in greater encapsulation efficiency and a more homogenous aggregation profile.

To further examine the morphology of the particles formed from the formulation, transmission emission microscopy images were taken of the formulations and compared with the naked GCPQ nanoparticle:

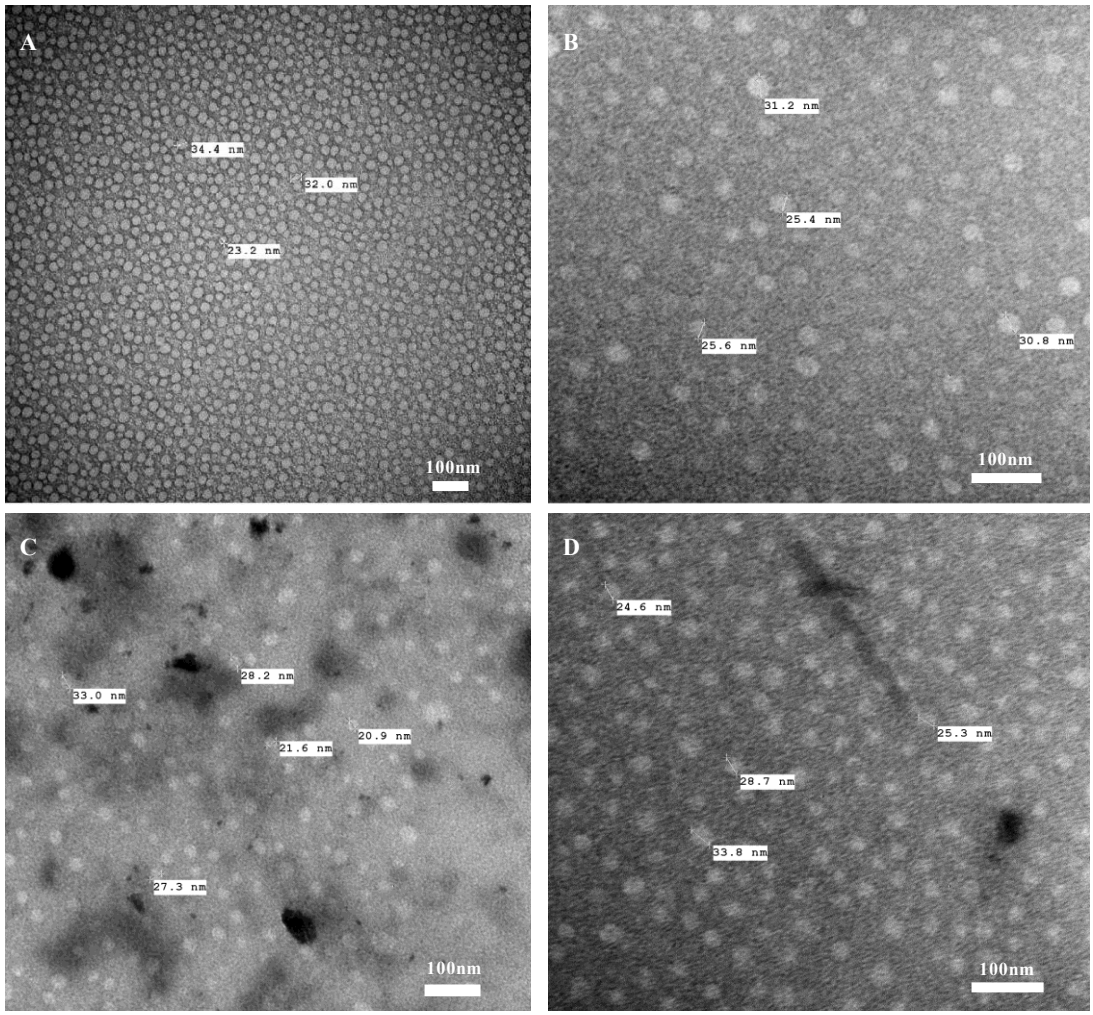

Figure 4-7: Transmission Electron Microscopy (TEM) image of GCPQ-cyclosporine A (GCPQ-CYS A) formulations showing. A. naked GCPQ 06 micelles B. GCPQ06-CYS A nanoparticles C. GCPQ05-CYS A nanoparticles D. GCPQ10-CYS A nanoparticles

Figure 4-7 shows the transmission electron microscope images of GCPQ-cyclosporine A formulations. The particles formed are mostly of similar sizes, around 30 nm and mostly comparable with the naked particles formed by the GCPQ polymers. This image shows that the larger sizes shown in table 4-4 are probably indicative of aggregation of the nanoparticles, with the more hydrophobic polymer prone to more aggregation, thus having a larger size.

Table 4-5: Table showing encapsulation efficiency of GCPQ-cyclosporine A formulations preserved at 4^{o}C decrease over a 1year period

DAYS	GCPQ03+CYS A	GCPQ05+CYS A	GCPQ06+CYS A	GCPQ10+CYS A
1	83.86±1.43	106.77±1.94	68.99±1.58	84.79±1.50
10	78.03±0.21	94.57±0.44	71.35±0.19	81.63±0.44
15	75.41±0.04	90.91±0.20	65.59±1.04	86.95±0.73
325	74.22±0.05	105.09±0.43	75.77±0.05	95.30±0.00
374	67.87±0.03	84.83±0.29	54.18±0.00	76.45±0.01
377	63.48±1.74	82.84±0.45	52.58±2.68	73.09±0.69

Table 4-5 shows the changes in encapsulation efficiency of GCPQ- cyclosporine A formulations over a 1-year period. GCPQ03-CYS A decreased from about 84 % to about 63 %, a decline of about 25%. GCPQ05+CYS A decreased by about 20 %, GCPQ06+CYS A decreased from about 69 % to about 53 %, a decrease of about 23 % while GCPQ10+CYS A decreased from about 85 % to about 73 %, a decrease of about 16 %. These results show that GCPQ10 which had the highest level of palmitoyl group substitution offered superior protection to the encapsulated cyclosporine A over a long period. Also, even though GCPQ05 which is the most hydrophobic polymer retained the highest amount of cyclosporine A, it still had a similar stability profile compared with the other more hydrophilic polymers.

Table 4-6: Size distribution of GCPQ-cyclosporine A formulations preserved at 4°C after 11months

		Day 1		Month 11	
Formulation	**GCPQ**	**Z-average±SD (nm)**	**PDI±SD**	**Z-average±SD (nm)**	**PDI±SD**
GCPQ03+CYS A	GCP19Q12	159.7±13.66	0.54±0.16	ND	ND
GCPQ05+CYS A	GCP19Q09	339.4±17.39	0.14±0.06	247.23±3.53	0.24±0.01
GCPQ06+CYS A	GCP20Q22	158.2±95.96	0.58±0.25	97.54±53.34	0.50±0.22
GCPQ10+CYS A	GCP37Q23	93.32±2.80	0.72±0.05	53.27±1.36	0.53±0.01

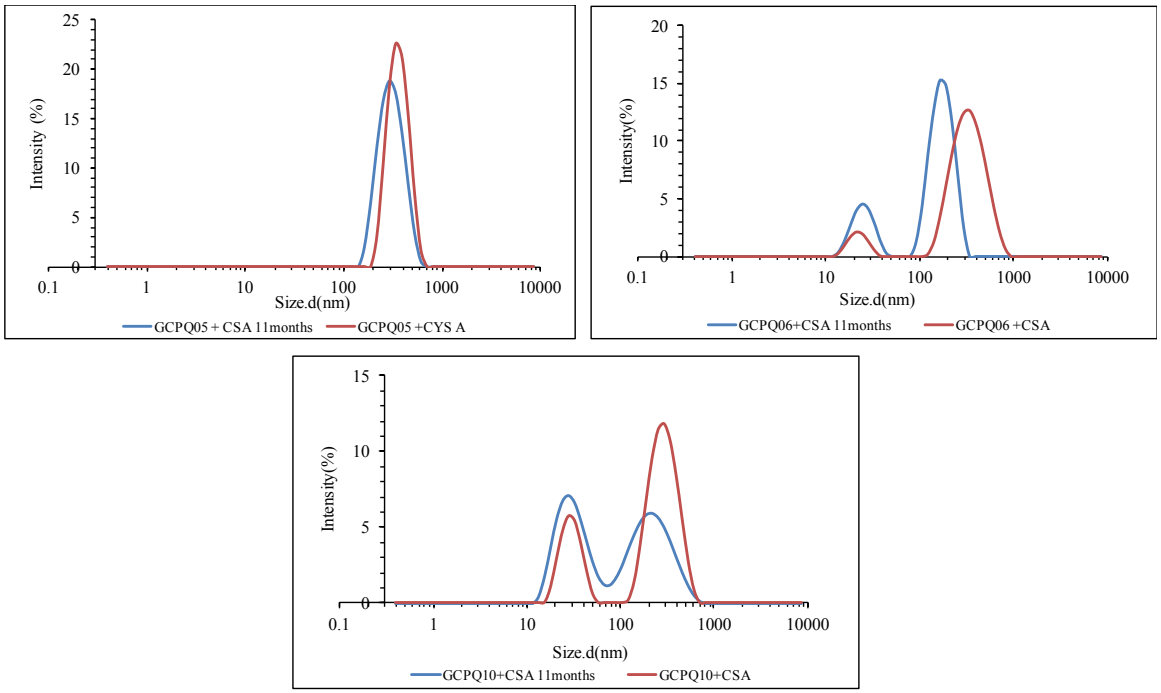

Figure 4-8: Size distribution of GCPQ-CYS A formulations on the 11th month compared with day 1 of the formulation

Table 4-6 and Figure 4-8 show the size distribution and size parameters of GCPQ cyclosporine A formulations 11 months after being stored at 4 °C compared with day 1 of

the formulation. The size distribution graphs show a narrowing of the population sizes and a slight shift towards smaller sizes. This is consistent with the z-average data shown in table 4-6 which shows a decrease in the size of the formulations. GCPQ05+CYS A decreased from about 340 nm to aout 250 nm, a decrease of about 29 %, GCPQ06+CYS A decreaed from about 160nm to about 100 nm, a decrease of about 37 % while GCPQ10+CYS A decreased from about 95 nm to about 54 nm, a decrease of about 43 %.

4.3.2 Discussion

The formulation of paclitaxel with GCPQ results in two structural conformations depending on the ratio of DQ to DP. GCPQ06 (GCP20Q22) which has a ratio of DQ to DP (QPR) of 1.1 formed crystalline nanostructures with paclitaxel while GCPQ10 (GCP37Q23) with a QPR of 0.62 and GCPQ14 with a QPR of 0.37 both formed spherical nanostructures (Figures 4-3).

These results show that structural modifications on GCPQ provides a tool for enhancing the encapsulation of different classes of drugs. Paclitaxel, a taxane with a rigid structure is a BCS class IV drug with logP of about 3.96 is very poorly soluble in aqueous solutions and in oil – a behaviour which is attributed to its physicochemical properties. Its lack of ionisable groups makes it particularly difficult to improve solubility using pH adjustments, hence the resort to the use of pro-drug synthesis, solubilisers and Nano formulations as approaches for formulation of paclitaxel for therapeutic purposes (Surapaneni et al., 2012). These include the development of liposomes, lipid nanoparticle conjugates, emulsions and polymers nanoparticles. Clinically, paclitaxel is currently available as Taxol® and Abraxane® both of

which are administered intravenously. Taxol is formulated by inclusion of a vehicle consisting of a 1:1 ratio of Cremphor® EL and ethanol while Abraxane is a Cremophor® free albumin conjugate of paclitaxel that is reported to have reduced toxicity.

The formulation of paclitaxel using polymeric nanoparticles yields different results, depending mostly on the method of formulation employed. A study using PEGylated PLGA to formulate paclitaxel nanoparticles yielded encapsulation efficiency of 70 ± 4 % when prepared by nanoprecipitation and 37 ± 2.5% when formulated as an emulsion with sizes of 112 ± 4 nm and 190 ± 4.5 nm for both methods of formulation respectively. The report also suggested that the presence of paclitaxel did not affect the size of the nanoparticle, agreeing with previous reports on PLGA based formulations of paclitaxel (Danhier et al., 2009). Another report using PLGA to formulate paclitaxel by oil in water emulsification, solvent evaporation method produced spherical shaped nanoparticles with sizes ranging from 200 to 800 nm having an encapsulation efficiency of about 88.5 % and drug loading of about 5 % (Jin et al., 2007).

Another study using methoxy poly(ethylene glycol)-poly(lactide) copolymer (MPEG-PLA) to formulate paclitaxel by the nanoprecipitation method reported the formation of spherical micelles ranging in sizes from 80 nm to 110 nm and with varying encapsulation efficiencies between 21 % and 48 %. These variabilities were reported to be due to differing amounts of components of the formulation and paclitaxel loading (Dong and Feng, 2004). Furthermore, paclitaxel nanocrystals formulated using N-((2-hydroxy-3-trimethylammonium) propyl) chitosan chloride (HTCC) had sizes of about 130.27 ± 6.73 nm and encapsulation efficiency of 83.12 ± 4.89 % with very high drug loading of 38.91 ± 4.02 % while chitosan formulated

paclitaxel nanocrystals had sizes of 125.19 ± 5.92 nm, encapsulation efficiency of 86.69 ± 5.52 % and drug loading efficiency of 35.42 ± 3.02 % (Lv et al., 2011).

Our results therefore show that GCPQ can be structurally modified to form GCPQ-paclitaxel nanoparticles which have spherical or rod-shaped nanostructures with fairly similar sizes close to 200 nm except GCPQ 10 which has a size greater than 300 nm. Furthermore, these structural modifications can lead to encapsulation efficiency values as high as 99 % and with drug loading levels above 15 %, making GCPQ comparably more efficient for encapsulating paclitaxel than several previously reported polymers. The reason for the higher encapsulation efficiency observed for GCPQ 06 and GCPQ10 which both have higher DQ values is not clear but might be related to conformational adjustments of the nanoparticle to favour a very strong hydrophobic bonding with paclitaxel at the core of the nanostructure in response to potentially high hydrogen bonding of the hydrophilic groups with the water molecules in the aqueous environment. This could lead to a more rigid structure as is suggested by the rod-shaped lattice structure of the GCPQ-Paclitaxel nanoparticle (Figure 4-6), that is a thermodynamically more favourable state. GCPQ 10 potentially achieves that much stability but has the added advantage of a greater number of hydrophobic DP groups, helping it to form a larger, more spherical structure because it is able to have a bulkier core with more encapsulated paclitaxel.

Cyclosporine A, a BCS Class II compound, is a cyclic peptide which has 11 amino acid residues, including 7 N-methylated ones. Its rigid structure, the result of extensive intramolecular hydrogen bonding, coupled with the hydrophobic nature of its amino acid residues confers on it its hydrophobic character. It has an octanol/water logP value of 2.92

and is very poorly soluble in water but readily soluble in most organic solvents. Like Paclitaxel, it lacks accessible ionisable groups on its structure which makes solubilisation by pH adjustments difficult to achieve, hence the use of pro-drug formation, complexation, micellization and co-solvency as approaches to improve cyclosporine A solubility (Czogalla, 2008).

A recent study reported on the formulation of Cyclosporine A in a PEGylated chitosan-modified lipid-based nanoparticle. The nanoformulation consisted of spherical nanoparticles of about 89 nm in size and achieved drug loading efficiency of about 37 % and encapsulation efficiency of about 69 % (Zhang et al., 2013). Another study reported formation of cyclosporine A loaded PLGA nanoparticles of about 163nm size and about 85 % encapsulation efficiency which stayed stable for about 3 months (Jain et al., 2010) while cyclosporine A formulated with Eudragit® S100 nanoparticles stabilised using Xanthan gum produced 60nm sized nanoparticles that were stable for 18 months (Wang et al., 2006). It is important to note that most of these reported formulations incorporate stabilisers to keep the formulation stable for extended periods. An exception to this is some nanospheres synthesized from an ABA type of triblock copolymer derived from Tyrosine which were about 65-70 nm in size, having encapsulation efficiency of about 60 % and stayed stable for about 4weeks at 4 ^{o}C (Goyal et al., 2015).

In comparison, GCPQ forms spherical nanoparticles with cyclosporine A which could be under 100nm in size, about 150nm in size or as large as 300 nm in size depending largely on the QPR ratio rather than the method of preparation. The QPR ratio also affects the encapsulation efficiency achieved. A low QPR ratio of 0.47 results in about 100 %

encapsulation, a QPR ratio of about 0.6 results in about 83 % encapsulation while a high QPR ratio above 1.0 results in about 69 % encapsulation efficiency. A low QPR ratio implies greater hydrophobicity which could potentially results in encapsulation of more of the hydrophobic cyclosporine A, leading to a higher drug load in each nanoparticle and consequently the higher particle size. Furthermore, GCPQ-cyclosporine A nanoparticles stayed stable for more than 1 year at 4 ^{o}C without the incorporation of a stabiliser. This enhanced stability is comparably better than previously reported nanoparticles without a stabiliser. Encapsulation efficiency reduced by about 20 % for all the formulations except GCPQ10 which had about 14 % reduction in encapsulation efficiency over this 1-year period. This reduction could be attributed to drug release instead of particle aggregation since the sizes of the nanoparticles decreased during this same period (Table 4-7). The comparably slower drug release from GCPQ10 could be attributed to its much higher DP value which could provide stronger local hydrophobic interaction with encapsulated cyclosporine A, decreasing the thermodynamic instability experienced by colloidal suspensions in aqueous solution.

4.4 Conclusions

GCPQ polymers can be engineered to formulate stable nanoparticles of encapsulated hydrophobic drugs from different BCS classes. For the encapsulation of paclitaxel, a BCS class IV drug, having a high DP of about 20 % or more coupled with a DQ of greater than 20 % is key to achieving a high encapsulation efficiency greater than 95%. Lower DQ values result in EE% of bout 50 %. A high QPR ratio greater than 1.0 results in rod shaped nanocrystals while a lower QPR ratio results in mostly spherical shaped nanoparticles. Nanoparticle sizes are typically under 200nm but a high DP greater than 30 % results in much larger particles closer to 300 nm in size. GCPQ-paclitaxel are stable for 28 days when stored at 4 ^{o}C without the addition of a stabiliser.

For the encapsulation of cyclosporine A, a hydrops class II, encapsulation is dependent on QPR ratio. A low QPR ratio of below 0.5 % results in about 100 % encapsulation efficiency while a high QPR ratio greater than 1.0 results in only about 69 % encapsulation efficiency. QPR also determines the size distribution of the nanoparticles. A lower QPR, which results in higher EE % also results in much bigger sizes of above 300 nm. Higher QPR values achieve nanoparticle smaller than 200 nm in size. GCPQ-Cyclosporine A nanoparticles are also very stable over a period of 1 year when stored at 4 ^{o}C without a stabiliser, releasing only about 20 % of the encapsulated cyclosporine A during that period. Increasing the level of DP results in slower release of cyclosporine A over the same period.

Chapter 5. Structure-Activity Relationships of GCPQ Polymeric Particles in Cellular and Rodent Models

5.0 Introduction

Quantitative structure activity relationship (QSR) represents a way to quantitatively correlate chemical structure to physiological effects (Asirvatham et al., 2016). The physiological properties of a chemical compound such as the molecular weight, hydrophilicity, hydrophobicity, solubility, partition coefficient and surface density can be used to predict the biological effects of the compound in different models (Verma et al., 2010). This approach will be used to examine the biological effects of structural modifications on GCPQ polymeric particles.

In the previous chapters, it was shown that modifying the level of palmitoyl and quaternary ammonium group substitutions resulted in different physicochemical properties. For example, the data obtained in chapter 3 showed that GCPQ has a very low critical micelle concentration of less than 10μM which is almost 10,000 times less than certain permeation enhancers like sodium caprate with a critical micelle concentration of about 85mM (Lisi et al., 1980). This implies that GCPQ is more likely to interact with biological membranes as polymeric micelle particles rather than as monomers if administered systemically. Additionally, the observation that a higher DQ confers better stability profiles in different

salt and pH environments might suggest that altering the level of substitutions will result in different effects in the different pH environments of the gut.

In this chapter, we examine the effects of these physicochemical properties on the biological effects of GCPQ. First, we examine effects on cytotoxicity and then effects on permeation enhancement as well as mechanisms involved.

5.1 Structure Activity Relationship of GCPQ polymeric particles on cellular toxicity

For every potential therapeutic agent or excipient, it is important to determine the concentration or dose at which the agent becomes unsafe for therapeutic purposes. A prototype of GCPQ with high molecular weight of 176 kDa, 6 mole % of palmitoylation and 4 mole % of quaternisation was reported to have an IC50 of 1.28 mg/mL in A431 cell line (Uchegbu et al., 2001). When compared with some other permeation enhancers, this value is much higher and represents a safer system for drug delivery. For example, the cationic polymer poly-L-lysine has an IC50 of 0.007 mg/mL while poly-L-ornithine has an IC50 of 0.004mg/mL also in the A431 cell line (Brown et al., 2000). Other anionic lipidic permeation enhancers such as sodium decanoate (C10) have been reported to show concentration and time dependent toxicities at levels ranging from 1 – 50mM in Caco-2 cell monolayer models using different assays such as the MTT [3-(4,5-dimethylthiazol-2-yl)-2,5-diphenyltetrazolium bromide] assay and Lactate dehydrogenase (LDH) assay (Shima et al., 1999, Quan et al., 1998, Zhou et al., 2009). Similarly, chitosan derivatives have been reported to show time dependent toxicity with cells recovering fully after removal of

treatment (Thanou et al., 2001b). For example, trimethylated chitosan derivatives were shown to have IC_{50} values ranging from about 0.05 mg/mL to about 1.0 mg/mL in MCF-7 cell lines. The IC50 values were lower for trimethyl chitosan derivatives with higher levels of trimethylation (Kean et al., 2005). The contribution of the lipidic chain in C10 and the charges in trimethyl chitosan to their respective toxicities represent a structure related impact of molecules on biological activities. Given the fact that the structural components of GCPQ includes the lipid palmitoyl chain and the positively charged quaternary ammonium group, we sought to examine what effects structural modifications involving these groups will have on the toxicity of GCPQ. we will do this using two assays: the MTT [3-(4,5-dimethylthiazol-2-yl)-2,5-diphenyltetrazolium bromide] assay and Lactate dehydrogenase (LDH) assay.

MTT Assay

The MTT assay is a colorimetric assay used to quantitatively measure cell survival and proliferation (Mosmann, 1983). The assay measures the ability of NAD(P)H dependent cellular oxidoreductase enzymes (such as the mitochondrial succinate dehydrogenase) to reduce the water soluble tetrazolium dye, 3-(4,5-dimethylthiazol-2-yl)-2,5-diphenyltetrazolium bromide to its insoluble purple formazan (Fotakis and Timbrell, 2006, Ciapetti et al., 1993). It is therefore more accurately a measure of the cellular activity of viable cells and by extension an indicator of cytotoxicity.

LDH Assay

The Lactate dehydrogenase assay is equally a colorimetric assay which measures the oxidation of β-NADH to β-NAD+ as a reduction in absorbance at 340nm. β-NADH is reduced to β-NAD+ when LDH reduces pyruvate to lactate(Moran and Schnellmann, 1996, Han et al., 2011). Lactate dehydrogenase is a 135kD (Hedrick and Smith, 1968) cytoplasmic enzyme to which the cell membrane is impermeable. It is therefore only released when there is a damage to the cell membrane (Allen et al., 1994). The LDH assay is therefore a measure of cell membrane damage and by extension an indicator of cytotoxicity. Both assays have been used and compared extensively as measures of cytotoxicity (Lobner, 2000, Fotakis and Timbrell, 2006, Arechabala et al., 1999, Weyermann et al., 2005) and the benefit of having both assays done is inherent in the fact that they both measure different parameters and indices of toxicity.

Both assays were used to determine the cytotoxic effects of treatment with GCPQ on 4T1, MDCK cells and caco-2 cells. The aim was to determine if the permeation enhancement effects observed with these polymers is due toxicity and if toxicity is correlated with structural modifications of GCPQ polymers.

5.1.1 Method

MTT Assay:

The method used was adapted from (Quan et al., 1998). Briefly, cells were seeded in 96 well plates at a density of $1X10^4$ cells per well and incubated at 37ºC in 5% CO_2, 95% for 24 hours in Minimum Essential Medium (MEM) supplemented with 10% Foetal Bovine Serum (FBS), 1% L-glutamine, 1% Non-essential Amino acids and 1% Penicillin-Streptomycin. Caco-2 cells were seeded at a density of $1X10^4$ cells per well and incubated at 37ºC in 5% CO_2, 95% humidity for 48 hours in Dulbecco's Modified Eagle's Medium with high glucose and l-glutamine, supplemented with 10% foetal bovine serum, 1% non-essential amino acids and 1% Penicillin-Streptomycin. On the day of treatment, the medium was removed and the cells washed twice with phosphate buffered saline (PBS, pH = 7.4). GCPQ (1 mg mL^{-1}) was suspended in HBSS and 200µL of the GCPQ treatment administered to the cells for 2 hours after which the treatment was removed and the cells washed with PBS twice again. An MTT stock solution (5mg mL^{-1}) was prepared in PBS from which a 0.5mg mL^{-1} concentration of the MTT reagent was prepared in cell culture medium. 200µl of this reagent was put in each well and the cells incubated 2 – 4 hours until the purple formazan crystals became visible under the microscope. After the incubation, the MTT reagent was removed using a multichannel pipette and 200µL of DMSO was put in each well and placed on a shaker, protected from light for 15 minutes to dissolve the crystals. The plates were then read on a UV spectrophotometer at 570nm. The cell viability was determined as a percentage of the negative control (HBSS). The positive control (lysis buffer) consisted of 1% Triton X-100 in PBS (pH = 7.4), 200 µL of which was applied to each positive control well for 15 minutes.

LDH Assay

The Assay was carried out using an LDH cytotoxicity detection Kit plus (04744926001, Roche Diagnostics Limited, UK) and according to the manufacturers protocol. Briefly, the cells were seeded in 96 well plates and treated as for the MTT assay. After two hours of treatment, 50μL of the supernatant from the 96 well plates was collected from each well into another 96 well plate and 100 μL of the LDH reaction dye and catalyst mixture was added to each well and the plates incubated for 20 minutes at room temperature in the dark. After the incubation, 50 μL of the stop solution was added to each well and the plate read on a UV spectrophotometer at 500nm. The cytotoxicity was determined as a percentage of the ratio of the difference between the absorbance of the treated cells and negative control and the difference between the absorbance of the positive control (a lysis buffer supplied in the kit, 5 μL of which was applied to each positive control well 15 minutes to the end of the treatment.) and the negative control (HBSS buffer).

$$\text{cytotoxicity (\%)} = \frac{\text{Treated} - \text{negative control}}{\text{positive control} - \text{negative control}} \text{x}100$$

5.1.2 Results and Discussion

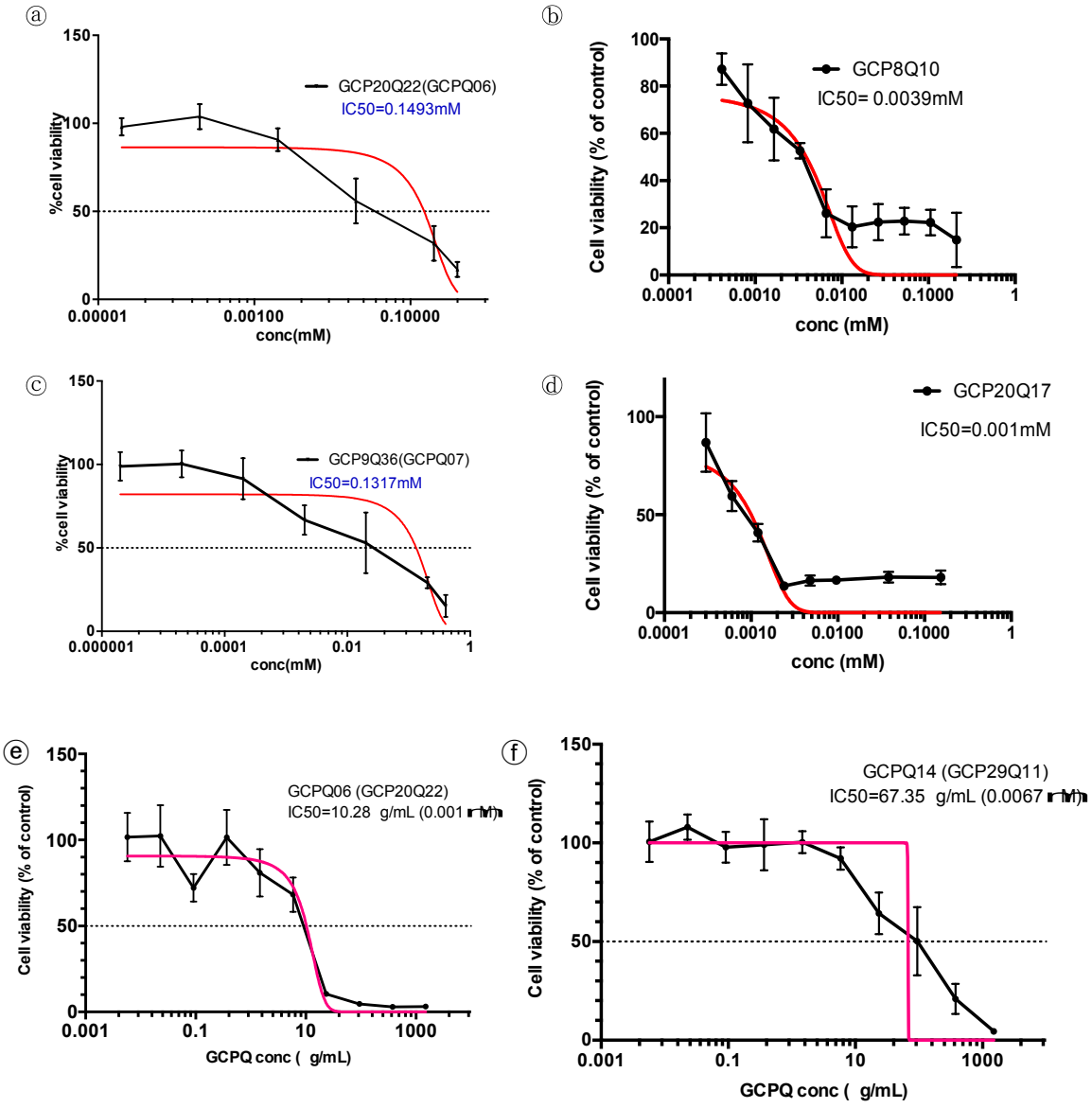

Figure 5-1: Cytotoxicity of GCPQ polymers on MDCK (A&C) and 4T1(B,D, E&F) cells using the MTT assay. The IC_{50} of GCPQ is lower in 4T1 cells than it is in MDCK cells. The red lines show the fit curves plotted from the data using log inhibitor vs normalised response model on Graph Pad Prism version 6.

Figure 5-1 shows the IC50 values of GCPQ polymers in MDCK and 4T1 cells using an MTT assay. GCPQ polymers with higher levels of DQ appear to have a lower IC50 value in both cell lines though the values are generally lower in the 4T1 cell line. GCPQ06 with a mole% DP of 20% and a DQ of 22% was used in both cell lines and has an IC50 value of about 0.15mM (about 1.5mg/mL) in MDCK cells but an IC50 value of 0.001mM (about 0.01mg/mL) in 4T1 cells which is about 150 times lower than the value in MDCK cells. GCPQ14 with DP of 29% and DQ of 11% has an IC50 value of 0.0067mM, about 7 times higher than the IC50 value of GCPQ 06 in 4T1 cells. Equally, GCP8Q10 has a higher IC50 value (0.0039mM) than GCP20Q17 (0.001mM, 0.0015mg/mL) in 4T1 cells. In MDCK cells, GCP9Q37 has an IC50 value of about 0.132mM (about 1.3mg/mL) which is only slightly lower than the IC50 value of GCP20Q22.

This observation of a lower IC50 value for GCPQ polymers which have a higher DQ was examined further using the caco-2 cell line and the MDCK cells line and caco-2 cell line and excluding the 4T1 cell line. Based on the data obtained from chapter 4 where a ratio of about 5:1 or 7.5:1 of GCPQ to encapsulated cargo was required to encapsulate a sufficiently high amount of cargo for therapeutic purposes, a high concentration of GCPQ (1mg/mL) was used to test for acute toxicity in the cell lines and to examine the effect of structural modification on toxicity. This concentration is slightly lower than the IC 50 value of GCPQ polymers in MDCK but much higher than the values in 4T1 cells, thus the 4T1 cell line was not used.

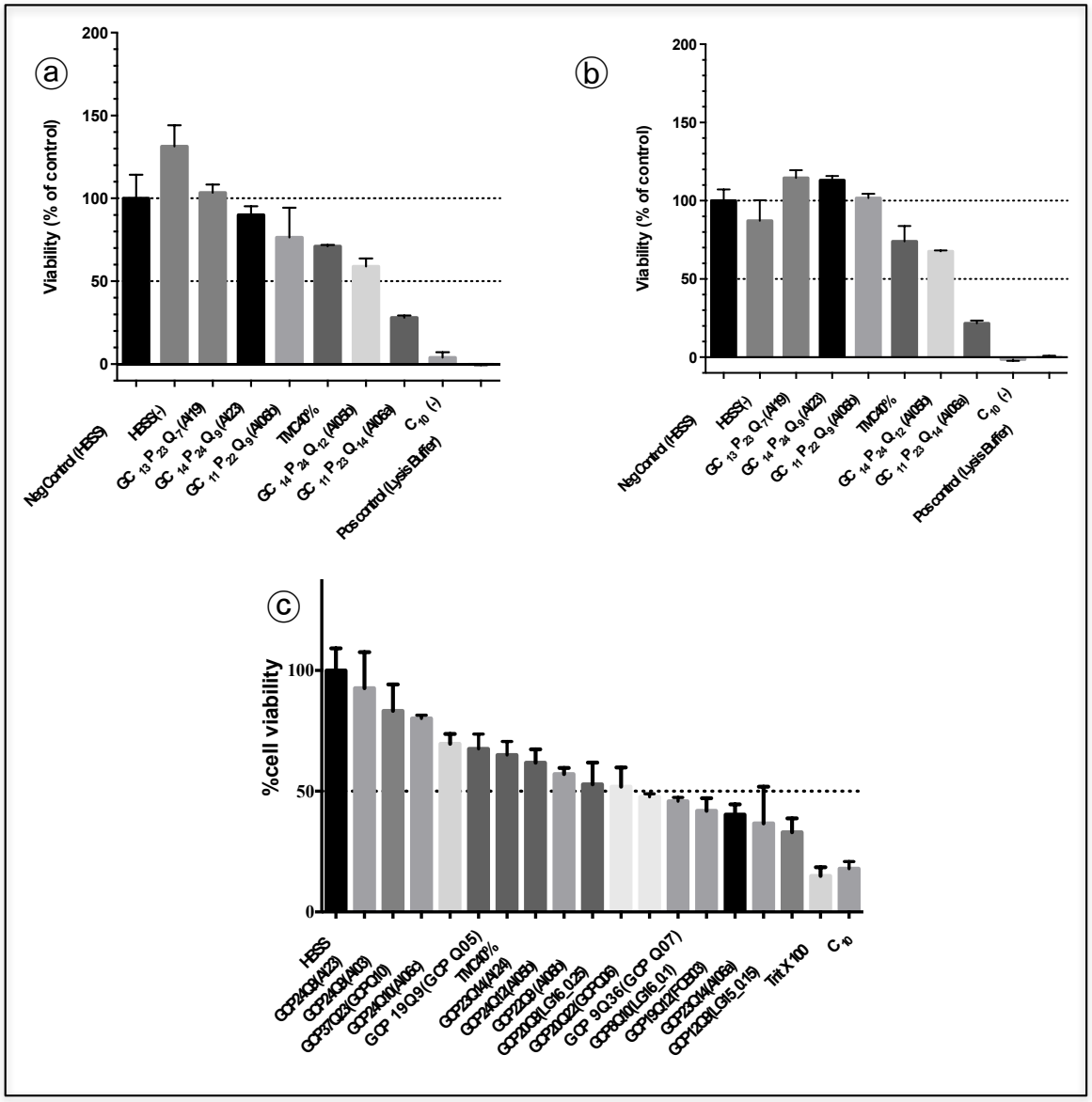

Figure 5-2: Cytotoxicity of GCPQ polymers on MDCK and Caco2 cells by MTT assay

(A) Caco-2 cells exposed to GCPQ polymer particles for 2 hours prior to assay. **(B)** Caco-2 cells allowed to recover for 24 hours after a 2-hour exposure to 1mg/mL GCPQ particles. **(C)** MDCK cells exposed to 1mg/mL GCPQ polymer particles for 2 hours prior to assay. HBSS(-) represents HBSS buffer without Ca^{2+} and Mg^{2+} ions. Cells were treated with C10 at a concentration of 1.9 mg/mL (10mM) for 2 hours. C10 was suspended in HBSS (-)

Figure 5-2 shows a trend of decreasing cell viability with increasing DQ % or decreasing DP % dev in both MDCK and caco-2 cells by the MTT assay. When compared with sodium caprate (C10) in both cell lines, cells treated with GCPQ have a higher viability than cells treated with C10. Also, cells treated with GCPQ particles recovered almost completely 24 hours after removal of the treatment while the cells treated with C10 failed to recover. GCPQ polymer particles also have a comparable level of toxicity with trimethyl chitosan having 40% degree of quaternisation (TMC 40%) in both cell lines.

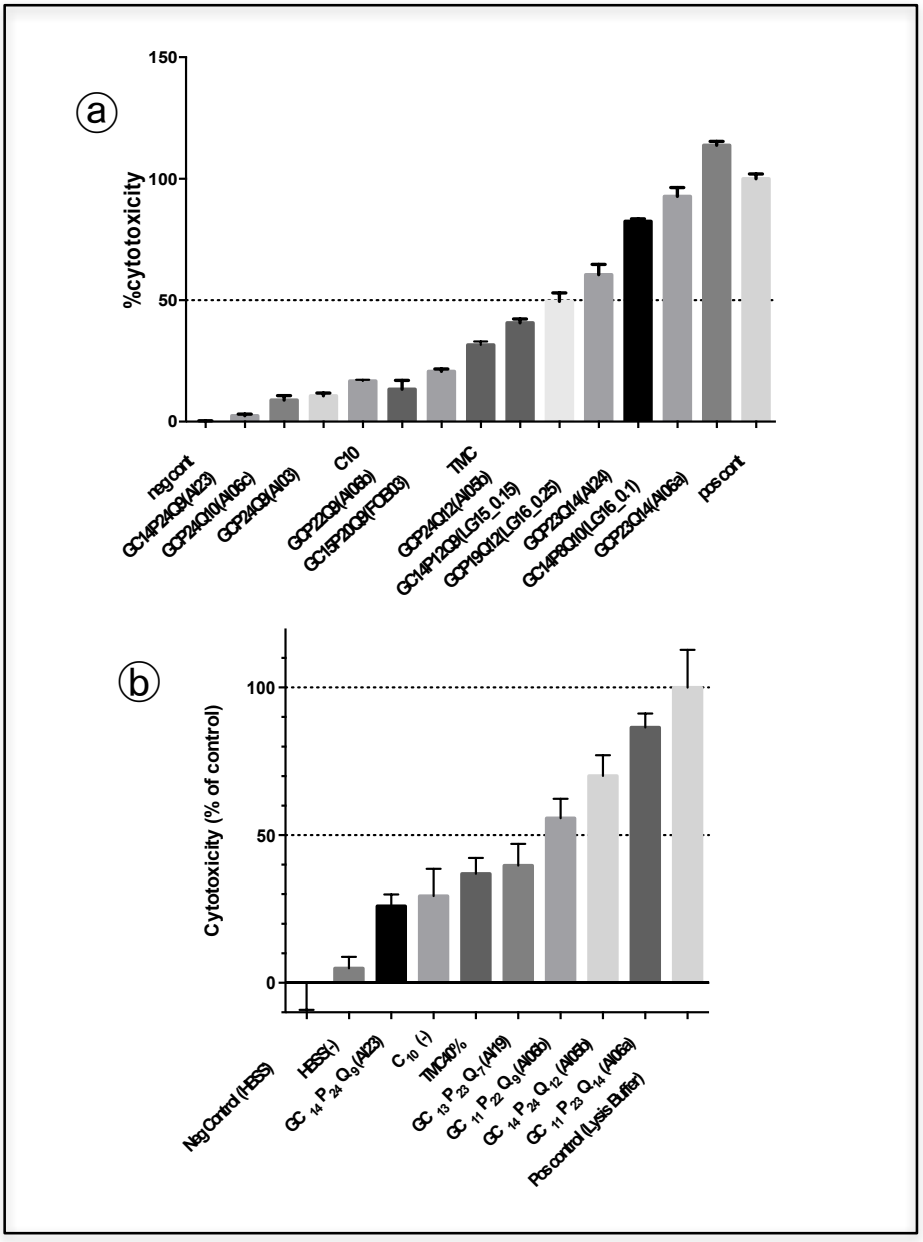

Figure 5-3: Cytotoxicity of GCPQ polymers on MDCK and Caco2 cells by LDH assay: (A) Caco-2 cells exposed to 1mg/mL GCPQ polymer particles, 1mg/mL TMC40% and 1.9 mg/mL C10 for 2 hours. (B) MDCK cells exposed to 1mg/mL GCPQ polymer particles, 1mg/mL TMC40% and 1.9 mg/mL C10 for 2 hours.

Figure 5-3 shows a trend of increasing cytotoxicity with increasing DQ% or decreasing DP% in both caco-2 and MDCK cells when measured by the LDH assay. Like with the MTT assay, most of the GCPQ polymers have a greater cytotoxicity than C10.

Table 5-1: The influence of QPR on cell cytotoxicity in the MDCK cell line

Polymer ID	QPR	% Cell viability (mean ± s.d.) in the MTT assay	% Cell viability (mean ± s.d.) in the LDH assay
GC14P24Q9	0.38	92.7 ± 29.86	97.6 ± 1.34
GC11P22Q9	0.41	52.9 ± 17.85**	86.7 ± 7.41*
GC12P24Q10	0.43	69.6 ± 8.20	91.1 ± 3.55
GC14P20Q9	0.45	51.8 ± 15.90**	39.5 ± 8.55****
GC14P24Q12	0.5	57.1 ± 5.12**	59.3 ± 3.06****
GCXP23Q14	0.6	61.8 ± 11.13*	17.5 ± 2.04****
GC14P12Q9	0.75	33.0 ± 11.40****	50.5 ± 6.90****
GC14P8Q10	1.25	41.9 ± 10.45***	7.3 ± 7.20****

Table 5-2: The influence of QPR on cytotoxicity in the Caco-2 cell line

Polymer ID	QPR	% Cell viability (mean ± s.d.) in the MTT assay	% Cell viability (mean ± s.d.) in the LDH assay
GC13P23Q7	0.3	103.4 ± 5.01	60.3 ± 7.35****
GC14P24Q9	0.38	90.0 ± 5.30	74.0 ± 3.95**
GC11P22Q9	0.41	76.3 ± 18.08*	44.2 ± 6.58****
GC14P24Q12	0.5	58.9 ± 4.82****	29.9 ± 6.96****

* = statistically significantly different when compared to the buffer control ($p < 0.05$)
** = statistically significantly different when compared to the buffer control ($p < 0.01$)
*** = statistically significantly different when compared to the buffer control ($p < 0.001$)
**** = statistically significantly different when compared to the buffer control ($p < 0.0001$)
One way ANOVA was used to determine statistical signifiance

Table 5-1 shows the effect of the ratio of DQ to DP (QPR) on cell viability of MDCK cells in both MTT and LDH assays. There appears to be a trend of decreasing viability with

increasing QPR in both assays. Polymers with DP of about 24% and a DQ of less than 10% do not cause a significant reduction of cell viability of MDCK cells. A QPR ratio of greater than 0.4 is required to cause significant reduction of cell viability in MDCK cells. Table 5-2 shows a similar trend in Caco-2 cells. Caco-2 cells appear to be more susceptible to membrane damage than MDCK cells as they show greater reduction of viability with the LDH assay and significantly so even for polymers with QPR ratios of about 0.3.

Figure 5-1 shows the IC 50 value of specific GCPQ polymers in MDCK and 4T1 cells. The figure shows that 4T1 cells are more susceptible to GCPQ than MDCK cells are. The 4T1 cell however, is a mouse mammary carcinoma cell line and not an epithelial tissue cell line like caco-2 and MDCK. Its inclusion here is not for a direct comparison but to indicate that cytotoxicity will be different depending on the tissues.

Figure 5-2 and Figure 5-3 show the cytotoxicity of GCPQ polymers at the concentration (1 mg/ml) used in the transport assays: MTT assay in **Figure 5-2** and LDH assay in **Figure 5-3**. The two assays measure different parameters as indicators of cell viability. The LDH assay measures the release of Lactate dehydrogenase, which is a cytosolic enzyme, into the extracellular environment. It is more directly a measure of membrane damage. The MTT assay is a measure of cell metabolic activity and may serve in some instances as an indicator of cell death. Both assays show a correlation between the DP and DQ and cell toxicity. Toxicity increases as DQ increases or as DP decreases. For both cell lines, MTT assay shows that C10 causes more toxicity than GCPQ polymers. For LDH assay however, both cell lines show higher toxicity with some GCPQ polymers than C10. This might suggest that at higher

DQ% or lower DP%, GCPQ causes more membrane damage than C10 but less damage to the metabolic activities of the mitochondrial oxidoreductase enzyme. This again suggests potential differences in the mechanism of permeation enhancement between GCPQ and C10.

Figure 5-2B shows the recovery of caco-2 cells 24 hours after a 2 hour exposure to GCPQ, TMC 40% and C10 with the MTT assay and suggests a reversible effect on epithelial membranes as is the case for some other derivatives of chitosan (Yeh et al., 2011, Dodane et al., 1999). The cells treated with C10 however, do not fully recover after 24 hours. A previous report showed a 78% MTT assay recovery and a 32% TEER recovery after five days following treatment of Caco2 cell monolayers with 10mM C10, this recovery being dependent on the duration of treatment (Shima et al., 1999). It is also important to note that most studies with C10 report a duration of treatment that is less than two hours (Anderberg et al., 1993).

The cytotoxicity data therefore raises the question of what effect these modifications will have on other biological processes in cells including permeation enhancement since there have been reports of correlation between cytotoxicity and permeation enhancement. To answer this question, we designed a series of experiments to test the hypothesis that increasing the level of DQ or decreasing the level of DP will increase permeation enhancement across epithelial barriers. We used two epithelial barrier models, one of the gut epithelia and the other of the kidney epithelia to see if this effect is conserved across different models as suggested by the cytotoxicity assay. We therefore treated MDCK cell and Caco-

2 cell monolayers with GCPQ polymers under similar conditions as the cytotoxicity assays and determined the effects on paracellular transport enhancement.

5.2 Effect of GCPQ Structural Modifications on Transport Across Epithelial Barriers

In common with several other chitosan-based nanoparticles, it is thought that GCPQ may act by protecting the drug from enzymatic degradation (Guggi and Bernkop-Schnürch, 2003, Zhang et al., 2015) and by mucoadhesion (Yin et al., 2009, Bernkop-Schnürch and Dünnhaupt, 2012). However, in contrast to other chitosan-based nanoparticles (Sonaje et al., 2012, Rosenthal et al., 2012, Kotzé et al., 1999), the available evidence suggests that the mechanism by which GCPQ augments oral bioavailability does not involve increased paracellular transport due to the opening of tight junctions between endothelial cells in the gut (Lalatsa et al., 2012a, Siew et al., 2012). In vitro transport experiments in the Caco-2 cell line found that GCPQ does not affect tight junction integrity, as measured by trans epithelial electrical resistance (TEER) and the transport of Lucifer Yellow, a marker of paracellular transport (Siew et al., 2012). Moreover, studies involving the cutting-edge and label-free coherent anti-Stokes Raman scattering (CARS) microscopy approach, in combination with analysis of the pharmacokinetics of radiolabelled GCPQ, suggest that that GCPQ nanoparticles may be transcytosed by enterocytes in the GIT following oral administration, resulting in an oral bioavailability of ~24% (Lalatsa et al., 2012a, Lalatsa et al., 2012b).

In the present studies, we aimed to further elucidate the exact mechanisms underlying GCPQ's oral bioavailability enhancing effects by conducting transport experiments in the well-established Caco-2 cell line and in the MDCK cell line as a model of other epithelial barriers. Caco-2 cells exhibit enterocytic differentiation when cultured as a monolayer on an appropriate support, expressing several physiologically relevant transport processes, and this model is among the best-characterized and most commonly used in vitro models of the human GIT epithelial barrier (Sambuy et al., 2005, Hubatsch et al., 2007). MDCK cells differentiate into a columnar epithelium when grown on a suitable membrane and also form tight junctions (Cho et al., 1989a, Cereijido et al., 1978) and are considered a good model for the simple epithelia (Rothen-Rutishauser et al., 1998). The cell line has been used extensively to study the trans epithelial transport of drug candidates with some reports showing similar Papp values as caco-2 cells (Ranaldi et al., 1996). In addition to being a comparable model to caco-2, it also has the advantage of a much higher throughput due to its faster growth and formation of tight junctions (Irvine et al., 1999). Both models were therefore considered useful tools with which to investigate the transport processes responsible for enterocytic uptake of nanoparticles (Gamboa and Leong, 2013, Irvine et al., 1999, Kaiser et al., 2015).

We hypothesized that the extent of GCPQ modification (i.e. different degrees of palmitoylation or quaternisation of the glycol chitosan polymer) may impact on its biological effects. Batches of GCPQ similar to those use in the toxicity assays were used for this assay and are shown in Table 5-3. A series of experiments were therefore designed to investigate the effect of DQ% and DP% on TEER and the permeability of a marker of paracellular

transport (fluorescein dextran 4 kDa) in the Caco-2 and MDCK cell lines. Further studies were carried out to ascertain the influence of pH on these effects, and to compare GCPQ to trimethyl chitosan (with 40% quaternisation) and sodium caprate (C_{10}), a well reported-on permeation enhancer (Krug et al., 2013). Finally, based on the results of the experiments, predictions of the effects of hypothetical GCPQ modifications on permeation enhancement and toxicity will be made to provide a guide for directed synthesis based on desired biological effects.

(Kean et al., 2005)

5.2.1 Methods:

Cell Culture and Maintenance

Caco-2 cells (passage number 35, ATCC: HTB-37) were obtained from collaborators in Veneto Nanotech (Padova, Italy) and Madine Darby Canine Kidney (MDCK) cells (passage number 12, ECACC 84121903) were obtained from an internal laboratory stock. Transport and trans epithelial electrical resistance (TEER) experiments were carried out using Corning Transwell® Inserts with polycarbonate membrane, 12 mm diameter and 0.4 μm pore size (VWR International, UK).

Caco-2 cells (passage number 38 – 46) were maintained in filter-topped cell culture flasks using Dulbecco's Modified Eagle's Medium with high glucose and L-glutamine (Sigma, UK, D5796), supplemented with 10% foetal bovine serum (Sigma, UK, F9665), 1% non-essential amino acids (Life Technologies, UK, 11140-035) and 1% Penicillin-Streptomycin (Gibco, 15140). Cell culture medium was replaced three times per week. Cells were incubated at

37°C in a humidified 5% CO_2 and 95% air atmosphere and passaged every 7-9 days with a seeding density of $2X10^5$ to $5X10^5$ cells in T75 flasks.

MDCK cells (Passage number 15-24), were grown in filter-topped cell culture flasks using Minimum Essential Medium Eagle (Sigma, M2279) supplemented with 10% foetal bovine serum (Life Technologies, UK, 11140-035), 1% Penicillin-Streptomycin (Gibco, 15140) and 1% GlutaMAX supplement (ThermoFisher Scientific, 35050061). Cell culture medium was replaced three times per week. Cells were incubated at 37°C in a humidified 5% CO_2 and 95% air atmosphere and passaged every 4-5 days with a seeding density of $3X10^5$ to $4X10^5$ cells in T-75 flasks.

Sample Preparation

Transport studies in the Caco-2 and MDCK cell lines were carried out using Hank's Balanced Salt Solution (HBSS). HBSS (Life Technologies, UK), supplemented with 10 M HEPES (4-(2-hydroxyethyl)-1-piperazineethanesulfonic acid) and 0.75% sodium bicarbonate, with pH adjusted to 6.8 (unless otherwise stated), was used in the present studies. A pH value of 6.8 was chosen as this lies within the pH range which is encountered in the small intestine in humans. GCPQ formulations (1 mg/ml) used in cell culture work were prepared by dissolving GCPQ at 2 mg/ml in autoclaved deionised water on the day before the experiment, before mixing with an equal volume of double strength HBSS shortly before applying onto the cells (i.e. within 20 min).

Caco-2 cells Monolayer preparation

For TEER and transport experiments in the Caco-2 cell line, cells (passage number: 38-46) were seeded in transwells at a density of $2.5x10^5$ cells per well and cultured according to standard protocols (Hubatsch et al., 2007). Briefly, cells were allowed to grow and differentiate on the transwells for 21-25 days prior to experimentation, with 0.5 ml of medium in the apical compartment and 1.5 ml of medium in the basolateral compartment. The cell culture medium in both apical and basolateral chambers was changed three times per week initially, and then daily 4 days prior to each experiment. Trans-epithelial electrical resistance (TEER) measurements were taken intermittently using a MILLIPORE Millicell^R-ERS voltohmmeter (Merck Millipore, UK) and corrected to account for the blank resistance of the transwell membrane. This measurement was carried out to monitor the development and integrity of the cell monolayer. Baseline TEER values on experimental days were typically in the range of 500-800 $\Omega.cm^2$.

For accelerated caco-2 monolayer growth, Corning ® semi permeable polycarbonate inserts were coated with 500µL of 0.7g/L rat tail collagen type I (Sigma-Aldrich, UK, C3867-1VL) in 0.02M acetic acid solution for 1hr based on a modification from Caldwell et al (Caldwell et al., 2014). The collagen solution was aspirated and the inserts washed three times with PBS (containing Ca^{2+} and Mg^{2+}). Seed 460000 cells/cm^2 suspended in DMEM (supplemented with 1% PEST, 1% Na pyruvate, 10%FBS) for 72 hours. After 72 hours, replace medium with STIM complete media (Entero-STIM® (Fischer Scientific, UK, 11553600) supplemented with 5% FBS, 0.5% PEST) every 48 hours for 6-8days. Baseline TEER values on experimental days were also about 500-800 $\Omega.cm^2$.

MDCK cell monolayer preparation

For experiments in the MDCK cell line, cells were seeded in transwells at a density of $5x10^5$ cells per well and cultured according to standard protocols (Cho et al., 1989b). Briefly, cells were allowed to grow and differentiate on the transwells for 5 days prior to experimentation, with 0.5 ml of medium in the apical compartment and 1.5 ml of medium in the basolateral compartment. The cell culture medium in both apical and basolateral chambers was changed every day from the second day. Trans-epithelial electrical resistance (TEER) measurements were taken intermittently using a MILLIPORE Millicell^R-ERS voltohmmeter (Merck Millipore, UK). Baseline TEER values on experimental days were typically in the range of 300-350 $\Omega.cm^2$.

Transport studies

All TEER/transport experiments were carried out in triplicate or quadruplicate (n = 3/4).

On the day of TEER/transport experiments, the cell culture medium was removed and monolayers were rinsed twice with buffer (HBSS, with 10mM HEPES and 0.75% sodium bicarbonate, adjusted to pH 6.8, unless otherwise stated), and then incubated for a further hour with HBSS at 37°C prior to taking a baseline TEER measurement.

Test GCPQ formulations (1 mg mL^{-1}) or blank HBSS serving as negative control solutions were then added to the apical chamber for a two-hour incubation period at 37°C, after which post-exposure TEER values were measured. The GCPQ control solutions were subsequently removed by aspiration, and both chambers washed once with HBSS before adding fresh blank HBSS to the basolateral chamber and fluorescein dextran 4 kDa (FD-4), a commonly

used marker of paracellular transport (Ye et al., 2015), to the apical chamber. The effect of GCPQ exposure on FD-4 permeability across the Caco-2 monolayer was determined by measuring FD-4 accumulation in the basolateral chamber. Samples (250 µl) were taken from the basolateral chamber (and replaced with 250 µl of HBSS) at 30 min intervals over a two-hour incubation period and analysed for FD-4 concentration using a BioTek Synergy™ HT Multi detection micro plate reader (BioTek Instruments, USA) at an excitation wavelength of 485 nm and emission wavelength of 528 nm. Throughout the FD-4 transport experiment, apical and basolateral chamber volumes were maintained at 0.5 and 1.5 ml, respectively, by replacing the volume removed from the chamber at each sampling point with an equal volume of blank transport buffer. In addition, a sample was taken from the apical chamber at the beginning of the experiment, to confirm the initial donor concentration (C_0), and at the end of the experiment, to facilitate mass balance calculations. It was decided to incubate GCPQ and FD-4 separately, following a protocol described by Kowapradit and colleagues (Kowapradit et al., 2010) because of the possibility of electrostatic interactions between the negatively charged FD4 and the positively charged GCPQ. TEER measurements were again taken after FD-4 incubation, followed by removal of the FD-4, washing once with HBSS and once with cell culture medium, before replacing with fresh cell culture medium and incubating cells overnight. Cell recovery TEER measurements were then taken 23 or 72 hours after exposure to treatment. Control permeation enhancers: TMC (1mg mL^{-1}) (Thanou et al., 2000b) obtained from a colleague in the lab and C10 (sodium caprate, 1.94 mg mL^{-1}) (Brayden et al., 2015a) purchased from Sigma, UK were applied in a similar manner to the apical chamber and the Papp values measured.

Calculating P_{app}

The apparent permeability coefficient (P_{app}; unit: $cm.s^{-1}$) of FD-4 in each individual well was calculated using the equation below:

$$P_{app} = \frac{dQ}{dt} \text{ X } \frac{1}{AC}$$

where, dQ/dt = rate of change of concentration in basolateral chamber, A = surface area of the cell monolayer (= 4.67 cm^2), C= initial concentration in the apical chamber.

The concentration of the collected samples was determined from a standard curve with $r^2 \approx 0.9988$ (Figure 5-4).

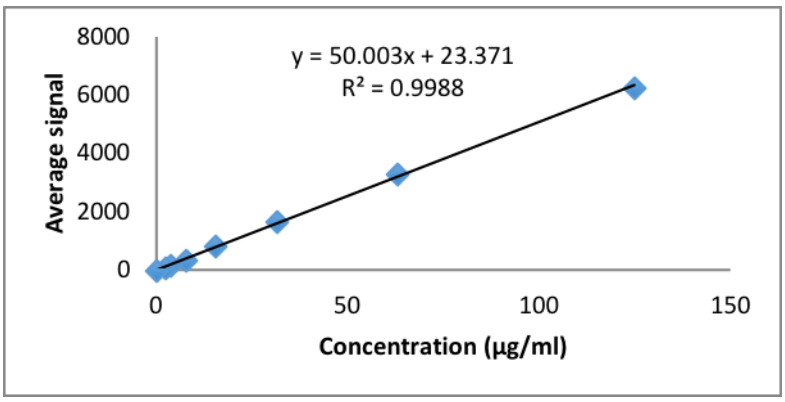

Figure 5-4: Sample standard curve of FD4 determined from fluorescence measurements and used to calculate concentration of transported FD4 after treatment with GCPQ.

Size Selectivity Assays:

For assays to determine the limits of tight junction modulation, different sizes of FITC-dextrans were used as paracellular transport markers, including FD4 (4kDa), FD10 (10kDa), FD20 (20kDa), FD40 (40kDa), FD70 (70kDa), FD250 (250kDa) and FITC-albumin (66.5kDa) (Sigma-Aldrich, UK) with hydrodynamic radii of ≈14Å, 23 Å, 33 Å, 44 Å, 60 Å,

105 Å and 34.8 Å respectively. MDCK and Caco2 cells were treated with GCPQ polymers and C10 following the method described earlier. TEER and Papp measurements were also carried out as described previously. Standard curves for higher molecular weight FITC dextrans are in the Appendix.

In Vitro CLSM Imaging

For fixed cell imaging, MDCK cells were seeded at a density of $5x10^5$ on 12 mm cover slips placed in 12 well plates and incubated at 37ºC in 5 % CO_2, 95 % for three days in Minimum Essential Medium (MEM) supplemented with 10 % Fetal Bovine Serum (FBS), 1 % L-glutamine, 1% Non-essential Amino acids and 1 % Penicillin-Streptomycin. The medium was changed every day until the day of the experiment. On the day of the experiment, the medium was removed from the wells and the cells were washed with phosphate buffered saline (PBS). The cells were then treated with Texas red labelled GCPQ (Synthesis and purification described in Chapter 2) suspended in HBSS for two hours. After the treatment, the cells were washed with PBS twice and stained with 1:1000 cell mask in PBS for 2 minutes, washed and fixed with freshly prepared 4% paraformaldehyde (PFA) for 10 minutes. The PFA was then removed and the cells washed twice with PBS. The cells were then stained with DAPI (Life Technologies, UK) for 5 minutes and washed again with PBS. The cover slip was then mounted on a glass slide with VECTASHIELD antifade mounting medium and then imaged on an inverted Zeiss LSM 710 confocal microscope.

For labelling of tight junctions, Caco2 cells were seeded on cover slips in 12 well plates and incubated until fully confluent. Antibody staining was done using a method adapted from

published literature (Kawauchiya et al., 2011) Cells were treated with GCPQ, sodium caprate or serum free medium for 120 minutes and then washed with PBS and fixed with 4 % PFA for 10 minutes. Cells were then blocked with blocking buffer (10 % goat serum, 1 % bovine serum albumin (BSA) in Tris buffered saline (TBS)) for 1 hour and then incubated with ZO-1 rabbit polyclonal anitbody (10 μg/mL in 1 % BSA in TBS) overnight at 4ºC, washed with PBS and then incubated with goat anti-rabbit antibody (1:1000 in 1 % BSA in TBS) for 1 hour. Cells were washed with PBS and stained with DAPI before mounting on a slide and viewing under the microscope.

For live cell imaging, the cells were seeded in a MatTek Glass Bottom Microwell Dish (Maryland, USA) and incubated in the same medium as with the fixed cell and under the same conditions until the cells were confluent. Imaging was done using the inverted Zeiss LSM 710 confocal microscope while incubating at 37ºC and 5% CO_2.

5.2.2 Results and Discussion

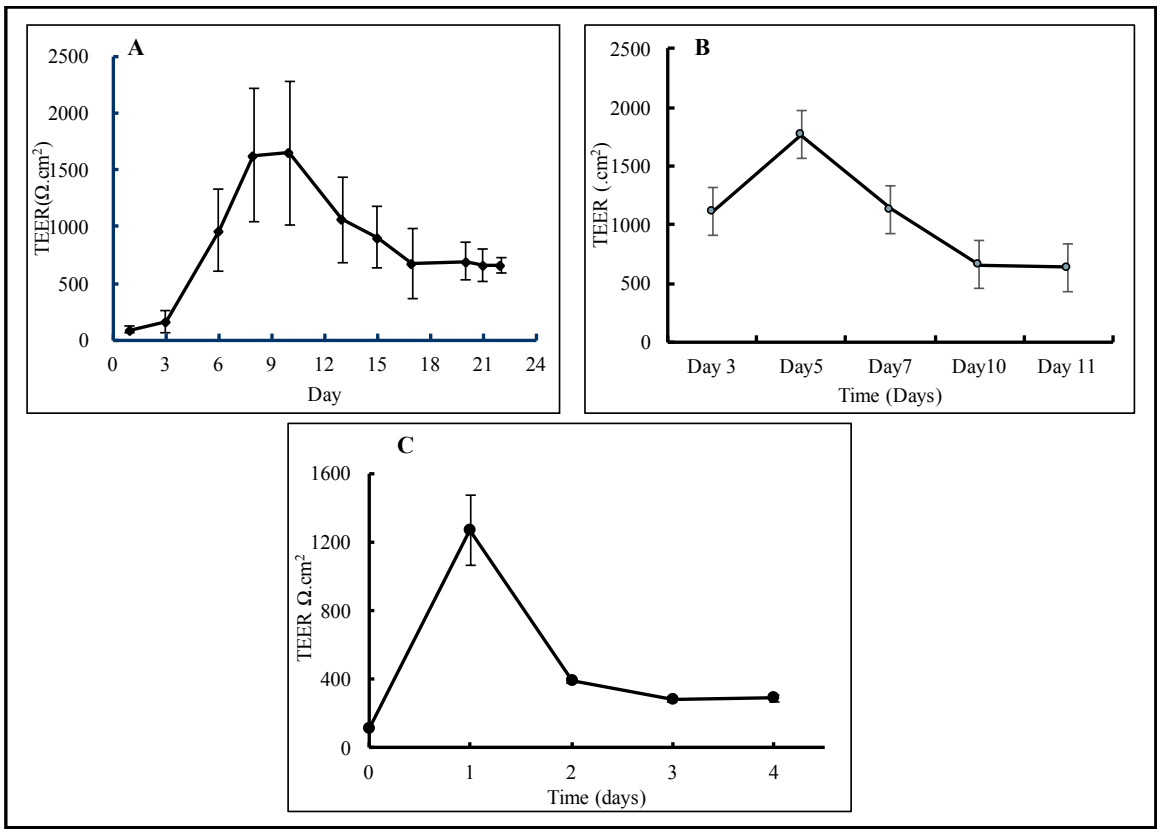

Figure 5-5: Development of TEER for cell monolayers grown on transwells A. caco-2 cells grown over 21 days. **B**. caco-2 cells grown by the accelerated method over 11 days. **C**. MDCK cells grown over 5 days.

Figure 5-5 shows the development of tight junctions in caco-2 and MDCK cells as measured using TEER. All cell lines show an initial period of rapid exponential increase in TEER values before a peak is reached followed by a steep decline and then a period where the TEER values are stable. Caco-2 cells grown without collagen coating (Figure 5-5A) show increase in TEER values up to about 1800 $\Omega.cm^2$ by day 9 and then decrease until a stable value of about 800$\Omega.cm^2$ is reached on day 21. Caco-2 cells grown with collagen coating

reach the peak of about 1800 $\Omega.cm^2$ by day 4 and then decrease until a stable value of about 800 $\Omega.cm^2$ is reached by day 10. MDCK cells however reach a peak value of about 1200 $\Omega.cm^2$ on day 1 after seeding and then decrease to a stable value of about 300 $\Omega.cm^2$ by day 4.

Reaching a stable value of TEER is regarded as an indication of full differentiation of the epithelial monolayer with the formation of tight junctions in caco-2 and MDCK cells (Hidalgo et al., 1989, Rothen-Rutishauser et al., 1998). The initial period of steep increase in TEER corresponds to growth and multiplication of cells before reaching confluence. For caco-2 cells, this takes about 8 days while MDCK cells become confluent within 48 hours. The subsequent drop in TEER has been attributed to variation in time course of tight junction sealing and formation of channels. The subsequent periods of stability in TEER represent a phase of morphological development of the epithelial cells as well as the thickening of the cytoskeleton to form a fully differentiated and polarised epithelial monolayer (Gonzalez-Mariscal et al., 1985, Rothen-Rutishauser et al., 1998)

Based on these observations, the subsequent transport assays were carried out during the periods of stable TEER values: day 4-5 for MDCK cells, day 21-23 for caco-2 cells grown without collagen and day 12 for caco-2 cells grown with collagen.

Table 5-3 Characteristics of the different batches of GCPQ used in the present studies

ID	Nomenclature	Molecular weight (kD)	%DP	%DQ
GCPQ08	GC8P10Q14	8	10	14
GCPQ07	GC9P9Q36	9	9	36
FOB03	GC9P19Q12	9	19	12
GCPQ10	GCP37Q23	≈10	37	23
GCPQ06	GC10P20Q22	10	20	22
AI06b	GC11P22Q9	11	22	9
AI06c	GC12P24Q10	12	24	10
GCPQ05	GC12P19Q9	12	19	9
AI19	GC13P23Q7	13	23	7
AI03	GC13P24Q9	13	24	9
AI23	GC14P24Q9	14	24	9
LG16_0.25	GC14P20Q9	14	20	9
LG16_0.1	GC14P8Q10	14	8	10
LG15_0.15	GC14P12Q9	14	12	9
AI24	GC14P23Q14	14	23	14
AI05b	GC14P24Q12	14	24	12

Table 5-3 shows the characteristics of GCPQ polymers used in these studies. A wide range of GCPQ polymers with different molecular weight, DP % and DQ % were used as for the cytotoxicity assay to establish the effect of structural modifications on cellular transport mechanisms.

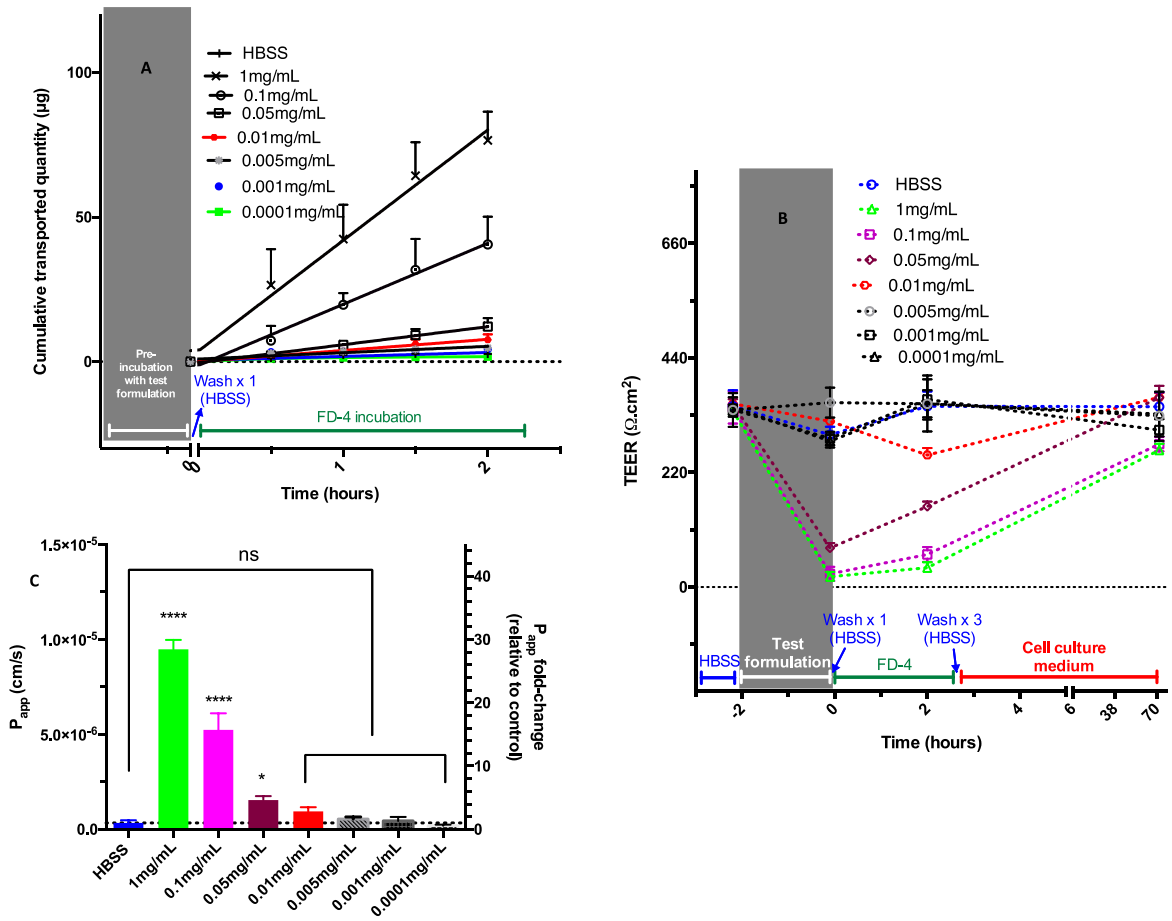

Figure 5-6: Concentration dependence of GCPQ polymer (GCPQ06) effects on paracellular transport across MDCK cell monolayer.

A. cumulative transport of FITC-Dextran 4KDa (FD4) from the apical to the basolateral chamber of the transwell after treatment with different concentrations of GCPQ06. **B**. permeability coefficient of the MDCK cell monolayer to FD4 after treatment with different concentrations of GCPQ06. **C**. Trans epithelial resistance (TEER) of MDCK monolayers after treatment with different concentrations of GCPQ06 for 2hours. Statistical significance was determined by two-way ANOVA with Bonferroni post- test. n=4; *= P<0.05; **=P<0.01; ***=P<0.001

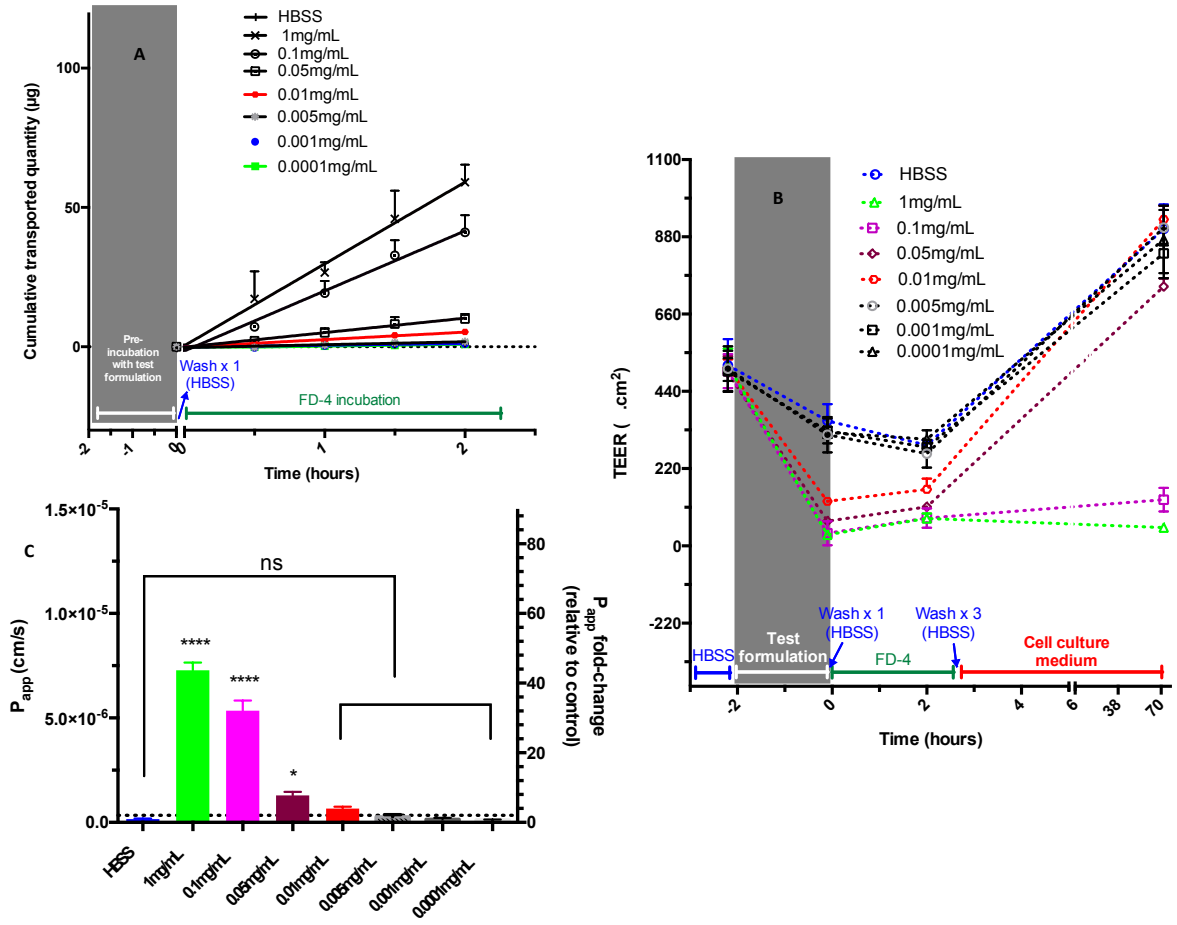

Figure 5-7: Concentration dependence of GCPQ polymer (GCPQ06) effects on paracellular transport across Caco-2 cell monolayer.

A. cumulative transport of FITC-Dextran 4KDa (FD4) from the apical to the basolateral chamber of the transwell after treatment with different concentrations of GCPQ06. **B**. permeability coefficient of the caco-2 cell monolayer to FD4 after treatment with different concentrations of GCPQ06. **C**. Trans epithelial resistance (TEER) of Cacco-2 monolayers after treatment with different concentrations of GCPQ06 for 2hours. Statistical significance was determined by two-way ANOVA with Bonferroni post- test. n=4; *= P<0.05; **=P<0.01; ***=P<0.001

Figures 5-6 and 5-7 show the concentration dependence of GCPQ 06 on TEER and FD4 transport in both MDCK (**Figure 5-6**) and Caco-2 (**Figure 5-7**) cell monolayers. A concentration of 0.05 mg/mL significantly increases the transport of a 4 kDa FITC-dextran across both monolayers. Lower concentrations were not effective in increasing transport. In MDCK cells, there was full recovery of the cells 72 hours after treatment with all concentrations of GCPQ06 whereas in Caco-2 monolayers, cells treated with 0.1 mg/mL and 1 mg/mL of GCPQ06 failed to recover 72 hours after treatment as shown by the TEER measurement. This compares closely with previous reports which observed that caco-2 cells treated with 0.01 % (0.1 mg/mL) of chitosan failed to recover (Ranaldi et al., 2002). At a concentration of 0.005 % w/v, GCPQ polymers are able to enhance paracellular transport at a lower concentration than most derivatives of chitosan (Kotzé et al., 1998).

These results are in contrast to previous reports on the mechanism of permeation enhancement by GCPQ which suggested that there is no involvement of the paracellular transport pathway. (Lalatsa et al., 2012a, Siew et al., 2012). Given that these previous reports used a prototype of GCPQ with a molecular weight of about 12kDa, DP% of 16% and DQ% of about 8% at a concentration of 5 mg/mL in a Caco-2 cell model, the question was raised about whether the effect on paracellular transport is affected by DP% and DQ%. Our results show that GCPQ 06 with about 20% DP and about 22% DQ opens tight junctions and increases paracellular transport of FD4. We will therefore carry out further experiments using other GCPQ polymer prototypes to determine if DQ and DP affect paracellular transport.

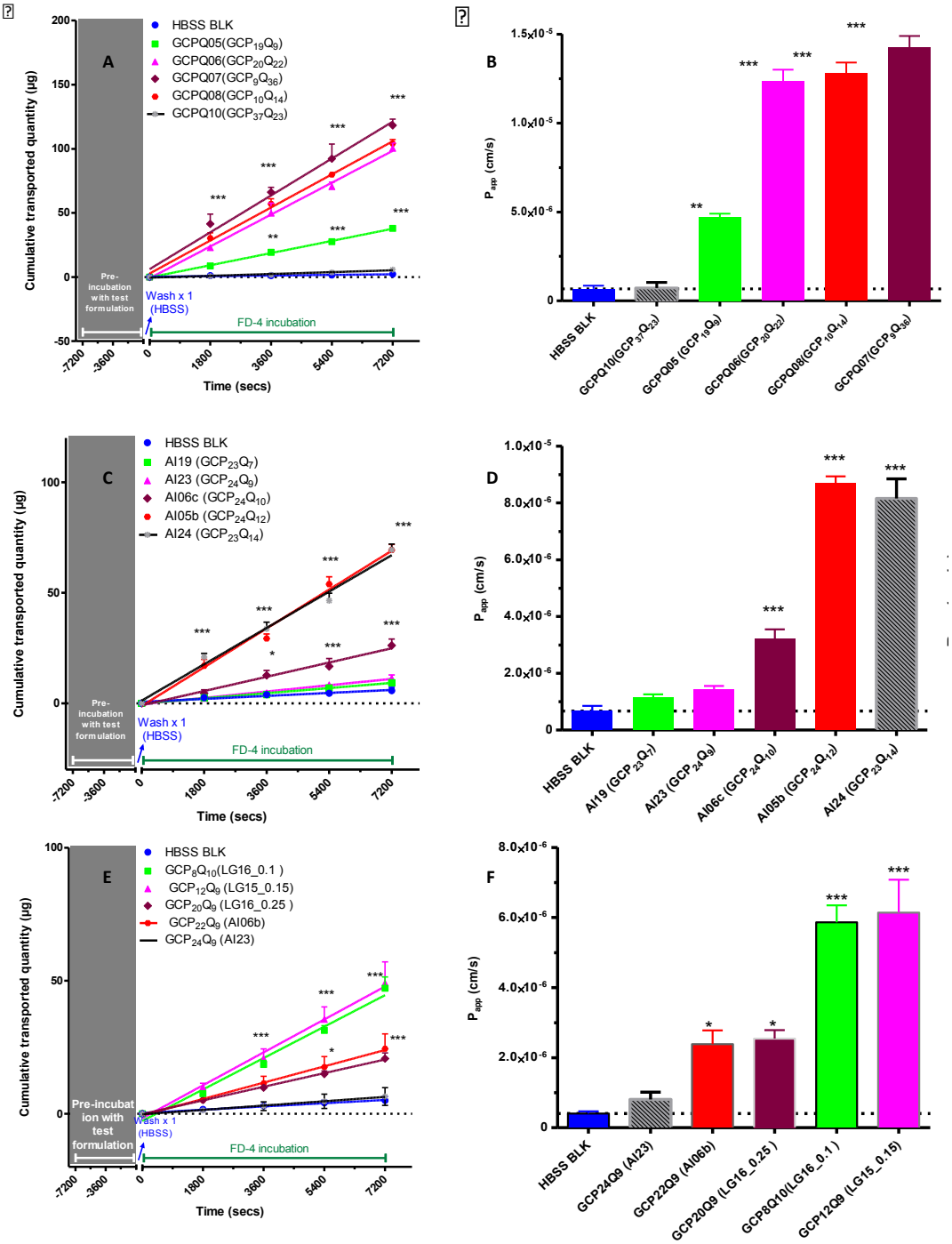

Figure 5-8: Effect of GCPQ (1mg/mL) on the paracellular transport of FD4 across MDCK cell monolayer. a. Cummulative transport of FD4 after exposure to GCPQ polymers having different properties but with similar molecular weight. **b**. Papp of FD4 corresponding to (a) (c) Cummulative transport of FD4 after exposure to GCPQ polymers having similar % DP (≈ 24 %) but different % DQ. (d) P_{app} of FD4 corresponding to (c). (e) Cummulative transport

of FD4 after exposure to GCPQ polymers having similar % DQ (≈ 9 %) but different % DP. (f) Papp of FD4 corresponding to (e). Statistical significance was determined by two-way ANOVA with Bonferroni post- test. n=4; *= P<0.05; **=P<0.01; ***=P<0.001

Figure 5-8a shows the cumulative transport of FD4 across MDCK cell monolayer after exposure to GCPQ polymers having a molecular weight between 8-10 kDa. The graph shows a positive linear slope suggesting a constant rate of increase of FD4 transport across the MDCK cell monolayer layer treatment with GCPQ. No increase in transport is seen with cells treated with HBSS which served as the negative control. There is also a higher rate of increase for polymers with higher DQ% or lower DP %. Figure 5-8b shows the apparent permeability coefficient of FD4 across MDCK cells determined from the slopes in Figure 5-8a. The figure shows that there is no significant transport of FD4 when MDCK cells are treated with GCPQ 10 while there is a very significant transport of FD4 when MDCK cells are treated with GCPQ 06. Both GCPQ10 and GCPQ06 have similar % DQ of about 22 % but GCPQ10 has a very high DP of about 37% while GCPQ 06 has a lower DP of about 20 %. This shows that % DP also plays a role in paracellular transport of FD4. GCPQ 05 and GCPQ 06 also have similar % DP but different % DQ (GCPQ05 being lower at about 9%) and the figure shows that the Papp of FD4 is more than 2 times greater with GCPQ06 than it is with GCPQ05. This shows that % DQ also plays a role in paracellular transport of FD4. GCPQ06, GCPQ07 and GCPQ08 have similar Papp values even though they do not share the same number of DP or DQ. However, for all three polymers, the ratio of DQ to DP (QPR) is greater than 1.0. which might suggest that there is an upper limit to the extent of

permeation enhancement so that there is no increase achieved with increasing the DQ beyond a certain level.

Figure 5-8 c and d shows what effects are observed when the level of DP is kept constant at about 24 % while the level of DQ is varied. As was observed in Figure 5-8 a and b, there is an increase in the rate of paracellular transport of FD4 and Papp with an increase in % DQ as is seen between GCP24Q9 and GCP24Q10 (Figure 5-8c & d). Furthermore, there is no significant increase in FD4 transport when the level of DQ is less than 9 and the % DP is greater than 23 as is seen for GCP23Q7 and GCP24Q9 (Figure 5-8d). Figure 5-8 e and d show what effects are observed when the DQ is kept constant at about 9 % and the % DP is varied. The figures show that there is an increase in FD4 transport when there is a decrease in % DP.

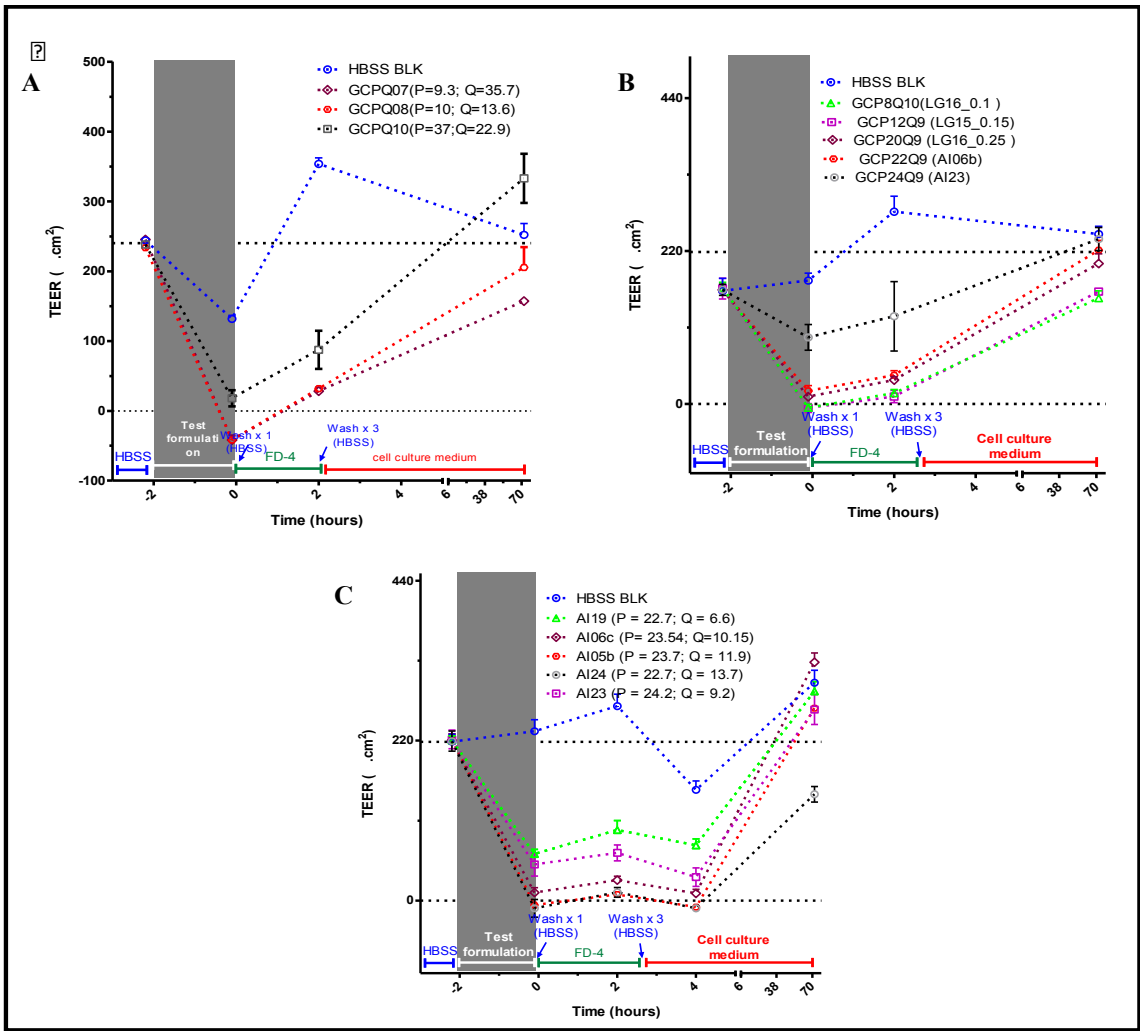

Figure 5-9: Effect of GCPQ on Trans epithelial Resistance (TEER). **a.** GCPQ polymers having different properties but with similar molecular weight. **b**. GCPQ polymers having similar percentage of quaternary ammonium groups (DQ) but with different percentage of palmitoyl groups (DP). **c**. GCPQ polymers with similar DP but different DQ.TEER was measured before and after treatment. Statistical significance was determined by two-way ANOVA with Bonferroni post- test. n=4; *= P<0.05; **=P<0.01; ***=P<0.001

The Trans epithelial resistance (TEER) is a measure of the integrity of cell monolayer tight junction. **Figure 5-9** shows the effect of GCPQ polymers with different properties on the tight junctions of MDCK monolayers after a 2-hour treatment period. It is obvious that the TEER values for cells treated with GCPQ decreased significantly following treatment. The extent of decrease in TEER values differs for each polymer with polymers having very high DQ and or low DP causing bigger decreases. The observation corresponds with the effects on FD4 transport and the effect on Papp and shown in the previous two figures. This reinforces the point that the observed increase in transport of FD4 is due to an effect on the tight junctions and the effect is dependent on the properties of the polymer. The cells treated with GCPQ appear to recover fully 72 hours after treatment except for a few polymers having very high DQ and/or very low DP.

There appears to be a balance between the effect of DP and the effect of DQ on the paracellular permeability enhancing effect of GCPQ. These graphs show different effects at DP≈10, DP≈20, and DP≈30 on the transport of FD4 across an MDCK monolayer. The effect of DQ appears to be hugely dependent on the degree of Palmitoylation. At about the same QPR, polymers with higher DP tend to have higher FD4 flux, probably because a much higher DQ is required to maintain the QPR. A steep increase in flux is observed at QPR just below 1 after which the flux increases at a slower rate over a wide QPR range. A maximum flux appears to be reached at a QPR just under 2, so that increasing the QPR further does not cause significant increase flux.

For polymers of fairly similar DP, the effect on paracellular transport is graded upwards with increasing DQ as is obvious for polymers DP of about 22% Similarly, decreasing DP at constant DQ appears to have the same graded increase in paracellular transport as with increasing DQ. The effect of DQ is enhanced at lower DP but this enhancement appears to reach a plateau as is shown by the fairly similar effects for GCPQ 06, 07 and 08 despite their large differences in DP Polymers with DP above 22% appear to need a DQ of more than 10% to have statistically significant paracellular transport enhancement. It is also worth noting that for GCPQ10 with a high DP of about 37%, even a very high DQ of 23% was not sufficient to cause statistically significant paracellular transport. These observations seem to suggest that DP is the more important parameter for achieving a graded effect on paracellular transport in MDCK cells.

Given the observation therefore, that GCPQ is able to enhance paracellular transport across an MDCK cell monolayer, and that these enhancement increases with an increase in % DQ or a decrease in % DP, it is important to determine how this permeation enhancement compares with other established permeation enhancers. We therefore examined the effect of Trimethyl chitosan having 40% quaternisation, an established permeation enhancer and a derivative of chitosan, as well as the effect of sodium caprate. The both reference compounds were used in toxicity assays for comparison with GCPQ.

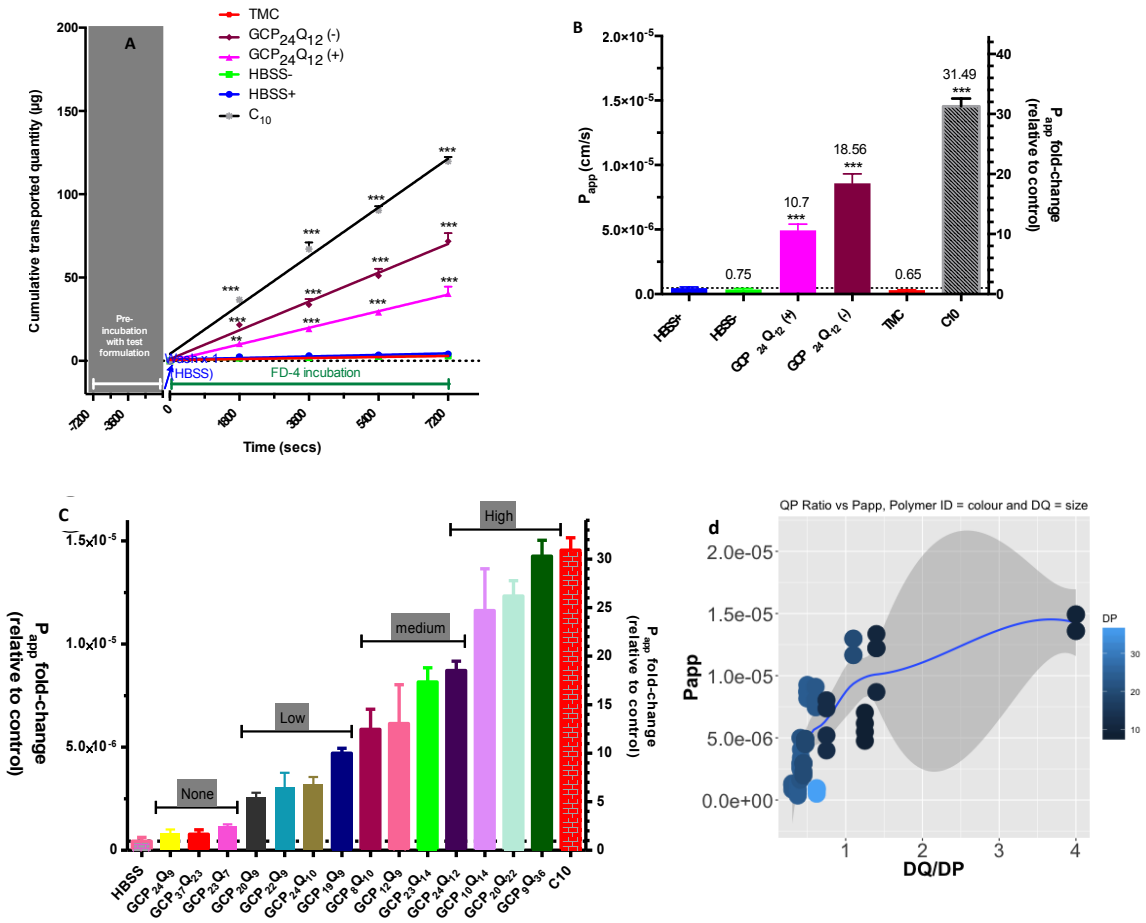

Figure 5-10: Effect of GCPQ on measured indices of paracellular transport compared with sodium caprate (C10) and Trimethyl chitosan (TMC)

(+) implies sample was prepared in HBSS containing Ca^{2+} and Mg^{2+}; (-) implies HBSS lacking Ca^{2+} and Mg^{2+} was used in preparing sample. **a**. Effect on FD4 transport. **b**. Effect on Apparent permeability, Papp. **c**. Papp of GCPQ polymers compared with C10 and graded according to extent of permeation enhancement. **d.** Plot of Papp against QPR for GCPQ polymers grouped by %DP Statistical significance was determined by two-way ANOVA with Bonferroni post- test and one-way ANOVA with Dunnett's multiple comparison post-test. n=4; *= P<0.05; **=P<0.01;***=P<0.001

Table 5-4: Ranking of GCPQ polymers by Papp in MDCK cells compared with HBSS and C10

ID	Nomenclature	Mean Papp (cm/s)	SD	Papp foldΔ	QPR
HBSS	HBSS	4.44E-07	1.83E-07	1	
GCPQ10	GCP37Q23	7.83E-07	2.11E-07	1.8	0.62
AI23	GC14P24Q9	8.08E-07	4.14E-07	1.8	0.38
AI19	GC13P23Q7	1.15E-06	2.17E-07	2.6	0.29
LG16_0.25	GC14P20Q9	2.54E-06	4.88E-07	5.7	0.45
AI06b	GC11P22Q9	3.04E-06	1.42E-06	6.9	0.41
AI06c	GC12P24Q10	3.20E-06	7.00E-07	7.2	0.43
GCPQ05	GC12P19Q9	4.71E-06	2.37E-07	10.6	0.49
LG16_0.1	GC14P8Q10	5.86E-06	9.70E-07	13.2	1.25
LG15_0.15	GC14P12Q9	6.14E-06	1.88E-06	13.8	0.75
AI24	GC14P23Q14	8.16E-06	6.90E-07	18.4	0.6
AI05b	GC14P24Q12	8.71E-06	4.53E-07	19.6	0.5
GCPQ08	GC8P10Q14	1.16E-05	2.03E-06	26.2	1.36
GCPQ06	GC10P20Q22	1.23E-05	7.57E-07	27.7	1.12
GCPQ07	GC9P9Q36	1.43E-05	7.66E-07	32.1	3.84
C10	C10	1.45E-05	6.12E-07	32.8	

Figures 5-10 show a comparison of GCPQ polymers with TMC40% and C10, both well reported on their roles as permeation enhancers (Brayden et al., 2015b, Thanou et al., 2000a, Krug et al., 2013). Sodium caprate has been reported to enhance paracellular transport by causing the release of intracellular Ca^{2+} from stores through the activation of protein kinase C, resulting in the contraction of actin microfilament and thus the dilation of paracellular space (Tomita et al., 1995, Lindmark et al., 1998, Del Vecchio et al., 2012). The close similarity between the reported mechanism of action of C10 and chitosan derivatives (activation of PKC, increasing intracellular Ca^{2+} and displacement of tight junctional proteins) (Wang et al., 2017) formed the basis for a comparison with GCPQ. GCPQ suspension and the negative control (HBSS) used were prepared in similar conditions as the positive control (C10). HBSS without calcium and magnesium was used in the apical chamber to prevent the precipitation of C10 (Lindmark et al., 1998). In MDCK cells, C10 has a 31.49-fold increase in Papp compared to the control (HBSS) but GCP24Q12 an 18.35-fold increase in Papp. While no difference was observed between the control treatment in the presence and absence of Ca^{2+} and Mg^{2+}, the effect of GCPQ was increased in the absence of calcium and magnesium in the medium in both caco-2 and MDCK cells. Reports suggest that the presence or absence of mucosal Ca2+ does not change the effect of C10 on a Caco2 cell monolayer (Tomita et al., 1995), however, it will seem that the absence of both ions increases the effect of GCPQ on MDCK cell monolayers. This might point to possible mechanisms of action relating to both ions which is not necessarily implicated with C10. However, when treated with TMC40%, MDCK cells showed a decrease in permeability to FD 4 compared to HBSS. It should be noted however, that a concentration of 0.1% TMC 40% was used in these assays for parallel comparison with GCPQ. Reports which have

suggested an increase in paracellular transport with TMC40% have typically used higher concentrations of 0.25% (Thanou et al., 2000a). These observations imply that while Papp values for FD4 following treatment with GCPQ and the controls are largely different between the two cell lines, the general trend of increasing Papp with increasing QPR can be observed in both cell lines

Table 5-4 shows C10 in comparison with different GCPQ polymers in MDCK cells and a proposed grading of the polymers based on Papp. FD4 Papp value of 1.45E-05 ± 6.12E-07 cm/s for C10 are comparable with values (0.82 ± 0.08 E-5 to 1.71 ± 0.21 E-5cm/s) reported in the literature following treatment with 10 mM C10 (Krug et al., 2013). The polymers are ranked based on QPR and show that a QPR of greater than 0.4 is required to have statistically significant paracellular transport enhancement with the exception of GCPQ10 which has a QPR of about 0.6 but doesn't significantly increase Papp due to its very high % DP.

The QPR which is the ratio of DQ % to DP % serves as a measure of hydrophilicity and can be plotted against the Papp as shown in **figure 5-10d**. The figure shows that while the Papp increases with QPR, the effect is still dependent on the level of % DP as clusters can be seen at DP≈10, DP≈20, and DP≈30. At about the same QPR, polymers with higher DP tend need a much higher DQ to maintain the QPR which is consistent with what was observed in figure 5-8. The effect of DQ is enhanced at lower DP but this enhancement appears to reach a plateau as is shown by the fairly similar Papp fold change for GCPQ 06, 07 and 08 despite their large differences in DP (**table 5-4**). Polymers with DP above 22% appear to need a DQ of more than 10% to have statistically significant paracellular transport enhancement. For

polymers with DP above 30%, such as GCPQ10 with a high DP of about 37%, even a very high DQ of 23% was not sufficient to cause statistically significant paracellular transport (Table 5-4). The steep increase in Papp for QPR values below 1.5 and the subsequent decline in slope at higher QPR suggests that not much benefit is realised from increasing the QPR beyond 1.0 as can be seen from the Papp fold change in Table 5-4. The positive correlation between Papp and QPR therefore suggests that hydrophilicity increases permeation enhancement while hydrophobicity decreases permeation enhancement.

The observation of a graded permeation enhancement mirrors the graded cytotoxicity observed in **figures 5-2 and 5-3.** Also, the recovery of TEER values for MDCK cells treated with GCPQ mirrors the recovery of cell viability shown with the toxicity assays which suggests a reversible effect on epithelial membranes as is the case for some other derivatives of chitosan (Yeh et al., 2011, Dodane et al., 1999). Previous reports have shown that increasing the degree of quaternisation of some derivatives of chitosan resulted in an increase in transport of FD4 and reduction in TEER (Thanou et al., 2000a, Kowapradit et al., 2010). Some other studies have also shown that an increase in N-substitution of chitosan is related to an increase in FD4 transport. There are also suggestions that an increase in aliphatic chain substitutions increases paracellular transport while aryl substitutions with benzyl groups decreases paracellular transport and toxicity (Kowapradit et al., 2010, Kowapradit et al., 2008). Apparently, positive charges contribute to the effects of chitosan and its derivatives on paracellular transport (Wang et al., 2017) but our results also suggest that an increase in the hydrophobic palmitic acid chains reduces the ability of positive charges on the polymer to modulate the tight junctions. The exact reason for this is not clear, but one plausible

explanation might be steric hindrances to electrostatic interactions between the positive charges and the negatively charged membrane components.

Furthermore, considering that cells treated with C10 failed to recover fully as suggested by the cytotoxicity assays in Figure 5-2b, our data shows that GCPQ is at least as potent as C10 in enhancing paracellular transport in MDCK cells but is safer for use and has a shorter recovery time. This is an important observation especially considering that the critical micelle concentration for GCPQ polymers is less than 10 μM compared with the CMC of C10 which is about 85 mM. This means that at a concentration of 1 mg/mL (approximately 10 mM), which is about 1000 times greater than the CMC of GCPQ, we are likely administering GCPQ polymeric particles to the cell monolayers. A concentration of 10 mM of sodium caprate is however almost $1/10^{th}$ of the CMC of C10 which means that we are administering monomers of C10 instead of particles. This offers an GCPQ an advantage over C10 of an ability to facilitate the uptake of an encapsulated cargo at a relatively lower concentration than C10. C10 will have to be administered at a much higher concentration to achieve a concentration at least 10 times more than 10mM at the epithelial surface to able to effectively protect any loaded cargo while facilitating its uptake (Maher et al., 2009b). This will obviously introduce toxicity issues since 10 mM is already sufficiently toxic to prevent cell recovery as is evident from a previous report which showed that regional administration of 100mM of C10 resulted in abrasion of the surface of the epithelium in rats (Maher et al., 2009a).

This difference between the characteristics of C10 and GCPQ in the *in vitro* models used might also point to differences in mechanisms. To understand the mechanisms involved in GCPQ paracellular transport enhancement, we will be try to gain understand better the role of the positive charges of the quaternary ammonium group. This is important since C10 is negatively charged and causes similar permeation enhancement. To do this, we will check for paracellular transport enhancement at different pH levels found in the gastrointestinal tract. We assume that at higher pH values, the GCPQ polymers will be deprotonated to an extent. We will use different polymers with different levels of DP and DP to determine if deprotonation is sufficient to cause a loss of tight junction modulation effect.

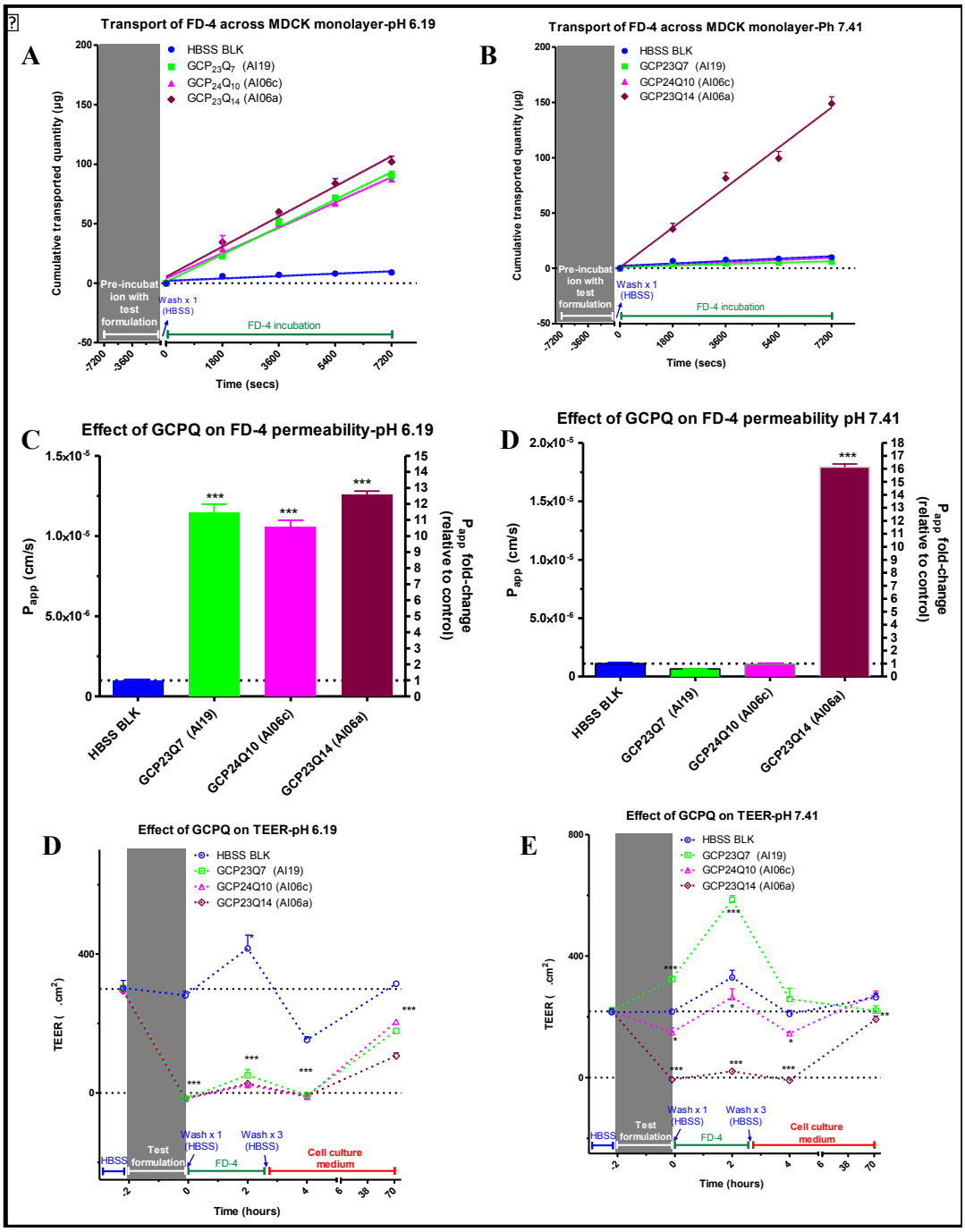

Figure 5-11: The role of pH on the effect of GCPQ on MDCK cell monolayer.

a. FD4 transport at pH 6.2 .**b**. FD4 transport at pH 7.4. **c**. Apparent permeability at pH 6.2. **d**. Apparent permeability at pH 7.2. **e** Effect on Trans epithelial resistance at pH 6.2. **f**. Effect on Trans epithelial resistance at pH 7.4. Statistical significance was determined by two-way ANOVA with Bonferroni post- test and one-way ANOVA with Dunnett's multiple comparison post- test. n=4; *= P<0.05; **=P<0.01; ***=P<0.001

Figure 5-11 shows the effect pH has on the paracellular enhancing effect of GCPQ.

Three polymers with similar DP but different DQ were compared. At pH 6.2, all three polymers which would ordinarily have a graded response at pH 6.8 (**see figure 5-10c**) were not different in their effect on the measured indices of paracellular transport. At pH 7.4 however, the polymer with the highest DQ retained its potency but the other polymers lost theirs completely. The striking difference at these three pH values point to the potential utility of these polymers in different physiological pH environments. At acidic pH, all the polymers are likely to enhance paracellular transport. At intestinal pH of 6.8, we can expect a graded response depending on the DQ. At the pH of the blood, only polymers with very high QPR will enhance tight junction opening and thus paracellular transport. By inference, GCP23Q14 will be potentially useful in opening the blood brain barrier and other endothelial barriers while the other polymers will be better suited for enhancing paracellular transport in the intestine. The pKa of GCPQ is reportedly about 6.0 (Chooi et al., 2014a). This means that GCPQ is less protonated at pH 7.4 than it is at pH 6.8 and at pH 6.2, establishing the fact that the positive charge on the polymer is important for tight junction modulation. This suggests that for a polymer like GCP37Q22 which did not cause significant permeation enhancement, there might be a conformation of the particles that limits the interaction of the positive charges of the polymer with the epithelial surface- hence the observation of a decrease in Papp with an increase in %DP.

Similar to our observation, a previous report showed a similar effect on paracellular transport using trimethyl chitosan pH 6.2 and 7.2. This study showed that TMC 60 (60 % quaternisation) was more potent than TMC40 (40 % quaternisation) in enhancing the

transport of a paracellular marker at both pH levels (Thanou et al., 2000a). Another study reported that the interaction of chitosan with integrin and by extension, its ability to open tight junctions is pH dependent, decreasing with increasing pH due to a loss of positive charges (Hsu et al., 2013). GCPQ is thus able to be structurally modified to retain its charge at neutral pH and thus retain its paracellular permeability enhancement effect.

This observation raises another question on the mechanism of tight junction modulation. Since the effect of GCPQ appears to be related to positive charges and as was observed from figure 5-10 d and Table 5-4 that GCPQ paracellular transport enhancement appears to reach a plateau, we were curious about why we had the plateau despite increasing the QPR to about 4.0. The toxicity data from figures 5-2 and 5-3 suggest that there is an increase in toxicity with increasing QPR. Since this is the case, why do we not have a continuously increasing transport of FD4 with higher QPR. We reasoned that since the cells recovered after GCPQ treatment, it must imply that toxicity does not result in permanent damage to the epithelial membrane. Therefore, we decided to determine what the upper limit of tight junction modulation was after treatment with GCPQ. This is important because of the role the tight junctions play in protecting against the uptake of harmful substances and also because of the association of tight junction modulation with certain disease conditions including Irritable Bowel Syndrome (IBS) (Bertiaux-Vandaële et al., 2011), Crohn's disease (D'Incà et al., 1999), celiac (Madara and Trier, 1980), gastroenteritis (Marshall et al., 2004) and infection with *Campilobacter jejuni* (Spiller et al., 2000).

To do this, we treated MDCK and Caco-2 cell monolayers with two GCPQ polymers with different levels of DQ but similar levels of DP, one which provides the upper limit of tight junction modulation

(GCP20Q22) and the other which provides less (GCP19Q12). We then examined the transport of different sized FITC dextran molecules up to 250kDa as well as the transport of a rigid molecule FITC albumin.

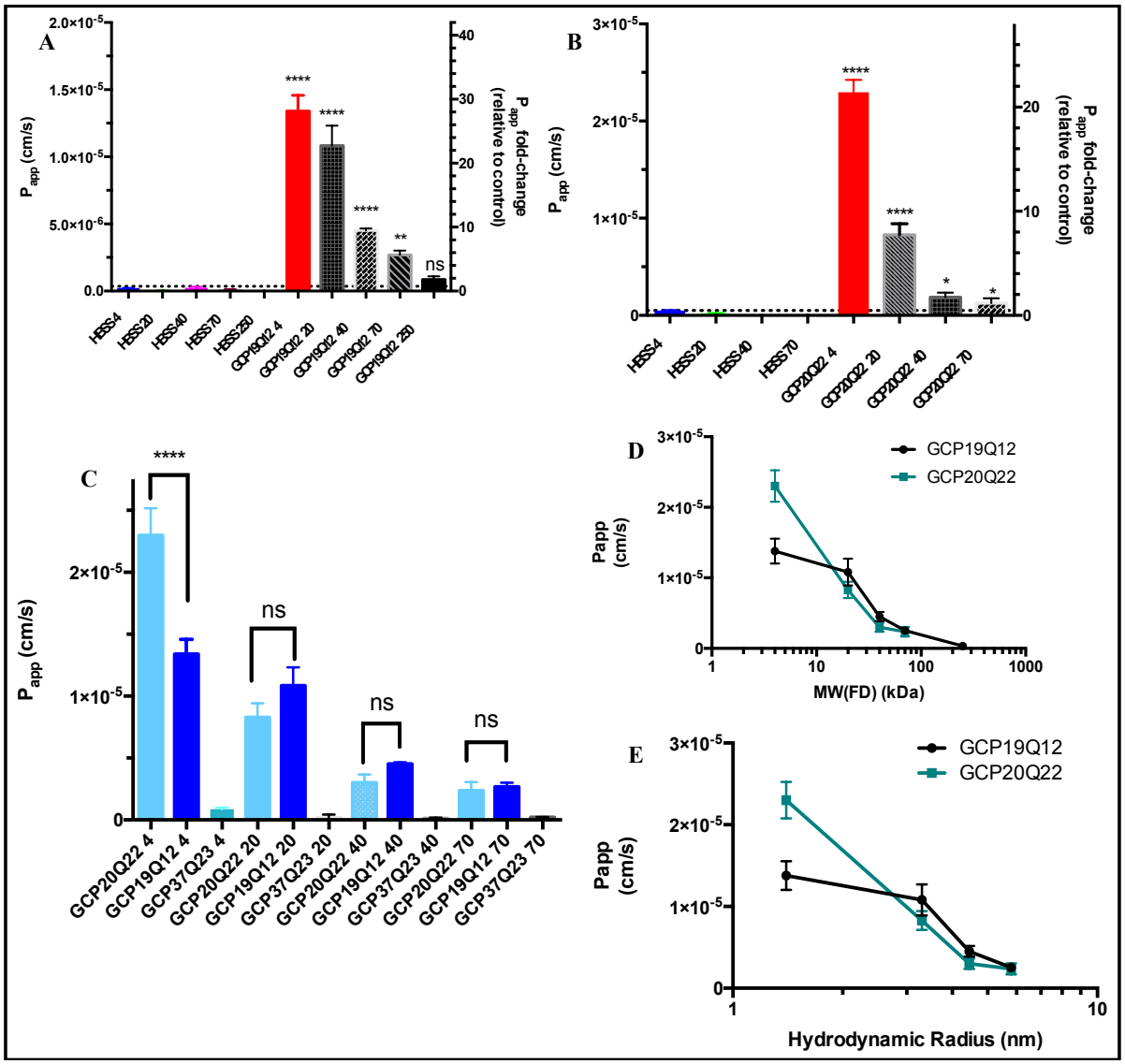

Figure 5-12: Effect of GCPQ on the paracellular transport of different sizes of FITC dextran across MDCK monolayers at pH 6.8.

A. Effect of GCPQ03 (GCP19Q12) on the Papp of different sizes of dextran. **B**. effect of GCPQ06 (GCP20Q22) on the Papp of different sizes of dextran. **C**. Comparison of the effects of GCPQ 03 and GCPQ06 on the Papp of different sizes of Dextran. **D**. Plot of Papp against molecular weight of different sizes of FITC dextran after treatment with GCPQ03, GCPQ06 and GCPQ10 (GCP37Q23). **E**. Plot of Papp against hydrodynamic radius of different sizes of FITC dextran after treatment with both GCPQ03 and GCPQ06. Statistical significance was determined by two-way ANOVA with Bonferroni post- test and one-way

ANOVA with Dunnett's multiple comparison post- test. n=4; *= P<0.05; **=P<0.01; ***=P<0.001.

Figure 5-12a shows that treatment with GCP19Q12 increases the permeability of MDCK cell monolayer to 4kDa, 20kDa, 40kDa and 70kDa FITC dextran but not 250kDa FITC dextran. There is a decrease in the Papp of dextran as the molecular weight increases. The same is shown when MDCK cell monolayers are treated with GCP20Q22 as shown in **Figure 5-12b**. **Figure 5-12c** shows that while there is significant difference between the Papp values of FD4 after treatment with GCP20Q22 and GCP19Q12 as is expected from the previous data, there is no significant difference between the Papp of the higher molecular weight dextrans after treatment with GCP19Q12 and GCP20Q22 . This is also shown in the line plots of Papp against molecular weight in Figure **5-12d** and the line plot of Papp against hydrodynamic radii as shown in **figure 5-12e**. the hydrodynamic radii of the dextrans as obtained from the product information (Sigma , UK) are : FD4: kDa ≈14Å (1.4nm), 10kDa ≈ 23 Å (2.3nm), 20kDa ≈ 33 Å (3.3nm), 40kDa ≈ 44 Å (4.4nm), 70kDa ≈ 60 Å (6.0nm).

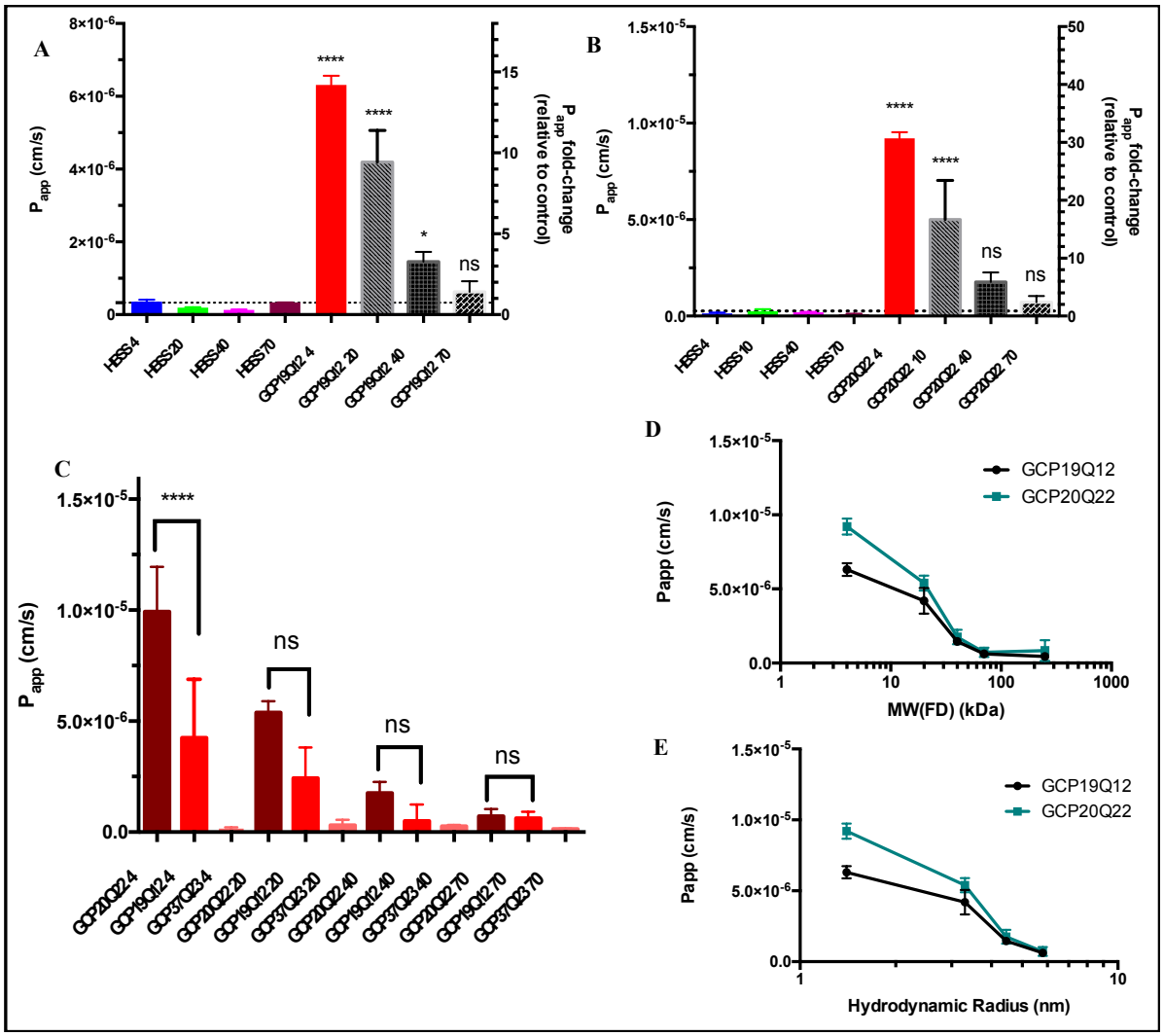

Figure 5-13: Effect of GCPQ on the paracellular transport of different sizes of FITC dextran across Caco-2 monolayers at pH 6.8.

A. Effect of GCPQ03 (GCP19Q12) on the Papp of different sizes of dextran. **B**. effect of GCPQ06 (GCP20Q22) on the Papp of different sizes of dextran. **C**. Comparison of the effects of GCPQ 03 and GCPQ06 on the Papp of different sizes of Dextran. **D**. Plot of Papp against molecular weight of different sizes of FITC dextran after treatment with GCPQ03, GCPQ06 and GCPQ10 (GCP37Q23). **E**. Plot of Papp against hydrodynamic radius of different sizes of FITC dextran after treatment with both GCPQ03 and GCPQ06. Statistical significance was determined by two-way ANOVA with Bonferroni post- test and one-way ANOVA with Dunnett's multiple comparison post- test. n=4; *= P<0.05; **=P<0.01; ***=P<0.001

Figure 5-13a shows that treatment with GCP19Q12 increases the permeability of Caco-2 cell monolayer to 4kDa, 20kDa and marginally to 40kDa but 70kDa FITC dextran. There is a decrease in the Papp of dextran as the molecular weight increases. A similar observation is shown when Caco-2 cell monolayers are treated with GCP20Q22 but was shown in **Figure 5-13b**. This is slightly different from the observation with MDCK cells where FD40 and FD70 both had significantly higher Papp values than the negative control, suggesting that MDCK cells are more susceptible to GCPQ polymers tight junction modulations than Caco-2 cells. **Figure 5-13c** shows that while there is significant difference between the Papp values of FD4 after treatment with GCP20Q22 and GCP19Q12 as is expected from the previous data, there is no significant difference between the Papp of the higher molecular weight dextrans after treatment with GCP19Q12 and GCP20Q22, like was observed with MDCK cells . This is also shown in the line plots of Papp against molecular weight in Figure **5-13d** and the line plot of Papp against hydrodynamic radii as shown in **figure 5-13e**, again similar to what was observed in MDCK cells.

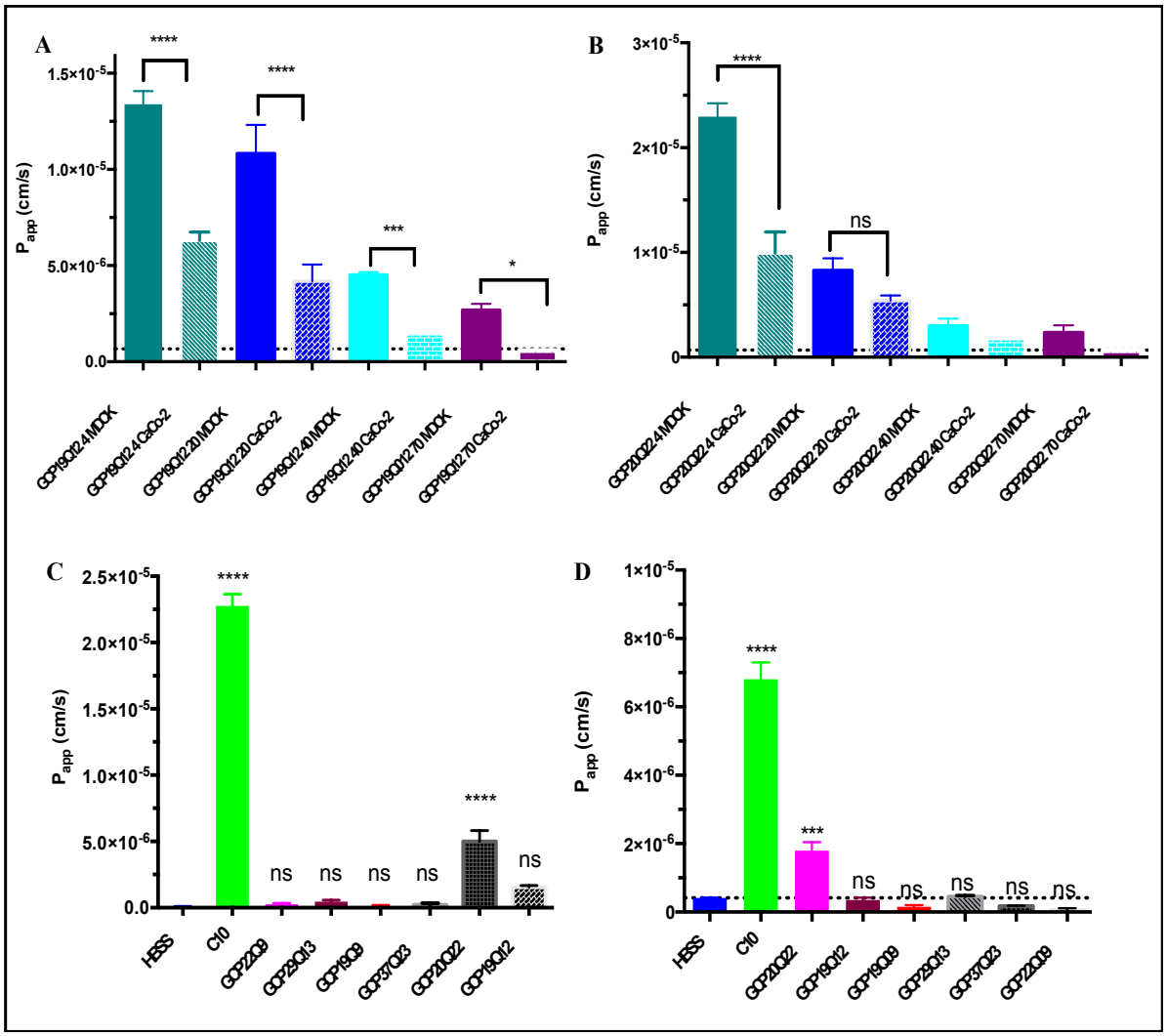

Figure 5-14: Effect of GCPQ on the paracellular transport of different sizes of FITC dextran and FITC albumin across MDCK and Caco-2 monolayers at pH 6.8.

A. Effect of GCPQ03 (GCP19Q12) on the Papp of different sizes of dextran. **B**. Effect of GCPQ06 (GCP20Q22) on the Papp of different sizes of dextran. **C**. Effect of different GCPQ polymers and C10 on the transport of FITC-albumin across an MDCK cell monolayer. **D**. Effect of different GCPQ polymers and C10 on the transport of FITC-albumin (1mg/mL) across a Caco-2 cell monolayer. Statistical significance was determined by two-way ANOVA with Bonferroni post- test and one-way ANOVA with Dunnett's multiple comparison post- test. n=4; *= P<0.05; **=P<0.01; ***=P<0.001

Figure 5-14a shows the comparison between the Papp of different sizes of FITC dextran molecules after treatment with GCP19Q12 in MDCK cells and Caco-2 cells. The Papp values are significantly greater in MDCK cells than they are in Caco-2 cell, again supporting the observation that MDCK cells are more susceptible to tight junction modulation after treatment with GCPQ than Caco-2 cells are. Following treatment with GCP20Q22 however, only the Papp values of FD4 are significantly higher in MDCK cells than in Caco-2 cells. The Papp of higher molecular weight dextrans are not significantly different in both cell lines though they are slightly higher in the MDCK cells than in the Caco-2 cells (Figure 4-14b). Figure 5-14c shows that while C10 was able to significantly increase the permeability of MDCK cell monolayers to FITC albumin which has a molecular weight of 69kDa (hydrodynamic radius =3.8 nm), GCPQ polymers failed to significantly do so except GCP20Q22. Figure 5-14d shows a similar result as only C10 and GCP20Q22 were able to significantly increase the Papp of FITC-albumin in Caco-2 cells. In both MDCK and Caco-2 cell lines, C10 caused about 4 times more permeation of FITC albumin than GCP20Q22.

Discussion

To determine the extent of tight junction modulation after GCPQ treatment, different sizes of FITC labelled dextran were administered to MDCK cell monolayers after GCPQ treatment and the quantity transported to the basolateral chamber determined by fluorescence spectroscopy. According to the product information (Sigma-Aldrich), the different sizes of Dextran are noted to have different Stoke's radii: FD4: kDa ≈14Å (1.4nm), 10kDa ≈ 23 Å (2.3nm), 20kDa ≈ 33 Å (3.3nm), 40kDa ≈ 44 Å (4.4nm), 70kDa ≈ 60 Å (6.0nm) and conformation (2-10kDa: expandable coil; >10kDa: branched flexible polymers)

Figures 5-12 and 5-13 show that smaller molecules of about 4kDa are transported most in both MDCK and Caco-2 cells. GCPQ 06 which has a very high DQ and QPR enhances the transport of FD4 more than GCPQ03 does in both MDCK and Caco-2 cells. No difference in the transport of bigger sized dextrans is observed in either cell line. This implies that the graded effect observed with FD4 might be lost with higher sizes of dextrans, suggesting that there is a size limit to tight junction permeability following treatment with GCPQ. This might also suggest differences in channels for the transport of the different sized molecules in both cell monolayer. **Figure 5-12d and 5-12e** as well **as Figure 5-13d and 5-13e** show the relationship between the flux and the size of the transported molecules, the gradient being steeper at lower molecular weight and slower at bigger molecular weight. This is consistent with previous reports suggesting that the relationship is bi-phasic with high permeability for molecules at about 4 Å but lower for larger molecules (Shen et al., 2011). Dextrans are flexible polymers which could adapt to different shapes to facilitate their passage through channels. This raised the question about whether the conformation of dextran enabled the

higher molecular weight FITC dextran to permeate the modulated tight junctions, possibly explaining the lower gradients observed with the high molecular weight dextrans. To answer this question, we treated both cell monolayers with a molecule which had a more rigid structure. We chose albumin which is a protein and has a similar molecular weight as 70 kDa FITC dextran but a hydrodynamic radius similar to a 20 kDa dextran (3.8 nm).

Figure 5-14c and 5-14d show the effect of different GCPQ polymers and sodium caprate on the transport of FITC albumin. Albumin is a 69 kDa protein with a hydrodynamic radius of about 3.8 nm which is more than the hydrodynamic radius of 20 kDa FD4 (3.3 nm) but less than the hydrodynamic radius of FD40 (4.4 nm). Albumin was used in this assay to determine if the transport of bigger sized dextran was due to their structural conformation, the fact that they are flexible and can stretch out to pass through the small pore size of the tight junction. Figure 5-14c and 5-14d show that while C10 increased the permeability of the MDCK and Caco-2 cells to albumin, GCPQ mostly doesn't except GCP20Q22. This shows that the actual limit of tight junction is less than 3.8 nm and that FITC dextran molecules with higher molecular weight than 20 kDa likely permeated the tight junctions because of conformational changes. A few studies suggest that the diffusion of dextran is more limited by the geometric conformation than by the Stokes radii (Pluen et al., 1999, Ta et al., 2009) which agrees with our observation that higher molecular weight FITC dextrans with higher hydrodynamic radii than 3.8 nm likely diffused because they could adopt a conformation that allowed them to pass through the modulated tight junctions.

The tight junction has both size and charge restrictive functions. The claudin family of tight junction proteins are reported to be responsible for the charge restrictive functions while the occludin and other members of the Tight junction Associates MARVEL proteins (TAMP) are reported to regulate the transport of macromolecules across the tight junction. The claudin based channels of the bicellular tight junction reportedly allows a high capacity charge and size-selective passage of small molecules and ions (Krug et al., 2014). Larger sized macromolecules reportedly pass through structural discontinuities on the bicellular tight junction and through the tricellular tight junction (Krug et al., 2009). This route is considered charge- and size- non selective as well as low capacity (Shen et al., 2011). This route, which is regulated by occludin and the TAMP proteins is potentially the pathway for passage of the larger sized dextran molecules considering the lack of significant difference in their passage through and the loss of correlation with QPR of GCPQ polymers. Interestingly, these leaky channels are reported to allow the transport of molecules up to 38 Å (3.8 nm) when distorted (Al-Sadi et al., 2011) and the tricellular tight junction has a pore size of up to 100 Å and is considered a weak point in the tight junction (Staehelin et al., 1969). Occludin (Balda et al., 1996) and Tricellulin (Ikenouchi et al., 2005) have also both been implicated in the increased transport of 4 kDa FITC dextran and 20KDa macromolecules. GCPQ and C10 thus potentially act by creating these discontinuities at the bicellular tight junctions and consequently increase the transport of large molecules, GCPQ being much less in severity than C10.

Following on from this observation, we sought to establish the involvement of these leaky channels in the uptake of larger sized dextrans following treatment with GCPQ. To do this,

we stain the tight junction proteins after treatment with GCPQ and observe their distribution using confocal microscope. We chose to stain the Zona occludens-1 (ZO-1) protein which is an intracellular component of the adherens junction that links the occludin and the actin cytoskeleton (Fanning et al., 1998). Disrupting the interaction between occludin and ZO-1 will invariably alter the integrity of the tight junctions (Van Itallie et al., 2009, Liang and Weber, 2014) and facilitate passage through the leaky channels . We therefore treated Caco-2 cell monolayers with GCPQ06 (GCP20Q22) and sodium caprate (C10) and labelled the ZO-1 tight junction using the method described in the method section of this chapter, and subsequently obtained confocal images of the cell monolayers.

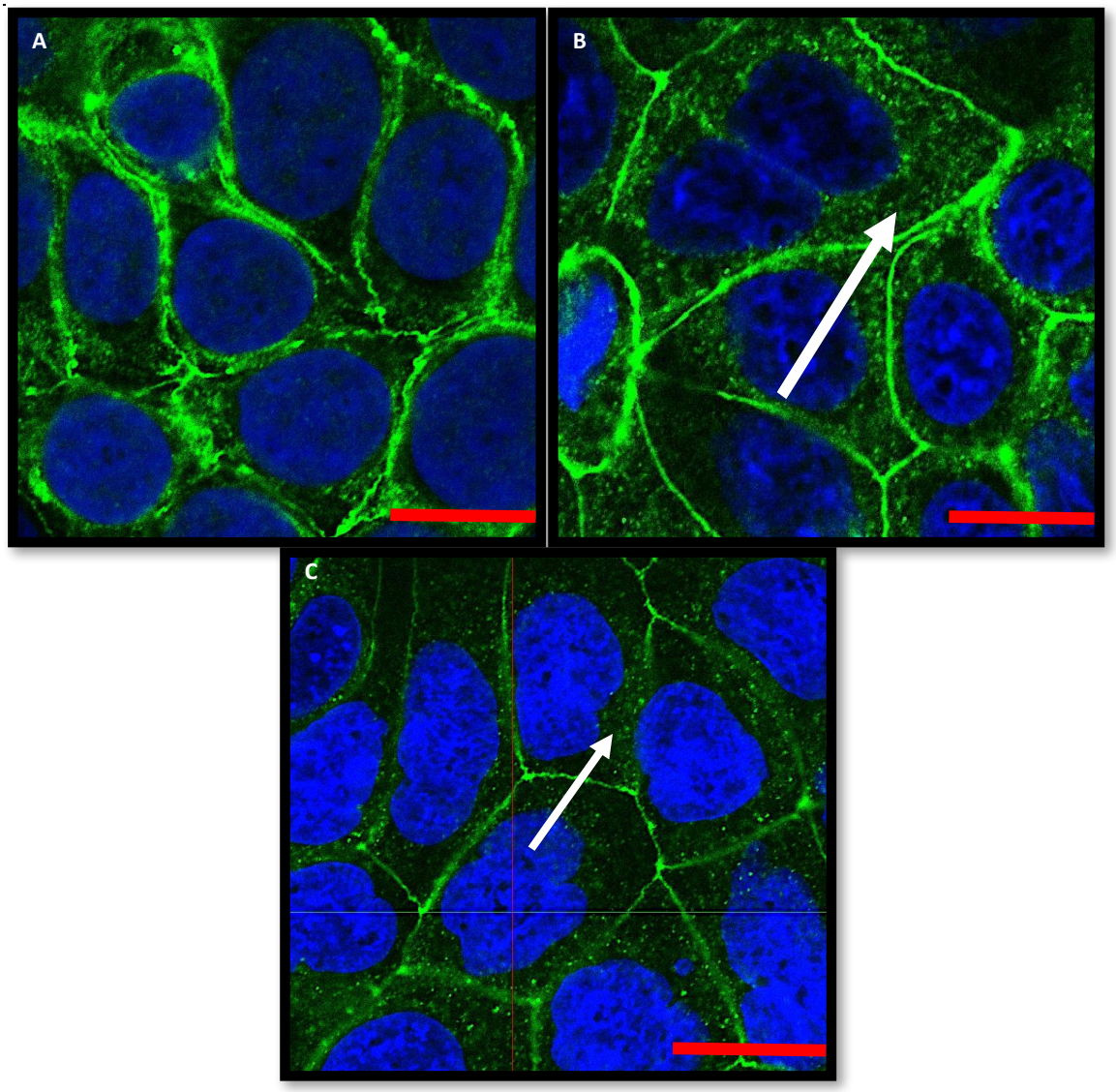

Figure 5-15: Confocal microscopy images of Caco 2 cells showing effect of GCPQ on tight junction protein zona occludens-1 (ZO-1). A. control cells treated with serum free medium, B. caco-2 cells treated with 1mg/ml of GCPQ06 for 2 hours. C. Caco-2 cells treated with 10mM sodium caprate for 1 hour. Arrows indicate distortion of cytoskeletal components of tight junction protein. Blue: DAPI, green, Alexa Fluor 488 showing ZO1. Arrows show relocation of ZO1 proteins. Scale bar = 20 μm

Figure 5-15 shows the effect of GCP20Q22 and C10 on the ZO-1 proteins in Caco-2 cells. Figure 5-15A shows ZO-1 closely aligned with the cell membrane, around the intercellular

junctions as would be expected in an undisturbed conformation. GCPQ06 **(B)** and C10 (**C**) treated cells however show signs of re-distribution into the cytosol, suggesting that the adhesion of ZO-1 to the extracellular components of the tight junction has been distorted. This has been suggested in a previous report as one of the events that occur when there is tight junction disassembly resulting in increased paracellular transport (Anderson and Van Itallie, 1995). This therefore shows that GCPQ, like C10 increases paracellular transport through a ZO-1 dependent mechanism which invariably utilises the occludin dependent, charge and size-non-selective, low capacity leaky channels (Al-Sadi et al., 2011) and explains the slower rate of transport of higher molecular weight dextran molecules which have a greater hydrodynamic radius than 3.8 nm as well as

After determining that tight junction modulation with GCPQ involves re-location of tight junction proteins and also that the charges of GCPQ are important for this mechanism, we sought to examine the nature of GCPQ interactions with the epithelial cell surface. Since GCPQ has a permanent positive charge and is administered at concentrations higher than the CMC, we postulated that GCPQ will be electrostatically attached to the negatively charged membrane in particulate form. We therefore treated MDCK cells with Texas-red labelled GCPQ polymers and stained the cell membrane and nucleus and examined the nature of interactions of GCPQ with the cell membrane using confocal microscopy. The method used for this experiment is described in the method section of this chapter.

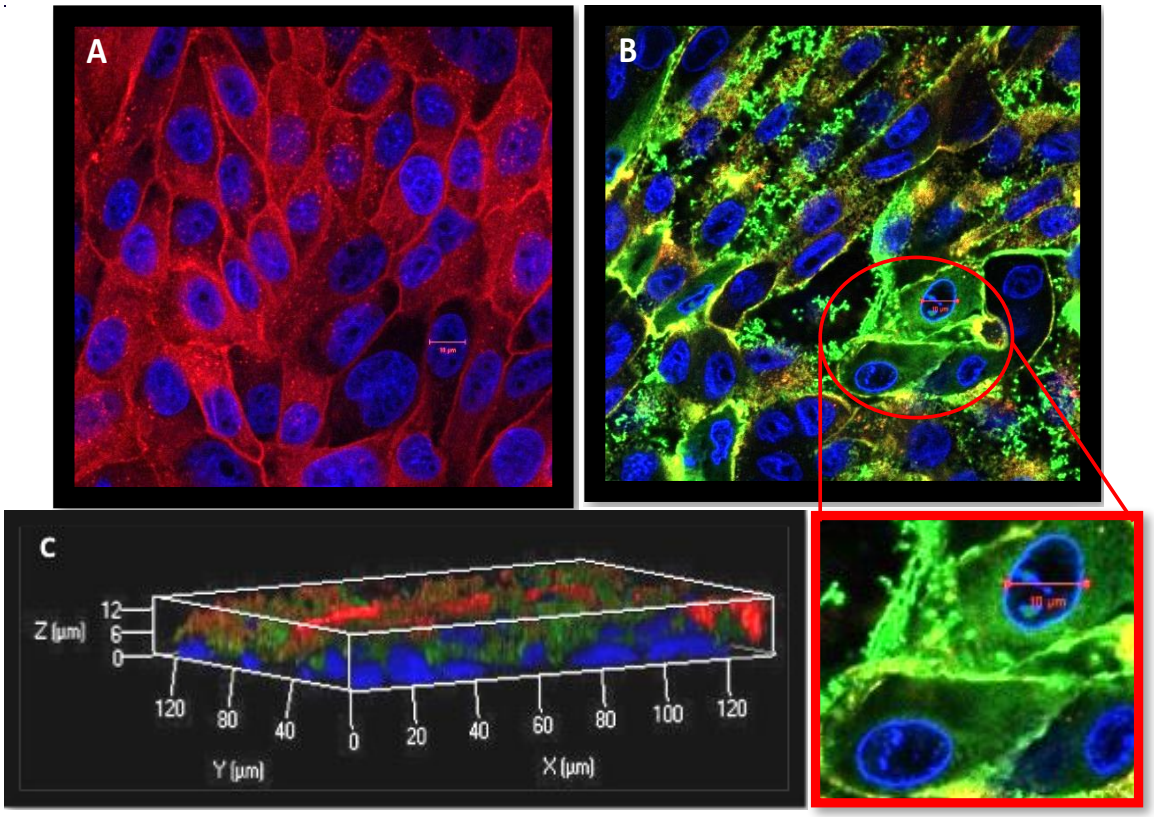

Figure 5-16: CLSM images showing GCPQ-TR particles adhering to an MDCK monolayer. **A**. Control cells treated with HBSS buffer. **B**. MDCK cells treated with 1mg/mL of GCPQ-TR. **C**. Z-stack image of MDCK cells treated with GCPQ-TR showing close adherence to the epithelial membrane and interactions around the intercellular junction. Blue: DAPI, Red: Cell Mask Deep Red, Green: GCPQ-TR. Scale bar: 10µm.

Figure 5-16 shows GCPQ-Texas red attached around the cell membrane, at the intercellular junctions and some passage across the cell membrane after exposure of MDCK cells to GCPQ-Texas red for 2 hours. The strong adherence to the cell surface is due to the strong attraction between the positive charges of GCPQ and the largely negative charges of the cell membrane components. The cut-out from figure 5-16b shows what appears to be a strong disperse green within the cytoplasm, indicating that some GCPQ-Texas red molecules got taken up over the 2-hour period, corresponding with previous reports that GCPQ facilitates

uptake by endocytosis. This raises the question of whether the effect of GCPQ on tight junction modulation is a direct effect, or an in direct effect- questions about whether GCPQ binding to extracellular membrane components or receptors is sufficient to trigger tight junction modulation or whether the uptake of GCPQ is necessary to cause this modulation.

To help us answer this question, we decided to use confocal images to identify the onset of effects and if GCPQ interacts with the membranes as particles or as monomers. To do this, we carried out a live cell imaging using the same concentration of GCPQ-TR on MDCK cells.

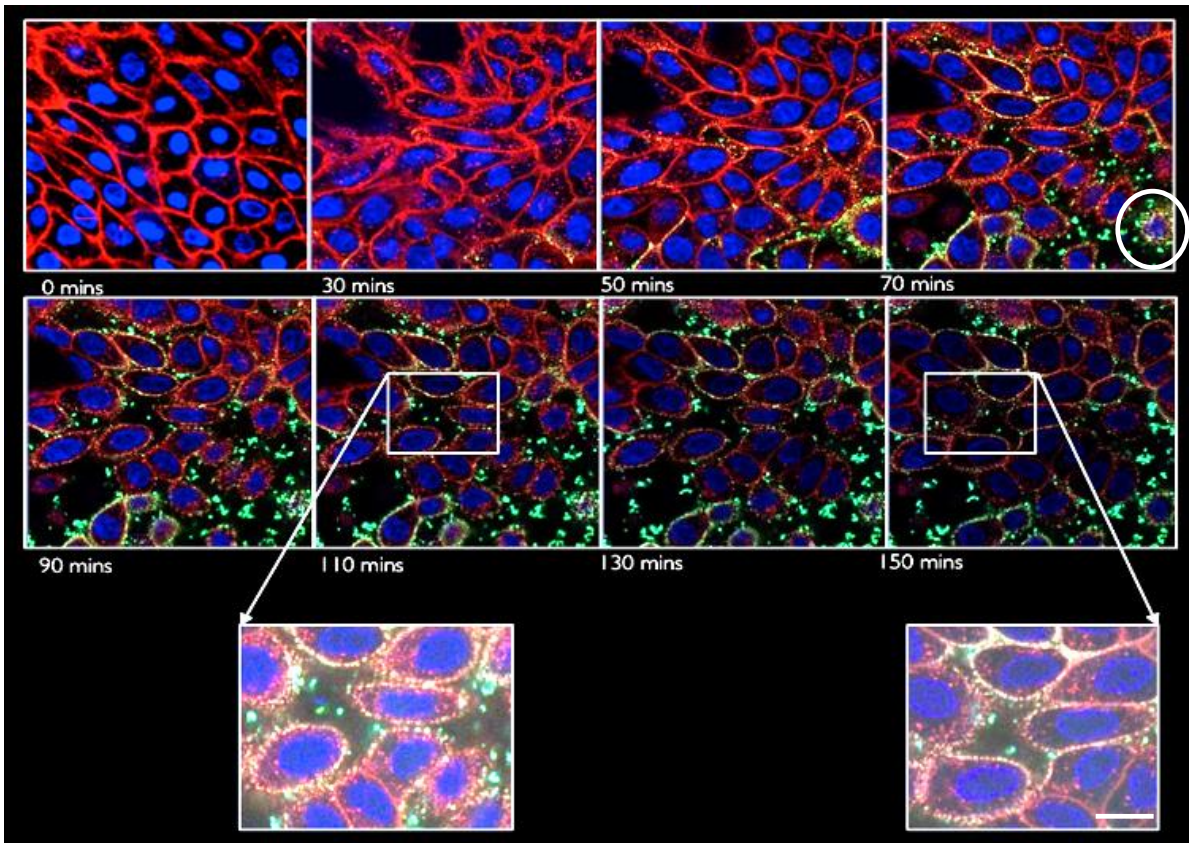

Figure 5-17: Live CLSM images of MDCK cells treated with Texas red labelled GCPQ showing time scale (time in minutes) of events during treatment. Blue stain: Hoechst; Red stain: Cell mask deep red; Green stain: GCPQ-Texas Red. Scale bar = 10μm

In **Figure 5-17**, GCPQ appears to cluster around the cell membrane and at the intercellular junctions as was seen in Figure 5-16. This observations correspond with previous reports that chitosan derivatives adhere to cell membranes as they transiently open tight junctions (Pan et al., 2002). The effect is seen to start about 30 minutes after exposure to GCPQ-TR. With increasing time, more GCPQ-TR molecules can be seen attaching to the membrane and between the intercellular junctions. GCPQ-TR also appears to be in the form of particles

as it attaches to the epithelial cell surface. Furthermore, the images show that as GCPQ attaches to the membranes, the cells appear to pull away from each other. This is obvious from about 50 minutes after treatment. At about 70 minutes, a cell which has a high local concentration of GCPQ-TR appears to lose much of its cell membrane (circled). This might explain the release of LDH after treatment with certain GCPQ polymers as shown in Figure 5-3a.

It appears, as can be seen from the enlargement at 110 minutes, that GCPQ-TR is taken up in membrane bound vesicles. This is clear from the appearance of strong yellow particulate discontinuities on the cell membranes and the presence of red vesicles in the cytoplasm. What is striking is that the vesicles within the cytoplasm are closer to red than yellow, suggesting that the strong yellow colour on the membrane is due to high local concentration of GCPQ-TR but that the intracellular vesicles perhaps carry only few GCPQ-TR particles. At about 150 minutes, the cells appear to start regaining their close contact (as shown in the enlargement) and the level of GCPQ-TR on the membrane appears to be reduced. This is probably explained by the recycling of the membrane components (Brown, 1989, Goldenring, 2015) after possibly releasing GCPQ-TR from the intracellular vesicles or degrading GCPQ-TR in the vesicles. In line with our observations in other in vitro assays; the fact that the cells begin to regain their close conformation corresponds with our finding that the TEER values return to pre-treatment values, 24 to 72 hours after treatment and cells recover from toxicity after 24 hours.

Uptake through the paracellular pathway using chitosan and some of its derivatives has been shown to involve modulation of the tight junction with suggested mechanisms including chelation or depletion of Ca^{2+}, resulting in the activation of protein kinase C (PKC) – a

process which is mediated by the calcium dependent cell adhesion protein cadherin. This results in the internalization of cadherin family proteins and triggers a cellular signalling cascade that causes the disassembly of cellular junction components including Zonula Occludens-1 (ZO-1) (Citi, 1992, Noach et al., 1993, Tomita et al., 1996, Salamat-Miller and Johnston, 2005). Recent studies have also shown an association between surface proteins - integrin and a downstream signalling pathway involving the phosphorylation of FAK and Src kinases, resulting in the dislodgement of claudin with subsequent destruction in lysosomal vessels. Chitosan was found to cause the clustering of integrins on the surface membrane, thereby triggering the subsequent downstream effects, resulting in altered tight junctions in Caco2 cells (Hsu et al., 2012). Interestingly, integrins and cadherins are important mechano-sensors, responsible for regulating cell adhesion, intercellular communication and mechano-transduction (Schwartz and DeSimone, 2008). In response to altered shear stress, cadherins facilitate the disassembly and subsequent reassembly of adherens junctions (Noria et al., 1999). Also, osmotic stress has been shown to trigger FAK and Src kinases in endothelial cells, a process which is associated with integrin (Browe and Baumgarten, 2003).

Our data show that GCPQ also causes the disassembly of tight junction protein ZO-1 but the specific molecular mechanisms are not clear. However, considering that GCPQ was administered at concentrations higher than the cmc, and the observation of effects being due to local concentration around cells, it is plausible to reason that osmotic stress from the high local concentration of GCPQ molecules in particulate forms as well as the altered shear stress from attachment of the polymers to the epithelial surfaces causes activation of integrin and

cadherin associated downstream effects that result in the disassociation of the junctional complex. But by internalising these extracellularly bound GCPQ molecules and subsequently releasing them extracellularly or degrading them, the cell membrane components can be recycled and membrane homeostasis restored – hence the reassembly of the tight junctional complex and recovery of cells.

Since it is clear that GCPQ gets taken up into the cells as shown in the images in figures 5-16 and 5-17, we decided to understand what mechanisms are involved in this uptake. To do this, we used flow cytometry to quantify how much GCPQ –TR is taken up by the cells and subsequently used pathway inhibitors to determine what mechanism was involved in the uptake.

5.3 Endocytosis of GCPQ polymeric particles

GCPQ has previously been reported to enhance uptake primarily by transcytosis (Siew et al., 2011). We have shown with preceding data that GCPQ can also be engineered to utilise the paracellular route of transport. We have also observed that GCPQ particles can be found within the cytoplasm of treated cells. We therefore decided to determine what pathways are involved in this uptake.

Endocytosis is a receptor mediated process through which cells take up materials from the extracellular fluid environment. Most of these molecules that have been taken up, including hormones, iron and proteins are ligands for specific receptors on the cell surface. However, several other molecules which do not have specific receptors get taken up by the same process (Pastan and Willingham, 1985). Endocytosis occurs by different mechanisms, including clathrin mediated endocytosis which is considered most important because of its predominance in endocytic processes (Doherty and McMahon, 2009). Clathrin mediated endocytosis involves the formation of clathrin coated pits with the associated cargo which eventually cleaves off the membrane and forms clathrin coated vesicles within the cytoplasm and can carry on to have different fates including eventual exocytosis (Sorkin, 2004). This process has been well studied and reported on and will be examined as a possible route of uptake of GCPQ nanoparticles. To examine this hypothesis, MDCK cells were be treated with Texas red labelled GCPQ nanoparticles with and without the inhibitor of clathrin mediated endocytosis, chlorpromazine (Ivanov, 2008) and the uptake of the fluorescent

nanoparticles was quantified using flow cytometry. Intracellular vesicles were also labelled and the internalisation of the fluorescent nanoparticles observed using confocal microscopy.

5.3.1 Method

Cell culture and maintenance

MDCK cells (Passage number 15-24), were grown in filter-topped cell culture flasks using Minimum Essential Medium Eagle (Sigma, M2279) supplemented with 10 % foetal bovine serum (Life Technologies, UK, 11140-035), 1 % Penicillin-Streptomycin (Gibco, 15140) and 1 % GlutaMAX supplement (ThermoFisher Scientific, 35050061). Cell culture medium was replaced three times per week. Cells were incubated at 37°C in a humidified 5 % CO_2 and 95 % air atmosphere and passaged every 4-5 days with a seeding density of 3 x 10^5 to 4 x 10^5 cells in T-75 flasks.

Flow cytometry

MDCK cells were seeded in 6-well plates at a density of 1 x 10^5 cells per well for 2 days until they were about 70 % confluent. Cells were then treated with 50 μg/ml of GCPQ-TR for different durations: 2 hours, 4 hours and 24 hours. Where inhibition was required, cells were pre incubated with 10μg/mL of chlorpromazine for 30 minutes before treatment with GCPQ-TR with or without the inhibitor for the duration of the treatment in accordance with a previously published method (Silva et al., 2017). After incubation, cells were washed twice with 3 mL of phosphate buffered saline (PBS) and collected by trypsinisation, pelleted by centrifuging at 300 rcf for 4 minutes at 4ºC, washed again with PBS and re-suspended in 1

mL of PBS. Cells were then kept at 4ºC prior to analysis using a MACSQuant analyser (Miltennyi Biotec, Surrey, UK). 10,000 events were collected for each analysis.

Confocal Microscopy

Cells were seeded on cover slips placed in 12 well plates at a density of 1 x 10^4 cells per well for 24 hours. On the day of the experiment, cells were incubated with 50 μg/ml of GCPQ-TR in serum free medium for 2 hours. Where inhibition was required, cells were pre-incubated with 10 μg/mL of chlorpromazine for 30 minutes before treatment with GCPQ-TR with or without 5 μg/mL of the inhibitor for the duration of the treatment. Negative control cells were incubated with serum free medium. After the treatment, cells were washed twice with 2 mL PBS and fixed with 1 mL 4 % paraformaldehyde for 10 minutes and subsequently washed twice again with 2 mL PBS after which they were stained with DAPI and imaged under the microscope.

For live cell imaging, the cells were seeded in a MatTek Glass Bottom Microwell Dish and incubated in the same medium as with the fixed cell and under the same conditions until the cells were confluent. Cells were also co-incubated with 1 μg/ml of LysoTracker green dye for the duration of the treatment. Imaging was done using the inverted Zeiss LSM 710 confocal microscope while incubating at 37ºC and 5 % CO_2.

5.3.2 Results and Discussion

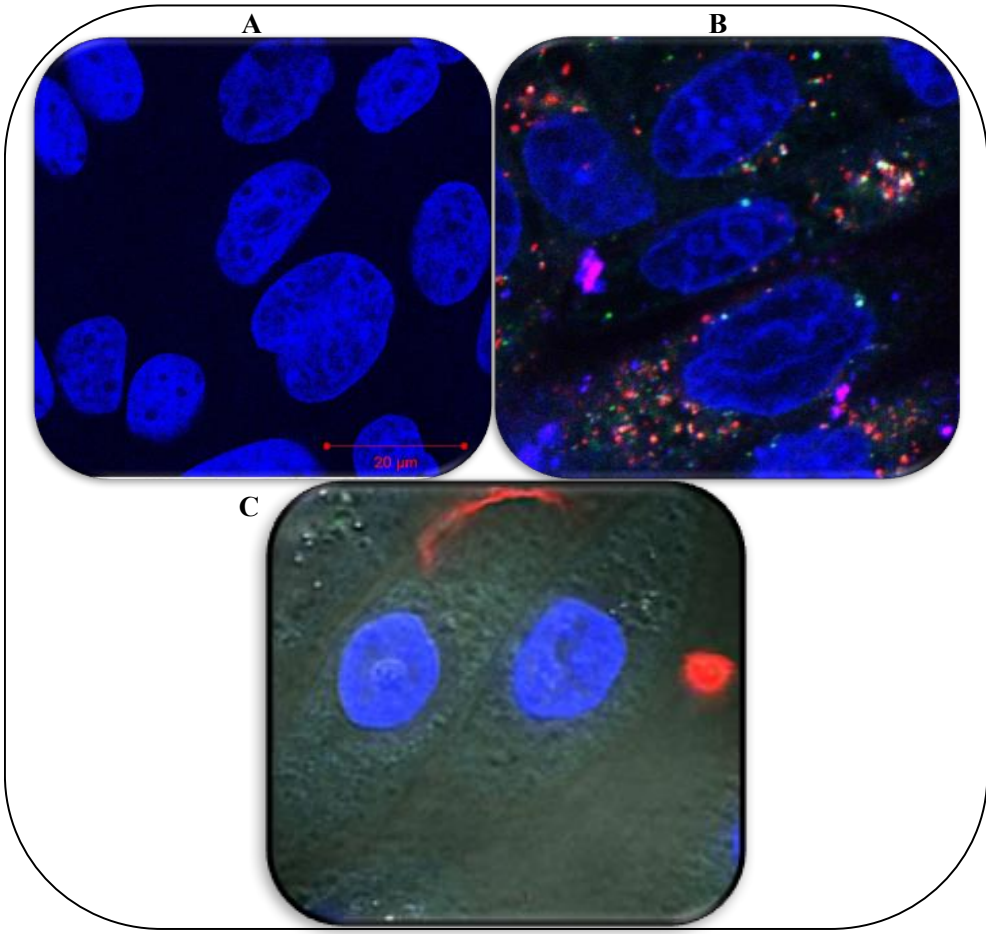

Figure 5-18: Confocal microscopy image showing uptake of GCPQ-TR into intracellular vesicles in MDCK cells.

A. Negative control cells treated with HBSS buffer. **B**. MDCK cells treated with 50µg/mL GCPQ-TR for 2 hours. C. MDCK cells treated with GCPQ-TR after inhibition with chlorpromazine (10 µg/mL). Bar: 20µm, Blue: DAPI, Red: GCPQ-TR, Green: Lysotracker Green.

Figure 5-18 shows the confocal microscopy image of MDCK cells treated with GCPQ-TR with and without CPZ. GCPQ-TR nanoparticles are seen co-localised with the lysotracker

green labelled intracellular vesicles, suggesting entrapment of these nanoparticles in these vesicles. Figure 5-18c shows that with CPZ inhibition, GCPQ-TR is still able to bind to the membrane but not readily internalised. This binding might be due to the positively charged GCPQ particles interacting with the negatively charged membrane components.

We then decided to quantify the uptake of GCPQ-TR using flow cytometry and determine how much inhibition is achieved by using chlorpromazine.

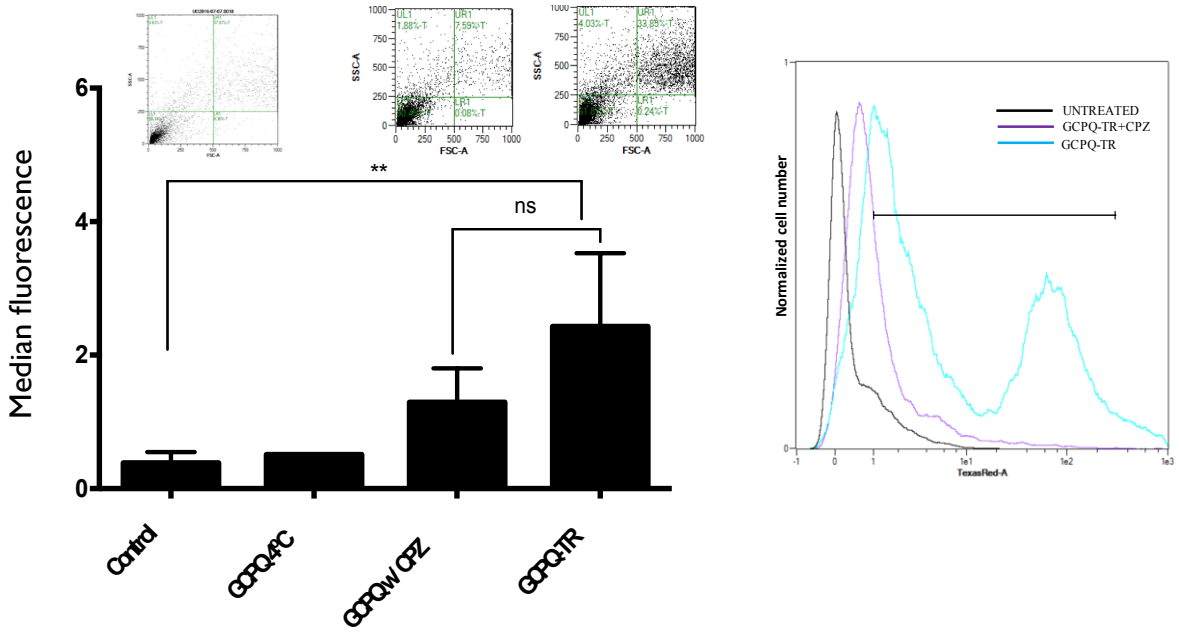

Figure 5-19: Uptake of GCPQ-TR with and without chlorpromazine (10µg/mL) inhibition at after 2 hours of treatment. Median fluorescence of Texas red labelled GCPQ (GCPQ-TR) measured by flow cytometry. Statistical analysis was determined by one-way ANOVA. . n=4; *= P<0.05; **=P<0.01.

Figure 5-19 shows the median fluorescence of MDCK cells after exposure to GCPQ-TR. MDCK Cells exposed to GCPQ-TR without chlorpromazine (an inhibitor of clathrin mediated endocytosis) took up about two times more GCPQ-TR than MDCK cells exposed to CPZ for 30 minutes before being exposed to GCPQ. This difference was however not found to be significant. When cells were incubated with GCPQ-TR at 4^{o}C, the uptake was also inhibited. Binding without uptake was also minimal as shown by the similarity between the negative control and the cells incubated at 4^{o}C. There is however the possibility that detachment by trypsinisation removed some of the bound GCPQ-TR and since the same process was applied to the other GCPQ-TR treated cells, it can be assumed that the fluorescence measured by flow cytometry was mostly due to particles taken up.

Since the figures show that pre-incubating cells with 10 μM CPZ for 30 minutes before incubation with GCPQ-TR does not completely inhibit the uptake of GCPQ-TR, we sought to determine if a longer incubation period will result in greater inhibition. We therefore pre-incubated MDCK cells with CPZ and then co-incubated with GCPQ-TR for the duration of treatment.

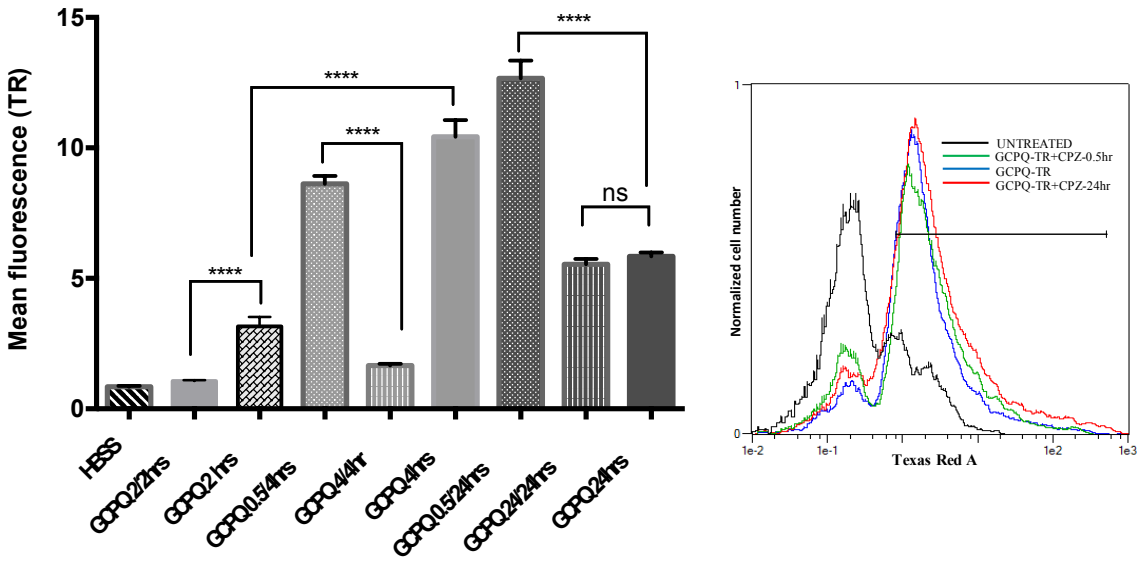

Figure 5-20: Fluorescence intensity of Texas red labelled GCPQ particles after uptake by MDCK cells incubated with or without the inhibitor, chlorpromazine (CPZ) (10µg/mL) for different durations. The fluorescent intensity curve represents MDCK cells treated for 24 hours. The grey curve represents untreated control cells. The blue curve represents MDCK cells incubated with GCPQ-TR for 24 hours without inhibition. The green curve represents MDCK cells pre-incubated with CPZ for 30 minutes before incubation with GCPQ-TR for 24 hours. The red curve represents MDCK cells co-incubated with GCPQ-TR and CPZ for 24 hours. Statistical analysis was determined by one-way ANOVA. N = 4; * = $P < 0.05$; ** = $P < 0.01$, **** = $P < 0.0001$.

Figure 5-20 shows the fluorescence intensity of GCPQ-TR taken up by MDCK cells with or without the clathrin mediated inhibitor, chlorpromazine (CPZ) after treatment for 2 hours, 4 hours and 24 hours. The mean fluorescence of GCPQ-TR increases with increasing duration of exposure and then decreases after 24 hours. The decrease at 24 hours is probably due to exocytosis of the nanoparticles during this period. Chlorpromazine inhibition

significantly prevented the uptake of GCPQ-TR when incubated for 2hours and 4hours while it appeared to significantly increase the uptake when exposed for 24hours. When cells are pre-incubated with chlorpromazine for only 30minutes and not co-incubated with GCPQ-TR, inhibition of uptake is significantly reduced, suggesting that co-incubation is important for extensive inhibition. For the 24-hour treatment, 30-minute pre-incubation with CPZ resulted in a much higher mean fluorescence than the non-inhibited cells and the cells co-incubated with CPZ for the duration of the treatment. This possibly suggests that the cells pre-incubated with CPZ had a slower internalisation which resulted in a slower rate of exocytosis or degradation, leaving a higher amount of the internalised nanoparticles within the cell after 24 hours. This assumption is supported by the observation that 30-minute pre-incubation with CPZ does not significantly inhibit uptake of GCPQ-TR in the 4 hours (figure 5-20) and 2 hour (figure 5-19) treated cells while the cells co-incubated with CPZ and GCPQ-TR for the duration of the treatment were not significantly different from the negative control cells. The alternative suggestion will be cytotoxicity resulting in indiscriminate uptake but this will not be supported by the lower mean fluorescence values observed for the 24-hour co-incubated cells.

Endocytosis is a process that results in the uptake of substances in the extracellular environment. It is conserved in eukaryotes and usually involves the invagination of components of that plasma membrane that form vesicles. The process can be carried out through different pathways differentiated by the size of the vesicles, the composition of the vesicular coat and the fate of the materials taken up (Khalil et al., 2006). These pathways are clathrin mediated (or receptor mediated) endocytosis, caveolae mediated endocytosis,

phagocytosis and micropinocytosis though clathrin mediated endocytosis is the most readily used pathway of uptake of nanoparticles (Conner and Schmid, 2003a). Clathrin mediated endocytosis is usually initiated by specific receptor-ligand interactions which results in internalization of particles and entrapment in endosomes which eventually fuse with acidic lysosomes where the cargo is degraded by lysosomal enzymes (Watson et al., 2005). This pathway can be inhibited by using chlorpromazine which specifically inhibits clathirn mediated endocytosis by dissociating clathrin from the surface membrane (Wang et al., 1993).

Our data show that by pre-incubating MDCK cells with Chlorpromazine for 30 minutes, the uptake of GCPQ can be reduced by about 30 % though not significant (Figure 5-19), however when MDCK cells are co-incubated with CPZ for 2 hours and 4 hours, the uptake of GCPQ is significantly reduced by about 90% (Figure 5-20). This suggests that clathrin mediated endocytosis is the major pathway of uptake of GCPQ-TR in MDCK cells. A previous study using a hydrophobically modified glycol chitosan showed a 20 % reduction in uptake when inhibited using 10μg/mL CPZ in a HeLa cell model. The same study that by including filipin, an inhibitor of caveolae mediated endocytosis, uptake was reduced by 60 % suggesting that the two pathways were involved (Nam et al., 2009). Another study found that cationization of nanoparticles facilitates their uptake by enhancing binding through electrostatic interactions between the positively charged nanoparticles and the anionic membrane components (Blau et al., 2000). The positive charges on GCPQ particles as well as the hydrophobic palmitoyl groups will therefore favour better binging and internalisation of the particles and especially though the clathrin mediated pathway.

Having therefore observed the uptake of GCPQ nanoparticles in vitro in epithelial cell monolayer models, we sought to observe the uptake in in vivo and *ex vivo* mouse models to determine if there are similarities in the processes observed in vitro.

5.4 GCPQ Nanoparticle interaction with the GIT epithelium

The translation of promising *in vitro* data to successful *in vivo* application is typically met with challenges, mostly because the *in vitro* assays rarely mirror i*n vivo* conditions perfectly, particularly following oral administration. Drug candidates administered through the oral route have to overcome multiple challenges to achieve sufficient bioavailability. Some of these problems including stability in the gastric environment, solubility at different pH environments, stability against enzymatic degradation and overcoming the mucus barrier (Ensign et al., 2012). The mucus layer is an important barrier because of the role it plays in protecting the epithelium from infectious agents and foreign particles, rapidly clearing them from the gut. Polymeric nano-formulations are also caught up in this 'clearance' from the gut, resulting in little retention and uptake through the epithelial cells (Galindo-Rodriguez et al., 2005). An attempt to reduce this clearance by making polymeric nanoparticles mucoadhesive has still been met with challenges. These mucoadhesive nanoparticles are thought to adhere tightly to the mucus at the loosely adherent top layer of the mucus, resulting in their inability to reach the firmly adherent layer of the mucus and thus becoming susceptible to rapid clearance (des Rieux et al., 2006). To overcome this challenge, nanoparticles are required to have certain size and surface charge parameters that make them more likely to penetrate the mucus and interact with the epithelial cells. Some of these properties include having a small size that can diffuse through the mucus mesh, having a

right balance of positive and negative charges to confer a net neutral charge, and being more hydrophilic with less hydrophobic surface modifications (Olmsted et al., 2001).

Our data so far has shown the importance of the positive charges of GCPQ polymeric particles to the interactions with the epithelial cell surfaces and to paracellular transport enhancement. We have shown that with increasing DQ, we can achieve higher paracellular transport of hydrophilic dextran and that the positive charges likely facilitate the adherence of the particles to membrane components and results in high endocytosis of GCPQ-TR. Going forward, we decided to determine if these positive charges will have an effect on the interactions of GCPQ with the intestinal epithelium. We expect that the positive charges of GCPQ and the hydrophobic palmitoyl group will make GCPQ mucoadhesive (Uchegbu et al., 2013a) but that its amphoteric nature will make it able to permeate the mucus barrier and be taken up. The biodistribution of GCPQ following oral administration had been shown using CARS microscopy (Lalatsa et al., 2012a) (Garrett et al., 2012). Here, we used confocal microscopy to describe the uptake of Texas red labelled GCPQ through the mouse intestinal epithelium.

5.4.1 Method

In vivo treated tissue imaging

A pilot study was carried out to determine the correlation of the in vitro observations in vivo. A male Wistar rat, 200 g was administered Texas red labelled GCPQ at a dose of 75mg kg^{-1} dissolved in distilled water by oral gavage. The animal was culled 2 hours after treatment

and the intestine harvested and cut into sections. Sections of the small intestine were washed with Normal saline, tied off at the ends and filled with optimal cutting temperature compound (OCT) and frozen in liquid nitrogen. The tissues were then sectioned into thin slices of a bout 10 μm using a cryostat (Leica CM1850) set at -25^{o}C. The slices were placed on poly-L-lysine microscope adhesion slides and fixed with freshly prepared paraformaldehyde (4 %). The slices were labelled with cell mask deep red and DAPI and washed with PBS. VECTASHIELD antifade agent (Vector Laboratories, USA) was then applied followed by a cover slip. The slices were imaged using an inverted Zeiss LSM 710 confocal microscope.

Mouse intestinal tissues:

Male CD-1 mice, ≈ 24 g were treated with the undiluted samples by oral gavage (200μL per mice) for different durations (45 mins, 60 mins, 120 mins and 180 mins). The mice were euthanized after the duration of treatment by CO2 asphyxiation and sections of the small intestine were harvested and tied off at either end to ensure preservation of the mucus membrane. Transverse sections of the intestine, approximately 2mm in length were cut carefully using cleaned razor blades and labelled with Cell Mask Deep Red and DAPI stains for 5 minutes after which they were placed between two coverslips, using multiple spacer layers of parafilm and imaged under the microscope. Direct instillation was done on excised intestine for approximately 15 minutes, suspended in PBS prior to tissue processing.

For effects of bile salts, a gut sac model was employed. Male CD1 mice were culled by CO2 asphixation and about 3 cm sections of the small intestine were collected and tied off on one

end. ≈50 μL solutions of GCPQ-TR or GCPQ-TR-Bile salt mixture was instilled into the sections, the other end tied off and the sections suspended in PBS buffer for 15 minutes. The sections were then fixed in 4 % PFA for about 15 minutes, washed in PBS and approximately 1mm transverse sections cut and stained with DAPI for viewing under the microscope.

For labelling of vascular endothelium with Dylight 488 Tomato lectin, the mouse was anaesthetized 15 minutes to the end of the duration of treatment and 0.1 ml of 1 mg/ml lectin injected through the tail vein. The mouse was allowed to recover from the anesthesia and culled by CO_2 asphyxiation after which it was perfused with 10 mL of 4 % paraformaldehyde over 10 minutes.

Preparation of GCPQ-Bile salts mixture

3.0 mg/mL of GCPQ-TR was prepared in deionised water and 8.3 mg/mL of bile salts (sigma, UK) was also prepared in deionised water. Equal volumes (0.5 mL) of both solutions were mixed by pipetting in a vial to produce 1.5 mg/mL of GCPQ-TR and 4.15 mg/mL of bile salts. The pH of the mixture was measured and the size and zeta potential also measure, the results for which are shown in table 5-5.

5.4.2 Results and Discussion

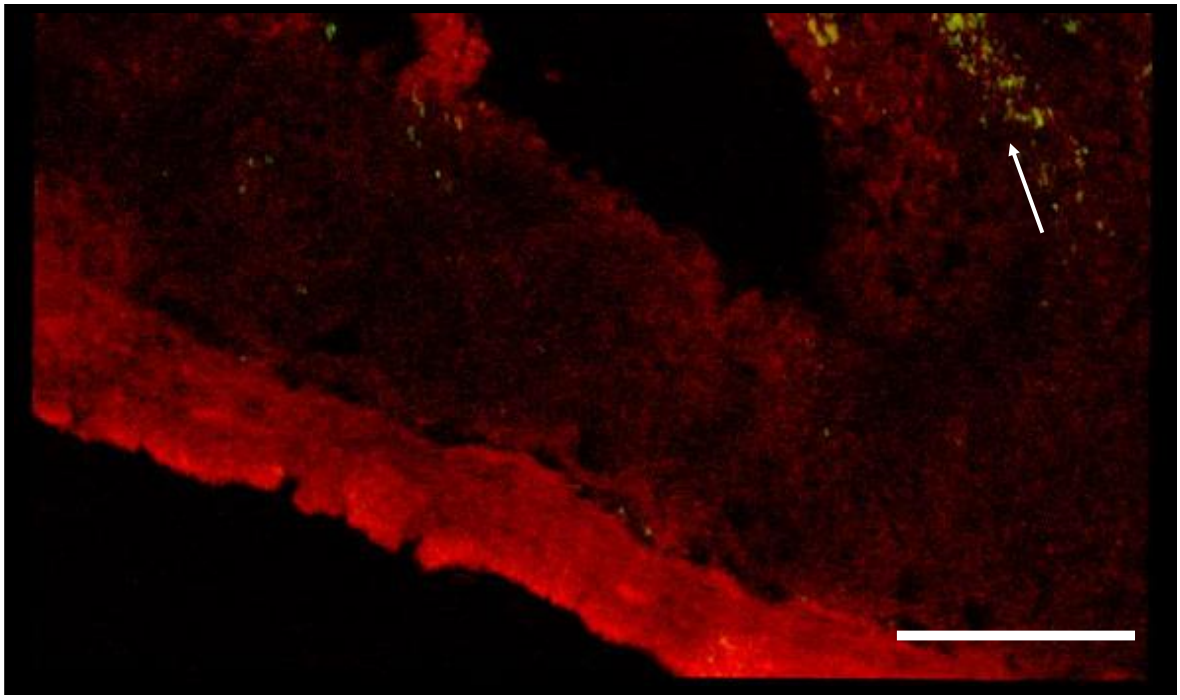

Figure 5-21: CLSM images of a transverse section of a rat small intestine after treatment with GCPQ. Arrows point to the location of GCPQ-Texas red. Red: Cell mask deep red; Green: GCPQ-Texas-Red. Scale bar: 500 μm.

Figure 5-21 shows the transverse section of a rat small intestine collected two hours after oral administration of GCPQ-TR (75 mg/kg). GCPQ can be seen adhering to the mucus layer of the intestine (arrows). The particles seen were more abundant at the top layer of the mucus which will represent the loosely adherent part of the mucus layer which might make them more susceptible to clearance.

We then decided to use an *ex vivo* gut sac model to instil GCPQ-TR into an intestinal section. We also tried to determine effect of neutralising the charges on GCPQ using bile salts (Sigma, UK) which contained a mixture of sodium cholate and sodium deoxycholate to mimic the interaction of orally administered GCPQ with bile.

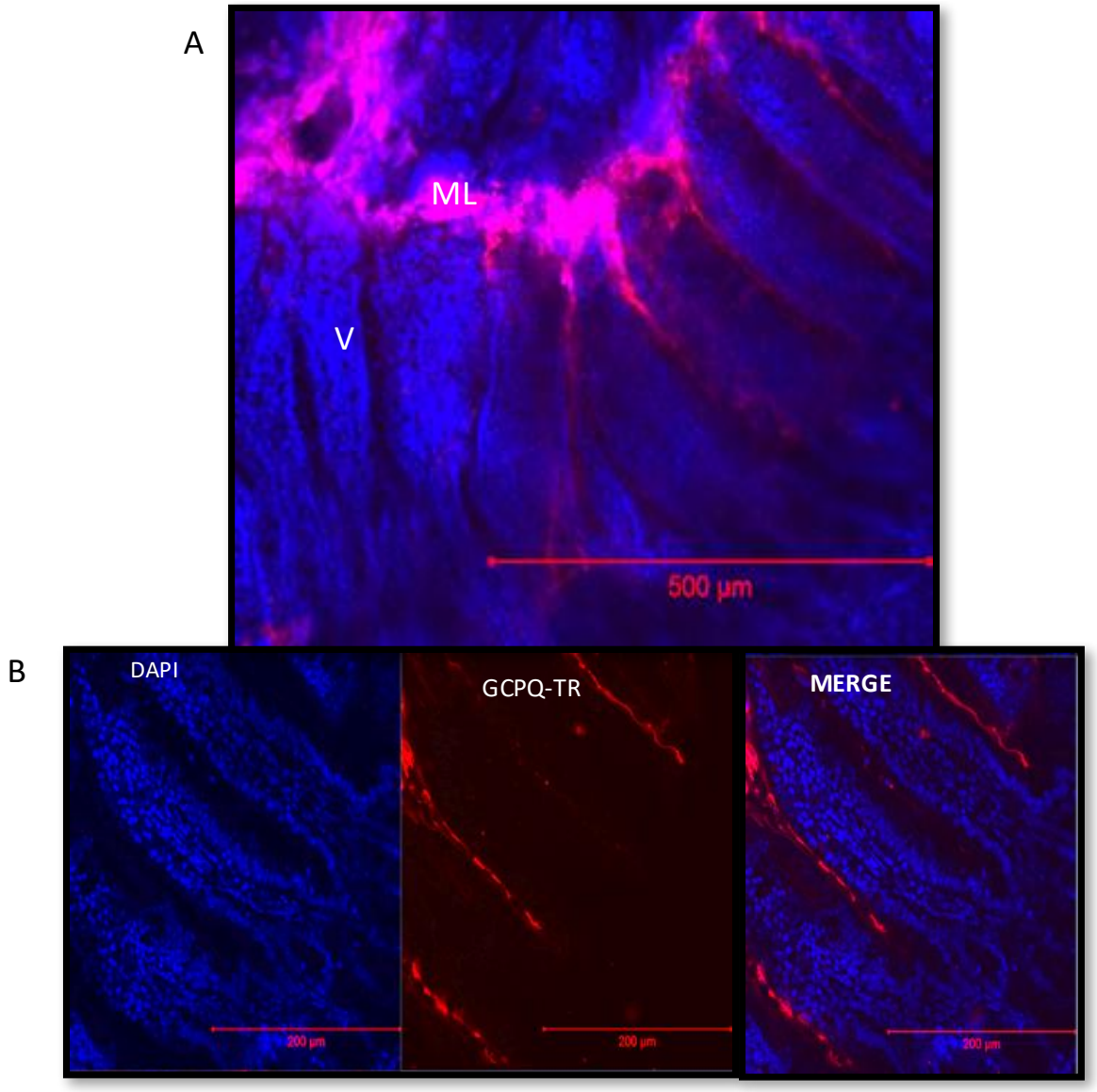

Figure 5-22: Sections of a CD1 mouse small intestine instilled with GCPQ-TR for 15 minutes. A. transverse section showing GCPQ-TR adhering to the mucus layer B. Transverse section showing GCPQ permeating between the villi. Blue: DAPI; Red: GCPQ-TR. V: villi, ML: mucus layer

Figure 5-22 shows GCPQ adhering closely to the mucus layer and permeating between the villi. This close adherence with the mucus is expected given the positive charges of GCPQ but the consistency in the permeation between the villi was unexpected for the same reason- the expectation that the strong attachment to the mucus layer will limit the access of GCPQ to the epithelial cell surface. We therefore repeated the experiments using GCPQ-TR polymers that were mixed with bile salts to lose their charges (see table 5-5).

Table 5-5: Properties of GCPQ and GCPQ bile salts instilled onto mouse intestine

	PH	Z.Ave (nm)	PDI	Zeta Potential (mV)
GCPQ03	4.5	71.1±12.54	0.835±0.01	37.5±1.34
GCPQ+Bile salts	7.4	502.1±32.24	0.19±0.12	-11.3±1.1

Table 5-5 shows that by mixing GCPQ with bile salts, we form negatively charged particles that are much larger in size.

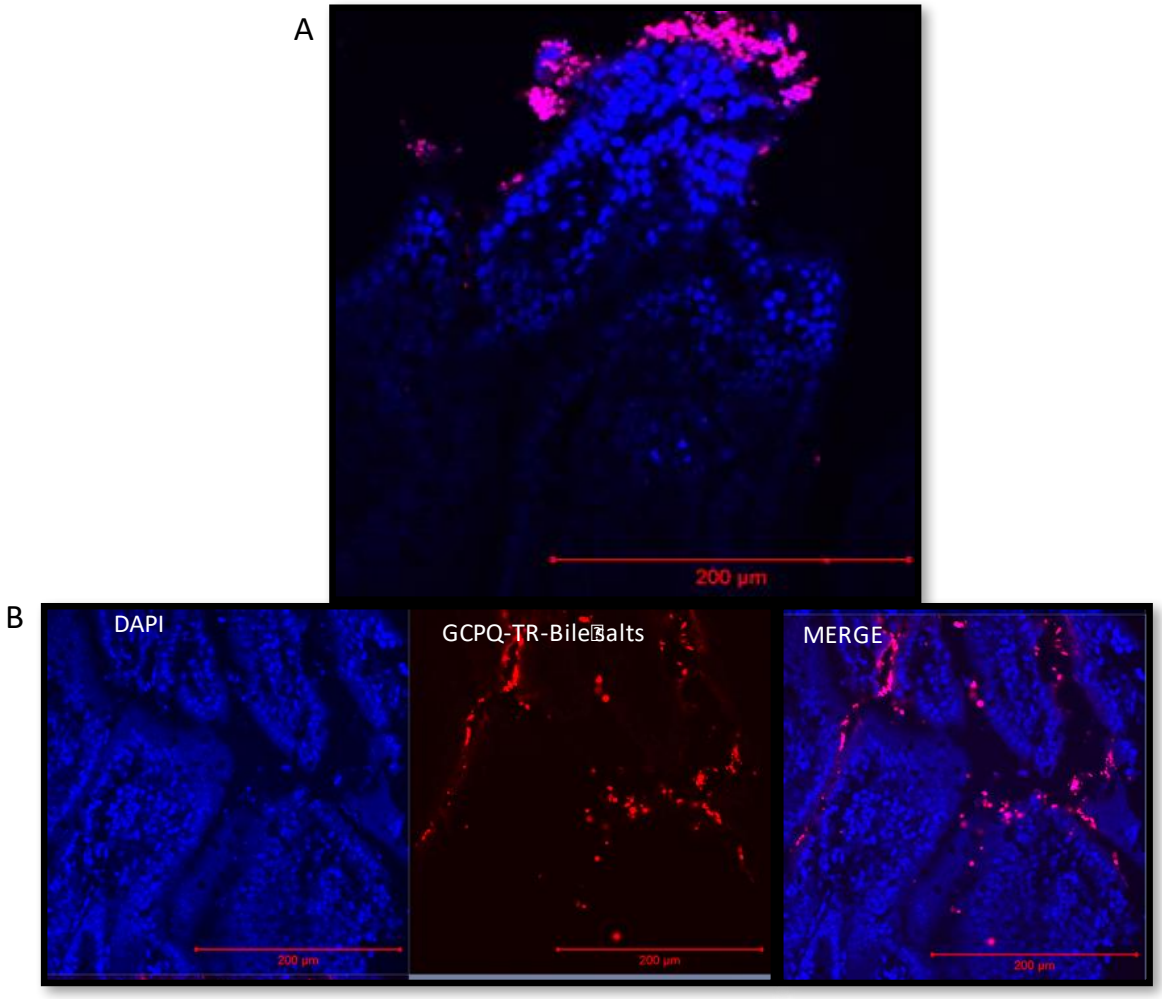

Figure 5-23: Sections of small intestine from CD1 mouse instilled with GCPQ-TR-Bile salts mixture for 15minutes. A. transverse section showing GCPQ-TR adhering to the mucus layer B. Transverse section showing GCPQ permeating between the villi. Blue: DAPI; Red: GCPQ-TR. V: villi, ML: mucus layer

Figure 5-23 shows the interaction of GCPQ-TR-bile salt particles with the intestinal epithelium. GCPQ-TR loses the fine consistence observed in figure 5-22 when it is mixed with bile salts and instead appears as large aggregates around in the mucus layer and between the villi. The figure shows that these large particles are still able to permeate the mucus barrier and get to the epithelial surface after interacting with bile. Having observed this, we

decided to administer GCPQ-TR orally to some mice to see if the interaction of GCPQ mirrors what was seen in the ex-vivo model.

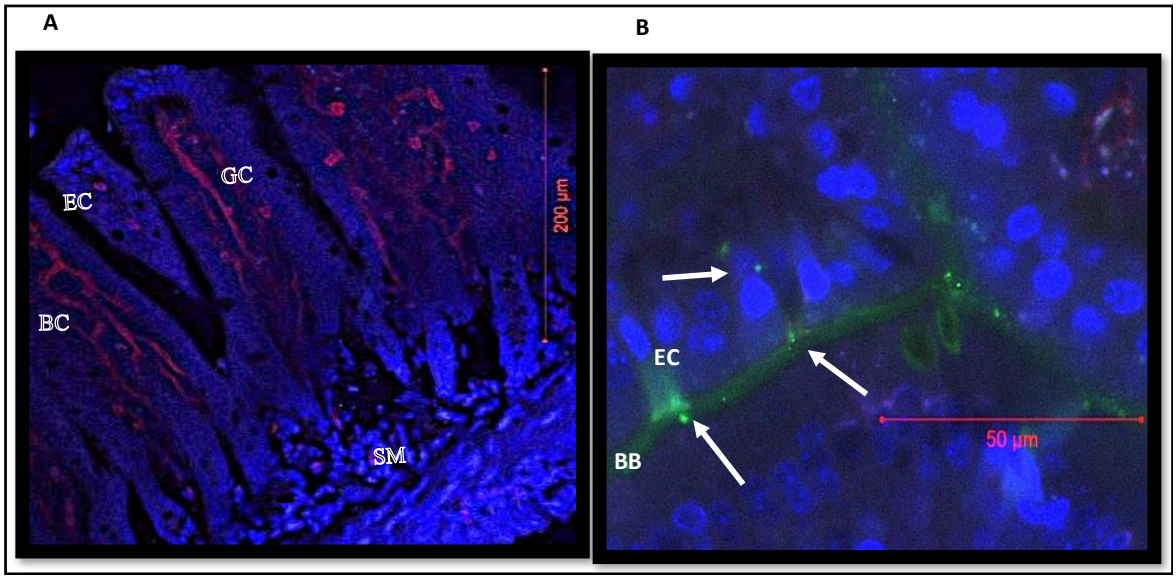

Figure 5-24: Section of villi from intestine of a male CD-1 mouse treated with **A**. PBS. **B.** 75mg/kg GCPQ-TR for 45minutes. Blue: DAPI; Red: DyLight 488 Tomato Lectin Green: GCPQ-TR. BB: Brush border; BC: Blood capillaries; GC: Goblet cell; EC: Epithelial cell. SM: Sub mucosa. Arrows show uptake of GCPQ-TR

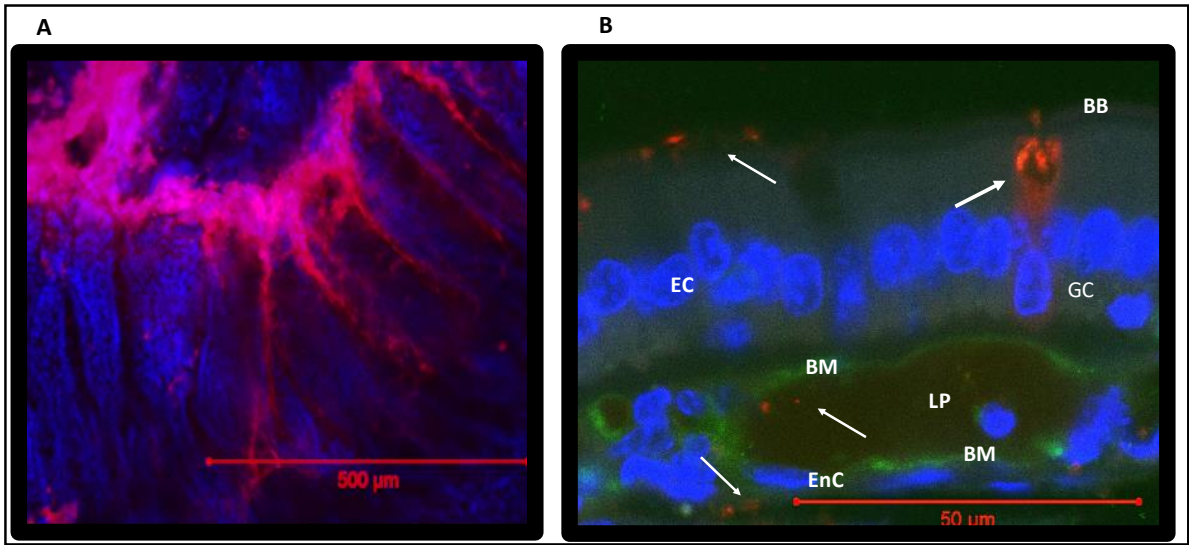

Figure 5-25: Section of villi from intestine of a male CD-1 mouse A. From figure 5-22A, small intestine instilled with GCPQ-TR showing GCPQ adhering tightly to the mucus and permeating between the villi. **B.** Treated with 75mg/kg GCPQ-TR by oral gavage for 45minutes showing GCPQ-TR around the brush border, taken up by Goblet cells and within the lamina propria and endothelium. Blue: DAPI; Green: DyLight 488 Tomato Lectin; Red: GCPQ-TR. BB: Brush border; GC: Goblet cell; EC: Epithelial cell; EnC: Endothelial cell; BM: Basal membrane; LP: Lamina Propria

Figure 5-24 and Figure 5-25 show GCPQ-TR adhering very closely to the brush border, appearing to be taken up by the epithelial cells and the goblet cells and getting distributed in the lamina propria and further down into the capaillary endothelium. Colocolisation with the Dylight 488 tomoato lectin might be suggestive of uptake into circulation. These images give strong suggestions of the nature of interaction between GCPQ and the epithelial cells and the pathways of uptake into circulation.

The images obtained from these experiments show GCPQ is abundantly distributed in the mucus layer and around the intestinal epithelium. GCPQ adheres closely to the mucus and permeates between the villi to get to lower regions of the intestinal epithelium. This is probably explained by the electrostatic interaction between the positively charged nanoparticles and the negatively charge mucus environment, causing fore-running nanoparticles to break through the mesh of the mucus and thus creating a path for advancing nanoparticles to interact further down the mucosa. The observed abundance in the mucosa agrees with reports that chitosan and its derivatives are muco-adhesive but also show that GCPQ does pass through the mucosal layer and accumulates at the boundary between the sub-mucosa and muscularis propria which is supported by previously reported observations using Coherent anti-Stoke Raman Scattering (CARS) microscopy technique (Garrett et al., 2012).

Bile is known to play a vital role in the uptake of certain drugs. Its high pH is also thought to neutralise the acidic chyme emptied from the stomach. Its negative charge will also likely alter the charges of protonated substances entering the intestine. GCPQ, like some other derivatives of chitosan, is thought to interact with the intestinal mucosa by binding electrostatically with the negatively charged components of the mucus and cell membrane. This type of interaction has been suggested to be essential for mucus adhesion i.e. allowing such particles to stay attached to the mucus over extended periods of time (Ensign et al., 2012). However, in general it is thought that neutral particles are most effective in penetrate into mucus (Olmsted et al., 2001)**. Figure 5-22** suggests**,** however, that catioinic GCPQ nanoparticles penetrate the mucus very well. We wanted to investigate whether coating of

GCPQ nanoparticles with bile salts could lead to the formation of a negatively charged bile slate 'corona' and thus facilitate mucus penetration. This interaction is thought to facilitate the permeation of chitosan through the mucus and enhance the eventual uptake of adminstered drugs. To investigate this hypothesises in more detail we determined the effect on pH, size and zeta potential (**Table 5-5)** and we instilled a GCPQ-TR-Bile salts mixture into an excised mouse intestine and observed the association with the intestinal epithelium by confocal microscopy

Figure 5-23 shows GCPQ-TR-Bile salts mixture abundant between the villi but with less consistency than GCPQ-TR (**Figure 5-22**) and what appears to be aggregates. **Table 5-5** shows that GCPQ-Bile salts mixture has a negative charge and a much bigger size than GCPQ. GCPQ however has a positive charge. While the close adherence and consistency obvious in **Figure 5-22** is probably suggestive of an electrostatic interaction between GCPQ and the negatively charged mucus and mucosal surface, **Figure 5-23** shows the size dependent diffusion of GCPQ through the mucus. Both phenomena were observed in the other images of GCPQ-TR treated mice and probably suggests that both processes are involved in the mechanism of GCPQ permeation enhancement. It can be expected that at the point of entry into the small intestine, mixing of Bile salts with the ingested GCPQ-TR polymers will not be uniform/wholistic and thus some of the particles will retain some positive charge and adhere closely to the mucus while those thoroughly mixed with bile salts will form negatively charged larger aggregates that can permeate through the mesh of the mucus and eventually interact with the epithelial cells.

5.5 Conclusion

We have been able to show that GCPQ can be engineered to have graded levels of paracellular transport enhancement in both caco-2 and MDCK cells. This graded effect is dependent on the ratio of DQ% to DP% (QPR) with polymers having higher QPR resulting in higher apparent permeability coefficient values for the para-cellular marker, FD4. This effect is also pH dependent. Polymers with high QPR values are likely to retain their permeation enhancement properties at higher pH values, giving utility for pH-controlled release formulations and site-specific formulation design.

GCPQ enhances paracellular transport by causing tight junction disassembly, affecting the low capacity occludin associated leaky pathway of macromolecule passage. This is however a temporary state which does not result in indiscriminate entry of large sized macromolecules. GCPQ-TR is also taken up by clathrin mediated endocytosis, a process which can be inhibited by chlorpromazine.

GCPQ also interacts closely with the intestinal epithelium, permeating through the mucus and adhering closely to the intestinal brush border. It gets taken up by the enterocytes and the Goblet cells into systemic circulation. GCPQ can thus be engineered to take advantage of both paracellular and transcellular pathways for particle uptake.

Chapter 6. In-vivo Bioavailability Studies

6.1 Introduction

The challenge of translating promising in vitro observations to clinical applications is one that is a common theme in a lot of failed drug prospects. Several reasons are associated with this challenge especially the inability to replicate physiological conditions in vitro. Factors such as the presence of enzymes, the homeostatic regulatory mechanisms, hormones, adequate dilution in biological milieu and the replication of the anatomical construct found in vivo all contribute to the challenge of designing a suitable in vitro screening method that can adequately predict in vivo outcomes (Lin, 1998). The conventional approach to closely mirroring the conditions found in humans is to use animal models where disease conditions can be simulated to resemble the targeted conditions in human.

In the previous chapters, we were able to establish that structural modifications on GCPQ polymers resulted in changes in physicochemical properties including critical micelle concentrations, thermodynamics of aggregation and stability in different environments. We were then able to show that these modifications resulted in different outcomes when the polymers were used to encapsulate different classes of drugs. Of particular significance was the formation of nanocrystals when a GCPQ polymer having a QPR of greater than 1.0 was used to encapsulate paclitaxel compared to micelles formed with GCPQ polymers having lower QPR. We observed also that the paclitaxel formulations had similar stability profiles

in 4ºC over a 28-day period but that encapsulation efficiency was higher for polymers which had a higher DQ than 20 %.

This chapter will seek to determine if these observations have any significance in vivo. First, we will look to determine if encapsulation of paclitaxel with GCPQ provides superior bioavailability of paclitaxel than other reported formulations. This is relevant because of the very low cmc of GCPQ which we expect will offer better protection to paclitaxel and prevent its premature release due to dilution systemically. Important also, is the question of whether this expected protection will reduce the bioavailability of paclitaxel due to non-release of the encapsulated drug. Another question that will be examined in this chapter is the significance of having a nanocrystal versus a micelle in the uptake and bioavailability of paclitaxel.

Paclitaxel is a well-known anti-cancer drug used clinically to treat a large number of solid tumours. It was originally developed and restricted for use in specific tumours that proved difficult to treat with more conventional therapies because of the scarcity of its source. However, because of its therapeutic effects, it has been subjected to extensive research to extend its use earlier on in treatment of tumours where there is a chance or remission or recovery. The advanced development of paclitaxel for this extended use is however confronted with challenges, primarily due to the properties of the molecule itself. First, paclitaxel is poorly soluble in aqueous solvents and in oils, making it difficult to solubilise it for formulations. It also has very poor pharmacokinetics after administration chiefly because it is a substrate for the P-glycoprotein (P-gp) which results in it being actively effluxed and thus resulting in resistance (Wang et al., 2014). Both of these challenges must

be overcome to successfully develop a therapeutic formulation of paclitaxel for clinical use. The two formulations which are currently in clinical use; Taxol® and Abraxane®, have improved solubility but poor pharmacokinetics. Taxol improves the solubility of paclitaxel by incorporating Cremophor EL and dehydrated ethanol (50:50) but this comes with associated toxicities, hypersensitivity reactions and non-linear pharmacokinetics. Abraxane, which is an albumin bound paclitaxel formulation improves the toxicity of Taxol and reduces the duration of infusion but does not necessarily improve bioavailability (Ma and Mumper, 2013). Both formulations are administered by intravenous infusions which adds a layer of inconvenience from being restrained for a duration of time, hospital visits and the need for skilled service, all of which add to the cost of treatment. Attempts have been made to improve the bioavailability of paclitaxel by incorporating P-gp inhibitors like verapamil with concomitant toxicity issues making it a complicated path for improving bioavailability (Berg et al., 1995, Baek and Cho, 2015).

This explains the need to develop better formulations that can be administered orally and have better or at least comparable bio distribution of paclitaxel to any of the current clinically available formulations. Nano formulations are the go-to systems for this approach owing to their potential biocompatibility, protection from biodegradation, small sizes which should enhance uptake and longer circulation times when in the plasma (Blanco et al., 2015). In this chapter, we administered two of the polymers which had the best encapsulation efficiency- GCPQ06+PTX and GCPQ10+PTX to CD1 mice and determined the bioavailability. We also compared the values obtained with previously reported values from other nano-enabled formulations.

6.2 Materials and Methods

6.2.1 Materials:

Paclitaxel powder was purchased from Cambridge Biosciences (Cambridge, UK), Docetaxel was purchased from Generon (Slough, UK), LC-MS Grade solvents were purchased from Fischer Scientific (Leicestershire, UK).

6.2.2 Methods:

Bioanalytical LC-MS/MS Assay

Preparation of stock solutions:

Paclitaxel was dissolved in methanol at a concentration of 1 mg/mL. A working solution of 10 μg/mL in 50:50 acetonitrile in deionized water was prepared from the stock solution. Standard concentrations ranging from 10 μg/mL to 0.5 μg/mL in 50:50 acetonitrile in deionized water were prepared from the working solution. Docetaxel was dissolved in methanol at a concentration of 1mg/mL. A working solution of 10 μg/mL was prepared in 50:50 acetonitrile in deionized water was prepared from the stock solution.

Preparation of standards and quality control solutions:

Standard dilutions of paclitaxel were prepared and used to obtain a standard curve. Ten (10) dilutions of paclitaxel were made in the mobile phase and ranged from 5000 ng/mL to 0.5 ng/mL. 50uL of blank plasma was collected and transferred into centrifuge tubes corresponding with each standard dilution. 50 μL of each dilution was transferred into

corresponding 15 mL centrifuge tubes and vortexed for 1 minute. 50 μL of a 10 μg/mL concentration of the internal standard was added to the samples and vortexed for 1 minute. 6mL of diethyl ether was added to each centrifuge tube and vortexed for 15 minutes. The tubes were centrifuged at 1000 g for 10 minutes and the organic layer collected into evaporating tubes. The samples were dried under a gentle stream of Nitrogen and reconstituted in 50 μL of the mobile phase, vortexed and centrifuged at 1000 g for 10 minutes, the supernatant collected into HPLC vials for LC-MS/MS analysis.

Sample preparation:

Plasma samples were collected from blood samples by spinning at 1000 g for 10 minutes. 50 μL of each plasma sample was collected into 15 mL centrifuge tubes and 50 μL of 10 μg/mL concentration of internal standard (Docetaxel in Acetonitrile:dH_2O, 50:50) was added to the plasma samples in the tubes and vortexed for 1minute. 50 μL of mobile phase (Acetonitrile : dH2O, 50:50) was added to each sample and vortexed for 1minute). 6 mL of diethyl ether was added to each tube and vortexed for 15 minutes. The tubes were centrifuged at 1000 g for 10 minutes and 5 mL of the organic layer was collected into evaporating tubes. The samples were dried under a gentle stream on Nitrogen gas and reconstituted in 50 μL of the mobile phase with vortexing. The tubes were centrifuged at 1000 g for 10 minutes and the clear supernatant was transferred into vials 0.4 mL HPLC vials for LC-MS/MS analysis.

Liquid Chromatography Tandem Mass Spectrometry (LC-MS/MS) Method:

Instrumentation:

Samples were analysed using an Agilent 6400 Series Triple Quadrupole LC/MS system (Agilent technologies, Berkshire, UK) comprising a degasser(HiP Degasser 1260/G4225A),

a binary pump (HiP 1260 binary pump/G1312B), an auto sampler (HiP sampler 1260/ G1367E), a column oven (G1316A) and a triple-quadrupole mass spectrometer (G6460A). Agilent MassHunter Workstation Software was used for system control, data acquisition and data processing.

Chromatographic conditions:

Samples (injection volume was 10 μL) were chromatographed over an Agilent Zorbax Extend C-18 50 X 2.1 mm column, pore size, 3.5 μm, equipped with a cartridge Gemini C18 4 x 2.0 mm guard column and at a temperature of 40ºC with the mobile flow rate of 0.200mL/min. The mobile phase was 50 % water and 50 % Acetonitrile containing 0.1% formic acid.

Mass Spectrometer Conditions:

Paclitaxel and docetaxel were monitored by positive Electrospray Ionisation (ESI) on an Agilent Jet Stream (AJS) ion source with ionisation source parameters of capillary voltage: 3500 V; Gas temperature: 300ºC; Gas flow: 5 L/min; collision energy: 20 V, nebuliser: 45 psi, fragmentation: 135V; Sheath gas heater: 250ºC; Sheath gas flow: 11 L. Samples were scanned using multiple reaction monitoring (MRM) mode for transitions of *m*/*z* 854 → 286 for Paclitaxel and *m*/*z* 808 → 181.9 for docetaxel respectively.

Plasma pharmacokinetics of paclitaxel:

Male CD1 mice 30-35 g were used for the studies. The animals were housed in groups of 5 in plastic cages under controlled laboratory conditions. Ambient temperature was

maintained at about 22^{o}C and humidity kept at 60 %. A 12-hour light and dark cycle was also maintained with food and water provided ad libitum. The mice were allowed to acclimatise for 5-7 days before being used for experimentation. All experiments were carried out under a UK Home Office Licence.

Three groups of mice were used for the study: a blank control, GCPQ06-paclitaxel and GCPQ10-paclitaxel. There were four time points: 30 minutes, 1 hour, 2 hours, 4 hours and 24 hours. Five mice were four mice were used per time point. 20 mg/kg of paclitaxel in 250 μL of the formulation was administered to the GCPQ treated mice by oral gavage. At each time point, mice from the treatment groups were culled by CO_2 asphyxiation and blood samples collected by cardiac puncture into EDTA coated plasma collection tubes and immediately placed kept at -80^{o}C until ready for processing.

6.3 Results and Discussion

Table 6-1: Preparation of Working Standards

	Dilutions			Final Conc
Code	Take (µL)	From	Diluent (µL)	PTXL(ng/mL)
WS1	400	PTX WKS	0	15000
WS2	200	WS1	300	6000
WS3	250	WS2	250	3000
WS4	250	WS3	250	1500
WS5	200	WS4	300	600
WS6	250	WS5	250	300
WS7	250	WS6	250	150
WS8	200	WS7	300	60
WS9	250	WS8	250	30
WS10	250	WS9	250	15
WS11	200	WS10	300	6
WS12	250	WS11	250	3
WS13	250	WS12	250	1.5
WS14	-	-	500	0

Table 6-2: Preparation of Calibration Standards

Sample No	Plasma (µL)	Spike (µL)	From	IS (µL)	Final conc (ng/mL)
STD1	50	50	WS1	50	5000
STD2	50	50	WS2	50	2000
STD3	50	50	WS3	50	1000
STD4	50	50	WS4	50	500
STD5	50	50	WS5	50	200
STD6	50	50	WS6	50	100
STD7	50	50	WS7	50	50
STD8	50	50	WS8	50	20
STD9	50	50	WS9	50	10
STD10	50	50	WS10	50	5
STD11	50	50	WS11	50	2
STD12	50	50	WS12	50	1
STD13	50	50	WS13	50	0.5
STD14	50	50	WS14	50	0

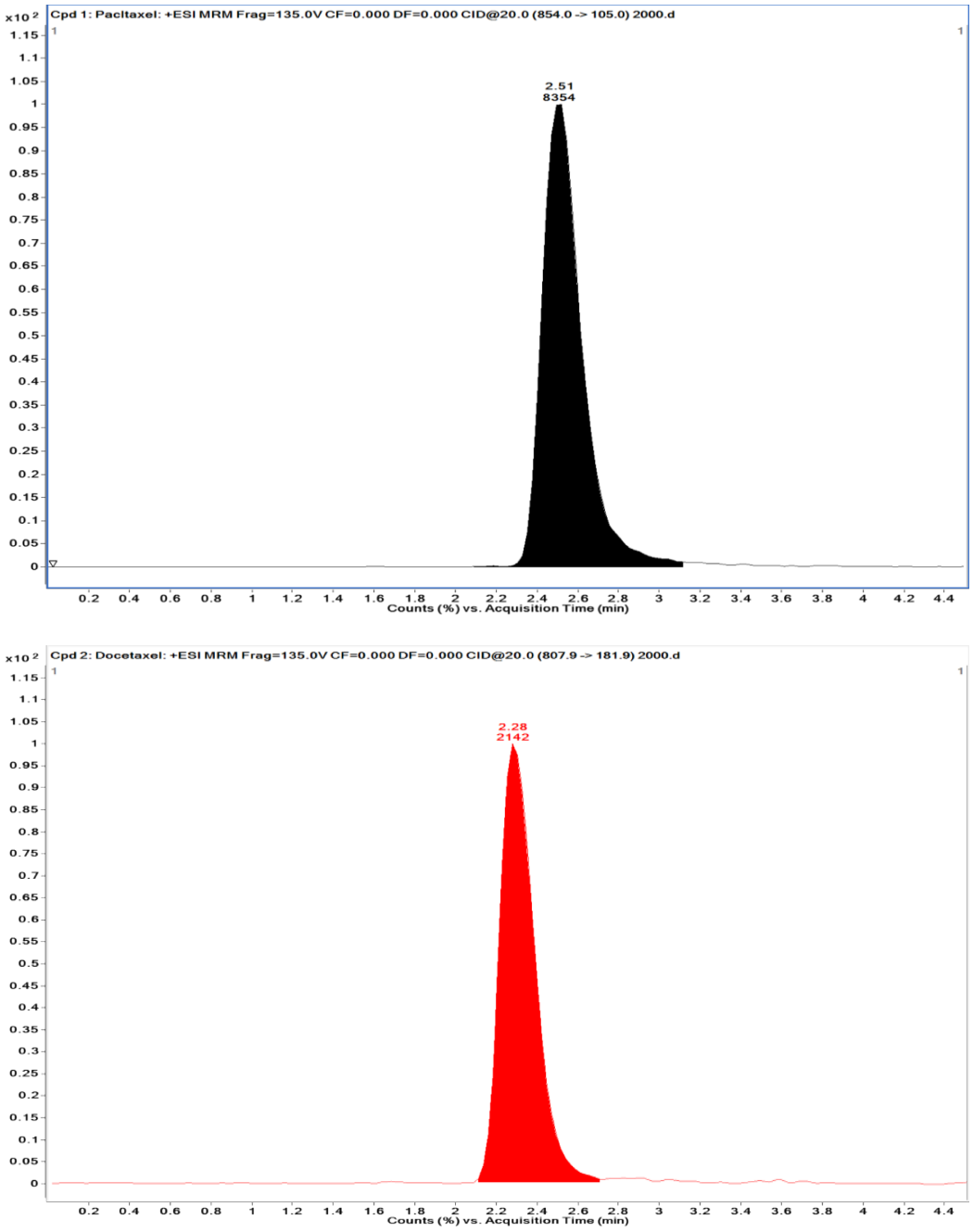

Figure 6-1: LC chromatogram for paclitaxel (2 µg/mL) with retention time at 2.5 minutes (top) and docetaxel (2 µg/mL) with retention time at 2.31 minutes (bottom) in 50:50 acetonitrile (+0.05% v/v Formic acid) and water.

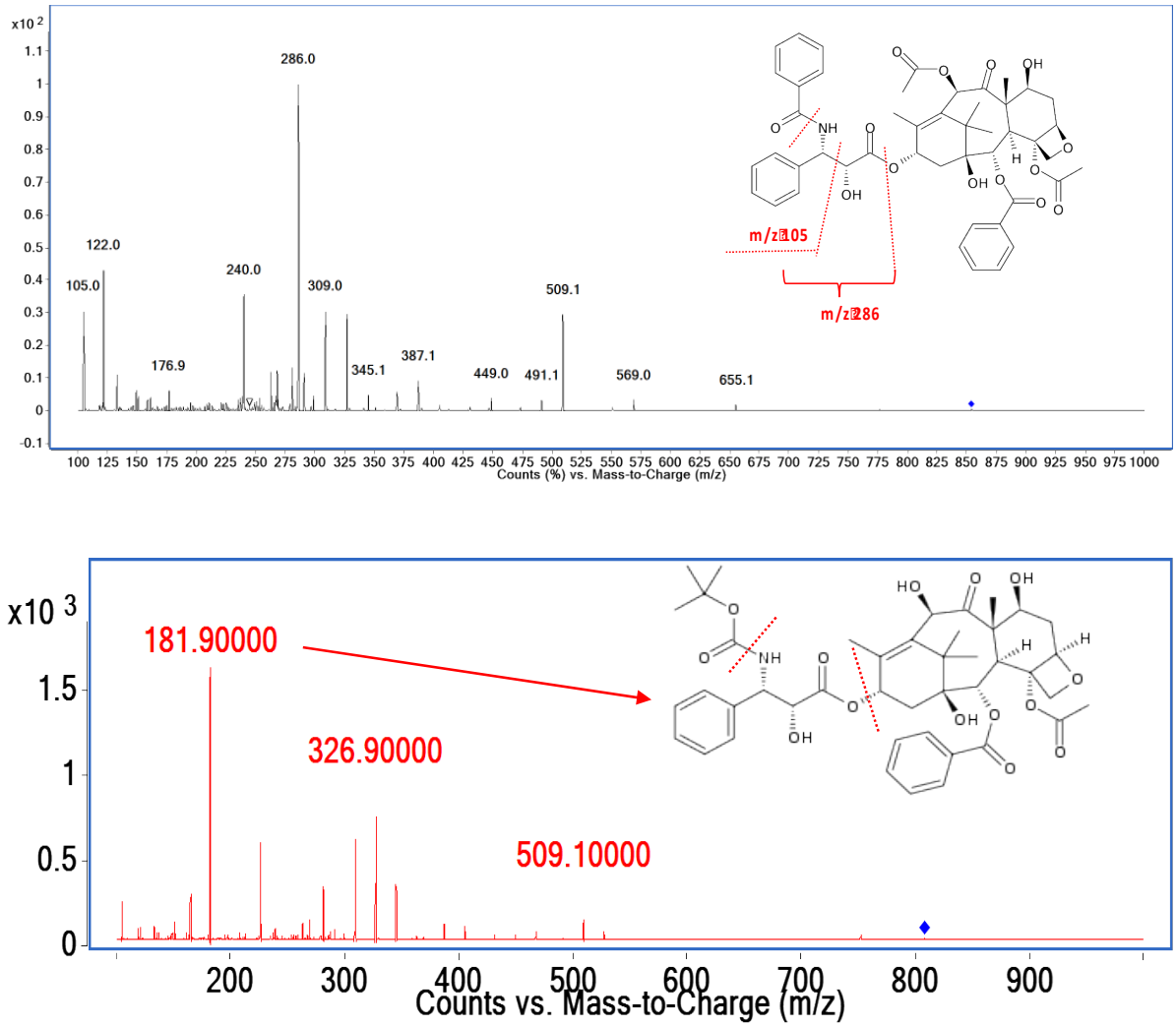

Figure 6-2: Mass spectrometry spectra for paclitaxel (10 µg/mL) (top) and docetaxel (10 µg/mL) (bottom) in 50:50 acetonitrile (+0.05% v/v Formic acid) and water by ESI^+ mode

Figure 6-1 and figure 6-2 show the chromatogram and mass spectra for paclitaxel and docetaxel. Both paclitaxel and docetaxel were ionised under the positive electrospray ionisation (ESI^+) for analyte quantitation, both having amide and hydroxyl groups. The parent ion to daughter ion transitions of *m/z* 854 → 286 and *m/z* 808 → 181.9 were chosen for paclitaxel and docetaxel respectively based on the most abundant daughter ion as shown

in the mass spectra in figure 7-2. Docetaxel was used as the internal standard because of its structural similarity to paclitaxel and its similar fragmentation pattern as shown in figure 7-2.

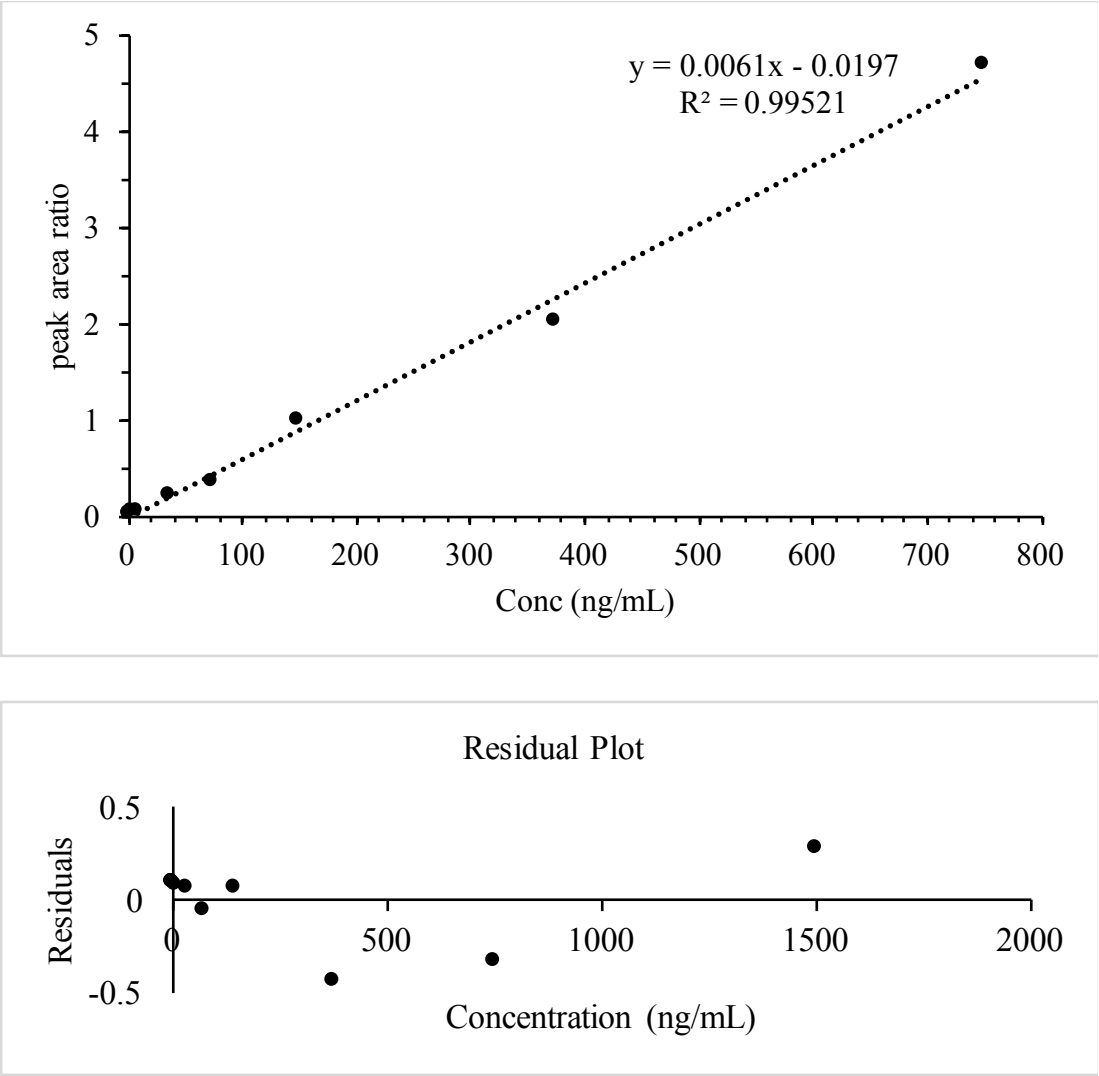

Figure 6-3: calibration curve for paclitaxel in mouse plasma samples run in 50:50 acetonitrile (+0.05% v/v Formic acid) (top) and residuals plot from least squares regression analysis of the calibration curve (bottom)

Figure 6-3 shows the calibration curve obtained by plotting the peak area ratios of paclitaxel to the internal standard, docetaxel. A least squares regression analysis, conducted to test for linearity and weighted against the inverse of the concentration, generated a coefficient of coefficient greater than 0.99. The calibration curve produces acceptable results within the concentration range of 0.5 ng/mL to 750 ng/mL.

Table 6-3 Table showing encapsulation efficiency (EE%) and Drug Loading (DL%) of GCPQ-Paclitaxel formulations

Formulation	GCPQ	Z-average±SD (nm)	PDI±SD	EE(%)	DL(%)
GCPQ03+PTXL	GCP19Q12	156.6±1.64	0.12±0.05	56.70±3.5	9.50±0.58
GCPQ06+PTXL	GCP20Q22	158.5±1.16	0.10±0.01	96.63±5.27	16.11±0.88
GCPQ10+PTXL	GCP37Q23	327.8±51.77	0.47±0.06	99.81±3.12	16.64±0.52
GCPQ14+PTXL	GCP29Q11	196.5±1.45	0.17±0.02	53.40±1.95	8.90±0.33

Table 6-3 shows the properties of the GCPQ-paclitaxel formulations discussed in chapter 4. Two of these formulations: GCPQ06-Paclitaxel and GCPQ10-Paclitaxel were used for the *in vivo* bio distribution studies. Both formulations were selected for a couple of reasons: they both had high encapsulation efficiencies above 95%, GCPQ10-paclitaxel (~99%) being slightly higher than GCPQ06-paclitaxel (~96%) they represent examples of different morphologies of GCPQ-paclitaxel formulations; GCPQ06-paclitaxel being a rod-like crystal and GCPQ10-paclitaxel being a spherical micellar formulation. Also, as was seen in chapter 5, GCPQ06 opens tight junctions significantly while GCPQ10 does not. Furthermore, both polymers have similar DQ% (~22%) but differ in DP% (20% and 37 % respectively) and finally, GCPQ10-paclitaxel has approximately twice the size (~327nm) of the other GCPQ-paclitaxel formulations (~150nm).

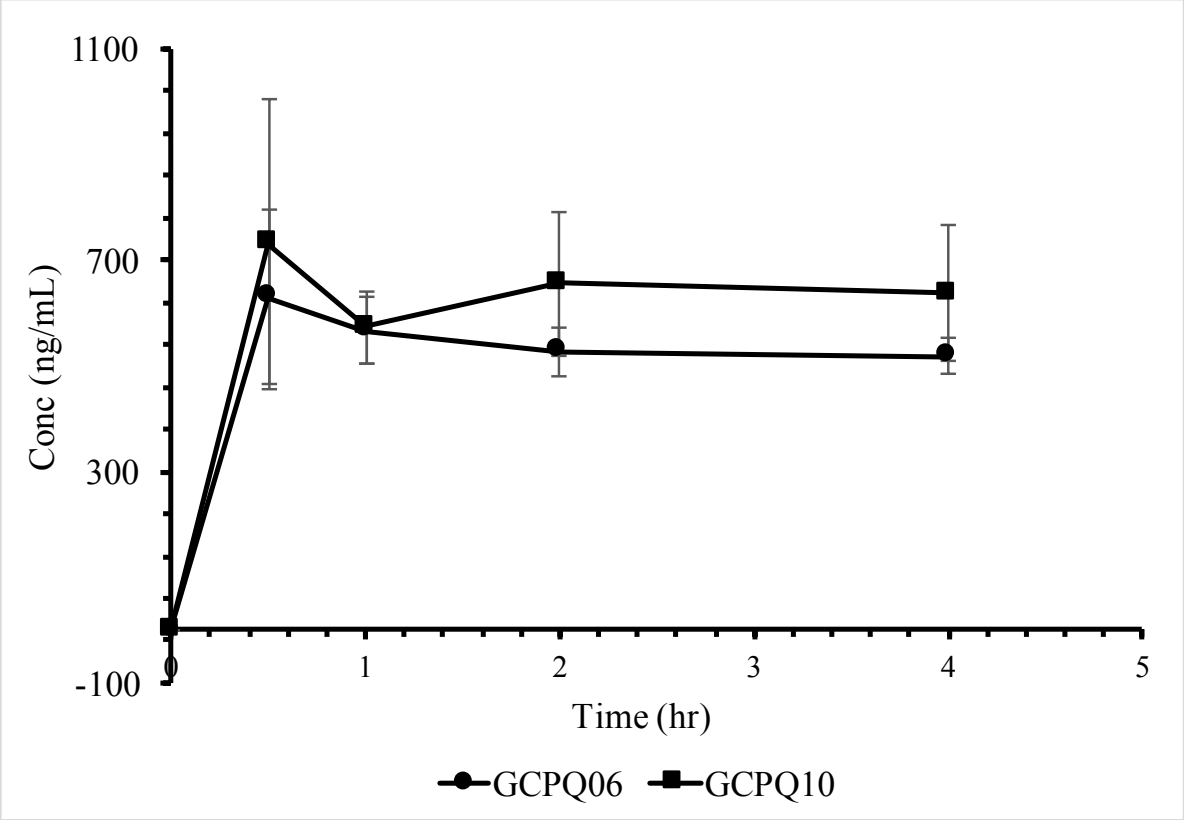

Figure 6-4: Plasma of GCPQ-Paclitaxel formulations over time after administration to male CD-1 mice by oral gavage at a dose of 20mg/kg. n=5

Figure 6-4 shows the plasma levels of paclitaxel following oral administration of GCPQ06-paclitaxel and GCPQ10-paclitaxel with the latter having slightly higher plasma levels than GCPQ06-paclitaxel but not significantly different.

Table 6-4: Bioavailability of GCPQ-Paclitaxel formulations administered by oral gavage at a dose of 20mg/kg to male CD-1 mice

Formulation	Dose ($mgKg^{-1}$)	AUC_{0-4h} (ng/hmL^{-1})	Cmax ($ngmL^{-1}$)	Tmax (h)
GCPQ06-PTXL	20	2048	629 ± 165	0.5
GCPQ10-PTXL	20	2417	731 ± 273	0.5

Table 6-4 shows the pharmacokinetic parameters of the GCPQ-paclitaxel formulations after oral administration. A high dose of 20mg/kg of paclitaxel in each formulation was chosen because we have previously shown that such a high dose was sufficient to saturate the P-gp receptors so that there was no improvement in plasma levels of paclitaxel when a P-gp inhibitor, verapamil was included (Soundararajan et al., 2016). The plasma levels of both GCPQ-paclitaxel formulations peaked at 30minutes which is earlier than 1hr which we previously reported for simulated Taxol but same as for a lower dose of a phenoxy acetyl derivative of glycol chitosan (GCPh) (Soundararajan et al., 2016). The peak concentration (Cmax) of GCPQ06-paclitaxel is slightly lower than that of GCPQ10-paclitaxel but the difference is not significant. Both Cmax values are comparable to the Cmax of simulated Taxol at the same concentration previously obtained under similar conditions (814 ± 331ng.hmL^{-1}) (Soundararajan et al., 2016). The AUC_{0-4h} of GCPQ10-paclitaxel (2417 ngmL^{-1}) is 18% higher than that of GCPQ06-paclitaxel (2048nghmL^{-1}) but this difference is again not significant. Both AUC values are comparable with the 2284nghmL^{-1} obtained for 20mg/kg simulated Taxol in the same previous study.

These results show that there is no significant difference in the plasma concentration of paclitaxel following oral administration with GCPQ06 and GCPQ10. Both formulations also compare well with simulated Taxol from previously reported data but have a faster Tmax. This faster Tmax perhaps is explained by the permeation enhancement effect of GCPQ, resulting in a more rapid uptake of paclitaxel. The comparable AUC and Cmax values which are not different from the values obtained when simulated Taxol was co-administered with verapamil (2333nghmL^{-1} and 718 ± 220 ngm^{L-1} respectively), indicates that similar concentrations are achieved when P-gp receptors are saturated or inhibited. The slightly higher Cmax and AUC values of GCPQ10-paclitaxel compared with GCPQ-paclitaxel could be attributed to a few factors: GCPQ10-PTXL had a slightly higher encapsulation efficiency than GCPQ06-PTXL but it also had a spherical shape while GCPQ06-PTXL was a rod-like crystal. Reports have suggested that while filamentous particles are likely to have a longer circulation half-life, spherical nanoparticles are likely to be internalised faster (Blanco et al., 2015). Another study in HeLa cells showed that rod shaped silica nanoparticles had a more rapid uptake at earlier time points but eventually achieve similar peak values as spherical nanoparticles at later time points, the differences being attributed to mechanisms of uptake (Hao et al., 2012) . The differences observed between GCPQ10-PTXL and GCPQ06-PTXL are however not significant enough to draw any conclusions, but they suggest that the paracellular route of uptake is perhaps not involved in the uptake of paclitaxel. This may not be surprising considering that paclitaxel will be confined to the Nano capsules after encapsulation and due to its low water solubility. The similarity of pharmacokinetics between paclitaxel nanocrystals and amorphous nanoparticles suggests furthermore that transport by diffusion along the lipid layers of the enterocytes may not be a qualitatively

important route. Our data is consistent with a mode of transport attributed to nanoparticles-namely endo/transcytosis. This will allow the crystalline as well as the amorphous drug in the nanoparticle to reach the plasma. It is unclear whether in terms of drugs being available, that is, in an active form as individual drug molecules, both formulations are equivalent. This could affect the pharmacodynamics effect available with either formulations but also disposition and accumulation in different compartments.

6.4 Conclusion

We have been able to show that structural modifications of GCPQ does not significantly alter the pharmacokinetic parameters of a hydrophobic BCS class IV drug. The pathway for uptake of these hydrophobic drugs is likely by endocytosis and while the shape and size differences resulting from structural modification might change the pathway, the differences are not significant enough to suggest one modification to be more efficient than the other.

Chapter 7. Conclusions and Future Plans

7.1 Conclusions

Comprehensive data from the series of experiments conducted suggest that GCPQ functionalization confers on it unique characteristics with potentially different applications. Thermodynamic analysis on self-aggregation suggests that the critical micelle concentration is very low (below 10μM) for all the polymers and increases with increasing temperature. Micellization can also be endothermic or exothermic, entropy driven or enthalpy driven depending on the proportion of palmitoyl and quaternary ammonium groups. The low CMC of GCPQ which compares well with that of Pluronic 127 and is more than 10,000 times lower than that of C10, confers on it an added advantage of stability after dilution in the aqueous milieu of the human body. This increased stability might imply that GCPQ is able to protect its encapsulated cargo after administration more efficiently than C10.

Drug encapsulation studies showed that GCPQ can be engineered to encapsulate poorly soluble drugs belonging to the BCS class II and IV, achieving encapsulation efficiencies as high as 99%. The nanoparticles formed also have a range of favourable properties including superior stability of cyclosporine A formulation, comparably good particle sizes under 200nm as well as rod shaped and spherical shaped paclitaxel nanoparticles.

In vitro assays on the transport of a paracellular marker, FITC dextran suggests that GCPQ does enhance paracellular permeability and this effect is pH dependent and can be graded

according to the degree of functionalization with palmitoyl and the quaternary ammonium groups. Furthermore, the results suggest that this effect is related to some reversible disruption of tight junctions, possibly related to the interactions between Zona occludens-1 and occludin. GCPQ can be engineered to be just as potent as C10 but much safer. Cytotoxicity experiments showed that cells treated with GCPQ recovered fully after 24 hours while those treated with C10 did not recover fully. The concentration of GCPQ used in the transport experiments is at least a thousand-fold higher than the CMC while C10 was below its CMC, implying that a higher concentration of C10 will be required to successfully encapsulate a cargo which comes with an increased risk of toxicity. GCPQ is thus a much safer permeation enhancer than C10, potentially more efficient for drug delivery while being at least as potent as C10. In vitro uptake studies also show that GCPQ is taken up by clathrin mediated endocytosis and that this uptake can be inhibited with chlorpromazine.

Ex vivo images show GCPQ is exceptionally mucoadhesive and muco-penetrative. It diffuses through the mucus mesh and adheres tightly to the epithelial cell surface, eventually getting taken up by the enterocytes and goblet cells. In vivo bioavailability data shows that GCPQ encapsulated paclitaxel attained as high plasma concentrations comparable with Taxol ® and remained in circulation at a high concentration up to 24hours after oral administration. This is indicative of GCPQ's ability to efficiently protect and deliver drugs with otherwise poor oral bioavailability, possibly through increasing local concentrations at the absorptive sites in the intestine and subsequently, protecting and carrying across the encapsulated drug into circulation.

7.2 Further work

We know, from this project that GCPQ does enhance paracellular transport across epithelial barriers and we know that the mechanism for this involves disruption of the integrity of the tight junction. From published literature, it is clear that this mechanism, for other derivatives of chitosan, involves a cascade of processes including Ca^{2+} and secondary messenger systems. It will be interesting to determine the exact molecular mechanisms of GCPQ's effects and if there are differences between the mechanism of GCPQ's effect and that of other permeation enhancers.

We have been able to show a correlation between cytotoxicity and permeation enhancement of GCPQ. This is consistent with what has been published for other permeation enhancers. Given that the toxicity assays conducted are measures of specific indices such as metabolic activity and membrane integrity, it will be interesting to conclusively draw a relationship between both indices and the mechanism of GCPQ's permeation enhancement effect. Furthermore, we know from the data that GCPQ gets taken up by receptor mediated endocytosis but we do not know if GCPQ is a ligand for any specific receptors and what the downfield effect of binding to one, should it do so.

We have shown that GCPQ is efficient in encapsulating hydrophobic drugs and in the literature, it is clear that GCPQ also enhances the uptake of hydrophilic drugs. It will be interesting to determine if GCPQ can be structurally modulated to affect positively or

negatively, the entrapment of hydrophilic drugs and how this translates affects oral bioavailability.

References

ADDERSON, J. & TAYLOR, H. 1970. The effects of temperature on the critical micelle concentrations of alkyl α-picolinium bromides. *Journal of Pharmacy and Pharmacology,* 22**,** 523-530.

AL-SADI, R., KHATIB, K., GUO, S., YE, D., YOUSSEF, M. & MA, T. 2011. Occludin regulates macromolecule flux across the intestinal epithelial tight junction barrier. *American Journal of Physiology-Gastrointestinal and Liver Physiology,* 300**,** G1054-G1064.

ALAVI, M., KARIMI, N. & SAFAEI, M. 2017. Application of various types of liposomes in drug delivery systems. *Advanced pharmaceutical bulletin,* 7**,** 3.

ALEXANDRIDIS, P., NIVAGGIOLI, T. & HATTON, T. A. 1995. Temperature Effects on Structural Properties of Pluronic P104 and F108 PEO-PPO-PEO Block Copolymer Solutions. *Langmuir,* 11**,** 1468-1476.

ALLEN, A., FLEMSTRÖM, G., GARNER, A. & KIVILAAKSO, E. 1993. Gastroduodenal mucosal protection. *Physiological reviews,* 73**,** 823-823.

ALLEN, M., MILLETT, P., DAWES, E. & RUSHTON, N. 1994. Lactate dehydrogenase activity as a rapid and sensitive test for the quantification of cell numbers in vitro. *Clinical materials,* 16**,** 189-194.

AMIDI, M., ROMEIJN, S. G., BORCHARD, G., JUNGINGER, H. E., HENNINK, W. E. & JISKOOT, W. 2006. Preparation and characterization of protein-loaded N-trimethyl chitosan nanoparticles as nasal delivery system. *Journal of Controlled Release,* 111**,** 107-116.

AMIDON, G. L., LENNERNÄS, H., SHAH, V. P. & CRISON, J. R. 1995. A theoretical basis for a biopharmaceutic drug classification: the correlation of in vitro drug product dissolution and in vivo bioavailability. *Pharmaceutical research,* 12**,** 413-420.

ANDERBERG, E. K., LINDMARK, T. & ARTURSSON, P. 1993. Sodium caprate elicits dilatations in human intestinal tight junctions and enhances drug absorption by the paracellular route. *Pharmaceutical research,* 10**,** 857-864.

ANDERSON, J. & VAN ITALLIE, C. 1995. Tight junctions and the molecular basis for regulation of paracellular permeability. *American Journal of Physiology-Gastrointestinal and Liver Physiology,* 269**,** G467-G475.

ARECHABALA, B., COIFFARD, C., RIVALLAND, P., COIFFARD, L. & DE ROECK-HOLTZHAUER, Y. 1999. Comparison of cytotoxicity of various surfactants tested on normal human fibroblast cultures using the neutral red test, MTT assay and LDH release. *Journal of applied toxicology,* 19**,** 163-165.

ASIRVATHAM, S., DHOKCHAWLE, B. V. & TAURO, S. J. 2016. Quantitative structure activity relationships studies of non-steroidal anti-inflammatory drugs: A review. *Arabian Journal of Chemistry*.

AZHDARZADEH, M., ATYABI, F., SAEI, A. A., VARNAMKHASTI, B. S., OMIDI, Y., FATEH, M., GHAVAMI, M., SHANEHSAZZADEH, S. & DINARVAND, R. 2016. Theranostic MUC-1 aptamer targeted gold coated superparamagnetic iron oxide nanoparticles for magnetic resonance imaging and photothermal therapy of colon cancer. *Colloids and Surfaces B: Biointerfaces,* 143**,** 224-232.

BAEK, J.-S. & CHO, C.-W. 2015. Controlled release and reversal of multidrug resistance by co-encapsulation of paclitaxel and verapamil in solid lipid nanoparticles. *International journal of pharmaceutics,* 478**,** 617-624.

BALDA, M. S., WHITNEY, J. A., FLORES, C., GONZÁLEZ, S., CEREIJIDO, M. & MATTER, K. 1996. Functional dissociation of paracellular permeability and transepithelial electrical resistance

and disruption of the apical-basolateral intramembrane diffusion barrier by expression of a mutant tight junction membrane protein. *The Journal of cell biology,* 134**,** 1031-1049.

BANERJEE, A., QI, J., GOGOI, R., WONG, J. & MITRAGOTRI, S. 2016. Role of nanoparticle size, shape and surface chemistry in oral drug delivery. *Journal of Controlled Release,* 238**,** 176-185.

BAYAT, A., DORKOOSH, F. A., DEHPOUR, A. R., MOEZI, L., LARIJANI, B., JUNGINGER, H. E. & RAFIEE-TEHRANI, M. 2008. Nanoparticles of quaternized chitosan derivatives as a carrier for colon delivery of insulin: ex vivo and in vivo studies. *International journal of pharmaceutics,* 356**,** 259-266.

BECK, I. 1973. The role of pancreatic enzymes in digestion. *The American journal of clinical nutrition,* 26**,** 311-325.

BEHRENS, S. H., CHRISTL, D. I., EMMERZAEL, R., SCHURTENBERGER, P. & BORKOVEC, M. 2000. Charging and aggregation properties of carboxyl latex particles: Experiments versus DLVO theory. *Langmuir,* 16**,** 2566-2575.

BEI, Y.-Y., YUAN, Z.-Q., ZHANG, L., ZHOU, X.-F., CHEN, W.-L., XIA, P., LIU, Y., YOU, B.-G., HU, X.-J. & ZHU, Q.-L. 2014. Novel self-assembled micelles based on palmitoyl-trimethyl-chitosan for efficient delivery of harmine to liver cancer. *Expert opinion on drug delivery,* 11**,** 843-854.

BERG, S. L., TOLCHER, A., O'SHAUGHNESSY, J. A., DENICOFF, A. M., NOONE, M., OGNIBENE, F. P., COWAN, K. H. & BALIS, F. M. 1995. Effect of R-verapamil on the pharmacokinetics of paclitaxel in women with breast cancer. *Journal of clinical oncology,* 13**,** 2039-2042.

BERNKOP-SCHNÜRCH, A., BRANDT, U. & CLAUSEN, A. 1999. Synthesis and in vitro evaluation of chitosan-cysteine conjugates. *Sci. Pharm,* 67**,** 196-208.

BERNKOP-SCHNÜRCH, A. & DÜNNHAUPT, S. 2012. Chitosan-based drug delivery systems. *European Journal of Pharmaceutics and Biopharmaceutics,* 81**,** 463-469.

BERNKOP-SCHNÜRCH, A., GUGGI, D. & PINTER, Y. 2004. Thiolated chitosans: development and in vitro evaluation of a mucoadhesive, permeation enhancing oral drug delivery system. *Journal of Controlled Release,* 94**,** 177-186.

BERNKOP-SCHNÜRCH, A., HORNOF, M. & ZOIDL, T. 2003. Thiolated polymers—thiomers: synthesis and in vitro evaluation of chitosan–2-iminothiolane conjugates. *International journal of pharmaceutics,* 260**,** 229-237.

BERTIAUX-VANDAËLE, N., YOUMBA, S. B., BELMONTE, L., LECLEIRE, S., ANTONIETTI, M., GOURCEROL, G., LEROI, A.-M., DÉCHELOTTE, P., MÉNARD, J.-F. & DUCROTTÉ, P. 2011. The expression and the cellular distribution of the tight junction proteins are altered in irritable bowel syndrome patients with differences according to the disease subtype. *The American journal of gastroenterology,* 106**,** 2165.

BLANCO, E., SHEN, H. & FERRARI, M. 2015. Principles of nanoparticle design for overcoming biological barriers to drug delivery. *Nature biotechnology,* 33**,** 941.

BLAU, S., JUBEH, T. T., HAUPT, S. M. & RUBINSTEIN, A. 2000. Drug targeting by surface cationization. *Critical Reviews™ in Therapeutic Drug Carrier Systems,* 17.

BOBO, D., ROBINSON, K. J., ISLAM, J., THURECHT, K. J. & CORRIE, S. R. 2016. Nanoparticle-based medicines: a review of FDA-approved materials and clinical trials to date. *Pharmaceutical research,* 33**,** 2373-2387.

BORISOV, O. V. & HALPERIN, A. 1998. Self-assembly of polysoaps. *Current opinion in colloid & interface science,* 3**,** 415-421.

BOUCHEMAL, K., AGNELY, F., KOFFI, A. & PONCHEL, G. 2009. A concise analysis of the effect of temperature and propanediol-1, 2 on Pluronic F127 micellization using isothermal titration microcalorimetry. *Journal of colloid and interface science,* 338**,** 169-176.

BRAVO-OSUNA, I., TEUTONICO, D., ARPICCO, S., VAUTHIER, C. & PONCHEL, G. 2007. Characterization of chitosan thiolation and application to thiol quantification onto nanoparticle surface. *International journal of pharmaceutics,* 340**,** 173-181.

BRAYDEN, D. J. & ALONSO, M.-J. 2016. Oral delivery of peptides: opportunities and issues for translation. *Adv Drug Deliv Rev,* 106**,** 193-5.

BRAYDEN, D. J., MAHER, S., BAHAR, B. & WALSH, E. 2015a. Sodium caprate-induced increases in intestinal permeability and epithelial damage are prevented by misoprostol. *Eur J Pharm Biopharm,* 94**,** 194-206.

BRAYDEN, D. J., MAHER, S., BAHAR, B. & WALSH, E. 2015b. Sodium caprate-induced increases in intestinal permeability and epithelial damage are prevented by misoprostol. *European Journal of Pharmaceutics and Biopharmaceutics*.

BROWE, D. M. & BAUMGARTEN, C. M. 2003. Stretch of β1 integrin activates an outwardly rectifying chloride current via FAK and Src in rabbit ventricular myocytes. *The Journal of general physiology,* 122**,** 689-702.

BROWN, D. 1989. Membrane recycling and epithelial cell function. *American Journal of Physiology-Renal Physiology,* 256**,** F1-F12.

BROWN, M., SCHÄTZLEIN, A., BROWNLIE, A., JACK, V., WANG, W., TETLEY, L., GRAY, A. & UCHEGBU, I. 2000. Preliminary characterization of novel amino acid based polymeric vesicles as gene and drug delivery agents. *Bioconjugate chemistry,* 11**,** 880-891.

BULBAKE, U., DOPPALAPUDI, S., KOMMINENI, N. & KHAN, W. 2017. Liposomal formulations in clinical use: an updated review. *Pharmaceutics,* 9**,** 12.

BUTTERWORTH, M., ILLUM, L. & DAVIS, S. 2001. Preparation of ultrafine silica-and PEG-coated magnetite particles. *Colloids and Surfaces A: Physicochemical and Engineering Aspects,* 179**,** 93-102.

BYE, W., ALLAN, C. & TRIER, J. 1984. Structure, distribution, and origin of M cells in Peyer's patches of mouse ileum. *Gastroenterology,* 86**,** 789-801.

CABRAL, H., MATSUMOTO, Y., MIZUNO, K., CHEN, Q., MURAKAMI, M., KIMURA, M., TERADA, Y., KANO, M., MIYAZONO, K. & UESAKA, M. 2011. Accumulation of sub-100 nm polymeric micelles in poorly permeable tumours depends on size. *Nature nanotechnology,* 6**,** 815-823.

CALDWELL, G. W., FERGUSON, C., BUERGER, R., KULP, L. & YAN, Z. 2014. Permeability Assessment Using 5-day Cultured Caco-2 Cell Monolayers. *Optimization in Drug Discovery: In Vitro Methods***,** 49-76.

CAMENISCH, G., ALSENZ, J., VAN DE WATERBEEMD, H. & FOLKERS, G. 1998. Estimation of permeability by passive diffusion through Caco-2 cell monolayers using the drugs' lipophilicity and molecular weight. *European journal of pharmaceutical sciences,* 6**,** 313-319.

CANTON, I. & BATTAGLIA, G. 2012. Endocytosis at the nanoscale. *Chemical Society Reviews,* 41**,** 2718-2739.

CEREIJIDO, M., ROBBINS, E., DOLAN, W., ROTUNNO, C. & SABATINI, D. 1978. Polarized monolayers formed by epithelial cells on a permeable and translucent support. *The Journal of cell biology,* 77**,** 853-880.

CHANDLER, D. 2005a. Interfaces and the driving force of hydrophobic assembly. *Nature,* 437**,** 640-7.

CHANDLER, D. 2005b. Interfaces and the driving force of hydrophobic assembly. *Nature,* 437**,** 640-647.

CHANG, R. 2005. *Physical chemistry for the biosciences*, University Science Books.

CHATTERJEE, A., MOULIK, S., SANYAL, S., MISHRA, B. & PURI, P. 2001. Thermodynamics of micelle formation of ionic surfactants: a critical assessment for sodium dodecyl sulfate, cetyl pyridinium chloride and dioctyl sulfosuccinate (Na salt) by microcalorimetric, conductometric, and tensiometric measurements. *The Journal of Physical Chemistry B,* 105**,** 12823-12831.

CHEN, L., TIAN, Z. & DU, Y. 2004a. Synthesis and pH sensitivity of carboxymethyl chitosan-based polyampholyte hydrogels for protein carrier matrices. *Biomaterials,* 25**,** 3725-3732.

CHEN, L.-T. & WEISS, L. 1973. The role of the sinus wall in the passage of erythrocytes through the spleen. *Blood,* 41**,** 529-537.

CHEN, S.-C., WU, Y.-C., MI, F.-L., LIN, Y.-H., YU, L.-C. & SUNG, H.-W. 2004b. A novel pH-sensitive hydrogel composed of N, O-carboxymethyl chitosan and alginate cross-linked by genipin for protein drug delivery. *Journal of Controlled Release,* 96**,** 285-300.

CHITHRANI, B. D., GHAZANI, A. A. & CHAN, W. C. 2006. Determining the size and shape dependence of gold nanoparticle uptake into mammalian cells. *Nano letters,* 6**,** 662-668.

CHO, E. C., XIE, J., WURM, P. A. & XIA, Y. 2009. Understanding the role of surface charges in cellular adsorption versus internalization by selectively removing gold nanoparticles on the cell surface with a I2/KI etchant. *Nano letters,* 9**,** 1080-1084.

CHO, K., WANG, X., NIE, S. & SHIN, D. M. 2008. Therapeutic nanoparticles for drug delivery in cancer. *Clinical cancer research,* 14**,** 1310-1316.

CHO, M. J., THOMPSON, D. P., CRAMER, C. T., VIDMAR, T. J. & SCIESZKA, J. F. 1989a. The Madin Darby canine kidney (MDCK) epithelial cell monolayer as a model cellular transport barrier. *Pharmaceutical research,* 6**,** 71-77.

CHO, M. J., THOMPSON, D. P., CRAMER, C. T., VIDMAR, T. J. & SCIESZKA, J. F. 1989b. The Madin Darby canine kidney (MDCK) epithelial cell monolayer as a model cellular transport barrier. *Pharm Res,* 6**,** 71-7.

CHOI, H. S., LIU, W., MISRA, P., TANAKA, E., ZIMMER, J. P., IPE, B. I., BAWENDI, M. G. & FRANGIONI, J. V. 2007. Renal clearance of quantum dots. *Nature biotechnology,* 25**,** 1165-1170.

CHOOI, K. W., CARLOS, M. I. S., SOUNDARARAJAN, R., GAISFORD, S., ARIFIN, N., SCHÄTZLEIN, A. G. & UCHEGBU, I. F. 2014a. Physical Characterisation and Long-Term Stability Studies on Quaternary Ammonium Palmitoyl Glycol Chitosan (GCPQ)—A New Drug Delivery Polymer. *Journal of pharmaceutical sciences,* 103**,** 2296-2306.

CHOOI, K. W., CARLOS, S., ISABEL, M., SOUNDARARAJAN, R., GAISFORD, S., ARIFIN, N., SCHÄTZLEIN, A. G. & UCHEGBU, I. F. 2014b. Physical Characterisation and Long-Term Stability Studies on Quaternary Ammonium Palmitoyl Glycol Chitosan (GCPQ)—A New Drug Delivery Polymer. *Journal of pharmaceutical sciences,* 103**,** 2296-2306.

CHOOI, K. W., GRAY, A. I., TETLEY, L., FAN, Y. & UCHEGBU, I. F. 2009. The molecular shape of poly (propylenimine) dendrimer amphiphiles has a profound effect on their self assembly. *Langmuir,* 26**,** 2301-2316.

CHOOI, K. W., GRAY, A. I., TETLEY, L., FAN, Y. L. & UCHEGBU, I. F. 2010. The molecular shape of poly(propylenimine) dendrimers has a profound effect on their self assembly. *Langmuir,* 26**,** 2301-2316.

CHOOI, K. W., HOU, X. L., QU, X., SOUNDARARAJAN, R. & UCHEGBU, I. F. 2013. Claw amphiphiles with a dendrimer core: Nanoparticle stability and drug encapsulation are directly proportional to the number of digits. *Langmuir,* 29**,** 4214-4224.

CHOOI, K. W., SIMAO CARLOS, M. I., SOUNDARARAJAN, R., GAISFORD, S., ARIFIN, N., SCHATZLEIN, A. G. & UCHEGBU, I. F. 2014c. Physical characterisation and long-term stability studies on quaternary ammonium palmitoyl glycol chitosan (GCPQ)--a new drug delivery polymer. *J Pharm Sci,* 103**,** 2296-306.

CHUNG, T.-H., WU, S.-H., YAO, M., LU, C.-W., LIN, Y.-S., HUNG, Y., MOU, C.-Y., CHEN, Y.-C. & HUANG, D.-M. 2007. The effect of surface charge on the uptake and biological function of mesoporous silica nanoparticles in 3T3-L1 cells and human mesenchymal stem cells. *Biomaterials,* 28**,** 2959-2966.

CIAPETTI, G., CENNI, E., PRATELLI, L. & PIZZOFERRATO, A. 1993. In vitro evaluation of cell/biomaterial interaction by MTT assay. *Biomaterials,* 14**,** 359-364.

CITI, S. 1992. Protein kinase inhibitors prevent junction dissociation induced by low extracellular calcium in MDCK epithelial cells. *The Journal of Cell Biology,* 117**,** 169-178.

CLOGSTON, J. 2009. NCL Method PCC-2: Measuring Zeta Potential of Nanoparticles. *Nanotechnology Characterization Laboratory, NCI, Ed*.

CONNER, S. D. & SCHMID, S. L. 2003a. Regulated portals of entry into the cell. *Nature,* 422**,** 37.

CONNER, S. D. & SCHMID, S. L. 2003b. Regulated portals of entry into the cell. *Nature,* 422**,** 37-44.

CORKILL, J., GOODMAN, J., HARROLD, S. & TATE, J. 1966. Thermodynamics of comicellization of ionic detergents. *Transactions of the Faraday Society,* 62**,** 994-1001.

COROT, C., PETRY, K. G., TRIVEDI, R., SALEH, A., JONKMANNS, C., LE BAS, J.-F., BLEZER, E., RAUSCH, M., BROCHET, B. & FOSTER-GAREAU, P. 2004. Macrophage imaging in central nervous system and in carotid atherosclerotic plaque using ultrasmall superparamagnetic iron oxide in magnetic resonance imaging. *Investigative radiology,* 39**,** 619-625.

COSTAS, M., KRONBERG, B. & SILVESTON, R. 1994. GENERAL THERMODYNAMIC ANALYSIS OF THE DISSOLUTION OF NONPOLAR MOLECULES INTO WATER - ORIGIN OF HYDROPHOBICITY. *Journal of the Chemical Society-Faraday Transactions,* 90**,** 1513-1522.

CROWTHER, R. S. & MARRIOTT, C. 1984. Counter-ion binding to mucus glycoproteins. *Journal of pharmacy and pharmacology,* 36**,** 21-26.

CUNDY, K. C., GALLOP, M. A. & ZHOU, C. X. 2005. Bile-acid conjugates for providing sustained systemic concentrations of drugs. Google Patents.

CZOGALLA, A. 2008. Oral cyclosporine A-the current picture of its liposomal and other delivery systems. *Cellular & molecular biology letters,* 14**,** 139.

D'INCÀ, R., DE LEO, V., CORRAO, G., MARTINES, D., D'ODORICO, A., MESTRINER, C., VENTURI, C., LONGO, G. & STURNIOLO, G. C. 1999. Intestinal permeability test as a predictor of clinical course in Crohn's disease. *The American journal of gastroenterology,* 94**,** 2956.

DA SILVA SANTOS, N. P., NASCIMENTO, S. C., WANDERLEY, M. S. O., PONTES-FILHO, N. T., DA SILVA, J. F., DE CASTRO, C. M. M. B., PEREIRA, E. C., DA SILVA, N. H., HONDA, N. K. & SANTOS-MAGALHÃES, N. S. 2006. Nanoencapsulation of usnic acid: an attempt to improve antitumour activity and reduce hepatotoxicity. *European Journal of Pharmaceutics and Biopharmaceutics,* 64**,** 154-160.

DANHIER, F., LECOUTURIER, N., VROMAN, B., JÉRÔME, C., MARCHAND-BRYNAERT, J., FERON, O. & PRÉAT, V. 2009. Paclitaxel-loaded PEGylated PLGA-based nanoparticles: in vitro and in vivo evaluation. *Journal of Controlled Release,* 133**,** 11-17.

DARAEE, H., ETEMADI, A., KOUHI, M., ALIMIRZALU, S. & AKBARZADEH, A. 2016. Application of liposomes in medicine and drug delivery. *Artificial cells, nanomedicine, and biotechnology,* 44**,** 381-391.

DAVIS, J. G., GIERSZAL, K. P., WANG, P. & BEN-AMOTZ, D. 2012a. Water structural transformation at molecular hydrophobic interfaces. *Nature,* 491**,** 582-5.

DAVIS, J. G., GIERSZAL, K. P., WANG, P. & BEN-AMOTZ, D. 2012b. Water structural transformation at molecular hydrophobic interfaces. *Nature,* 491**,** 582-585.

DE ASSIS, D. N., MOSQUEIRA, V. C. F., VILELA, J. M. C., ANDRADE, M. S. & CARDOSO, V. N. 2008. Release profiles and morphological characterization by atomic force microscopy and

photon correlation spectroscopy of 99m Technetium-fluconazole nanocapsules. *International Journal of Pharmaceutics,* 349**,** 152-160.

DE MELLO, C. G. C., BRANQUINHO, R. T., OLIVEIRA, M. T., MILAGRE, M. M., MOSQUEIRA, V. C. F. & DE LANA, M. 2016. Efficacy of lychnopholide polymeric nanocapsules after oral and intravenous administration in murine experimental Chagas disease. *Antimicrobial agents and chemotherapy,* 60**,** 5215-5222.

DEL VECCHIO, G., TSCHEIK, C., TENZ, K., HELMS, H. C., WINKLER, L., BLASIG, R. & BLASIG, I. 2012. Sodium caprate transiently opens claudin-5-containing barriers at tight junctions of epithelial and endothelial cells. *Molecular pharmaceutics,* 9**,** 2523-2533.

DERJAGUIN, B. & LANDAU, L. 1941. Theory of the stability of strongly charged lyophobic sols and of the adhesion of strongly charged particles in solutions of electrolytes. *Acta physicochim. URSS,* 14**,** 633-662.

DES RIEUX, A., FIEVEZ, V., GARINOT, M., SCHNEIDER, Y.-J. & PRÉAT, V. 2006. Nanoparticles as potential oral delivery systems of proteins and vaccines: a mechanistic approach. *Journal of controlled release,* 116**,** 1-27.

DESAI, M. P., LABHASETWAR, V., AMIDON, G. L. & LEVY, R. J. 1996. Gastrointestinal uptake of biodegradable microparticles: effect of particle size. *Pharmaceutical research,* 13**,** 1838-1845.

DESAI, M. P., LABHASETWAR, V., WALTER, E., LEVY, R. J. & AMIDON, G. L. 1997. The mechanism of uptake of biodegradable microparticles in Caco-2 cells is size dependent. *Pharmaceutical research,* 14**,** 1568-1573.

DIAB, C., WINNIK, F. & TRIBET, C. 2007. Enthalpy of interaction and binding isotherms of non-ionic surfactants onto micellar amphiphilic polymers (amphipols). *Langmuir,* 23**,** 3025-3035.

DILL, K. & BROMBERG, S. 2010. *Molecular driving forces: statistical thermodynamics in biology, chemistry, physics, and nanoscience*, Garland Science.

DIZAJ, S. M., VAZIFEHASL, Z., SALATIN, S., ADIBKIA, K. & JAVADZADEH, Y. 2015. Nanosizing of drugs: effect on dissolution rate. *Research in pharmaceutical sciences,* 10**,** 95.

DOBSON, J. 2006. Magnetic nanoparticles for drug delivery. *Drug development research,* 67**,** 55-60.

DODANE, V., KHAN, M. A. & MERWIN, J. R. 1999. Effect of chitosan on epithelial permeability and structure. *International journal of pharmaceutics,* 182**,** 21-32.

DODANE, V. & VILIVALAM, V. D. 1998. Pharmaceutical applications of chitosan. *Pharmaceutical Science & Technology Today,* 1**,** 246-253.

DOHERTY, G. J. & MCMAHON, H. T. 2009. Mechanisms of endocytosis. *Annual review of biochemistry,* 78**,** 857-902.

DONG, Y. & FENG, S.-S. 2004. Methoxy poly (ethylene glycol)-poly (lactide)(MPEG-PLA) nanoparticles for controlled delivery of anticancer drugs. *Biomaterials,* 25**,** 2843-2849.

DONOVAN, M. D., FLYNN, G. L. & AMIDON, G. L. 1990. Absorption of polyethylene glycols 600 through 2000: the molecular weight dependence of gastrointestinal and nasal absorption. *Pharmaceutical research,* 7**,** 863-868.

DREWE, J., FRICKER, G., VONDERSCHER, J. & BEGLINGER, C. 1993. Enteral absorption of octreotide: absorption enhancement by polyoxyethylene-24-cholesterol ether. *British journal of pharmacology,* 108**,** 298-303.

EASTMAN, J. 2009. Colloid stability. *Colloid Science: Principles, Methods and Applications***,** 36-49.

ENSIGN, L. M., CONE, R. & HANES, J. 2012. Oral drug delivery with polymeric nanoparticles: the gastrointestinal mucus barriers. *Advanced drug delivery reviews,* 64**,** 557-570.

FANNING, A. S., JAMESON, B. J., JESAITIS, L. A. & ANDERSON, J. M. 1998. The tight junction protein ZO-1 establishes a link between the transmembrane protein occludin and the actin cytoskeleton. *Journal of Biological Chemistry,* 273**,** 29745-29753.

FARAJI, A. H. & WIPF, P. 2009. Nanoparticles in cellular drug delivery. *Bioorganic & medicinal chemistry,* 17**,** 2950-2962.

FENG, Y., BILLON, L., GRASSL, B., BASTIAT, G., BORISOV, O. & FRANÇOIS, J. 2005. Hydrophobically associating polyacrylamides and their partially hydrolyzed derivatives prepared by post-modification. 2. Properties of non-hydrolyzed polymers in pure water and brine. *Polymer,* 46**,** 9283-9295.

FERRARI, M. 2005. Cancer nanotechnology: opportunities and challenges. *Nature Reviews Cancer,* 5**,** 161.

FLORENCE, A. T. 2005. Nanoparticle uptake by the oral route: fulfilling its potential? *Drug discovery today: technologies,* 2**,** 75-81.

FLORENCE, A. T. & HUSSAIN, N. 2001. Transcytosis of nanoparticle and dendrimer delivery systems: evolving vistas. *Advanced drug delivery reviews,* 50**,** S69-S89.

FORTE, J. & SCHULTZ, S. 1989. Handbook of Physiology: The Gastrointestinal System. Salivary, Gastric, Pancreatic, and Hepatobiliary Secretion. 567-596.

FOTAKIS, G. & TIMBRELL, J. A. 2006. In vitro cytotoxicity assays: comparison of LDH, neutral red, MTT and protein assay in hepatoma cell lines following exposure to cadmium chloride. *Toxicology letters,* 160**,** 171-177.

FRANK, P. G., WOODMAN, S. E., PARK, D. S. & LISANTI, M. P. 2003. Caveolin, caveolae, and endothelial cell function. *Arteriosclerosis, thrombosis, and vascular biology,* 23**,** 1161-1168.

FULLER, J. E., ZUGATES, G. T., FERREIRA, L. S., OW, H. S., NGUYEN, N. N., WIESNER, U. B. & LANGER, R. S. 2008. Intracellular delivery of core–shell fluorescent silica nanoparticles. *Biomaterials,* 29**,** 1526-1532.

GALINDO-RODRIGUEZ, S. A., ALLEMANN, E., FESSI, H. & DOELKER, E. 2005. Polymeric nanoparticles for oral delivery of drugs and vaccines: a critical evaluation of in vivo studies. *Critical Reviews™ in Therapeutic Drug Carrier Systems,* 22.

GAMBOA, J. M. & LEONG, K. W. 2013. In vitro and in vivo models for the study of oral delivery of nanoparticles. *Adv Drug Deliv Rev,* 65**,** 800-10.

GANGWAR, S., PAULETTI, G. M., WANG, B., SIAHAAN, T. J., STELLA, V. J. & BORCHARDT, R. T. 1997. Prodrug strategies to enhance the intestinal absorption of peptides. *Drug Discovery Today,* 2**,** 148-155.

GARDIEL, P., HILDEBRAND, A., NEUBERT, R. & BLUME, A. 2000. Thermodynamic characterization of bile salt aggregateion as a function of temperature and ionic strength using isothermal titration calorimetry. *Langmuir,* 16**,** 5267-5275.

GARRETT, N. L., LALATSA, A., UCHEGBU, I., SCHÄTZLEIN, A. & MOGER, J. 2012. Exploring uptake mechanisms of oral nanomedicines using multimodal nonlinear optical microscopy. *Journal of biophotonics,* 5**,** 458-468.

GEBHARDT, R. & MATZ-SOJA, M. 2015. Liposomes as carriers: not as innocent as one would like. *Archives of toxicology,* 89**,** 1399-1400.

GENG, Y., DALHAIMER, P., CAI, S., TSAI, R., TEWARI, M., MINKO, T. & DISCHER, D. E. 2007. Shape effects of filaments versus spherical particles in flow and drug delivery. *Nature nanotechnology,* 2**,** 249-255.

GHOSH, P. 2012. DLVO Theory and Non-DLVO Forces. *Nptel. ac. in***,** 1-17.

GILL, S. J. & WADSO, I. 1976. EQUATION OF STATE DESCRIBING HYDROPHOBIC INTERACTIONS. *Proceedings of the National Academy of Sciences of the United States of America,* 73**,** 2955-2958.

GILLIES, E. R. & FRECHET, J. M. 2005. Dendrimers and dendritic polymers in drug delivery. *Drug discovery today,* 10**,** 35-43.

GIUSTI, F., POPOT, J.-L. & TRIBET, C. 2012. Well-defined critical association concentration and rapid adsorption at the air/water interface of a short amphiphilic polymer, amphipol A8-35: a study by Forster resonance energy transfer and dynamic surface tension measurements. *Langmuir,* 28**,** 10372-10380.

GOLDBERG, M. & GOMEZ-ORELLANA, I. 2003a. Challenges for the oral delivery of macromolecules. *Nature Reviews Drug Discovery,* 2**,** 289-295.

GOLDBERG, M. & GOMEZ-ORELLANA, I. 2003b. Challenges for the oral delivery of macromolecules. *Nature reviews Drug discovery,* 2**,** 289.

GOLDENRING, J. R. 2015. Recycling endosomes. *Current opinion in cell biology,* 35**,** 117-122.

GONZALEZ-MARISCAL, L., DE RAMIREZ, B. C. & CEREIJIDO, M. 1985. Tight junction formation in cultured epithelial cells (MDCK). *The Journal of membrane biology,* 86**,** 113-125.

GOYAL, R., MACRI, L. & KOHN, J. 2015. Formulation strategy for the delivery of cyclosporine A: comparison of two polymeric nanospheres. *Scientific reports,* 5.

GRASSO, D., SUBRAMANIAM, K., BUTKUS, M., STREVETT, K. & BERGENDAHL, J. 2002. A review of non-DLVO interactions in environmental colloidal systems. *Reviews in Environmental Science and Biotechnology,* 1**,** 17-38.

GRCEV, S., SCHOENMAKERS, P. & IEDEMA, P. 2004. Determination of molecular weight and size distribution and branching characteristics of PVAc by means of size exclusion chromatography/multi-angle laser light scattering (SEC/MALLS). *Polymer,* 45**,** 39-48.

GUGGI, D. & BERNKOP-SCHNÜRCH, A. 2003. In vitro evaluation of polymeric excipients protecting calcitonin against degradation by intestinal serine proteases. *International journal of pharmaceutics,* 252**,** 187-196.

HA, P. T., LE, M. H., HOANG, T. M. N., LE, T. T. H., DUONG, T. Q., TRAN, T. H. H. & NGUYEN, X. P. 2012. Preparation and anti-cancer activity of polymer-encapsulated curcumin nanoparticles. *Advances in Natural Sciences: Nanoscience and Nanotechnology,* 3**,** 035002.

HAMMAN, J. H., ENSLIN, G. M. & KOTZÉ, A. F. 2005. Oral delivery of peptide drugs. *BioDrugs,* 19**,** 165-177.

HAN, H.-K. & AMIDON, G. L. 2000. Targeted prodrug design to optimize drug delivery. *AAPS PharmSci,* 2**,** 48-58.

HAN, X., GELEIN, R., CORSON, N., WADE-MERCER, P., JIANG, J., BISWAS, P., FINKELSTEIN, J. N., ELDER, A. & OBERDÖRSTER, G. 2011. Validation of an LDH assay for assessing nanoparticle toxicity. *Toxicology,* 287**,** 99-104.

HAO, N., LI, L., ZHANG, Q., HUANG, X., MENG, X., ZHANG, Y., CHEN, D., TANG, F. & LI, L. 2012. The shape effect of PEGylated mesoporous silica nanoparticles on cellular uptake pathway in Hela cells. *Microporous and Mesoporous Materials,* 162**,** 14-23.

HE, P., DAVIS, S. S. & ILLUM, L. 1998. In vitro evaluation of the mucoadhesive properties of chitosan microspheres. *International Journal of Pharmaceutics,* 166**,** 75-88.

HEDRICK, J. L. & SMITH, A. J. 1968. Size and charge isomer separation and estimation of molecular weights of proteins by disc gel electrophoresis. *Archives of Biochemistry and Biophysics,* 126**,** 155-164.

HIDALGO, I. J., RAUB, T. J. & BORCHARDT, R. T. 1989. Characterization of the human colon carcinoma cell line (Caco-2) as a model system for intestinal epithelial permeability. *Gastroenterology,* 96**,** 736-749.

HILL, C. S. 1995. When will adequate pain treatment be the norm? *JAMA,* 274**,** 1881-1882.

HINDS, K. D. & KIM, S. W. 2002. Effects of PEG conjugation on insulin properties. *Advanced drug delivery reviews,* 54**,** 505-530.

HOFFMANN, I., HOFFMANN, C., FARAGO, B., PRÉVOST, S. & GRADZIELSKI, M. 2018. Dynamics of small unilamellar vesicles. *The Journal of Chemical Physics,* 148**,** 104901.

HOFMANN, A. F. & ECKMANN, L. 2006. How bile acids confer gut mucosal protection against bacteria. *Proceedings of the National Academy of Sciences of the United States of America,* 103**,** 4333-4334.

HOFMANN, A. F. & MYSELS, K. J. 1987. Bile salts as biological surfactants. *Colloids and Surfaces,* 30**,** 145-173.

HOGBEN, C. A. M., SCHANKER, L. S., TOCCO, D. J. & BRODIE, B. B. 1957. Absorption of drugs from the stomach. II. The human. *Journal of Pharmacology and Experimental Therapeutics,* 120**,** 540-545.

HONG, S., BIELINSKA, A. U., MECKE, A., KESZLER, B., BEALS, J. L., SHI, X., BALOGH, L., ORR, B. G., BAKER, J. R. & BANASZAK HOLL, M. M. 2004. Interaction of poly (amidoamine) dendrimers with supported lipid bilayers and cells: hole formation and the relation to transport. *Bioconjugate chemistry,* 15**,** 774-782.

HOO, C. M., STAROSTIN, N., WEST, P. & MECARTNEY, M. L. 2008. A comparison of atomic force microscopy (AFM) and dynamic light scattering (DLS) methods to characterize nanoparticle size distributions. *Journal of Nanoparticle Research,* 10**,** 89-96.

HORNOF, M. D., KAST, C. E. & BERNKOP-SCHNÜRCH, A. 2003. In vitro evaluation of the viscoelastic properties of chitosan–thioglycolic acid conjugates. *European Journal of Pharmaceutics and Biopharmaceutics,* 55**,** 185-190.

HÖRTER, D. & DRESSMAN, J. 2001. Influence of physicochemical properties on dissolution of drugs in the gastrointestinal tract1. *Advanced drug delivery reviews,* 46**,** 75-87.

HSU, L.-W., HO, Y.-C., CHUANG, E.-Y., CHEN, C.-T., JUANG, J.-H., SU, F.-Y., HWANG, S.-M. & SUNG, H.-W. 2013. Effects of pH on molecular mechanisms of chitosan–integrin interactions and resulting tight-junction disruptions. *Biomaterials,* 34**,** 784-793.

HSU, L.-W., LEE, P.-L., CHEN, C.-T., MI, F.-L., JUANG, J.-H., HWANG, S.-M., HO, Y.-C. & SUNG, H.-W. 2012. Elucidating the signaling mechanism of an epithelial tight-junction opening induced by chitosan. *Biomaterials,* 33**,** 6254-6263.

HUBATSCH, I., RAGNARSSON, E. G. & ARTURSSON, P. 2007. Determination of drug permeability and prediction of drug absorption in Caco-2 monolayers. *Nat Protoc,* 2**,** 2111-9.

HUBER, D. L. 2005. Synthesis, properties, and applications of iron nanoparticles. *Small,* 1**,** 482-501.

HWANG, G., AHN, I.-S., MHIN, B. J. & KIM, J.-Y. 2012. Adhesion of nano-sized particles to the surface of bacteria: mechanistic study with the extended DLVO theory. *Colloids and Surfaces B: Biointerfaces,* 97**,** 138-144.

IKENOUCHI, J., FURUSE, M., FURUSE, K., SASAKI, H., TSUKITA, S. & TSUKITA, S. 2005. Tricellulin constitutes a novel barrier at tricellular contacts of epithelial cells. *The Journal of cell biology,* 171**,** 939-945.

ILLUM, L., FARRAJ, N. F. & DAVIS, S. S. 1994. Chitosan as a novel nasal delivery system for peptide drugs. *Pharmaceutical research,* 11**,** 1186-1189.

INSTRUMENTS, M. 2011. Zeta potential: An Introduction in 30 minutes. *Zetasizer Nano Serles Technical Note. MRK654-01*.

IRVINE, J. D., TAKAHASHI, L., LOCKHART, K., CHEONG, J., TOLAN, J. W., SELICK, H. & GROVE, J. R. 1999. MDCK (Madin–Darby canine kidney) cells: a tool for membrane permeability screening. *Journal of pharmaceutical sciences,* 88**,** 28-33.

IVANOV, A. I. 2008. Pharmacological inhibition of endocytic pathways: is it specific enough to be useful? *Exocytosis and Endocytosis***,** 15-33.

JAIN, S., MITTAL, A., K JAIN, A., R MAHAJAN, R. & SINGH, D. 2010. Cyclosporin A loaded PLGA nanoparticle: preparation, optimization, in-vitro characterization and stability studies. *Current Nanoscience,* 6**,** 422-431.

JAMES, T. L. 1998. Fundamentals of NMR. *Online Textbook: Department of Pharmaceutical Chemistry, University of California, San Francisco*, 1-31.

JANI, P., HALBERT, G. W., LANGRIDGE, J. & FLORENCE, A. T. 1990. Nanoparticle uptake by the rat gastrointestinal mucosa: quantitation and particle size dependency. *Journal of pharmacy and pharmacology,* 42, 821-826.

JAYAKUMAR, R., REIS, R. & MANO, J. 2007. Synthesis and characterization of pH-sensitive thiol-containing chitosan beads for controlled drug delivery applications. *Drug Delivery,* 14, 9-17.

JEONG, J., HA, T. H. & CHUNG, B. H. 2006. Enhanced reusability of hexa-arginine-tagged esterase immobilized on gold-coated magnetic nanoparticles. *Analytica Chimica Acta,* 569, 203-209.

JIANG, W., KIM, B. Y., RUTKA, J. T. & CHAN, W. C. 2008. Nanoparticle-mediated cellular response is size-dependent. *Nature nanotechnology,* 3, 145-150.

JIN, C., WU, H., LIU, J., BAI, L. & GUO, G. 2007. The effect of paclitaxel-loaded nanoparticles with radiation on hypoxic MCF-7 cells. *Journal of clinical pharmacy and therapeutics,* 32, 41-47.

JOHNSON, J. & PORTER, R. 1970. Gel permeation chromatography. *Progress in Polymer Science,* 2, 201-256.

KAISER, M., PEREIRA, S., POHL, L., KETELHUT, S., KEMPER, B., GORZELANNY, C., GALLA, H.-J., MOERSCHBACHER, B. & GOYCOOLEA, F. 2015. Chitosan encapsulation modulates the effect of capsaicin on the tight junctions of MDCK cells. *Scientific reports,* 5, 10048.

KAKDE, D., TARESCO, V., BANSAL, K. K., MAGENNIS, E. P., HOWDLE, S. M., MANTOVANI, G., IRVINE, D. J. & ALEXANDER, C. 2016. Amphiphilic block copolymers from a renewable ε-decalactone monomer: prediction and characterization of micellar core effects on drug encapsulation and release. *Journal of Materials Chemistry B,* 4, 7119-7129.

KAST, C. E. & BERNKOP-SCHNÜRCH, A. 2001. Thiolated polymers—thiomers: development and in vitro evaluation of chitosan–thioglycolic acid conjugates. *Biomaterials,* 22, 2345-2352.

KAWASHIMA, Y., YAMAMOTO, H., TAKEUCHI, H. & KUNO, Y. 2000. Mucoadhesive DL-lactide/glycolide copolymer nanospheres coated with chitosan to improve oral delivery of elcatonin. *Pharmaceutical development and technology,* 5, 77-85.

KAWAUCHIYA, T., TAKUMI, R., KUDO, Y., TAKAMORI, A., SASAGAWA, T., TAKAHASHI, K. & KIKUCHI, H. 2011. Correlation between the destruction of tight junction by patulin treatment and increase of phosphorylation of ZO-1 in Caco-2 human colon cancer cells. *Toxicology letters,* 205, 196-202.

KE, W., ZHAO, Y., HUANG, R., JIANG, C. & PEI, Y. 2008. Enhanced oral bioavailability of doxorubicin in a dendrimer drug delivery system. *Journal of Pharmaceutical sciences,* 97, 2208-2216.

KEAN, T., ROTH, S. & THANOU, M. 2005. Trimethylated chitosans as non-viral gene delivery vectors: cytotoxicity and transfection efficiency. *Journal of Controlled Release,* 103, 643-653.

KESHARWANI, P., JAIN, K. & JAIN, N. K. 2014. Dendrimer as nanocarrier for drug delivery. *Progress in Polymer Science,* 39, 268-307.

KHALIL, I. A., KOGURE, K., AKITA, H. & HARASHIMA, H. 2006. Uptake pathways and subsequent intracellular trafficking in nonviral gene delivery. *Pharmacological reviews,* 58, 32-45.

KHAN, J. & ISLAM, M. N. 2012. *Morphology of the intestinal barrier in different physiological and pathological conditions*, INTECH Open Access Publisher.

KIM, J.-S. 2016. Liposomal drug delivery system. *Journal of Pharmaceutical Investigation,* 46, 387-392.

KIRBY, B. J. & HASSELBRINK, E. F. 2004. Zeta potential of microfluidic substrates: 2. Data for polymers. *Electrophoresis,* 25, 203-213.

KLINGLER, J., VARGAS, C., FIEDLER, S. & KELLER, S. 2015. Preparation of ready-to-use small unilamellar phospholipid vesicles by ultrasonication with a beaker resonator. *Analytical biochemistry,* 477, 10-12.

KOMAROVA, Y. & MALIK, A. B. 2010. Regulation of endothelial permeability via paracellular and transcellular transport pathways. *Annual review of physiology,* 72**,** 463-493.

KOPER, G. J., MINKENBERG, C. B., UPTON, I. S., VAN ESCH, J. H. & SUDHÖLTER, E. J. 2009. Quantitatively interpreting thermal behavior of self-associating systems. *The Journal of Physical Chemistry B,* 113**,** 15597-15601.

KOTZÉ, A. F., LUESSE, H. L., DE LEEUW, B. J., VERHOEF, J. C. & JUNGINGER, H. E. 1998. Comparison of the effect of different chitosan salts and N-trimethyl chitosan chloride on the permeability of intestinal epithelial cells (Caco-2). *Journal of controlled release,* 51**,** 35-46.

KOTZÉ, A. F., THANOU, M. M., LUEBEN, H. L., DE BOER, A., VERHOEF, J. & JUNGINGER, H. E. 1999. Enhancement of paracellular drug transport with highly quaternized N-trimethyl chitosan chloride in neutral environments: In vitro evaluation in intestinal epithelial cells (Caco-2). *Journal of pharmaceutical sciences,* 88**,** 253-257.

KOTZÉ, A. R., LUEBEN, H. L., DE LEEUW, B. J., VERHOEF, J. C. & JUNGINGER, H. E. 1997. N-trimethyl chitosan chloride as a potential absorption enhancer across mucosal surfaces: in vitro evaluation in intestinal epithelial cells (Caco-2). *Pharmaceutical research,* 14**,** 1197-1202.

KOWAPRADIT, J., OPANASOPIT, P., NGAWHIRANPAT, T., APIRAKARAMWONG, A., ROJANARATA, T., RUKTANONCHAI, U. & SAJOMSANG, W. 2008. Methylated N-(4-N, N-dimethylaminobenzyl) chitosan, a novel chitosan derivative, enhances paracellular permeability across intestinal epithelial cells (Caco-2). *AAPS PharmSciTech,* 9**,** 1143-1152.

KOWAPRADIT, J., OPANASOPIT, P., NGAWHIRUNPAT, T., APIRAKARAMWONG, A., ROJANARATA, T., RUKTANONCHAI, U. & SAJOMSANG, W. 2010. In vitro permeability enhancement in intestinal epithelial cells (Caco-2) monolayer of water soluble quaternary ammonium chitosan derivatives. *Aaps Pharmscitech,* 11**,** 497-508.

KRAEHENBUHL, J.-P. & NEUTRA, M. R. 2000. Epithelial M cells: differentiation and function. *Annual review of cell and developmental biology,* 16**,** 301-332.

KRALCHEVSKY, P. A., DANOV, K. D. & DENKOV, N. D. 1997. Chemical physics of colloid systems and interfaces. *Handbook of Surface and Colloid Chemistry,* 2.

KRONBERG, B., COSTAS, M. & SILVESTON, R. THERMODYNAMICS OF THE HYDROPHOBIC EFFECT IN SURFACTANT SOLUTIONS - MICELLIZATION AND ADSORPTION. 13th IUPAC International Conference on Chemical Thermodynamics, Jul 17-22 1994 Clermont Ferrand, France. 897-902.

KRONBERG, B., HOLMBERG, K. & LINDMAN, B. 2014. *Surface chemistry of surfactants and polymers*, John Wiley & Sons.

KRUG, S. M., AMASHEH, M., DITTMANN, I., CHRISTOFFEL, I., FROMM, M. & AMASHEH, S. 2013. Sodium caprate as an enhancer of macromolecule permeation across tricellular tight junctions of intestinal cells. *Biomaterials,* 34**,** 275-282.

KRUG, S. M., AMASHEH, S., RICHTER, J. F., MILATZ, S., GÜNZEL, D., WESTPHAL, J. K., HUBER, O., SCHULZKE, J. D. & FROMM, M. 2009. Tricellulin forms a barrier to macromolecules in tricellular tight junctions without affecting ion permeability. *Molecular biology of the cell,* 20**,** 3713-3724.

KRUG, S. M., SCHULZKE, J. D. & FROMM, M. Tight junction, selective permeability, and related diseases. Seminars in cell & developmental biology, 2014. Elsevier, 166-176.

KUMAR, M. N. R. 2000. A review of chitin and chitosan applications. *Reactive and functional polymers,* 46**,** 1-27.

KUMARI, A., YADAV, S. K. & YADAV, S. C. 2010. Biodegradable polymeric nanoparticles based drug delivery systems. *Colloids and Surfaces B: Biointerfaces,* 75**,** 1-18.

LAI, S. K., WANG, Y.-Y. & HANES, J. 2009. Mucus-penetrating nanoparticles for drug and gene delivery to mucosal tissues. *Advanced drug delivery reviews,* 61**,** 158-171.

LALATSA, A., GARRETT, N., FERRARELLI, T., MOGER, J., SCHATZLEIN, A. & UCHEGBU, I. 2012. Delivery of peptides to the blood and brain after oral uptake of quaternary ammonium palmitoyl glycol chitosan nanoparticles. *Molecular pharmaceutics,* 9**,** 1764-1774.

LALATSA, A., LEE, V., MALKINSON, J. P., ZLOH, M., SCHÄTZLEIN, A. G. & UCHEGBU, I. F. 2012. A prodrug nanoparticle approach for the oral delivery of a hydrophilic peptide, leucine5-enkephalin, to the brain. *Molecular pharmaceutics,* 9**,** 1665-1680.

LANGGUTH, P., BOHNER, V., HEIZMANN, J., MERKLE, H., WOLFFRAM, S., AMIDON, G. & YAMASHITA, S. 1997. The challenge of proteolytic enzymes in intestinal peptide delivery. *Journal of controlled release,* 46**,** 39-57.

LAVELLE, E., SHARIF, S., THOMAS, N., HOLLAND, J. & DAVIS, S. 1995. The importance of gastrointestinal uptake of particles in the design of oral delivery systems. *Advanced drug delivery reviews,* 18**,** 5-22.

LAWRENCE, X. Y., AMIDON, G. L., POLLI, J. E., ZHAO, H., MEHTA, M. U., CONNER, D. P., SHAH, V. P., LESKO, L. J., CHEN, M.-L. & LEE, V. H. 2002. Biopharmaceutics classification system: the scientific basis for biowaiver extensions. *Pharmaceutical research,* 19**,** 921-925.

LEE, V. H., YAMAMOTO, A. & KOMPELLA, U. B. 1991. Mucosal penetration enhancers for facilitation of peptide and protein drug absorption. *Critical reviews in therapeutic drug carrier systems,* 8**,** 91-192.

LEE, Y.-H. & SINKO, P. J. 2000. Oral delivery of salmon calcitonin. *Advanced drug delivery reviews,* 42**,** 225-238.

LEHR, C.-M., BOUWSTRA, J. A., SCHACHT, E. H. & JUNGINGER, H. E. 1992. In vitro evaluation of mucoadhesive properties of chitosan and some other natural polymers. *International journal of Pharmaceutics,* 78**,** 43-48.

LIANG, G. H. & WEBER, C. R. 2014. Molecular aspects of tight junction barrier function. *Current opinion in pharmacology,* 19**,** 84-89.

LIANG, J., ZHANG, X., MIAO, Y., LI, J. & GAN, Y. 2017. Lipid-coated iron oxide nanoparticles for dual-modal imaging of hepatocellular carcinoma. *International journal of nanomedicine,* 12**,** 2033.

LIN, J. H. 1998. Applications and limitations of interspecies scaling and in vitro extrapolation in pharmacokinetics. *Drug Metabolism and Disposition,* 26**,** 1202-1212.

LINDMARK, T., KIMURA, Y. & ARTURSSON, P. 1998. Absorption enhancement through intracellular regulation of tight junction permeability by medium chain fatty acids in Caco-2 cells. *Journal of Pharmacology and Experimental Therapeutics,* 284**,** 362-369.

LIPINSKI, C. A. 2016. Rule of five in 2015 and beyond: Target and ligand structural limitations, ligand chemistry structure and drug discovery project decisions. *Advanced drug delivery reviews,* 101**,** 34-41.

LIPINSKI, C. A., LOMBARDO, F., DOMINY, B. W. & FEENEY, P. J. 2001. Experimental and computational approaches to estimate solubility and permeability in drug discovery and development settings1. *Advanced drug delivery reviews,* 46**,** 3-26.

LISI, R. D., PERRON, G. & DESNOYERS, J. E. 1980. Volumetric and thermochemical properties of ionic surfactants: sodium decanoate and octylamine hydrobromide in water. *Canadian Journal of Chemistry,* 58**,** 959-969.

LOBNER, D. 2000. Comparison of the LDH and MTT assays for quantifying cell death: validity for neuronal apoptosis? *Journal of neuroscience methods,* 96**,** 147-152.

LÓPEZ-DÁVILA, V., MAGDELDIN, T., WELCH, H., DWEK, M. V., UCHEGBU, I. & LOIZIDOU, M. 2016. Efficacy of DOPE/DC-cholesterol liposomes and GCPQ micelles as AZD6244 nanocarriers in a 3D colorectal cancer in vitro model. *Nanomedicine*.

LUNDIN, S. & ARTURSSON, P. 1990. Absorption of a vasopressin analogue, 1-deamino-8-D-arginine-vasopressin (dDAVP), in a human intestinal epithelial cell line, Caco-2. *International journal of pharmaceutics,* 64**,** 181-186.

LUTZ, J.-F., STILLER, S., HOTH, A., KAUFNER, L., PISON, U. & CARTIER, R. 2006. One-pot synthesis of PEGylated ultrasmall iron-oxide nanoparticles and their in vivo evaluation as magnetic resonance imaging contrast agents. *Biomacromolecules,* 7**,** 3132-3138.

LV, P.-P., WEI, W., YUE, H., YANG, T.-Y., WANG, L.-Y. & MA, G.-H. 2011. Porous quaternized chitosan nanoparticles containing paclitaxel nanocrystals improved therapeutic efficacy in non-small-cell lung cancer after oral administration. *Biomacromolecules,* 12**,** 4230-4239.

MA, C. D., WANG, C., ACEVEDO-VÉLEZ, C., GELLMAN, S. H. & ABBOTT, N. L. 2015b. Modulation of hydrophobic interactions by proximally immobilized ions. *Nature,* 517**,** 347-350.

MA, P. & MUMPER, R. J. 2013. Paclitaxel nano-delivery systems: a comprehensive review. *Journal of nanomedicine & nanotechnology,* 4**,** 1000164.

MA, T. Y., HOLLANDER, D., KRUGLIAK, P. & KATZ, K. 1990. PEG 400, a hydrophilic molecular probe for measuring intestinal permeability. *Gastroenterology,* 98**,** 39-46.

MA, Z., LIM, T. M. & LIM, L.-Y. 2005. Pharmacological activity of peroral chitosan–insulin nanoparticles in diabetic rats. *International journal of pharmaceutics,* 293**,** 271-280.

MADAAN, K., LATHER, V. & PANDITA, D. 2016. Evaluation of polyamidoamine dendrimers as potential carriers for quercetin, a versatile flavonoid. *Drug delivery,* 23**,** 254-262.

MADARA, J. & TRIER, J. 1980. Structural abnormalities of jejunal epithelial cell membranes in celiac sprue. *Laboratory investigation,* 43**,** 254-261.

MAHER, S., KENNELLY, R., BZIK, V. A., BAIRD, A. W., WANG, X., WINTER, D. & BRAYDEN, D. J. 2009a. Evaluation of intestinal absorption enhancement and local mucosal toxicity of two promoters. I. Studies in isolated rat and human colonic mucosae. *European Journal of Pharmaceutical Sciences,* 38**,** 291-300.

MAHER, S., LEONARD, T. W., JACOBSEN, J. & BRAYDEN, D. J. 2009b. Safety and efficacy of sodium caprate in promoting oral drug absorption: from in vitro to the clinic. *Advanced drug delivery reviews,* 61**,** 1427-1449.

MAISEL, K., ENSIGN, L., REDDY, M., CONE, R. & HANES, J. 2015. Effect of surface chemistry on nanoparticle interaction with gastrointestinal mucus and distribution in the gastrointestinal tract following oral and rectal administration in the mouse. *Journal of Controlled Release,* 197**,** 48-57.

MALAM, Y., LOIZIDOU, M. & SEIFALIAN, A. M. 2009. Liposomes and nanoparticles: nanosized vehicles for drug delivery in cancer. *Trends in pharmacological sciences,* 30**,** 592-599.

MARSH, D. 2012. Thermodynamics of phospholipid self-assembly. *Biophys J,* 102**,** 1079-87.

MARSHALL, J., THABANE, M., GARG, A., CLARK, W., MEDDINGS, J. & COLLINS, S. 2004. Intestinal permeability in patients with irritable bowel syndrome after a waterborne outbreak of acute gastroenteritis in Walkerton, Ontario. *Alimentary pharmacology & therapeutics,* 20**,** 1317-1322.

MCMAHON, H. T. & BOUCROT, E. 2011. Molecular mechanism and physiological functions of clathrin-mediated endocytosis. *Nature reviews Molecular cell biology,* 12**,** 517-533.

MELZACK, R. & WALL, P. D. 1983. The challenge of pain.

MEYER, E. E., ROSENBERG, K. J. & ISRAELACHVILI, J. 2006. Recent progress in understanding hydrophobic interactions. *Proceedings of the National Academy of Sciences,* 103**,** 15739-15746.

MORA-HUERTAS, C., FESSI, H. & ELAISSARI, A. 2010. Polymer-based nanocapsules for drug delivery. *International journal of pharmaceutics,* 385**,** 113-142.

MORAN, J. H. & SCHNELLMANN, R. G. 1996. A rapid β-NADH-linked fluorescence assay for lactate dehydrogenase in cellular death. *Journal of pharmacological and toxicological methods,* 36**,** 41-44.

MOSMANN, T. 1983. Rapid colorimetric assay for cellular growth and survival: application to proliferation and cytotoxicity assays. *Journal of immunological methods,* 65**,** 55-63.

MOURYA, V. & INAMDAR, N. N. 2008. Chitosan-modifications and applications: opportunities galore. *Reactive and Functional polymers,* 68**,** 1013-1051.

MUCHA, M. 1997. Rheological characteristics of semi-dilute chitosan solutions. *Macromolecular Chemistry and Physics,* 198**,** 471-484.

MUHEEM, A., SHAKEEL, F., JAHANGIR, M. A., ANWAR, M., MALLICK, N., JAIN, G. K., WARSI, M. H. & AHMAD, F. J. 2016. A review on the strategies for oral delivery of proteins and peptides and their clinical perspectives. *Saudi Pharmaceutical Journal,* 24**,** 413-428.

MUZZARELLI, R. A., TANFANI, F., EMANUELLI, M. & MARIOTTI, S. 1982. N-(carboxymethylidene) chitosans and N-(carboxymethyl) chitosans: novel chelating polyampholytes obtained from chitosan glyoxylate. *Carbohydrate Research,* 107**,** 199-214.

MYERS, D. 1999. Colloids and colloidal stability. *Surfaces, Interfaces, and Colloids: Principles and Applications, Second Edition***,** 214-252.

NAGAVARMA, B., YADAV, H. K., AYAZ, A., VASUDHA, L. & SHIVAKUMAR, H. 2012. Different techniques for preparation of polymeric nanoparticles-a review. *Asian J. Pharm. Clin. Res,* 5**,** 16-23.

NAM, H. Y., KWON, S. M., CHUNG, H., LEE, S.-Y., KWON, S.-H., JEON, H., KIM, Y., PARK, J. H., KIM, J. & HER, S. 2009. Cellular uptake mechanism and intracellular fate of hydrophobically modified glycol chitosan nanoparticles. *Journal of Controlled Release,* 135**,** 259-267.

NELLANS, H. N. 1991. (B) Mechanisms of peptide and protein absorption:(1) Paracellular intestinal transport: modulation of absorption. *Advanced drug delivery reviews,* 7**,** 339-364.

NEUTRA, M. 1987. Gastrointestinal mucus: synthesis, secretion, and function. *Physiology of the gastrointestinal tract***,** 975-1009.

NOACH, A. B., KUROSAKI, Y., BLOM-ROOSEMALEN, M. C., DE BOER, A. G. & BREIMER, D. D. 1993. Cell-polarity dependent effect of chelation on the paracellular permeability of confluent Caco-2 cell monolayers. *International journal of pharmaceutics,* 90**,** 229-237.

NOBBMANN, U., CONNAH, M., FISH, B., VARLEY, P., GEE, C., MULOT, S., CHEN, J., ZHOU, L., LU, Y. & SHENG, F. 2007. Dynamic light scattering as a relative tool for assessing the molecular integrity and stability of monoclonal antibodies. *Biotechnology and genetic engineering reviews,* 24**,** 117-128.

NORIA, S., COWAN, D. B., GOTLIEB, A. I. & LANGILLE, B. L. 1999. Transient and steady-state effects of shear stress on endothelial cell adherens junctions. *Circulation research,* 85**,** 504-514.

NORRIS, D. A., PURI, N. & SINKO, P. J. 1998. The effect of physical barriers and properties on the oral absorption of particulates. *Advanced drug delivery reviews,* 34**,** 135-154.

NORRIS, D. A. & SINKO, P. J. 1997. Effect of size, surface charge, and hydrophobicity on the translocation of polystyrene microspheres through gastrointestinal mucin. *Journal of applied polymer science,* 63**,** 1481-1492.

O'MAHONY, A. M., DOYLE, D., DARCY, R., CRYAN, J. F. & O'DRISCOLL, C. M. 2012. Characterisation of cationic amphiphilic cyclodextrins for neuronal delivery of siRNA: effect of reversing primary and secondary face modifications. *European Journal of Pharmaceutical Sciences,* 47**,** 896-903.

OHSHIMA, H. 2012. The derjaguin–landau–verwey–overbeek (dlvo) theory of colloid stability. *Electrical Phenomena at Interfaces and Biointerfaces: Fundamentals and Applications in Nano-, Bio-, and Environmental Sciences***,** 27.

OLMSTED, S. S., PADGETT, J. L., YUDIN, A. I., WHALEY, K. J., MOENCH, T. R. & CONE, R. A. 2001. Diffusion of macromolecules and virus-like particles in human cervical mucus. *Biophysical journal,* 81**,** 1930-1937.

ORTEGA-VINUESA, J., MARTIN-RODRIGUEZ, A. & HIDALGO-ALVAREZ, R. 1996. Colloidal stability of polymer colloids with different interfacial properties: mechanisms. *Journal of colloid and interface science,* 184**,** 259-267.

PAN, Y., LI, Y.-J., ZHAO, H.-Y., ZHENG, J.-M., XU, H., WEI, G. & HAO, J.-S. 2002. Bioadhesive polysaccharide in protein delivery system: chitosan nanoparticles improve the intestinal absorption of insulin in vivo. *International Journal of Pharmaceutics,* 249**,** 139-147.

PARK, M.-J., BALAKRISHNAN, P. & YANG, S.-G. 2013. Polymeric nanocapsules with SEDDS oil-core for the controlled and enhanced oral absorption of cyclosporine. *International journal of pharmaceutics,* 441**,** 757-764.

PASTAN, I. & WILLINGHAM, M. C. 1985. The pathway of endocytosis. *Endocytosis.* Springer.

PAULA, S., SUES, W., TUCHTENHAGEN, J. & BLUME, A. 1995a. Thermodynamics of micelle formation as a function of temperature: a high sensitivity titration calorimetry study. *The Journal of Physical Chemistry,* 99**,** 11742-11751.

PAULA, S., SUS, W., TUCHTENHAGEN, J. & BLUME, A. 1995b. THERMODYNAMICS OF MICELLE FORMATION AS A FUNCTION OF TEMPERATURE - A HIGH-SENSITIVITY TITRATION CALORIMETRY STUDY. *Journal of Physical Chemistry,* 99**,** 11742-11751.

PETIT-AGNELY, F., ILIOPOULOS, I. & ZANA, R. 2000. Hydrophobically modified sodium polyacrylates in aqueous solutions: association mechanism and characterization of the aggregates by fluorescence probing. *Langmuir,* 16**,** 9921-9927.

PLUEN, A., NETTI, P. A., JAIN, R. K. & BERK, D. A. 1999. Diffusion of macromolecules in agarose gels: comparison of linear and globular configurations. *Biophysical journal,* 77**,** 542-552.

PODZIMEK, S. 1994. The use of GPC coupled with a multiangle laser light scattering photometer for the characterization of polymers. On the determination of molecular weight, size and branching. *Journal of applied polymer science,* 54**,** 91-103.

POHLMANN, A. R., MEZZALIRA, G., DE GARCIA VENTURINI, C., CRUZ, L., BERNARDI, A., JÄGER, E., BATTASTINI, A. M., DA SILVEIRA, N. P. & GUTERRES, S. S. 2008. Determining the simultaneous presence of drug nanocrystals in drug-loaded polymeric nanocapsule aqueous suspensions: a relation between light scattering and drug content. *International journal of pharmaceutics,* 359**,** 288-293.

POWELL, D. 1987. Intestinal water and electrolyte transport. *Physiology of the gastrointestinal tract,* 2**,** 1286-1287.

PRABAHARAN, M. 2008. Review paper: chitosan derivatives as promising materials for controlled drug delivery. *Journal of Biomaterials Applications,* 23**,** 5-36.

PREGO, C., TORRES, D. & ALONSO, M. J. 2005. The potential of chitosan for the oral administration of peptides. *Expert opinion on drug delivery,* 2**,** 843-854.

PRIDGEN, E. M., ALEXIS, F. & FAROKHZAD, O. C. 2015. Polymeric nanoparticle drug delivery technologies for oral delivery applications. *Expert opinion on drug delivery***,** 1-15.

QUAN, Y.-S., HATTORI, K., LUNDBORG, E., FUJITA, T., MURAKAMI, M., MURANISHI, S. & YAMAMOTO, A. 1998. Effectiveness and toxicity screening of various absorption enhancers using Caco-2 cell monolayers. *Biological and Pharmaceutical Bulletin,* 21**,** 615-620.

QUARTERMAN, J. 1987. Metal absorption and the intestinal mucus layer. *Digestion,* 37**,** 1-9.

RAJU, B. B., WINNIK, F. M. & MORISHIMA, Y. 2001. A look at the thermodynamics of the association of amphiphilic polyelectrolytes in aqueous solutions: strengths and limitations of isothermal titration calorimetry. *Langmuir,* 17**,** 4416-4421.

RAMALINGAM, P. & KO, Y. T. 2015. Enhanced oral delivery of curcumin from N-trimethyl chitosan surface-modified solid lipid nanoparticles: pharmacokinetic and brain distribution evaluations. *Pharmaceutical research,* 32**,** 389-402.

RAN, F., LEI, W., CUI, Y., JIAO, J., MAO, Y., WANG, S. & WANG, S. 2018. Size effect on oral absorption in polymer-functionalized mesoporous carbon nanoparticles. *Journal of colloid and interface science,* 511**,** 57-66.

RANALDI, G., MARIGLIANO, I., VESPIGNANI, I., PEROZZI, G. & SAMBUY, Y. 2002. The effect of chitosan and other polycations on tight junction permeability in the human intestinal Caco-2 cell line. *The Journal of nutritional biochemistry,* 13**,** 157-167.

RANALDI, G., SENECI, P., GUBA, W., ISLAM, K. & SAMBUY, Y. 1996. Transport of the antibacterial agent oxazolidin-2-one and derivatives across intestinal (Caco-2) and renal (MDCK) epithelial cell lines. *Antimicrobial agents and chemotherapy,* 40**,** 652-658.

RAY, G. B., CHAKRABORTY, I. & MOULIK, S. P. 2006. Pyrene absorption can be a convenient method for probing critical micellar concentration (cmc) and indexing micellar polarity. *Journal of colloid and interface science,* 294**,** 248-254.

REISS, G. & HÜTTEN, A. 2005. Magnetic nanoparticles: applications beyond data storage. *Nature materials,* 4**,** 725.

ROLS, M.-P. 2017. Molecular Transmembrane Transport with Giant Unilamellar Vesicles (GUVs). *Handbook of Electroporation***,** 95-111.

ROSENTHAL, R., GÜNZEL, D., FINGER, C., KRUG, S. M., RICHTER, J. F., SCHULZKE, J.-D., FROMM, M. & AMASHEH, S. 2012. The effect of chitosan on transcellular and paracellular mechanisms in the intestinal epithelial barrier. *Biomaterials,* 33**,** 2791-2800.

ROTHEN-RUTISHAUSER, B., KRÄMER, S. D., BRAUN, A., GÜNTHERT, M. & WUNDERLI-ALLENSPACH, H. 1998. MDCK cell cultures as an epithelial in vitro model: cytoskeleton and tight junctions as indicators for the definition of age-related stages by confocal microscopy. *Pharmaceutical research,* 15**,** 964-971.

SAHU, A., KASOJU, N., GOSWAMI, P. & BORA, U. 2011. Encapsulation of curcumin in Pluronic block copolymer micelles for drug delivery applications. *Journal of biomaterials applications,* 25**,** 619-639.

SALAMAT-MILLER, N. & JOHNSTON, T. P. 2005. Current strategies used to enhance the paracellular transport of therapeutic polypeptides across the intestinal epithelium. *International journal of pharmaceutics,* 294**,** 201-216.

SAMBUY, Y., DE ANGELIS, I., RANALDI, G., SCARINO, M. L., STAMMATI, A. & ZUCCO, F. 2005. The Caco-2 cell line as a model of the intestinal barrier: influence of cell and culture-related factors on Caco-2 cell functional characteristics. *Cell Biol Toxicol,* 21**,** 1-26.

SÁNCHEZ-IGLESIAS, A., GRZELCZAK, M., ALTANTZIS, T., GORIS, B., PEREZ-JUSTE, J., BALS, S., VAN TENDELOO, G., DONALDSON JR, S. H., CHMELKA, B. F. & ISRAELACHVILI, J. N. 2012. Hydrophobic interactions modulate self-assembly of nanoparticles. *ACS nano,* 6**,** 11059-11065.

SANDRI, G., ROSSI, S., BONFERONI, M. C., FERRARI, F., ZAMBITO, Y., DI COLO, G. & CARAMELLA, C. 2005. Buccal penetration enhancement properties of N-trimethyl chitosan: influence of quaternization degree on absorption of a high molecular weight molecule. *International journal of pharmaceutics,* 297**,** 146-155.

SANTANDER-ORTEGA, M., PEULA-GARCÍA, J., GOYCOOLEA, F. & ORTEGA-VINUESA, J. 2011. Chitosan nanocapsules: effect of chitosan molecular weight and acetylation degree on electrokinetic behaviour and colloidal stability. *Colloids and Surfaces B: Biointerfaces,* 82**,** 571-580.

SANTANDER-ORTEGA, M. J., LOZANO-LÓPEZ, M. V., BASTOS-GONZÁLEZ, D., PEULA-GARCÍA, J. M. & ORTEGA-VINUESA, J. L. 2010. Novel core-shell lipid-chitosan and lipid-poloxamer nanocapsules: stability by hydration forces. *Colloid and Polymer Science,* 288**,** 159-172.

SCHOLZ, J. & WOOLF, C. J. 2002. Can we conquer pain? *Nature neuroscience,* 5**,** 1062-1067.

SCHWARTZ, M. A. & DESIMONE, D. W. 2008. Cell adhesion receptors in mechanotransduction. *Current opinion in cell biology,* 20**,** 551-556.

SERRANO, D. R., LALATSA, A., DEA-AYUELA, M. A., BILBAO-RAMOS, P. E., GARRETT, N. L., MOGER, J., GUARRO, J., CAPILLA, J., BALLESTEROS, M. P. & SCHÄTZLEIN, A. G. 2015a. Oral particle uptake and organ targeting drives the activity of amphotericin B nanoparticles. *Molecular pharmaceutics,* 12**,** 420-431.

SERRANO, D. R., LALATSA, A., DEA-AYUELA, M. A., BILBAO-RAMOS, P. E., GARRETT, N. L., MOGER, J., GUARRO, J., CAPILLA, J., BALLESTEROS, M. P., SCHATZLEIN, A. G., BOLAS, F., TORRADO, J. J. & UCHEGBU, I. F. 2015b. Oral particle uptake and organ targeting drives the activity of amphotericin B nanoparticles. *Mol Pharm,* 12**,** 420-31.

SHAKWEH, M., PONCHEL, G. & FATTAL, E. 2004. Particle uptake by Peyer's patches: a pathway for drug and vaccine delivery. *Expert opinion on drug delivery,* 1**,** 141-163.

SHARMA, K. S., DURAND, G. G., GABEL, F., BAZZACCO, P., LE BON, C., BILLON-DENIS, E., CATOIRE, L. J., POPOT, J.-L., EBEL, C. & PUCCI, B. 2012. Non-ionic amphiphilic homopolymers: synthesis, solution properties, and biochemical validation. *Langmuir,* 28**,** 4625-4639.

SHEN, L., WEBER, C. R., RALEIGH, D. R., YU, D. & TURNER, J. R. 2011. Tight junction pore and leak pathways: a dynamic duo. *Annual review of physiology,* 73**,** 283-309.

SHEN, W.-C. 2003. Oral peptide and protein delivery: unfulfilled promises? *Drug discovery today,* 8**,** 607-608.

SHIMA, M., KIMURA, Y., ADACHI, S. & MATSUNO, R. 1999. Recovery of Caco-2 cell monolayers to normal from the transport-enhanced state induced by capric acid sodium salt and its monoacylglycerol. *Bioscience, biotechnology, and biochemistry,* 63**,** 680-687.

SHIMIZU, S., PIRES, P. A. R. & EL SEOUD, O. A. 2004. Thermodynamics of micellization of benzyl(2-acylaminoethyl)dimethylammonium chloride surfactants in aqueous solutions: A conductivity and titration calorimetry study. *Langmuir,* 20**,** 9551-9559.

SIEVAL, A., THANOU, M., KOTZE, A., VERHOEF, J., BRUSSEE, J. & JUNGINGER, H. 1998. Preparation and NMR characterization of highly substitutedN-trimethyl chitosan chloride. *Carbohydrate Polymers,* 36**,** 157-165.

SIEVÄNEN, E. 2007. Exploitation of bile acid transport systems in prodrug design. *Molecules,* 12**,** 1859-1889.

SIEW, A., LE, H., THIOVOLET, M., GELLERT, P., SCHATZLEIN, A. & UCHEGBU, I. 2011. Enhanced oral absorption of hydrophobic and hydrophilic drugs using quaternary ammonium palmitoyl glycol chitosan nanoparticles. *Molecular pharmaceutics,* 9**,** 14-28.

SILVA, E., BARREIROS, L., SEGUNDO, M. A., LIMA, S. A. C. & REIS, S. 2017. Cellular interactions of a lipid-based nanocarrier model with human keratinocytes: Unravelling transport mechanisms. *Acta biomaterialia,* 53**,** 439-449.

SIMÕES, S. M., FIGUEIRAS, A. R., VEIGA, F., CONCHEIRO, A. & ALVAREZ-LORENZO, C. 2015. Polymeric micelles for oral drug administration enabling locoregional and systemic treatments. *Expert opinion on drug delivery,* 12**,** 297-318.

SINHA, V. & KUMRIA, R. 2001. Colonic drug delivery: prodrug approach. *Pharmaceutical research,* 18**,** 557-564.

SOGIAS, I. A., WILLIAMS, A. C. & KHUTORYANSKIY, V. V. 2008. Why is chitosan mucoadhesive? *Biomacromolecules,* 9**,** 1837-1842.

SONAJE, K., CHUANG, E.-Y., LIN, K.-J., YEN, T.-C., SU, F.-Y., TSENG, M. T. & SUNG, H.-W. 2012. Opening of epithelial tight junctions and enhancement of paracellular permeation by chitosan: microscopic, ultrastructural, and computed-tomographic observations. *Molecular pharmaceutics,* 9**,** 1271-1279.

SORKIN, A. 2004. Cargo recognition during clathrin-mediated endocytosis: a team effort. *Current opinion in cell biology,* 16**,** 392-399.

SOUNDARARAJAN, R., SASAKI, K., GODFREY, L., ODUNZE, U., FEREIRA, N., SCHÄTZLEIN, A. & UCHEGBU, I. 2016. Direct in vivo evidence on the mechanism by which nanoparticles facilitate the absorption of a water insoluble, P-gp substrate. *International journal of pharmaceutics,* 514**,** 121-132.

SPILLER, R., JENKINS, D., THORNLEY, J., HEBDEN, J., WRIGHT, T., SKINNER, M. & NEAL, K. 2000. Increased rectal mucosal enteroendocrine cells, T lymphocytes, and increased gut permeability following acuteCampylobacter enteritis and in post-dysenteric irritable bowel syndrome. *Gut,* 47**,** 804-811.

SRIKANTH, K., TRINDADE, T., DUARTE, A. & PEREIRA, E. 2017. Cytotoxicity and oxidative stress responses of silica-coated iron oxide nanoparticles in CHSE-214 cells. *Environmental Science and Pollution Research,* 24**,** 2055-2064.

STAEHELIN, L. A., MUKHERJEE, T. & WILLIAMS, A. W. 1969. Freeze-etch appearance of the tight junctions in the epithelium of small and large intestine of mice. *Protoplasma,* 67**,** 165-184.

STEIN, H., SPINDLER, S., BONAKDAR, N., WANG, C. & SANDOGHDAR, V. 2017. Production of Isolated Giant Unilamellar Vesicles under High Salt Concentrations. *Frontiers in physiology,* 8**,** 63.

STODGHILL, S. P., SMITH, A. E. & O'HAVER, J. H. 2004. Thermodynamics of micellization and adsorption of three alkyltrimethylammonium bromides using isothermal titration calorimetry. *Langmuir,* 20**,** 11387-11392.

SUH, J.-K. F. & MATTHEW, H. W. 2000. Application of chitosan-based polysaccharide biomaterials in cartilage tissue engineering: a review. *Biomaterials,* 21**,** 2589-2598.

SUN, C., LEE, J. S. & ZHANG, M. 2008. Magnetic nanoparticles in MR imaging and drug delivery. *Advanced drug delivery reviews,* 60**,** 1252-1265.

SUN, S. 2006. Recent advances in chemical synthesis, self-assembly, and applications of FePt nanoparticles. *Advanced Materials,* 18**,** 393-403.

SURAPANENI, M. S., DAS, S. K. & DAS, N. G. 2012. Designing Paclitaxel drug delivery systems aimed at improved patient outcomes: current status and challenges. *ISRN pharmacology,* 2012.

SUWA, M., HASHIDZUME, A., MORISHIMA, Y., NAKATO, T. & TOMIDA, M. 2000. Self-association behavior of hydrophobically modified poly (aspartic acid) in water studied by fluorescence and dynamic light scattering techniques. *Macromolecules,* 33**,** 7884-7892.

SVENSON, S. 2009. Dendrimers as versatile platform in drug delivery applications. *European Journal of Pharmaceutics and Biopharmaceutics,* 71**,** 445-462.

SWANSON, J. A. & WATTS, C. 1995. Macropinocytosis. *Trends in cell biology,* 5**,** 424-428.

SZYMAŃSKA, E. & WINNICKA, K. 2015. Stability of chitosan—a challenge for pharmaceutical and biomedical applications. *Marine drugs,* 13**,** 1819-1846.

TA, H. T., HAN, H., LARSON, I., DASS, C. R. & DUNSTAN, D. E. 2009. Chitosan-dibasic orthophosphate hydrogel: a potential drug delivery system. *International journal of pharmaceutics,* 371**,** 134-141.

TADROS, T. F. 2005. Physical chemistry of surfactant solutions. *Applied Surfactants: Principles and Applications***,** 19-51.

TAKEUCHI, H., YAMAMOTO, H. & KAWASHIMA, Y. 2001. Mucoadhesive nanoparticulate systems for peptide drug delivery. *Advanced drug delivery reviews,* 47**,** 39-54.

TANFORD, C. 1980. *The hydrophobic effect: formation of micelles and biological membranes,* New York, John Wiley and Sons.

TATE, P., STEPHENS, T. & SEELEY, R. 2003a. Anatomy & Physiology 6th edition Digestive System: Clinical Application 1. 860-891.

TATE, P., STEPHENS, T. & SEELEY, R. 2003b. Anatomy & Physiology 6th edition Digestive System: Clinical Application 1. 882-883.

THANOU, M., KOTZE, A., SCHARRINGHAUSEN, T., LUESSEN, H., DE BOER, A., VERHOEF, J. & JUNGINGER, H. 2000a. Effect of degree of quaternization of N-trimethyl chitosan chloride for enhanced transport of hydrophilic compounds across intestinal Caco-2 cell monolayers. *Journal of Controlled Release,* 64**,** 15-25.

THANOU, M., NIHOT, M., JANSEN, M., VERHOEF, J. C. & JUNGINGER, H. 2001a. Mono-N-carboxymethyl chitosan (MCC), a polyampholytic chitosan derivative, enhances the intestinal absorption of low molecular weight heparin across intestinal epithelia in vitro and in vivo. *Journal of pharmaceutical sciences,* 90**,** 38-46.

THANOU, M., VERHOEF, J. & JUNGINGER, H. 2001b. Oral drug absorption enhancement by chitosan and its derivatives. *Advanced drug delivery reviews,* 52**,** 117-126.

THANOU, M., VERHOEF, J. C., VERHEIJDEN, J. H. & JUNGINGER, H. E. 2001c. Intestinal absorption of octreotide using trimethyl chitosan chloride: studies in pigs. *Pharmaceutical research,* 18**,** 823-828.

THANOU, M. M., KOTZE, A. F., SCHARRINGHAUSEN, T., LUESSEN, H. L., DE BOER, A. G., VERHOEF, J. C. & JUNGINGER, H. E. 2000b. Effect of degree of quaternization of N-trimethyl chitosan chloride for enhanced transport of hydrophilic compounds across intestinal caco-2 cell monolayers. *Journal of controlled release : official journal of the Controlled Release Society,* 64**,** 15-25.

TOAN, N. V., NG, C. H., AYE, K. N., TRANG, T. S. & STEVENS, W. F. 2006. Production of high-quality chitin and chitosan from preconditioned shrimp shells. *Journal of Chemical Technology and Biotechnology,* 81**,** 1113-1118.

TOMITA, M., HAYASHI, M. & AWAZU, S. 1995. Absorption-enhancing mechanism of sodium caprate and decanoylcarnitine in Caco-2 cells. *Journal of Pharmacology and Experimental Therapeutics,* 272**,** 739-743.

TOMITA, M., HAYASHI, M. & AWAZU, S. 1996. Absorption-enhancing mechanism of EDTA, caprate, and decanoylcarnitine in Caco-2 cells. *Journal of pharmaceutical sciences,* 85**,** 608-611.

TONG, W., ZHENG, Q., SHAO, S., LEI, Q. & FANG, W. 2010. Critical micellar concentrations of quaternary ammonium surfactants with hydroxyethyl substituents on headgroups determined by isothermal titration calorimetry. *Journal of Chemical & Engineering Data,* 55**,** 3766-3771.

TORCHILIN, V. P. 2005. Recent advances with liposomes as pharmaceutical carriers. *Nature reviews Drug discovery,* 4**,** 145.

TRAN, P., NGUYEN, H. T., FOX, K. & TRAN, N. 2018. In vitro cytotoxicity of iron oxide nanoparticles: Effects of chitosan and polyvinyl alcohol as stabilizing agents. *Materials Research Express*.

TREFALT, G. & BORKOVEC, M. 2014. Overview of DLVO Theory.

TUMA, P. L. & HUBBARD, A. L. 2003. Transcytosis: crossing cellular barriers. *Physiological Reviews,* 83**,** 871-932.

UCHEGBU, I. F. 2013. Low Molecular Weight Micelles. *Fundamentals of Pharmaceutical Nanoscience.* Springer.

UCHEGBU, I. F., CARLOS, M., MCKAY, C., HOU, X. & SCHÄTZLEIN, A. G. 2014. Chitosan amphiphiles provide new drug delivery opportunities. *Polymer International,* 63**,** 1145-1153.

UCHEGBU, I. F., LALATSA, A. & WONG, D. 2013a. Polymeric nanoparticles. *Fundamentals of pharmaceutical nanoscience.* Springer.

UCHEGBU, I. F., SADIQ, L., ARASTOO, M., GRAY, A. I., WANG, W., WAIGH, R. D. & SCHÄTZLEIN, A. G. 2001. Quaternary ammonium palmitoyl glycol chitosan—a new polysoap for drug delivery. *International journal of pharmaceutics,* 224**,** 185-199.

UCHEGBU, I. F., SCHATZLEIN, A. G. & HOU, X. 2013b. Polymeric micellar clusters and their uses in formulating drugs. Google Patents.

UCHEGBU, I. F. & SIEW, A. 2013. Nanomedicines and nanodiagnostics come of age. *J Pharm Sci,* 102**,** 305-10.

UPADHYAYA, L., SINGH, J., AGARWAL, V. & TEWARI, R. P. 2014. The implications of recent advances in carboxymethyl chitosan based targeted drug delivery and tissue engineering applications. *Journal of Controlled Release,* 186**,** 54-87.

VAN DER LUBBEN, I., KONINGS, F., BORCHARD, G., VERHOEF, J. & JUNGINGER, H. 2001a. In vivo uptake of chitosan microparticles by murine Peyer's patches: visualization studies using confocal laser scanning microscopy and immunohistochemistry. *Journal of drug targeting,* 9**,** 39-47.

VAN DER LUBBEN, I., VERHOEF, J., VAN AELST, A., BORCHARD, G. & JUNGINGER, H. 2001b. Chitosan microparticles for oral vaccination:: preparation, characterization and preliminary in vivo uptake studies in murine Peyer's patches. *Biomaterials,* 22**,** 687-694.

VAN ITALLIE, C. M. & ANDERSON, J. M. 2006. Claudins and epithelial paracellular transport. *Annu. Rev. Physiol.,* 68**,** 403-429.

VAN ITALLIE, C. M., FANNING, A. S., BRIDGES, A. & ANDERSON, J. M. 2009. ZO-1 stabilizes the tight junction solute barrier through coupling to the perijunctional cytoskeleton. *Molecular biology of the cell,* 20**,** 3930-3940.

VERMA, A. & STELLACCI, F. 2010. Effect of surface properties on nanoparticle–cell interactions. *Small,* 6**,** 12-21.

VERMA, J., KHEDKAR, V. M. & COUTINHO, E. C. 2010. 3D-QSAR in drug design-a review. *Current topics in medicinal chemistry,* 10**,** 95-115.

VERWEY, E. J. W., OVERBEEK, J. T. G. & OVERBEEK, J. T. G. 1999. *Theory of the stability of lyophobic colloids*, Courier Corporation.

VILA, A., SANCHEZ, A., TOBIO, M., CALVO, P. & ALONSO, M. 2002. Design of biodegradable particles for protein delivery. *Journal of Controlled Release,* 78**,** 15-24.

VILLANUEVA, A., CANETE, M., ROCA, A. G., CALERO, M., VEINTEMILLAS-VERDAGUER, S., SERNA, C. J., DEL PUERTO MORALES, M. & MIRANDA, R. 2009. The influence of surface functionalization on the enhanced internalization of magnetic nanoparticles in cancer cells. *Nanotechnology,* 20**,** 115103.

VILLARI, V., MAZZAGLIA, A., DARCY, R., O'DRISCOLL, C. M. & MICALI, N. 2013. Nanostructures of cationic amphiphilic cyclodextrin complexes with DNA. *Biomacromolecules,* 14**,** 811-817.

WALKER, W. A. 2004. *Pediatric gastrointestinal disease: pathophysiology, diagnosis, management*, PMPH-USA.

WANG, J., KONG, M., ZHOU, Z., YAN, D., YU, X., CHENG, X., FENG, C., LIU, Y. & CHEN, X. 2017. Mechanism of surface charge triggered intestinal epithelial tight junction opening upon chitosan nanoparticles for insulin oral delivery. *Carbohydrate Polymers,* 157**,** 596-602.

WANG, L.-H., ROTHBERG, K. G. & ANDERSON, R. 1993. Mis-assembly of clathrin lattices on endosomes reveals a regulatory switch for coated pit formation. *The Journal of cell biology,* 123**,** 1107-1117.

WANG, X.-Q., HUANG, J., DAI, J.-D., ZHANG, T., LÜ, W.-L., ZHANG, H., ZHANG, X., WANG, J.-C. & ZHANG, Q. 2006. Long-term studies on the stability and oral bioavailability of cyclosporine A nanoparticle colloid. *International journal of pharmaceutics,* 322**,** 146-153.

WANG, Y., WANG, D., FU, Q., LIU, D., MA, Y., RACETTE, K., HE, Z. & LIU, F. 2014. Shape-controlled paclitaxel nanoparticles with multiple morphologies: rod-shaped, worm-like, spherical, and fingerprint-like. *Molecular pharmaceutics,* 11**,** 3766.

WANG, Y.-S., JIANG, Q., LI, R.-S., LIU, L.-L., ZHANG, Q.-Q., WANG, Y.-M. & ZHAO, J. 2008. Self-assembled nanoparticles of cholesterol-modified O-carboxymethyl chitosan as a novel carrier for paclitaxel. *Nanotechnology,* 19**,** 145101.

WATSON, P., JONES, A. T. & STEPHENS, D. J. 2005. Intracellular trafficking pathways and drug delivery: fluorescence imaging of living and fixed cells. *Advanced drug delivery reviews,* 57**,** 43-61.

WEBBER, S. 1998. Polymer micelles: an example of self-assembling polymers. ACS Publications.

WEYERMANN, J., LOCHMANN, D. & ZIMMER, A. 2005. A practical note on the use of cytotoxicity assays. *International Journal of Pharmaceutics,* 288**,** 369-376.

WHITCOMB, D. C. & LOWE, M. E. 2007. Human pancreatic digestive enzymes. *Digestive diseases and sciences,* 52**,** 1-17.

WILHELM, C., BILLOTEY, C., ROGER, J., PONS, J., BACRI, J.-C. & GAZEAU, F. 2003. Intracellular uptake of anionic superparamagnetic nanoparticles as a function of their surface coating. *Biomaterials,* 24**,** 1001-1011.

WORKING, P. & DAYAN, A. 1996. Pharmacological-toxicological expert report. CAELYX.(Stealth liposomal doxorubicin HCl). *Human & experimental toxicology,* 15**,** 751-785.

WU, D., ABEZGAUZ, L., DANINO, D. & HO, C.-C. 2008. Alternating polymer vesicles. *Soft Matter,* 4**,** 1066-1071.

XU, T., XIN, M., LI, M., HUANG, H. & ZHOU, S. 2010. Synthesis, characteristic and antibacterial activity of N, N, N-trimethyl chitosan and its carboxymethyl derivatives. *Carbohydrate Polymers,* 81**,** 931-936.

YE, D., DAWSON, K. A. & LYNCH, I. 2015. A TEM protocol for quality assurance of in vitro cellular barrier models and its application to the assessment of nanoparticle transport mechanisms across barriers. *Analyst,* 140**,** 83-97.

YEH, T.-H., HSU, L.-W., TSENG, M. T., LEE, P.-L., SONJAE, K., HO, Y.-C. & SUNG, H.-W. 2011. Mechanism and consequence of chitosan-mediated reversible epithelial tight junction opening. *Biomaterials,* 32**,** 6164-6173.

YIN, L., DING, J., HE, C., CUI, L., TANG, C. & YIN, C. 2009. Drug permeability and mucoadhesion properties of thiolated trimethyl chitosan nanoparticles in oral insulin delivery. *Biomaterials,* 30**,** 5691-5700.

ZHANG, L., ZHAO, Z.-L., WEI, X.-H. & LIU, J.-H. 2013. Preparation and in vitro and in vivo characterization of cyclosporin A-loaded, PEGylated chitosan-modified, lipid-based nanoparticles. *International journal of nanomedicine,* 8**,** 601.

ZHANG, M.-Q. & WILKINSON, B. 2007. Drug discovery beyond the 'rule-of-five'. *Current opinion in biotechnology,* 18**,** 478-488.

ZHANG, Y., FENG, J., CUI, L., ZHANG, Y., LI, W., LI, C., SHI, N., CHEN, Y. & KONG, W. 2015. Investigation into efficiency of a novel glycol chitosan–bestatin conjugate to protect thymopoietin oligopeptides from enzymatic degradation. *Journal of pharmaceutical sciences*.

ZHENG, Y., CAI, Z., SONG, X., YU, B., BI, Y., CHEN, Q., ZHAO, D., XU, J. & HOU, S. 2009. Receptor mediated gene delivery by folate conjugated N-trimethyl chitosan in vitro. *International journal of pharmaceutics,* 382**,** 262-269.

ZHOU, L., CHOW, M. S. & ZUO, Z. 2009. Effect of sodium caprate on the oral absorptions of danshensu and salvianolic acid B. *International journal of pharmaceutics,* 379**,** 109-118.

ZIMM, B. H. & STOCKMAYER, W. H. 1949. The dimensions of chain molecules containing branches and rings. *The Journal of Chemical Physics,* 17**,** 1301-1314.

Appendix

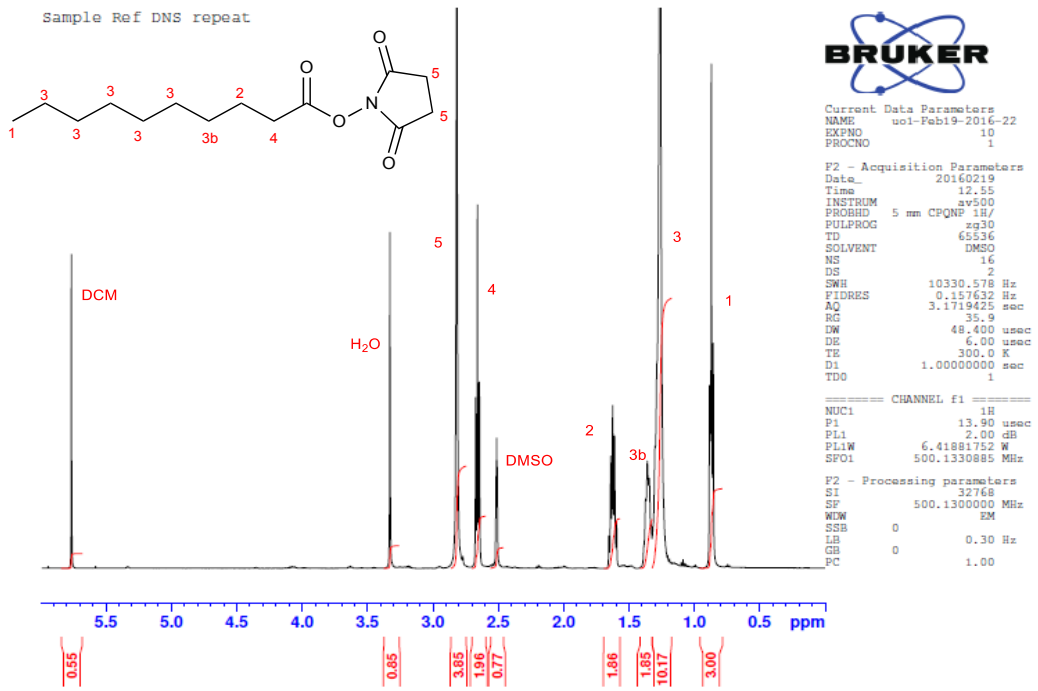

Figure 7-1: NMR plots of synthesized Decanoic acid-N-hydroxysuccinimide ester

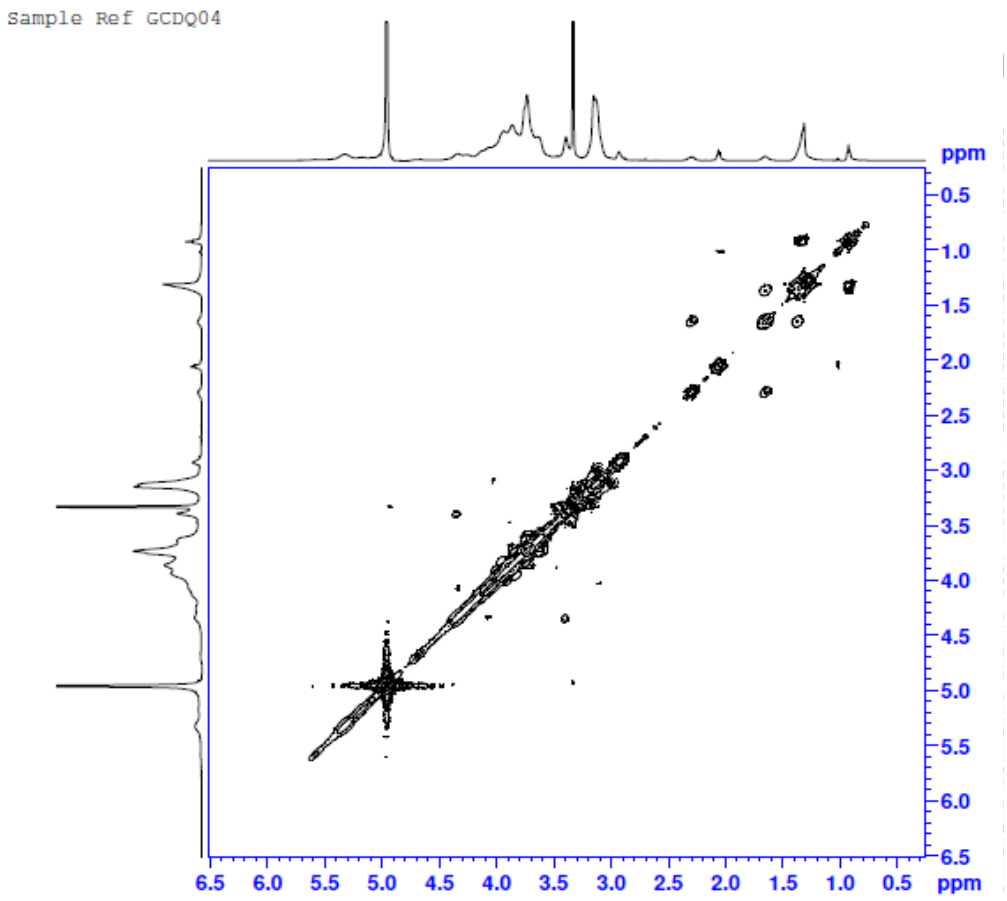

Figure 7-2: ^{1}H-^{1}H-COSY NMR of GCDQ in MeOD with decanoylation level of 8.7% and quaternisation level of 7%

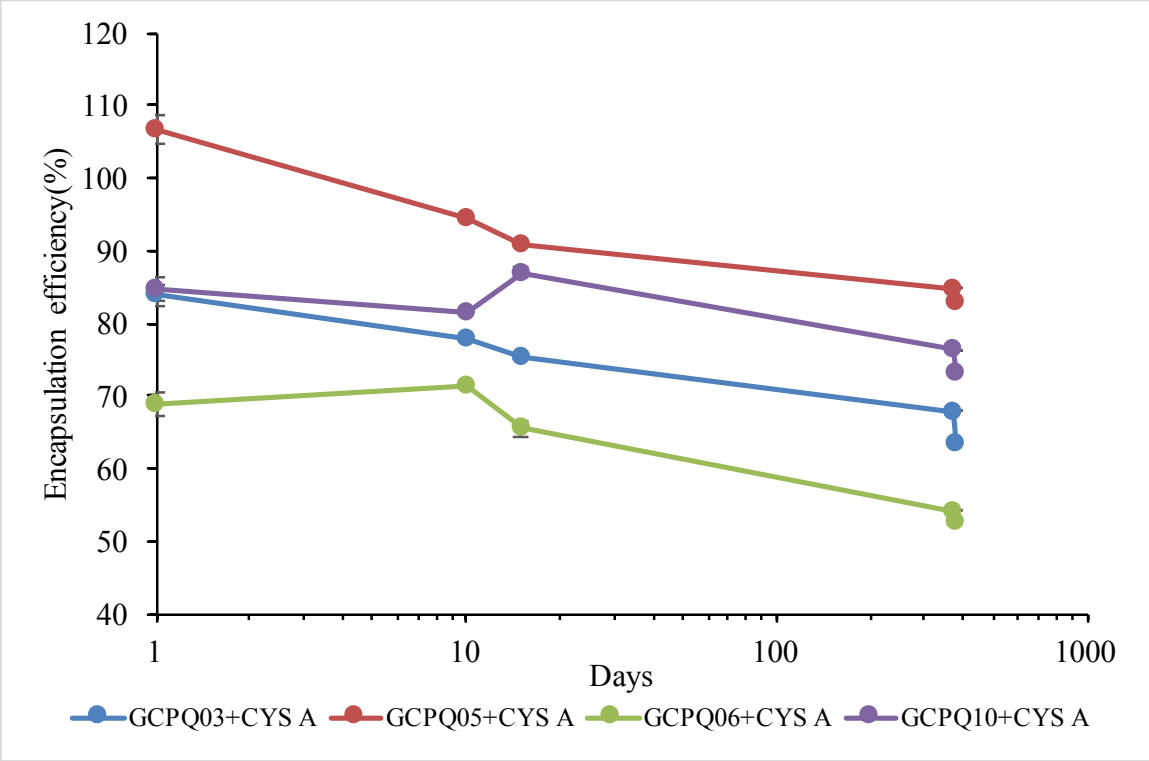

Figure 7-3: Encapsulation efficiency of GCPQ-Cyclosporine A formulations preserved at 4^{o}C decreased by about 20% over a one-year period.